TURBULENCE AND COHERENT STRUCTURES ACROSS AIR-WATER INTERFACE AND RELATIONSHIP WITH GAS TRANSFER

A Dissertation

Presented to the Department of Global Environment Engineering

of Kyoto University

in Partial Fulfillment of the Requirements for the Degree of

Doctor of Philosophy

by

Tadanobu Nakayama

2000

ABSTRACT

Tadanobu Nakayama, Ph.D.
Kyoto University, Japan, 2000

In this study, the relationship between the turbulence and coherent structures in both layers and the gas transfer across the interface was evaluated in view of both the physical and chemical aspects. At that time, three types of turbulent conditions were examined; that is to say, (A) bottom-shear generated turbulence, (B) wind-shear generated turbulence and (C) combined wind/stream turbulent conditions.

The turbulence and the coherent structures near the free surface in "*smooth open-channel flow*" were firstly evaluated. It was found that the free surface affects greatly the damping characteristics of turbulence intensity near the free surface in quiet open-channel flow in comparison with the DNS data in duct flow. However, when the Froude number increases and the surface-wave fluctuations occur, this damping characteristic disappears. So, the relationship between the turbulence structure near the free surface and the surface-wave fluctuations was considered by the simultaneous measurements of LDA (Laser-Doppler anemometer) and the ultrasonic depth meter. These turbulence characteristics are closely related to the coherent structure, and therefore, the space-time correlation structures were considered in order to relate to the Chapter 3.

Next, the "*mutual-interaction between bursts and boils*" was evaluated. The variation of turbulent energy redistributions near the free surface including the effect of Froude number was estimated. Next, PIV (Particle-Image Velocimetry) method is used to measure evolutionary patterns of coherent vortices. In this chapter, a relationship between the "*bursting phenomenon*" generated near the wall and the "*surface renewal eddies*" near the free surface was evaluated in the flows whether or not the surface-wave fluctuations are generated at the free surface. It was clarified that the agglemeration occurs in the higher Froude number flow and that this results in the longer bursting-period and the increase of turbulence intensity.

For reproducing the above-mentioned experimental data, the "*numerical simulation by using RSM (Reynolds stress model)*" was conducted. The turbulent redistribution near the free surface could be reproduced by considering the effect of Froude number and the surface-wave fluctuations. At that time, two methods, that is to say, (1) giving the boundary conditions of the turbulent redistributions at the free surface, and (2) the expansion of Shir model, were used.

Comparing the smooth bed flow, the "*rough-bed flow with large roughness elements*" was examined. The tendency toward isotropy becomes stronger near the roughness elements in comparison with smooth open-channel flow. As for the coherent structure, the inhomogeneity of the coherent structure predominates near the rough bed, which results in the generation of boil near the free surface. Furthermore, the wave-induced flow is evaluated for comparing "*wave-effect*" with "*turbulence-effect*".

Next, the "*turbulence structure in air-water interface with wind shear above the still water*" was estimated. Firstly, the fundamental characteristics of wind waves were considered in view of the momentum transfer and the relation between roughness height and surface wave, *etc*. Furthermore, the turbulence structures across air-water interface were evaluated. At that time, LFT (Linear Filtration Technique) method was used for decomposing the velocity component into the mean, wave and turbulence components. The energy budgets in both air and water layers are closely related with each other, and the energy transfer through the air-water interface increases when the wind velocity increases.

Considering the actual river, the "*two-layer flows when both the bed shear and the interface shear coexist*" were evaluated. In this chapter, the mixing-length model in wind wave is extended in the air

ABSTRACT

flow of two-phase flows. As for the roughness height, it was clarified that the value has a close relationship with the relative velocity of both layers.

Furthermore, the "*characteristic of gas transfer across the interface*" was estimated to compare with the previous empirical models including the effects of shear velocity and dissipation rate by measuring the DO (dissolved oxygen) concentrations. About two-layer flows, these models were expanded by considering the effect of the bed and interfacial shears, and the gas transfer coefficient in two-layer flows could be estimated by using the square-root matching technique.

Finally, the "*mechanism of relationship between the coherent structures in both layers and the gas transfer across the interface*" was clarified. By using PIV and the phase-averaged method, it was found that the separation of air flow on the leeward of the crest is closely related to the higher vorticity region of water on the leeward. In the faster wind speed, there occur a pair of vortices both in air and water layers. Furthermore, the effect of enhanced surface area on the gas transfer could be ignored in open-channel flow, and the higher frequency-energy of surface-wave fluctuations contributes greatly on the rapid increase of gas transfer.

ACKNOWLEDGEMENTS

The author wishes to express his thanks to Prof. Dr. Iehisa Nezu, Dept. of Global Environment Engineering, Faculty of Engineering, Kyoto University, for giving a chance to conduct this research at Kyoto University.

The author also wishes to thank Prof. Dr. Satoru Komori, Dept. of Mechanical Engineering, Faculty of Engineering, Kyoto University, for his idea, comments, and advices, in particular, about the turbulence structure near the free surface and gas transfer.

The author also wishes to thank Prof. Dr. Hirotake Imamoto, Ujigawa Hydraulics Laboratory, DPRI, Kyoto University, for his essential advices and sincere comments of this study.

About numerical simulation, the technical supports and comments of Prof. Dr. Dan Naot, Center of Tech. Ed., Israel, Prof. Dr. Ayodeji O. Demuren, Dept. of Mechanical Engineering, Old Dominion University, USA, Dr. Yoshihisa Kawahara, the Ministry of Construction, and Dr. Nobukazu Tanaka, Central Research Institute of Electric Power Industry, are appreciated.

The author is indebted very much to Dr. Douglas B. Moog, Dept. of Civil Engineering, Cornell University, USA, and Dr. Shohachi Kakuno, Dept. of Civil Engineering, Faculty of Engineering, Osaka City University, for their good and helpful discussion regarding the gas transfer model and how to measure the gas transfer.

The author also wishes to thank Prof. Dr. John C. Wells, College of Civil and Environmental Systems Engineering, Faculty of Science and Engineering, Ritsumeikan University, for his sincere and honest comments as a scientist and grammatical check of this thesis.

The author also is indebted to Dr. Norihisa Tsuda, Nippon Steel, Mr. Jyoji Mizoguti and Mr. Hideyuki Nagasaki, Kanomax Co. Ltd. and Mr. Masanori Matsumoto and Mr. Hiroshi Kumagai, Matsushita Inter-Techno Co. Ltd., for their frequent help about measuring systems (PTV, PIV and LDA systems).

This work was partially supported by the Japan Society for the Promotion of Science (JSPS).

Sincere thanks to all the students and graduates of Water Environment Engineering laboratory for helping experiments and data acquisitions.

Finally, the author wishes to express his deep sense of gratitude to his advisor, Prof. Dr. Hiroji Nakagawa, College of Civil and Environmental Systems Engineering, Faculty of Science and Engineering, Ritsumeikan University, and Professor emeritus of Kyoto University, for teaching an environmental importance of this study, a pride as researcher, and an enjoyment of pursuing a truth !

ACKNOWLEDGEMENTS

SUBMITTED PAPERS

[1] Nezu, I., Abe, T., Shimura, T. and Nakayama, T. : Characteristics of compound open-channel flows with FLDA and PTV, *Proc. of 2nd Symposium on River Hydraulics and Environments*, pp.45-52, 1995 (in Japanese).
[2] Nezu, I., Shimura, T. and Nakayama, T. : Analyses of coherent vortices between main-channel and flood-plains by means of PTV, *Annual Journal of Hydraulic Engineering*, Vol.40, pp.1059-1064, 1996a (in Japanese).
[3] Nezu, I., Abe, T., Shimura, T. and Nakayama, T. : Space-time correlation analysis in compound open-channel flows by making use of Particle-Tracking Velocimetry, *Journal of Hydraulic Engineering*, JSCE, No.539/II-35, pp.89-98, 1996b (in Japanese).
[4] Nezu, I., Shimura, T., Nakayama, T. and Kamiya, H. : Hydraulic effects on secondary currents in compound open-channel flows, *1st Symposium on Environmental Fluid Mechanics*, Vol.1, pp.331-332, 1996c (in Japanese).
[5] Nezu, I. and Nakayama, T.: Measurements of horizontal coherent vortices between main-channel and flood-plains by using Particle-Tracking Velocimetry, *Flow Modeling and Turbulence Measurements VI*, Chen, Shih, Lienau and Kung (eds), pp.229-236, 1996d.
[6] Nezu, I., Nakayama, T. and Itoh, Y. : Turbulent structures in steep open-channel flows, *1st Symposium on Environmental Fluid Mechanics*, Vol.1, pp.323-324, 1996e (in Japanese).
[7] Nezu, I. and Nakayama, T.: Space-time correlation structures of horizontal coherent vortices in compound open-channel flows by using Particle-Tracking Velocimetry, *J. Hydraulic Res.*, IAHR, Vol.35, No.2, 1997a.
[8] Nezu, I., Nakayama, T. and Itoh, Y. : Comparison of 3-D experimental database with direct numerical simulation, *Annual Journal of Hydraulic Engineering*, Vol.41, pp.1055-1060, 1997b (in Japanese).
[9] Nezu, I., Nakayama, T. and Kita, A. : Relationship between turbulence structures near the free-surface and surface-wave-fluctuations, *Annual Journal of Hydraulic Engineering*, Vol.41, pp.657-662, 1997c (in Japanese).
[10] Nezu, I. and Nakayama, T.: Relationship between turbulent structure near the free-surface and surface-wave-fluctuations, *Proc. of 27th IAHR Congress*, ASCE, IAHR, pp.245-250, 1997d.
[11] Nezu, I. and Nakayama, T. : Relationship between turbulent structures near the free-surface and surface-wave-fluctuations, *Journal of Hydraulic Engineering*, JSCE, No.593/II-43, pp.69-78, 1998a (in Japanese).
[12] Nezu, I. and Nakayama, T. : Space-time correlation structures of coherent vortices near the free surface, *Journal of Hydraulic Engineering*, JSCE, No.586/II-42, pp.51-60, 1998b (in Japanese).
[13] Nezu, I. and Nakayama, T. : Effect of the surface-wave fluctuations on coherent structures near the free-surface, *Annual Journal of Hydraulic Engineering*, Vol.42, pp.853-858, 1998c (in Japanese).
[14] Nezu, I. and Nakayama, T. : Characteristics of turbulent energy redistribution in an open-channel flow, *Proc. of 1998 Meeting of Japan Society of Fluid Mechanics*, pp.319-320, 1998d (in Japanese).
[15] Nezu, I. and Nakayama, T. : Relationship between bursts and boils in open-channel flows, *Journal of the Visualization Society of Japan*, Vol.18, No.1, pp.137-140, 1998e (in Japanese).
[16] Nezu, I., Nakayama, T. and Fujita, M. : Turbulence and free-surface sluctuations in open channel flows over macro-roughness, *Journal of Applied Mechanics*, JSCE, Vol.1, pp.709-718, 1998f (in Japanese).
[17] Nezu, I. and Nakayama, T.: Effect of the surface-wave fluctuations on coherent structures near the free surface, *11th Congress of the IAHR-APD*, pp.507-516, 1998g.
[18] Nezu, I. and Nakayama, T.: Turbulent redistribution near the free surface by using numerical

simulation, *11th Congress of the IAHR-APD*, pp.537-546, 1998h.
[19] Nezu, I. and Nakayama, T.: Separation between turbulence and water-wave effects in an open-channel flow, *Flow Modeling and Turbulence Measurements VII*, pp.67-76, 1998i.
[20] Nezu, I. and Nakayama, T.: Effect of macro-roughness on coherent structures by using PIV methods, *Flow Modeling and Turbulence Measurements VII*, pp.617-626, 1998j.
[21] Nezu, I. and Nakayama, T.: Mutual-interaction between bursts and boils very near the free surface in open-channel flows, *Environmental Hydraulics*, J.H.W.Lee *et al.* (eds), Balkema Pub., pp.297-303, 1998k.
[22] Nezu, I., Nakayama, T. and Inoue, R. : Turbulence structures in air-water interface with wind shear, *Annual Journal of Hydraulic Engineering*, Vol.43, pp.413-418, 1999a (in Japanese).
[23] Nezu, I. and Nakayama, T. : Effect of turbulence components below wind water waves, *Annual Journal of Hydraulic Engineering*, Vol.43, pp.407-412, 1999b (in Japanese).
[24] Nezu, I. and Nakayama, T. : Fundamental study at air-water interfaces with wind shear, *28th IAHR Congress*, IAHR, 1999c.
[25] Nezu, I. and Nakayama, T.: Effect of turbulence components below wind water waves, *28th IAHR Congress*, IAHR, 1999d.
[26] Nakayama, T. and Nezu, I. : Bursts near the free surface in open-channel flows and their relationship with turbulence structures, *Journal of Hydraulic Engineering*, JSCE, No.635/II-49, pp.31-40, 1999e (in Japanese).
[27] Nakayama, T. and Nezu, I. : Relationship between turbulence structures and gas transfer across air-water interface, *Journal of Hydraulic Engineering*, JSCE, N 635/II-49, pp.85-95, 1999f (in Japanese).
[28] Nakayama, T. and Nezu, I. : Numerical simulation of turbulence structures near the free surface by using Reynolds Stress Model, *Journal of Hydraulic Engineering*, JSCE, 1999g (in Japanese, to be accepted).
[29] Nezu, I., Nakayama, T. and Inoue, R. : Influence of turbulence structure on gas transfer across air-water interface, *Journal of Applied Mechanics*, JSCE, Vol.2, pp.673-684, 1999h (in Japanese).
[30] Nezu, I., Nakayama, T. and Inoue, R. : Relation between turbulence structure and gas transfer coefficient near the free surface, *Proc. of Water, Environment, Ecology, Socio-Economics, and Health Engineering*, pp.203-216, 1999i.
[31] Nezu, I. and Nakayama, T : Numerical calculation of steep open-channel flows by considering effects of surface-wave fluctuations, *Proc. of Water, Environment, Ecology, Socio-Economics, and Health Engineering*, pp 33-48, 1999j.
[32] Nezu, I. and Nakayama, T. . Numerical simulation of steep open-channel flows by using RSM, *Proc. of 1999 Meeting of Japan Society of Fluid Mechanics*, pp.383-384, 1999k (in Japanese).
[33] Nakayama, T. and Nezu, I. : Turbulence structures of wind/stream combined flow, *Journal of Hydraulic Engineering*, JSCE, 1999m (in Japanese, to be accepted).
[34] Nakayama, T. and Nezu, I. : Turbulence structures of wind water waves, *Journal of Hydraulic Engineering*, JSCE, No.642/II-50, 2000a (in Japanese).
[35] Nakayama, T. and Nezu, I. : Effect of increase of surface area and other factor on gas transfer in two-layer flows, *Annual Journal of Hydraulic Engineering*, Vol.44, pp.891-896, 2000b (in Japanese).
[36] Nezu, I. and Nakayama, T. : Instantaneous structures of air and water layers in wind water waves, *Annual Journal of Hydraulic Engineering*, Vol.44, pp.897-902, 2000c (in Japanese).

TABLE OF CONTENTS

TABLE OF CONTENTS

LIST OF TABLES

LIST OF FIGURES

CHAPTER 1

CHAPTER 2

CHAPTER 3

CHAPTER 4

CHAPTER 5

CHAPTER 6

CHAPTER 7

CHAPTER 8

CHAPTER 9

CHAPTER 1

INTRODUCTION

Natural river in mountains

1.1 Motivation

Under the sunshine in a warm spring, the fish vigorouly swim around a calm stream, beside which the animal and the insect play with a growing bloom and the little birds seem delightful to twitter. When we are in these situations, we feel not only a mere unit of the nature, a peace of mind, and a pleasure, but also a duty not to have our own way to destroy this property and to leave this for the future people. On the other hand, when the water resources are urgently needed for satisfying the rapidly increasing population in the city and the natural disaster occurs such as flood, debris flow, tsunami and storm surge, we feel powerless and try to conquer the nature for protecting the human life. Up to now, the destruction of the system of the ecologies such as the environmental pollution and contamination occurs and the environmental problem has begun to be exposed because the "*water management*" and the "*flood control*" have been regarded as much important for water resources. In particular, the global environment ploblems on earth are most serious, as shown in Fig.1.1. There occur enormous ploblems, for example, global warming, destruction of ozone layer, acid rain, occurrence of dioxins, and water pollution, *etc*. It is clear that carbon dioxide has a "*greenhouse effect*" (the increase of temperature is in proportion to the logarithm of concentration). Why there occur many ploblems on earth ? Insufficient understanding of nature, human and life as "*unified system*" ? This is due to the same reason as the failure example of Marxism which had destroyed the modern civilization itself due to the pursuit of an absolutely universal law to the nature and human beings, and is a caution to the limitations of material civilization, as pointed out by Takeiti and Tsunetoshi (1988). In such a case, the Oriental concept, "*coexistence with nature*" becomes very important instead of Western concept, "*rule of nature*". This means the necessity of engineering considering such a theory as "*habitat segregation*".

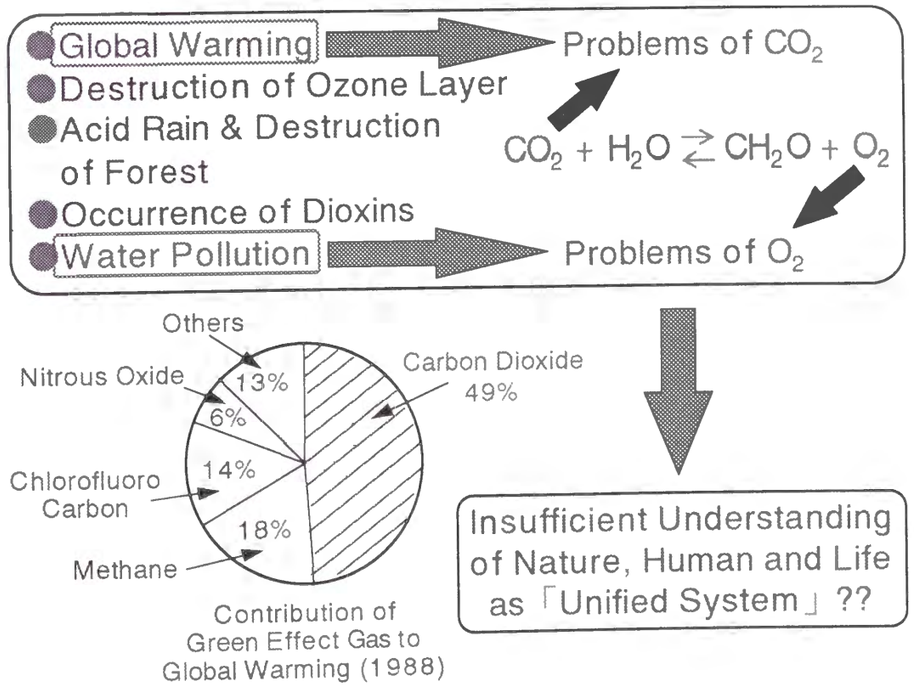

Fig.1.1 Global environment problems on earth.

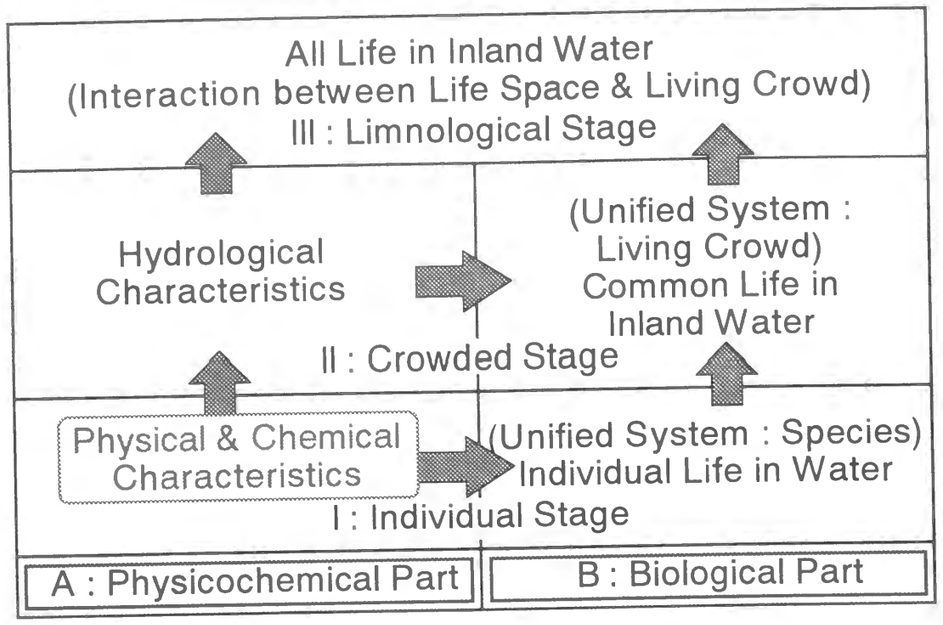

Fig.1.2 Construction of limnology by Thienemann (1955).

The former functions such as water management and flood control have been a symbol of politics itself, which led to the adherence to the huge construction such as enormous dams and artificial rivers, *etc*. On the other hand, there have been traditions of coexistence, such as well in the village, Canat in Iran, huge reservoir in India and Sri Lanka, and separated channel in Bangladesh, *et al*. The mountain streams may have infinite "*gross natural product*" instead of "*gross national product* (GNP)" in the economics. In such a situation, the objection against the construction of dam has recently become powerful like "*the dam as the weapon to take away the common things for a specific interest*", as pointed out by an English researcher of water resources (Pearce (1992)). This implies that it is necessary to regard river in view of broader aspects in philosophers such as Laozi and Zhuangzi instead of as only a connected line or a object for conquest called by Confucian in ancient China.

In addition to the above-mentioned water management and flood control, the "*environmental*" function has recently become more important, in particular, as the waterfront of the source of vision, hearing, smell, taste, and touch in the city, as mentioned by Yokouchi (1994). From this point of view, the concept proposed by Thienemann (1955) was a pioneer in the study of limnology (in this situation, it is better to include ocean in limnology), as shown in Fig.1.2. The field is divided into three stages, that is to say, I : individual stage, II : crowded stage, and III : limnological stage, respectively. The first two stages have A : physicochemical part and B : biological part. However, in the last stage, these two parts are combined with each other. In environmental research, it is ultimately necessary to evaluate all life at limnological stage for solving various environmental problems. However, the final stage is affected by many elements. In other words, physicochemical part at individual stage affects all the others directly or indirectly. Therefore, there occurs once again the necessity of local study, as shown in Fig.1.3. In order to overcome the global environment problems on earth, it is urgent to develop numerical simulation of atmosphere-water global-circulation. Recently, it has become clear that the middle size of vortex (about a radius of 100km) is very important for convecting the more heat,

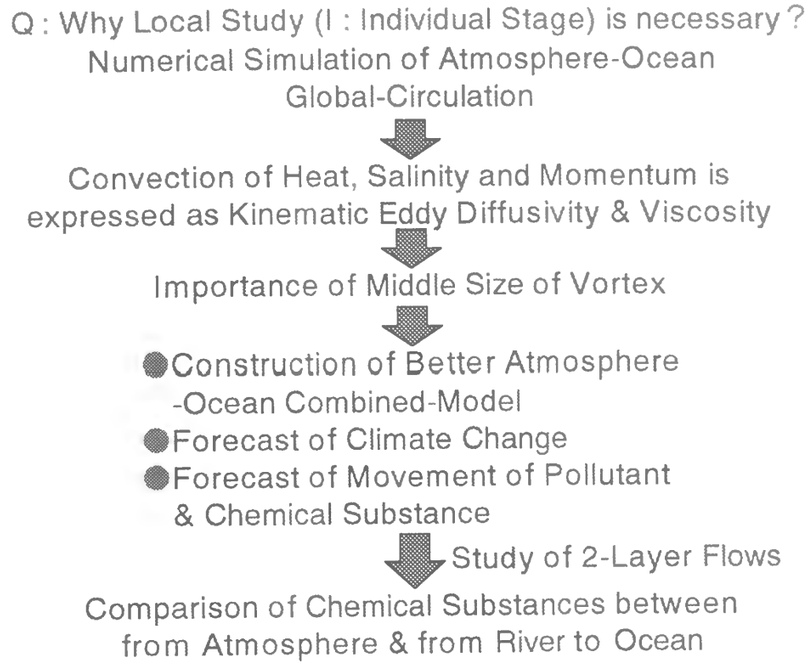

Fig.1.3 Necessity of local study.

salinity and momentum in the field of ocean science (Horibe (1977)). The further local study may result in the construction of better atmosphere-ocean combined-model, the forecast of climate change, and the movement of pollutant and chemical substance. In particular, the study of two-layer flows (air and water) may contribute to the comparison of chemical substances between from atmosphere and from river to ocean in the future.

The ideas of technical development, such as "not to waste the resources", "not to destroy the ecological environment", "to ensure the safety and healthy of human beings", and "not to control intensively but to let all the people participate", are becoming attractive in the field of technology instead of the former "*huge technology*". At that time, the managed society inevitably spreads as a bad influence independent of the difference of systems (capitalism or socialism, *etc*.), which is characterized by the three kinds of technology, that is to say, "technology for production and profit", "technology for rule" and "technology as ideology". Under these technologies, "1984 year" by Orwell (1970) becomes a good mirror of managed society. Dickson (1980) has supposed the strategy for resisting the managed society, as follows;

(1) the dispersion and decentralization from the central management
(2) the saving type from the mass consumption of energy
(3) the small scale production from the mass production
(4) the serious consideration of qualitative standard from quantitative standard
(5) the incorporation with the nature from the alienation from the nature
(6) the coexistence with the local culture from the destruction of the local culture
(7) the technique of public itself from at the professional
(8) the integrated science from the alienated science from the culture

The above-mentioned suggestions imply that the previous scientific idea originated in Descartes (1966) (which is a little different from the original meaning in the point that he desired the construction

of "*pratique*" natural science) is not necessarily universal in the today's situation where there are no unique relations between the cause and the result due to the extension of scale, the complexity of matter and the feedback operation. This also means that the science does not always have an absolute truth in spite of the intuition based on the experience of nature and the logical construction of concept, as pointed out by Nakagawa (1995). Instead, another idea is necessary which is the point of view not always to understand the matter systematically, that is to say, to reconsider the environment as system based on the thought that the "*independence of system*" only belongs to the essence of nature, as derived by Ishikawa (1998). In other words, we are now in the time where the consistency of understanding is necessary by the "*Hermeneutischer circulation*" based on the transformation of paradigm. In this situation, the "secondary nature" does not necessarily refer to the destruction of nature, and we can understand the environmental system itself by accumulating the understanding for "*characteristics in a specific place*" in the same idea as Gadamer and Apel (1984). We have to make the most of technology for pursuing the best possibility in each place on the "*environmental*" idea of Watsuji (1963) harmonized with the surroundings. This idea depends on giving up the insolence that the technology is all-round and pursuing the truth realistically, which is a kind of "*Husserlism*", as mentioned by Ogawa (1990). However, it is necessary of rationalism based on a reality in order not to fall in mysticism, and of the moral sense like "*Ren*" in order to go back to tradition and to bring out the new order. This empiricism respecting the actual state than the style is similar to the tradition of Kyoto supported by the merchant culture, for example, Jinsai Itoh, as mentioned by Hayashiya (1962).

Levi-Strauss and Eribon (1996) mention the following phrases in the series of mythology; "the power and dignity which were possessed for impressing mysteriously the people and fascinating the listener's mind in the deep forest of image and symbol". This means the necessity not only to throw light on the "*encounter to the outer mystery*" but also to clear the "*encounter to the inner mystery*", which is the dynamic consistency between "*Prometeus*" aspect and "*Orpeus*" aspect and the urgent necessity of "*speculation*" instead of "*scholarship*", as mentioned by Mumford (1956). That is to say, it is not until we regard the nature as related closely to ourselves that we can get "*sustainable development*" with success. At that situation, the following words by Bacon become meaningful again. "If we do not follow the nature, we can not rule the nature" (Anderson (1948)). In this situation, the importance of air-water interface study can be clearly recognized, as shown in Fig.1.4. The variations of dissolved oxygen (O_2) and carbon dioxide (CO_2) are closely related with each other, as shown in Fig.1.1. The variation O_2 of is affected by gas transfer, consumption due to resolution of life, and increase due to photosynthesis, *etc*., as mentioned by Ichikawa (1980). On the other hand, the movement of CO_2 is related to gas transfer, photosynthesis of plant and breathi··, and combustion of fossil fuel due to human activity (greater increase in recent years), *etc*. It is c··r that the gas transfer plays an important role on both gases. Furthermore, the majority of environmentally important gases have low solubility, and the difference of gases can be explained by Schmidt number *Sc*. On the above-mentioned background of idea, this thesis was written for looking forward to the contribution toward the environmental engineering in view of the study about air-water interface.

1.2 Scope and Objectives

So far, many hydraulic researchers and engineers of open-channel flow have laid much emphasis on the interaction between the fluid motion and the perimeter (bed and side wall), which is a critical aspect of the flood control and river improvement. However, there are not so many important researches in environmental and geophysical problems except for "*rich-in-nature typed works*" or "*river restoration works*". On the other hand, there exists another boundary in open-channel flow, that is to say, a free

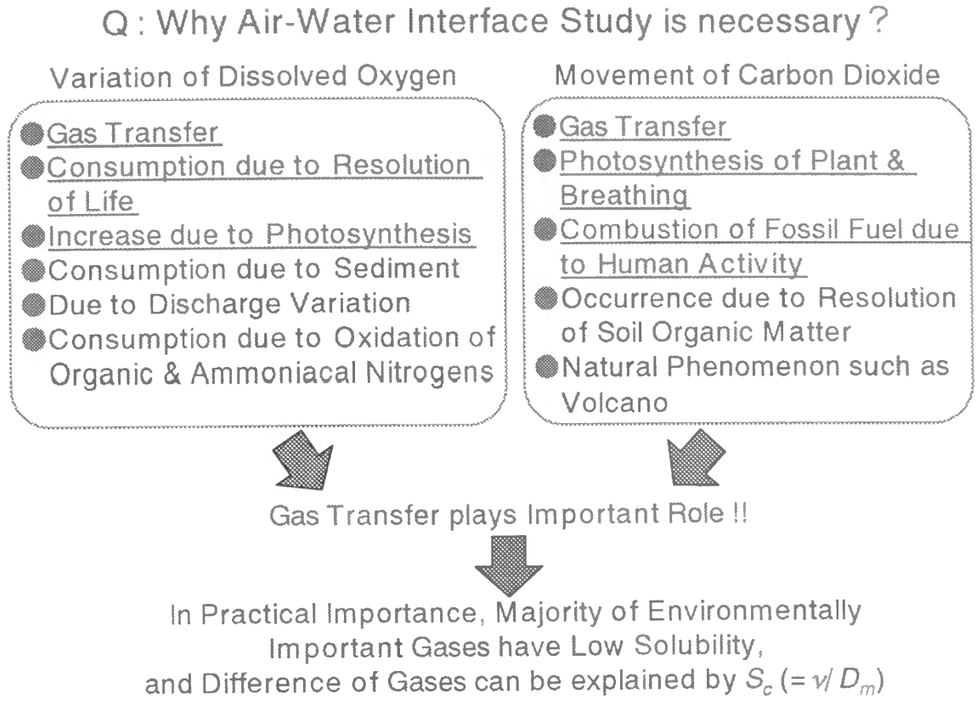

Fig.1.4 Necessity of air-water interface study.

surface, and this causes a great difference from closed-channel flow (duct flow). About duct flow, there have been a lot of researches in mechanical engineering. In this way, research about open-channel flow is peculiar to hydraulics, and it has a possibility that free-surface problems contribute much to the environmental problems of chemical and sanitary engineering. However, there may occur different phenomena in flowing water because water layer is usually still in chemical and sanitary engineering.

Let us consider two aspects of the fluctuating free-surface in actual rivers, lakes and oceans, as shown in Fig.1.5. One is the fluid mechanics and hydraulics aspect. Free surface peculiar to open-channel flow is not a rigid boundary, but a continuously moving boundary. The surface-wave fluctuations affect the turbulent redistributions near the free surface, which are greatly dependent on Froude number and the bed slope, *etc*. Furthermore, coherent structures such as the bursting phenomena which are generated near the bed wall are closely related to the air-water mutual interaction near the interface. The other aspect considered here is the chemical and environmental aspect. In view of gas transfer phenomena due to the air-water interaction, there exists a very-thin concentration boundary-layer (CBL) near the free surface where the DO concentration changes dramatically, and oxygen transport is controlled by this interfacial resistance. In particular, the gas transfer is more promoted by the fluctuating free surface in addition to conduction. Although there are various explanations based on the film theory and the surface-renewal theory, *etc*. about these transport phenomena, a purely chemical approach is not sufficient for the evaluation of these complex interfacial phenomena. In particular, it is urgent to throw more light on the characteristics of turbulence structure and coherent structure. These mechanical and chemical aspects are dependent on each other. So, studying this inter-relationship furthers understanding of the air-water interfacial phenomena, and will help us create a richer water environment, which are the objectives of this thesis.

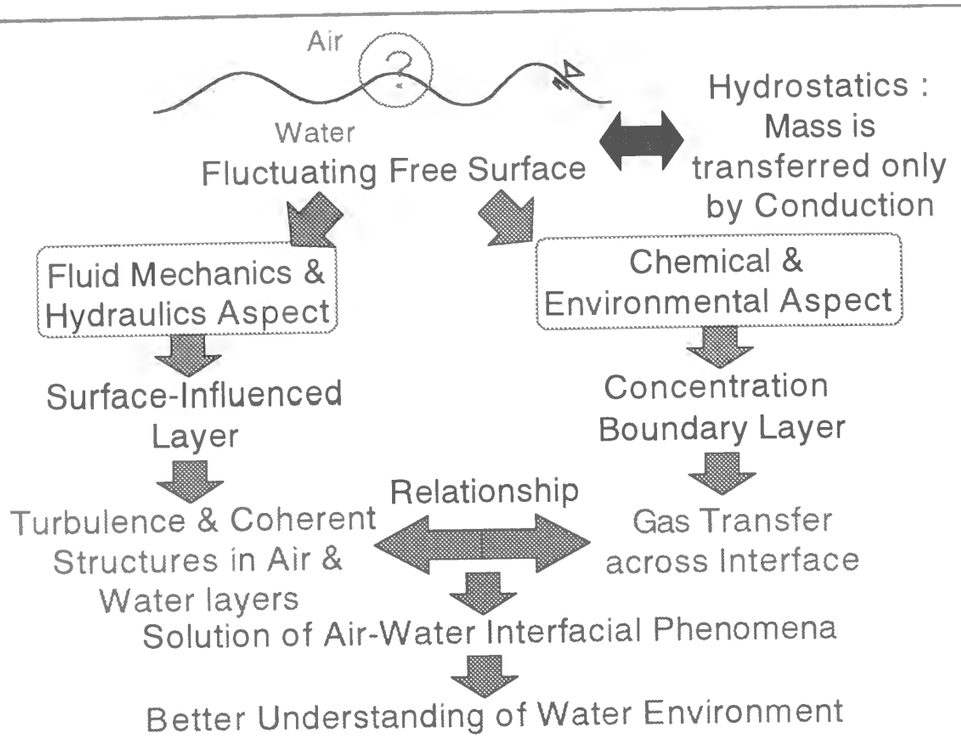

Fig.1.5 Objective of this study.

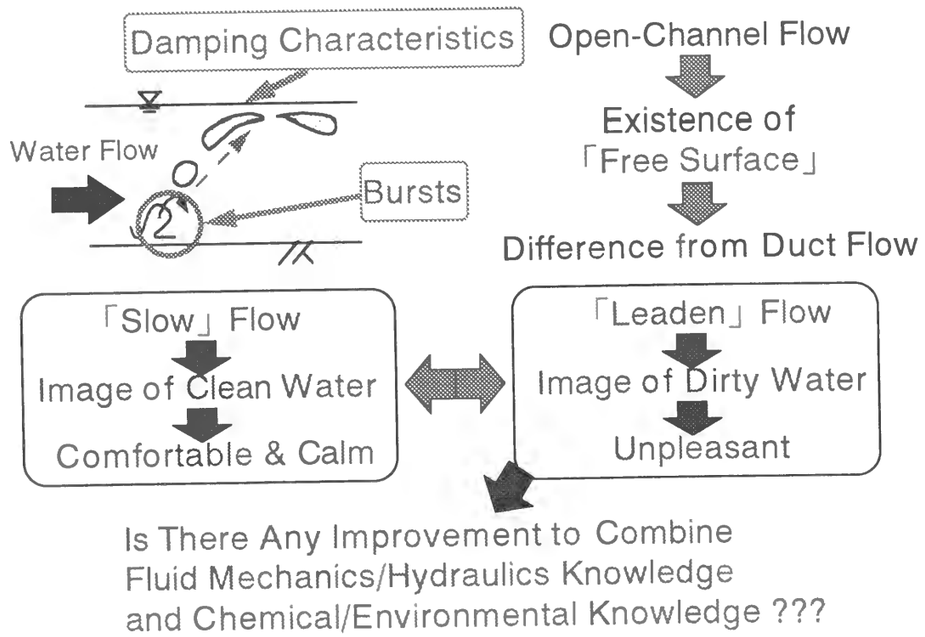

Fig.1.6 Tranquil open-channel flow.

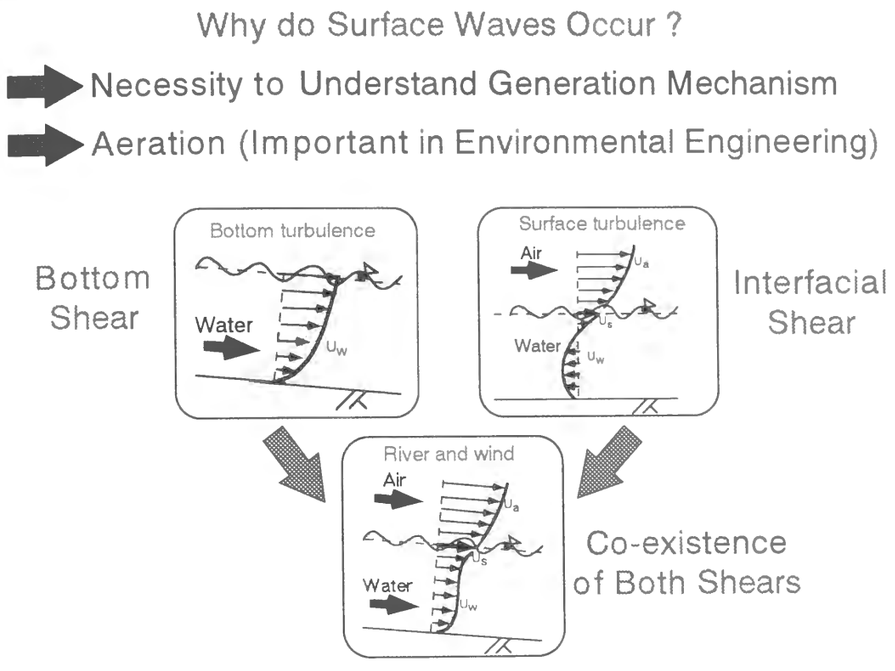

Fig.1.7 Three types of turbulent conditions in this study.

In this way, the free surface is very important for defining physically and chemically the characteristic of open-channel flow. The image of open-channel flows in rivers, streams and drains changes variously depending on a single word, and one can do suitably by combining the physical and chemical knowledge, as shown in Fig.1.6. So, this study is very significant for the recently vigorous environmental problem, as pointed out by Chanson (1996) and Toba (1996). Furthermore, evaluating the turbulence characteristics near the free surface is also necessary for defining the boundary conditions in numerical simulations.

The aim of this study is to improve understanding of the mutual interaction near the air-water interfacial region by the laboratory experiment and numerical simulation, which is an approach from a micro point of view rather than from a global one. At that time, the relationship between the surface-wave fluctuations and the gas transfer characteristics is focused on, about which there have been less studies till now. Furthermore, when one would like to construct a comprehensive model by GIS and GPS, *etc*., to understand the natural and water environmental systems, to forecast future situations, to prevent environmental pollution and contamination, and to utilize water resources efficiently, this study is very important in order to clarify the physical and chemical boundary conditions at the air-water interface. From the above-mentioned point of view, in this study, it is firstly necessary to evaluate three types of turbulent conditions in order to study the relationship between the turbulence structure near the free surface and the gas transfer across the air-water interface, as shown in Fig.1.7, as suggested by Plate and Friedrich (1984); that is to say, (A) bottom-shear generated turbulence, (B) wind-shear generated turbulence and (C) combined wind/stream turbulent conditions.

(A) Bottom-shear generated turbulence means a normal "*open-channel flow*" as have been studied by many researchers in hydraulics, for example, Nezu and Nakagawa (1993). This type of flow is an "*ideal*" river or stream. In an open-channel flow, turbulence structure is affected by the presence of a free surface, and therefore, its characteristics are quite different from those of a duct flow near the

plane of symmetry, that is to say, "*damping characteristic*". Furthermore, the turbulence structure near the free surface has a close relationship with surface-wave fluctuations and the Froude number, which is an important characteristic of steep open-channel flow and an essential phenomenon in view of the environmental engineering. This phenomenon is called "*self-aeration*", and is an important part of air-water transfer in open-channel flow, as pointed out by Chanson (1996).

On the other hand, (B) wind-shear generated turbulence is "*wind-water wave*" as can be seen in the sea or lake when the wind blows above the almost still water-surface. When the wind blows over the water, there occur drift currents and wind waves due to the wind shear across an air-water interface. These flows have been studied in the field of coastal engineering and geophysical sciences, for example, Toba (1996), and also have a great effect on mass transfer and energy transfer across a gas/liquid interface from the air layer toward the water layer. Furthermore, in the water layer, there occurs the energy transport from the wave field to the mean field and from the mean field to the turbulent field. So, the "*coupling*" and the interaction among the three fields exist among the mean, wave and turbulent fields, and this is a very interesting phenomenon.

As for (C) combined wind/stream turbulence, there exist both air flow and water flow together, and the bed shear and the interfacial shear coexist in the water layer. This flow can be seen commonly in actual rivers. Furthermore, in chemical, mechanical and nuclear engineering, the evaluation of these flow characteristics and interfacial heat transfer coefficients is important for the need to estimate accurately the heat transfer rate at the liquid surface of cooling reactors. The final objective of this thesis is to clarify the relationship between the turbulence structure near the free surface and the gas-transfer mechanism in these flows.

1.3 Overviews

A brief overviews of this thesis is given here as a guide to selective reading of this report. From "Chapter 2" to "Chapter 7", three types of flow conditions, as shown in Fig.1.7, are discussed in view of the physical aspect. "Chapter 8" deals with the chemical aspect about three types of flow conditions. In "Chapter 9", the above-mentioned physical and the chemical aspects are related with each other.

"Chapter 2" describes about the turbulence structure and the coherent structure near the free surface in smooth open-channel flow in comparison with duct flow from the experimental point of view. At that time, the relationship between the turbulence structure and the surface-wave fluctuations is considered by the simultaneous measurements of a Laser-Doppler anemometer (LDA and an ultrasonic depth meter (Figs.1.6 and 1.8).

"Chapter 3" considers a relationship between the "*bursting phenomenon*" generated near the wall and the "*surface renewal eddies*" near the free surface. At that time, one of the newest image analyses, PIV (Particle-Image Velocimetry) method is used to measure evolutionary patterns of coherent vortices (Figs.1.6 and 1.8).

"Chapter 4" discusses a numerical simulation by using a Reynolds stress model (RSM). The aim of this chapter is to propose a new boundary conditions at the free surface including the effect of Froude number and the surface-wave fluctuations, and to reproduce the turbulent redistribution near the free surface in steep open-channel flow (Fig.1.9).

"Chapter 5" treats rough-bed flow. In comparison with smooth-bed flow, the effect of macro-roughness on the turbulence structure near the free surface and surface-wave fluctuations is investigated by using LDA and PIV. At the same time, the wave-induced flow is evaluated for comparing "*wave-effect*" with "*turbulence-effect*" (Fig.1.10).

"Chapter 6" deals with the turbulence structure at an air-water interface with wind shear above the

still water. This chapter describes the turbulence structure and the energy budget in both the air and water layers. Furthermore, the wave component and turbulence component of the water flow were separated by a spectral separation method (LFT) (Fig.1.11).

"Chapter 7" studies the turbulence structure in a wind-stream combined flow when both the bed shear and the interfacial shear coexist. In this chapter, mixing-length model in wind wave is extended in the air flow of two-phase flows, and the description of the shear stress distribution in the water flow is refined for two-layer flows (Fig.1.12).

"Chapter 8" relates the characteristics of gas transfer across the interface to the previous empirical models including the effects of shear velocity and dissipation rate and expands these models to air-water two layer flows in view of the chemical aspect. This chapter tries to find the key for relating the physical aspect to the chemical one (Fig.1.13).

"Chapter 9" relates the coherent structures of both layers with each other by using PIV and the phase-averaged method. Furthermore, the effect of surface area and other factor on the gas transfer is evaluated in order to clarify the relationship between the coherent structures and the gas transfer characteristics in two layer flows (Fig.1.14).

"Chapter 10" summarizes the findings of this study and gives concluding remarks. Then, some applicabilities of this study are mentioned in view of the global environment problems on earth. Finally, some recommendations for future studies are given in order to utilize and extend this study to the solve of various environment problems.

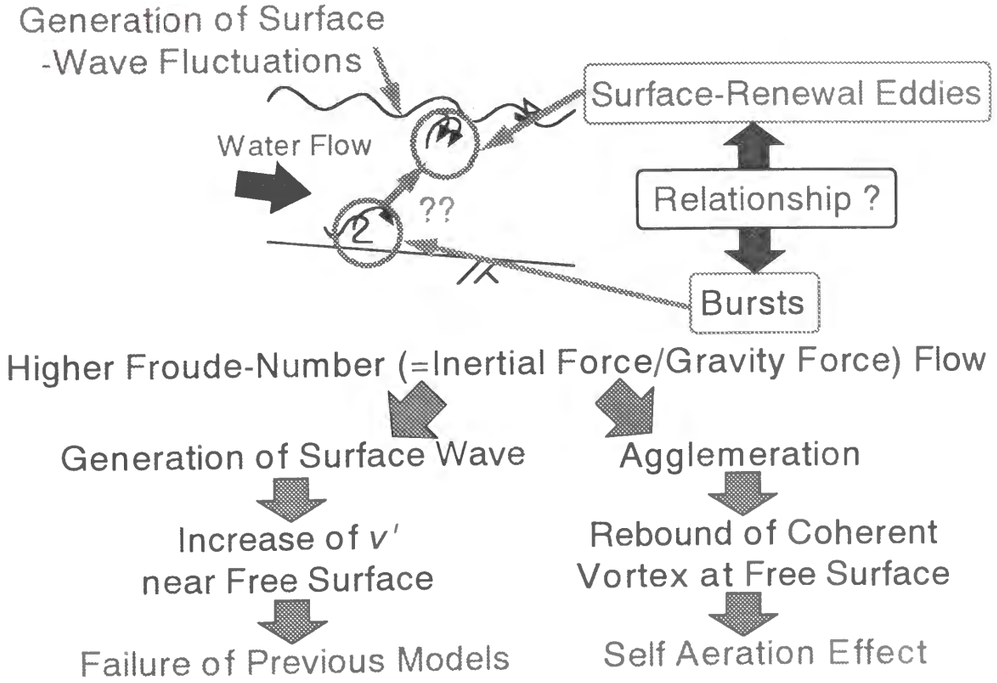

Fig.1.8 Steep open-channel flow.

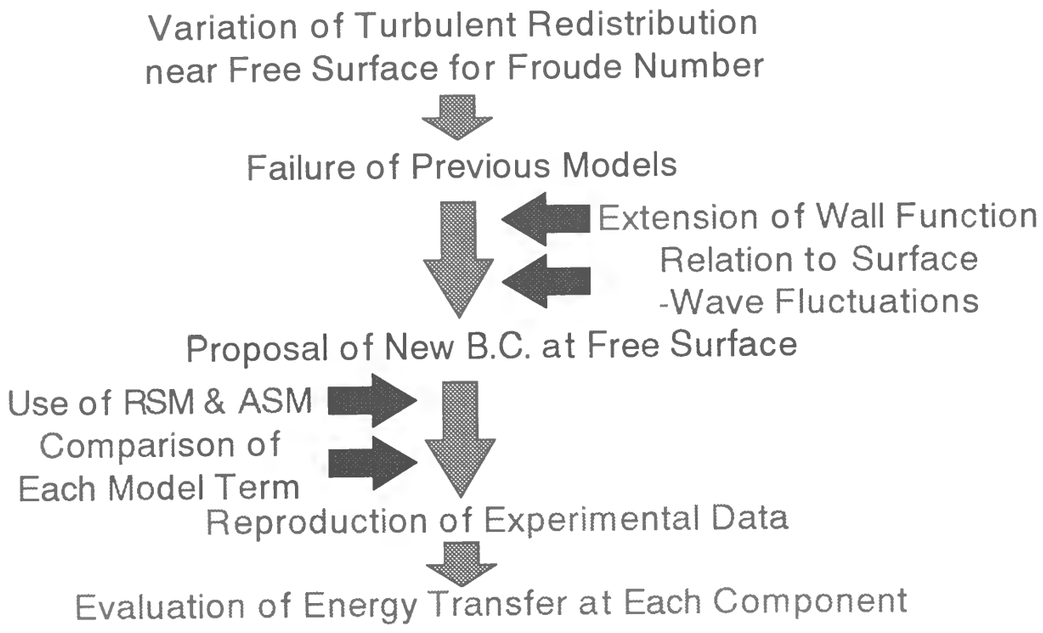

Fig.1.9 Reproduction of turbulent redistribution by numerical simulation.

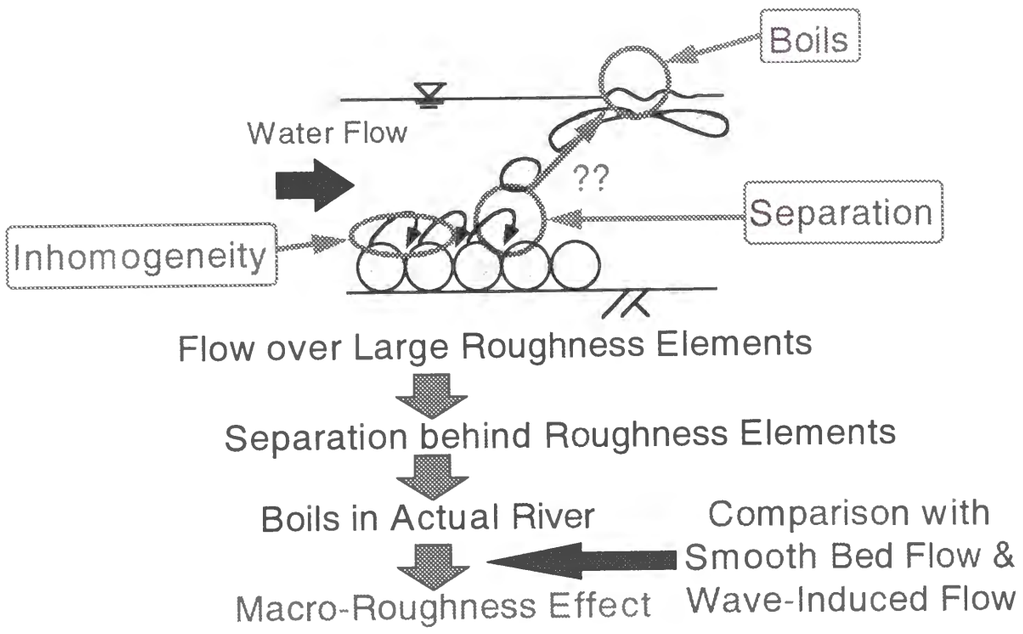

Fig.1.10 Rough bed flow with large roughness elements.

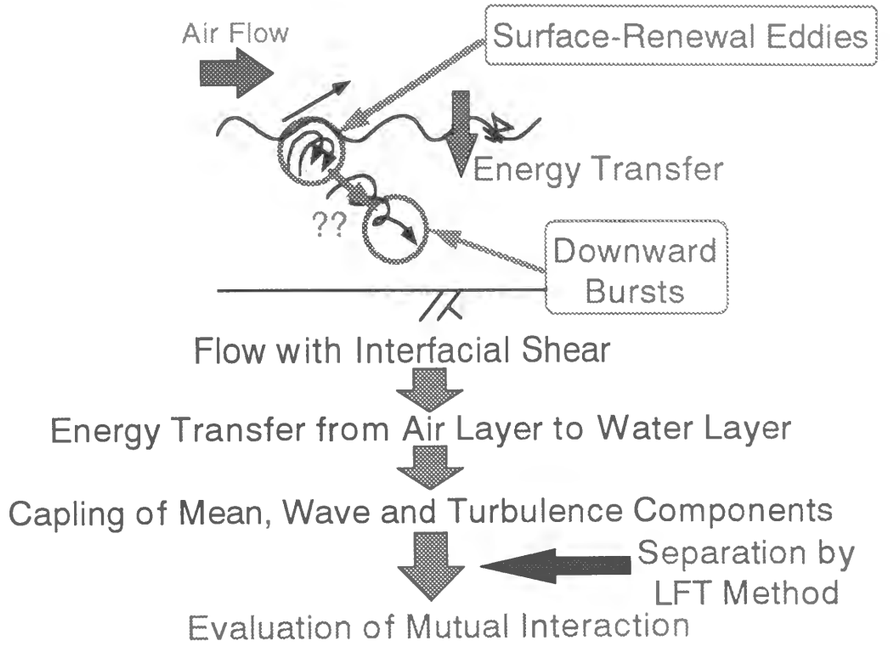

Fig.1.11 Flow with wind shear.

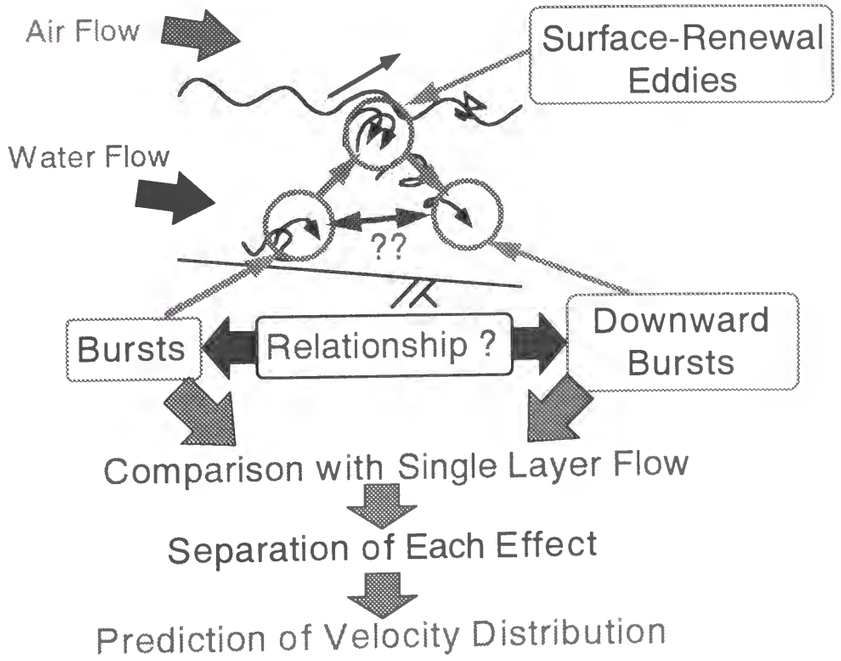

Fig.1.12 Two layer flows.

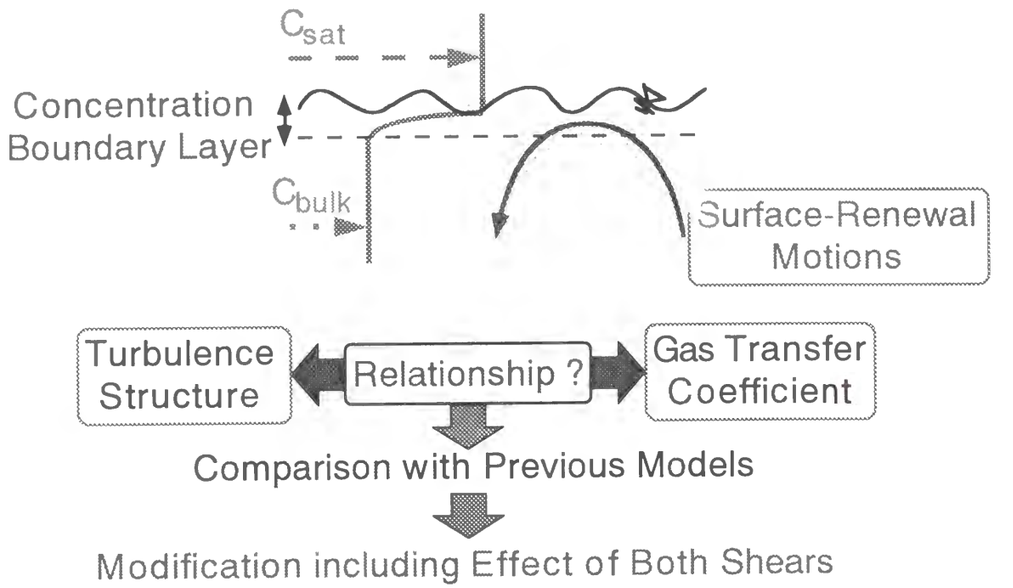

Fig.1.13 Gas transfer across air-water interface.

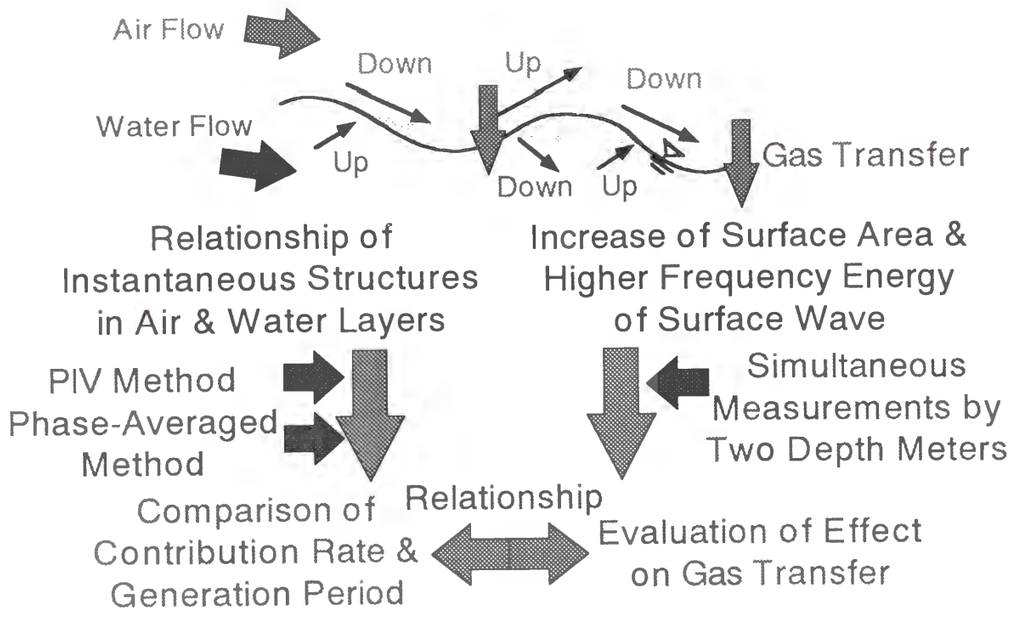

Fig.1.14 Relationship between coherent structure and gas transfer.

References

[1] Anderson, F.H. : The philosophy of Francis Bacon, Chicago, 1948.
[2] Ichikawa, A. : Environmental science in urban river, Baifu-Kan, 1980 (in Japanese).
[3] Imanishi, K. : The logic of animals and plants, Shisaku-Sya, 1971 (in Japanese).
[4] Imanishi, K. : The world of life, Kodan-Sya, 1972 (in Japanese).
[5] Ishikawa, T. : The difference of environmentology from environmental science, *Technical Report, Tokyo Institute of Technology*, No.57, pp.69-74, 1998 (in Japanese).
[6] Chanson, H. : Air bubble entrainment in free-surface turbulent shear flows, Academic Press, 1996.
[7] Descartes, R. : Discours de la methode, Translated by T.Ochiai, Iwanami Publisher, 1966 (in Japanese).
[8] Dickson, D. : Alternative technology, Translated by M.Takubo, Jijitsushin-Sya, 1980 (in Japanese).
[9] Gadamer, H.G. and Apel, K.O. : Transformation of philosophy, Translated by A.Takeiti, Iwanami Publisher, 1984 (in Japanese).
[10] Hayashiya, T. : Kyoto, Iwanami Publisher, 1962 (in Japanese).
[11] Horibe, Y. : Science of ocean environment, University of Tokyo Press, 1977 (in Japanese).
[12] Kitano, Y. : Mechanism of water pollution and its analysis, Sangyo-Tosyo, 1978 (in Japanese).
[13] Kuhn, T.S. : The structure of scientific revolutions, University of Chicago Press, 1970.
[14] Levi-Strauss, C. and Eribon, D. : Myth and meaning, Translated by Y.Ohashi, Misuzu Publisher, 1996 (in Japanese).
[15] Matsui, S. : Guidelines of lake management volume4 : Toxic substances management in lakes and reservoirs, *International Lake Environment Committee Foundation and United Nations Environment Programme*, 1991.
[16] Mumford, L. : The transformations of man, Harper and Row Publishers, 1956.
[17] Nakagawa, H. : Forty years together with rivers and persons, *Commemorative Publication in Celebration of His Retirement from Kyoto University*, 1995 (in Japanese).
[18] Nezu, I. and Nakagawa, H. : Turbulence in open-channel flows, IAHR-Monograph, Balkema, 1993.
[19] Ogawa, T. : Phenomenologie and structuralism, Sekai-Syoin, 1990 (in Japanese).
[20] Orwell, G. : The collected essays, journalism and letters of George Orwell, Translated by S.Tsurumi, Heibon-Sya, 1970-71 (in Japanese).
[21] Pearce, F. : The dammed, Random House UK Limited, 1992.
[22] Plate, E.J. and Friedrich, R. : Reaeration of open channel flow, *Gas Transfer at Air-Water Interfaces*, W. Brutsaert and G.H. Jirka (eds.), pp.333-346, 1984.
[23] Takeiti, A. and Tsunetoshi, S. : What is philosophy, Keisou Publisher, 1988 (in Japanese).
[24] Thienemann, A. : Die binnengewasser in natur und kultur, Springer-Verlag, 1955.
[25] Toba, Y. : Atmosphere-Ocean Interactions, University of Tokyo Press, 1996 (in Japanese).
[26] Yokouchi, N. : Planning notes for waterfront development, Kyoritsu Press, 1994 (in Japanese).
[27] Watsuji, T. : Environment, Iwanami Publisher, 1963 (in Japanese).

CHAPTER 2

TURBULENCE STRUCTURE AND CHARACTERISTICS OF COHERENT VORTICES NEAR FREE SURFACE IN OPEN-CHANNEL FLOW

Abstract

In an open-channel flow, turbulence structure is affected by the presence of a free surface, and therefore, its characteristics are quite different from those of a duct flow near the plane of symmetry. Furthermore, the turbulence structure near the free surface has a close relationship with surface-wave fluctuations and the Froude number. In particular, the turbulence structure may become unstable in a critical flow, and this phenomenon can be seen in the complexity of turbulent redistribution and the undulation property of surface-wave fluctuations. Furthermore, it has been pointed out that the turbulence structures near a free surface have a close relationship with coherent vortices, and that its characteristics are greatly affected by the presence of the free surface. In a higher Froude-number flow, a coherent structure, so-called the "*surface renewal eddies*", can be seen clearly at the free surface. The macro-scale of turbulence is an important quantitative descriptor of the turbulent eddies, and this macro-scale depends greatly on the surface-wave fluctuations and the coherent structures. In this study, turbulence measurements were three-dimensionally conducted in open-channel flows by using two sets of fiber-optic LDA systems, and simultaneously, the surface-wave fluctuations were measured by an ultrasonic depth-meter instrument. Furthermore, the coherent structure near the free surface is evaluated by using space-time correlation analyses and conditional sampling methods. The aim of this study is to clarify the relationship between the turbulence structure near the free surface and the surface-wave fluctuations.

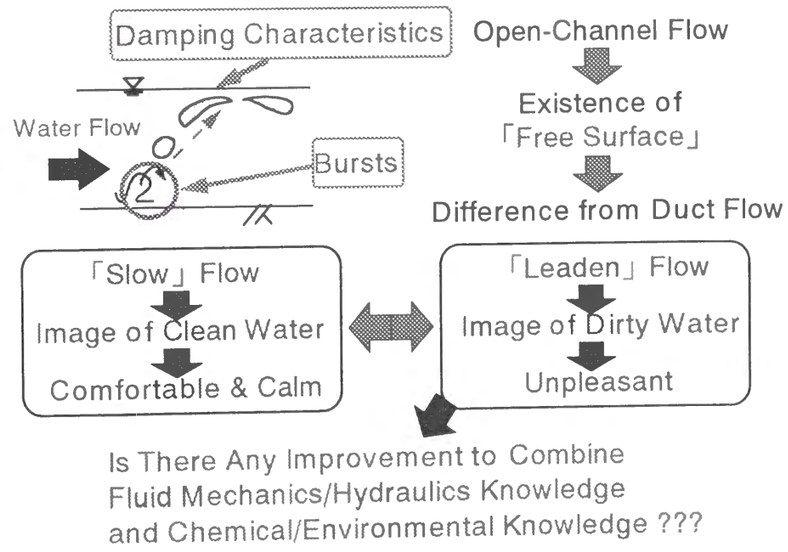

CHAPTER 2 TURBULENCE STRUCTURE AND CHARACTERISTICS OF COHERENT VORTICES NEAR FREE SURFACE IN OPEN-CHANNEL FLOW

Parts of this chapter were presented in the following papers.

[1] Nakayama, T. : Turbulent structures and characteristics of coherent vortices near the free surface, *M.E. Thesis presented to Kyoto University*, 1997 (in Japanese).
[2] Nezu, I., Nakayama, T. and Itoh, Y. : Turbulent structures in steep open-channel flows, *1st Symposium on Environmental Fluid Mechanics*, Vol.1, pp.323-324, 1996e (in Japanese).
[3] Nezu, I., Nakayama, T. and Itoh, Y. : Comparison of 3-D experimental database with direct numerical simulation, *Annual Journal of Hydraulic Engineering*, Vol.41, pp.1055-1060, 1997b (in Japanese).
[4] Nezu, I., Nakayama, T. and Kita, A. : Relationship between turbulence structures near the free-surface and surface-wave-fluctuations, *Annual Journal of Hydraulic Engineering*, Vol.41, pp.657-662, 1997c (in Japanese).
[5] Nezu, I. and Nakayama, T.: Relationship between turbulent structure near the free-surface and surface-wave-fluctuations, *Proc. of 27th IAHR Congress*, ASCE, IAHR, pp.245-250, 1997d.
[6] Nezu, I. and Nakayama, T. : Relationship between turbulent structures near the free-surface and surface-wave-fluctuations, *Journal of Hydraulic Engineering*, JSCE, No.593/II-43, pp.69-78, 1998a (in Japanese).
[7] Nezu, I. and Nakayama, T. : Space-time correlation structures of coherent vortices near the free surface, *Journal of Hydraulic Engineering*, JSCE, No.586/II-42, pp.51-60, 1998b (in Japanese).
[8] Nezu, I. and Nakayama, T.: Effect of the surface-wave fluctuations on coherent structures near the free surface, *11th Congress of the IAHR-APD*, pp.507-516, 1998g.

2.1 Introduction

It has been pointed out that turbulence structure is affected by the presence of a free surface and turbulent energy redistribution changes variously within a surface-influenced layer which is roughly ten per cent of the flow depth. Hunt (1978, 1984) has analyzed a grid turbulence convected by a free stream past a rigid surface moving at the same speed as the free stream; he used a boundary-layer theory and spectral methods, and has discussed the turbulence characteristics near the free surface in an open-channel flow. Furthermore, he has compared the turbulence in the presence of large shear near the surfaces with the turbulence in the small shear stresses near the surfaces, and he mentioned the peculiar characteristics near the free surface in open-channel flow.

Many researchers have pointed out that a turbulence structure is affected by the presence of a free surface and turbulent redistributions change variously within a "*surface-influenced layer*" roughly ten per cent of the flow depth. In particular, the characteristics near the free surface depend greatly on the Froude number Fr, and a damping effect on the vertical motions is gradually lost out as surface-wave fluctuations increase. This means that Fr is one of the important factors for analyzing the turbulence structure near the free surface. Bradshaw (1967) proposed the idea that "*turbulence consists of active motions and inactive motions*", and it is necessary to clarify the effect of the free surface on the turbulence structure and to investigate inactive motions such as surface-wave fluctuations.

In order to evaluate the turbulence structure near the free surface, there have been many researches about oscillating-grid turbulence. Komatsu *et al.* (1995) have measured the turbulence and pressure disturbance simultaneously in the oscillating grid, and pointed out that the pressure fluctuation has an important role on the turbulent redistribution near the free surface. Furthermore, Brumly and Jirka (1987) and Drayton (1993) have investigated the characteristics of turbulence intensities, integral-length scales and dissipation rate in a grid-stirred tank, and compared them with Hunt's theory. In these previous works, attention was restricted to the damping characteristics of turbulent quantities. Rashidi and Banerjee (1988) and Komori *et al.* (1982, 1989) have related surface renewal to some more organized motions (bursting motions and coherent flow structures) occurring in the flow. Tamburrino and Gulliver (1994, 1999) have also considered the relationship between large-scale coherent vortices and the surface renewal by using spectral analyses and correlation analyses. Li, Dong and Chen (1995) have evaluated the skewness and flatness factors of velocity components in various Froude number flow. However, they did not clarify the effect of Froude number on the turbulence structures near the free surface. Thus there have been no considerations about the relationship between the turbulent energy redistributions and the surface-wave fluctuations when the surface-wave fluctuations occur.

Furthermore, the turbulence structures near a free surface in an open-channel flow have a close relationship with coherent vortices, whose characteristics are greatly affected by the presence of the free surface. Furthermore, the turbulence structure near the free surface has a close relationship with surface-wave fluctuations and the Froude numbers. In a higher Froude-number flow, a coherent structure, so-called surface renewal eddies, can be seen clearly at the free surface. Nakagawa and Nezu (1981), Rashidi and Banerjee (1988) and Komori *et al.* (1989) have investigated the surface renewal, boil vortex and some more organized motions (bursting motions and coherent flow structures) occurring in the flow. At that time, macro-scale of turbulence is an important quantitative descriptor of such turbulent eddies. Hunt (1984) discussed about the turbulent redistribution near the free surface, and pointed out that the vertical macro-scale L_y is substantially smaller than the streamwise macro-scale L_x near the free surface in a quiet flow. Furthermore, Handler *et al.* (1993), Komori *et al.* (1993) and Swean *et al.* (1991) conducted a direct numerical simulation (DNS) in an open-channel flow and Handler *et al.* (1993) and Swean *et al.* (1991) compared the space-time correlation coefficient and the

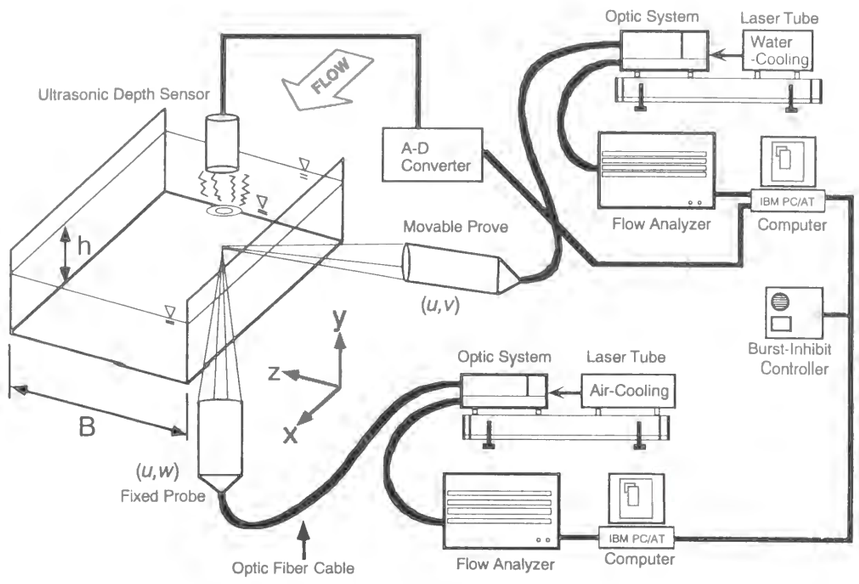

Fig.2.1 Experimental flume and LDA system in 3-D measurements.

Table 2.1 Hydraulic conditions in 3-D measurements of smooth-bed open-channel flow.

case	S_b	h (cm)	B/h	U_m (cm/s)	U^* (cm/s)	Fr	Re (x10^3)
L-FR01	1/25000	8.0	5.0	10.0	0.59	0.12	8.0
L-FR02	1/6000	5.0	8.0	16.0	0.99	0.23	8.0
L-FR03	1/3000	4.0	10.0	20.0	1.14	0.32	8.0
L-FR04	1/2000	3.5	11.4	22.9	1.33	0.39	8.0
L-FR05	1/1500	3.0	13.3	26.7	1.49	0.49	8.0
M-FR06	1/1200	5.0	8.0	40.0	2.10	0.57	20.0
M-FR07	1/900	4.5	8.9	44.4	2.32	0.67	20.0
M-FR08	1/600	4.0	10.0	50.0	2.50	0.80	20.0
M-FR09	1/455	3.7	10.8	54.1	2.78	0.90	20.0
M-FR10	1/316	3.5	11.4	57.1	2.90	0.98	20.0
M-FR11	1/273	3.2	12.5	62.5	3.24	1.12	20.0
M-FR12	1/250	3.0	13.3	66.7	3.36	1.23	20.0
H-FR11	1/300	5.0	8.0	75.0	3.80	1.07	37.5
H-FR13	1/240	4.5	8.9	83.3	4.00	1.25	37.5
H-FR15	1/167	4.0	10.0	93.8	4.75	1.50	37.5
H-FR18	1/111	3.5	11.4	107.1	5.42	1.83	37.5
H-FR23	1/77	3.0	13.3	125.0	6.09	2.30	37.5

S_b=channel slope, h=water depth, B=channel width,
U_m=bulk mean velocity, $Fr=U_m/(gh)^{0.5}$, $Re=U_m h/\nu$

macro scale in an open-channel flow with those in a closed-channel flow. They mentioned the damping characteristics of macro-scale near the free surface. However, the situation is quite different when the surface-wave fluctuations occur, and this macro scale depends greatly on the surface-wave fluctuations and the coherent structures.

The aim of this study is to clarify the turbulence and coherent structures near the free surface and the relationship with the surface-wave fluctuations in open-channel flows. Firstly, a comparison between experimental data and a DNS (Direct Numerical Simulation) database in duct flows without free

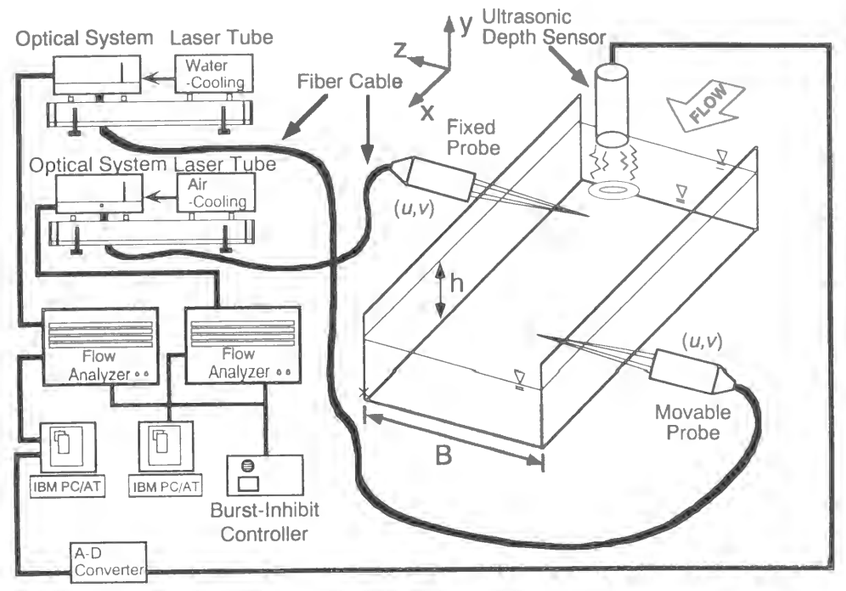

Fig.2.2 Experimental flume and LDA system for space-time correlation analyses.

Table 2.2 Hydraulic conditions in correlation analyses of smooth-bed open-channel flow.

case	S_b	h (cm)	B/h	U_m (cm/s)	U^* (cm/s)	Fr	Re (x10^3)
M-FR06	1/1200	5.0	8.0	40.0	2.10	0.57	20.0
M-FR10	1/316	3.5	11.4	57.1	2.90	0.98	20.0
S-FR31	1/41	3.0	13.3	166.7	8.47	3.07	50.0

S_b=channel slope, h=water depth, B=channel width,
U_m=bulk mean velocity, $Fr=U_m/(gh)^{0.5}$, $Re=U_m h/\nu$

surface by Kim *et al.* (1987) is made, and the effects of the free surface are considered. Furthermore, simultaneous measurements by using two-sets of laser Doppler anemometers (LDA) and an ultrasonic depth-meter instrument are conducted, and the relationship between the turbulence structure near the free surface and the surface-wave fluctuations and the coherent structure are considered by using their spectral analyses and correlation analyses.

2.2 Experimental Apparatus and Procedures

The experiments were conducted in a 10m long, 40cm wide and 30cm deep tilting flume, whose slope can be lifted up to 1/10 by jacks. The bed and side walls of the test section 6m downstream of the channel entrance were made of optical glass for LDA measurements. Coordinate axes in the streamwise, vertical and spanwise directions were defined respectively as x, y and z, and the corresponding velocity components as u, v, and w. The 3-D measurements were made in the center of the channel by using two sets of fiber-optic LDA systems (DANTEC-made), as shown in Fig.2.1. The sampling time was 60sec and the sampling frequency was about 200Hz. At that time, an ultrasonic depth-meter instrument (KEYENCE-made) was set above the free surface, and synchronized with the LDA. Hydraulic

conditions for the experiment are shown in Table 2.1. In this study, the aspect ratio was greater, *i.e.*, B/h>5, for two dimensional (2-D) flow with smooth bed.

Furthermore, by using two sets of LDA systems synchronized with burst-inhibit controller, the space-time correlation analyses were conducted. One is the air-cooling laser light as a fixed point (x=0), and the other is the water-cooling laser light as a movable point in the center of the channel. Fig.2.2 shows the experimental equipment for space-time correlation analyses. The focal lengths of both LDA probes are 300mm, which means that the measurement volumes are the same. When measuring at points within 2mm of each other, a biasing-light board was used for preventing fro. conflict of two laser lights. Hydraulic conditions for this experiment are shown in Table 2.2. In this study, three types of flow conditions were evaluated; (A) sub-critical flow in tranquil free surface, (B) critical flow in unstable and undulating free surface and (C) super-critical flow with large surface-wave fluctuations, respectively. The sampling time was 60sec, and the sampling frequency was about 200Hz for the water-cooled laser and about150Hz for the air-cooled laser. Instantaneous velocity data were interpolated linearly at 100Hz, and space-time correlation analyses were conducted after separating turbulence components. More detailed information on the present fiber-optic two-component LDA system is available in Nezu and Nakayama (1998b, 1998g).

2.3 Theoretical Considerations

2.3.1 Turbulence Characteristics in Open-Channel Flow

In fully-developed 2-D open-channel flow, the following shear stress equation is deduced from the streamwise momentum equation.

$$\frac{\tau}{\rho}\equiv-\overline{uv}+\nu\frac{dU}{dy}=U_*^2(1-\xi) \tag{2.1}$$

where $\xi=y/h$: non-dimensional vertical distance from the wall and ρ : the density of water, respectively. By applying Prandtl's (1925) mixing-length formulation to Eq.(2.1), the following expression for the dimensionless velocity gradient can be obtained.

$$\frac{dU^+}{dy^+}=\frac{2(1-\xi)}{1+\sqrt{1+4l^{+2}(1-\xi)}} \tag{2.2}$$

where $U^+=U/U_*$: normalized mean velocity, $y^+=yU_*/\nu$: vertical distance in law of the wall coordinates, and $l^+=lU_*/\nu$: normalized mixing length, respectively. By using Prandtl's (1925) mixing-length formulation and van Driest (1956) damping function in the above equation, the following famous velocity distribution can be obtained.

$$U^+=y^+ \quad for\, y^+<<A \tag{2.3}$$

$$U^+=\frac{1}{\kappa}\ln(y^+)+A_S \quad for\, A<y^+\le 0.2R_* \tag{2.4}$$

where A is van Driest's damping coefficient (=26), and $R_*=hU_*/\nu$ is turbulent Reynolds stress. Eq.(2.3) is the "*viscous-sublayer*" formula, and Eq.(2.4) is the "*log-law*" formula, both of which are governed by the law of the wall in the expression of the inner variables U_* and ν. For the intermediate region between Eq.(2.3) and Eq.(2.4), there exists a "*buffer layer*" in the range $5<y^+<30$ and no simple velocity formula is available, whose distribution can be calculated by integrating Eq.(2.2) directly. Furthermore, von Karman constant κ and integration constant A_s in Eq.(2.4) should be determined from experimental

data in the wall region (y/h<0.2). In the previous studies, κ=0.41 and A_s=5.3～5.5 have been usually used. On the other hand, recent investigations have indicated that the log law in Eq.(2.4) is applicable only in the wall region and that it is necessary to add a wake function to Eq.(2.4), which is a deviation from the standard log law. Coles (1956) has suggested the following wake function in the extension of Eq.(2.4).

$$w(\xi)=\frac{2\Pi}{\kappa}\sin^2\left(\frac{\pi}{2}\xi\right) \tag{2.5}$$

$$U^+=\frac{1}{\kappa}\ln(y^+)+A_s+w\left(\frac{y^+}{R_*}\right) \tag{2.6}$$

As for turbulence intensities u', v' and w' and turbulent kinetic energy k, the following semi-empirical formulae proposed by Nezu and Nakagawa (1993) are often quoted.

$$u'/U_*=2.30\exp(-\xi) \tag{2.7}$$

$$v'/U_*=1.27\exp(-\xi) \tag{2.8}$$

$$w'/U_*=1.63\exp(-\xi) \tag{2.9}$$

$$k/U_*^2=4.78\exp(-2\xi) \tag{2.10}$$

By applying Eq.(2.7)～(2.10), the turbulence intensity ratio (v'/u', w'/u') and the turbulent energy redistributions ($\overline{u^2}/2k$, $\overline{v^2}/2k$, $\overline{w^2}/2k$) take the following constant values:

$$v'/u'=0.55,\ w'/u'=0.71 \tag{2.11}$$

$$\overline{u^2}/2k=0.55,\ \overline{v^2}/2k=0.17,\ \overline{w^2}/2k=0.28 \tag{2.12}$$

As for u', Nezu and Nakagawa (1993) have refined Eq.(2.7) into Eq.(2.14) to account for the damping effect expressed in Eq.(2.13).

$$\Gamma(y^+)\equiv 1-\exp(-y^+/A') \tag{2.13}$$

$$u'/U_*=2.30\exp(-y^+/R_*)\cdot\Gamma(y^+)+D\cdot y^+\left(1-\Gamma(y^+)\right) \tag{2.14}$$

where A'=10 and D=0.3. About Reynolds stress, the following expressions are obtained from Eq.(2.1) and (2.6).

$$-\overline{uv}/U_*^2=(1-\xi)-V_t \tag{2.15}$$

$$V_t(\xi)=\frac{1}{\kappa R_*}\left(\xi^{-1}+\pi\Pi\sin(\pi\xi)\right) \tag{2.16}$$

The turbulent energy equations are obtained from the basic equations of normal turbulent stresses in fully-developed 2-D open-channel flow.

$$G=\varepsilon+(T_D+P_D)+V_D \tag{2.17}$$

$$G \equiv -\overline{uv}\left(\frac{\partial U}{\partial y}\right) \tag{2.18}$$

$$T_D \equiv \frac{\partial}{\partial y}\left(\frac{1}{2}\overline{(u^2+v^2+w^2)v}\right) \approx \frac{\partial}{\partial y}\left(\frac{\overline{u^2}v}{2}+\overline{v^3}\right) \tag{2.19}$$

$$P_D \equiv \frac{\partial}{\partial y}\left(\frac{\overline{pv}}{\rho}\right) \tag{2.20}$$

$$V_D \equiv -\nu\frac{\partial^2 k}{\partial y^2} \tag{2.21}$$

where G : turbulent generation (or production), T_D : turbulent energy diffusion, P_D : pressure energy diffusion, V_D : viscous diffusion, and ε : dissipation rate, respectively. There are various ways to evaluate ε. Nezu (1977) suggested that the dissipation rate ε can be most accurately evaluated from the –5/3 power law of FFT spectrum $F(f)$, as follows:

$$\varepsilon = \left(\frac{1}{C}\right)^{3/2} u'^3 \left(\frac{2\pi}{U}\right) f_c^{5/2} F(f_c)^{3/2} \tag{2.22}$$

where C : Kolmogoroff universal constant (about 0.5), U : local mean velocity, $F(f)$: normalized frequency spectrum ($\int_0^\infty F(f)df=1$), and f_c : frequency when $F(f_c)f_c^{5/3}$ becomes constant, respectively. In regions away from the wall at large Reynolds number, V_D is negligible and P_D can be obtained by the following expression.

$$P_D = G - \varepsilon - T_D \tag{2.23}$$

On the other hand, G can be expressed by substituting Eqs.(2.6) and (2.15) in Eq.(2.18), as follows:

$$Gh/U_*^3 = \left(1-\xi-\frac{1}{\kappa R_* \xi}\right)(\kappa\xi)^{-1} \tag{2.24}$$

Nezu and Nakagawa (1993) have suggested the following semi-empirical formula for ε.

$$\varepsilon h/U_*^3 = 9.8\xi^{-1/2}\cdot\exp(-3\xi) \tag{2.25}$$

2.3.2 Small-Amplitude Wave Theory

The ratio Λ of the surface-wave fluctuation energy to the total kinetic energy per unit area is expressed by evaluating the integral of turbulent kinetic energy according to Eq.(2.10), as follows:

$$\Lambda \equiv \frac{(\rho/2)\overline{g\eta^2}}{\int_0^h \rho k dy} = \frac{1}{4.13}\left(\frac{Um}{U_*}\right)^2 \cdot \frac{1}{Fr^2}\left(\frac{\sqrt{\overline{\eta^2}}}{h}\right)^2 \tag{2.26}$$

Iwasa (1967) has derived the following equation for surface-wave fluctuations by linearizing the momentum equation in open-channel flow.

$$(1-\beta Fr^2)\frac{\partial^2\eta}{\partial x^2} - 2\beta\frac{Fr^2}{U_m}\frac{\partial^2\eta}{\partial x\partial t} - \left(\frac{Fr}{U_m}\right)^2\frac{\partial^2\eta}{\partial t^2} - \frac{NS_b}{h}\frac{\partial\eta}{\partial x} - \frac{2S_b}{U_m h}\frac{\partial\eta}{\partial t} = 0 \tag{2.27}$$

where S_b : channel slope, β : momentum correction coefficient, and N : hydraulic exponent (=7/3+(1+2h/B)$^{-1}$), respectively. Let us assume that η is given by small-amplitude wave theory, as follows:

$$\eta = H\cdot\exp\{i(k_w x-\omega t)\} \tag{2.28}$$

$$\omega \equiv k_w V_w + i\tilde{\omega} \tag{2.29}$$

where k_w : wave number, ω : angular frequency, and V_w : the celerity of small-amplitude waves, respectively. The wave is developing (unstable) at $\tilde{\omega}>0$, damping (stable) at $\tilde{\omega}<0$, and critical at $\tilde{\omega}=0$. Substituting Eq.(2.28) into Eq.(2.27),

$$\left(\frac{\tilde{\omega}}{k_w U_m}\right)^2 = \frac{(N-2\phi)\left(1-Fr^2(\beta-2\beta\phi+\phi^2)\right)}{Fr^2(4\beta-N-2\phi)} \geq 0 \tag{2.30}$$

where $V_w/U_m=\phi$. The boundary curves for the existence of $\tilde{\omega}$ are given in the following.

$$\phi = N/2, \phi = 2\beta - N/2 \tag{2.31}$$

$$\phi = \beta \pm \sqrt{\beta(\beta-1)+Fr^{-2}} \tag{2.32}$$

Iwagaki (1955) derived the following expression by canceling ϕ in Eqs.(2.30)~(2.32).

$$\frac{\tilde{\omega}h}{U_m} = \frac{S(k_w h)^2}{8} \times \frac{Fr^2(N^2-4\beta N+4\beta)-4}{(k_w h)^2 Fr^2\left(\beta(2\beta-1)Fr^2+1\right)+S_b^2} \tag{2.33}$$

$$Fr,c \equiv \left((N/2)^2+\beta-\beta N\right)^{-1/2} \tag{2.34}$$

From the above equations, the flow is stable at $F_r<F_{r,c}$ and unstable at $F_r>F_{r,c}$. Nezu (1977) has pointed out that the flow is developing at $F_r>F_{r,c}=1.6$ and damping at $F_r<1.6$. So, the wave celerity is zero when $Fr=\beta^{1/2} \fallingdotseq 1$ from Eq.(2.32), whereas flow is stable at this condition. Therefore, the rapid growth of surface-wave fluctuations near critical flow cannot be explained by the above-mentioned small-amplitude wave theory, as mentioned later.

2.3.3 Non-Conditional Space-Time Correlation Analyses

Non-conditional space-time correlation coefficient $C_{u_i u_j}$ of velocity components u_i at a fixed point P and u_j at an arbitrary point Q is defined, as follows:

$$C_{u_i u_j}(x_0,y_0,z_0;\Delta x,\Delta y,\Delta z,\tau) = \frac{\overline{u_i(x_0,y_0,z_0,t_0)u_j(x_0+\Delta x,y_0+\Delta y,z_0+\Delta z,t_0+\tau)}}{u'_i(x_0,y_0,z_0)u'_j(x_0+\Delta x,y_0+\Delta y,z_0+\Delta z)} \tag{2.35}$$

where (Δx, Δy, Δz) is the lag distance from P to Q, τ is the lag time, and u_i' is the turbulence intensity of u_i, respectively.

A macro-scale gives not only a quantitative information about the turbulent eddy sizes, but also a qualitative picture of how the free surface modifies the coherent structure. The macro-scale $L_{u_i x_j}$ corresponding to velocity component u_i (=u) in the direction x_j (=x, z: homogeneous directions) is defined by

$$L_{u_i x_j} = \int_0^{x_{j,\max}} C_{u_i u_i}(\Delta x_j) dx_j \tag{2.36}$$

$$C_{u_i u_i}(\Delta x_j)\Big|_{\Delta x_j = x_{j,\max}} = 0 \tag{2.37}$$

where $x_{j,max}$ is the separation distance up to the zero-cross of $C_{u_i u_i}(\Delta x_j)$. In the inhomogeneous direction, Handler *et al.* (1993) have defined a vertical macro-scale $L_{u_i y}$ as follows:

$$L_{u_i y} = \int_0^1 C_{u_i u_i}(\Delta y) dy \tag{2.38}$$

On the other hand, $L_{u_i x}$ is obtained by the following two methods.

$$L_{u_i x} = \frac{\pi}{2} F_{u_i}(k_w = 0) \tag{2.39}$$

where F_{u_i} is normalized spectrum for wave number k_w ($\int_0^\infty F_{u_i}(k_w) dk_w = 1$). If "*Taylor's frozen turbulence hypothesis*" is valid, $L_{u_i x}$ can be evaluated from the integral time-scale $C_{u_i u_i}(0,\tau)$ and the convection velocity U_c, as follows:

$$L_{u_i x} = \int_0^\infty C_{u_i u_i}(\Delta x_j, 0) dx_j = \int_0^\infty C_{u_i u_i}(0, \Delta x_j / U_c) d(U_c \tau) = U_c \int_0^\infty C_{u_i u_i}(0,\tau) d\tau \tag{2.40}$$

As for the above-mentioned macro-scale, the following equation is generally effective in homogeneous isotropic turbulence.

$$\frac{L_{uy}}{L_{ux}} = 0.5, \quad \frac{L_{uz}}{L_{ux}} = 0.5 \tag{2.41}$$

The values of Eq.(2.41) are called the flatness ratio, and in general, not equal to 0.5 due to anisotropy.

2.4 Comparison between 3-D Measurements and DNS-Data in Low Reynolds-Number Flow

2.4.1 Turbulence Characteristics in Tranquil Open-Channel Flow

The friction velocity U_* is usually the most suitable velocity scale to normalize mean velocity and turbulence, and there are various methods to evaluate U_*, as follow; (1) log law, (2) formula of uniform flow, (3) Reynolds stress distribution, and (4) viscous-sublayer formula, *etc*. When there exists the viscous sublayer, *i.e.*, in low Reynolds number flow, method (4) is most appropriate due to its theoretical validity. However, it is usually difficult to obtain measurements in the viscous sublayer in the faster flows and then method (1) is most convenient both in the actual rivers and the experimental flumes. Therefore, first of all, the applicability of log law was evaluated in this study. Fig.2.3 shows the distribution of von Karman constant κ versus Froude number Fr, together with the experimental data

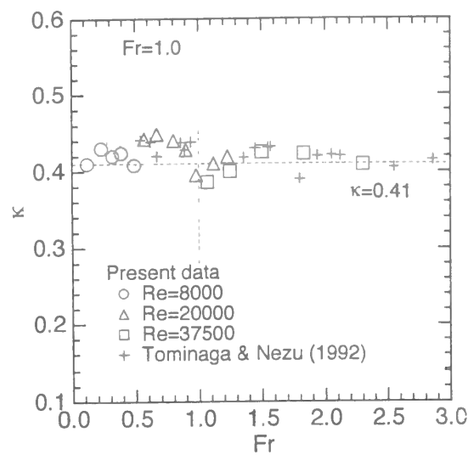

Fig.2.3 von Karman constant κ versus Froude number Fr.

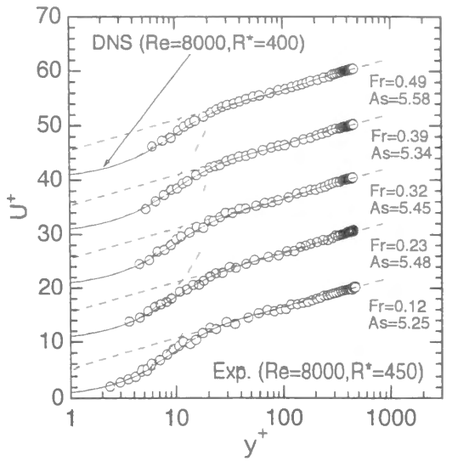

Fig.2.4 Primary mean velocity U^+ in tranquil flow.

by Tominaga and Nezu (1992). At that time, κ was evaluated from the log law by using U_* calculated from the Reynolds stress distribution $-\overline{uv}$ of Eq.(2.15). It can be seen that κ is the universal constant at 0.41 independent of Froude number, and therefore, the log law at κ=0.41 is effective regardless of Froude number and Reynolds number.

Next, it is necessary to verify the accuracy of these experiments. So, some comparisons were made between the experimental data and the DNS data. Fig.2.4 shows the distribution of a primary mean velocity U normalized by the friction velocity U_* in the wall region for the case-L, together with the DNS data by Kim *et al.* (1987) in a closed-channel. The experimental values of U_* were evaluated by three methods; (1) log law, (2) formula of uniform flow, and (3) Reynolds stress distribution. Three data coincided very well with one another, and the evaluation of U_* from the log law is effective, as mentioned in the former figure. In this figure, experimental and DNS data are in very good agreement with each other. This shows that in the wall region the primary mean velocity in open-channel flows is similar to that in closed-channel flows and is scarcely affected by the free surface. Furthermore, because this case is at low Reynolds number, the wake strength parameter Π proposed by Coles (1956) is zero and the log law is effective up to the free surface, as pointed out by Nezu and Nakagawa (1993).

Fig.2.5 shows the distribution of the turbulence intensities u', v', w' and turbulent kinetic energy k normalized by U_*, respectively. In this figure, the DNS data and the semi-empirical formulae proposed by Nezu and Nakagawa (1993) are also plotted together. It can be seen that in the wall region and intermediate region, all the values coincide well with the values in closed-channel. However, v' is damped near the free surface, that is to say, y/h>0.8, in comparison with the closed-channel, which is an important characteristic of tranquil open-channel flow. Furthermore, u' and w' increase a little near the free surface, as pointed out by Komori *et al.* (1987), while k coincides with the closed-channel. Fig.2.6 shows the high-order correlation terms $\overline{u^2 v}$ and $\overline{v^3}$ versus y^+. Both data are in good agreement with each other, which implies that this experimental data is highly accurate.

2.4.2 Turbulent Energy Budget near Free Surface

Fig.2.7 shows the turbulent energy budget (G : turbulent generation, T_D : turbulent energy diffusion, and ε : dissipation rate) versus y/h in tranquil flow, together with the DNS data by Kim *et al.* (1987) in closed-channel. G, T_D, and ε were calculated by Eqs.(2.18), (2.19) and (2.22), respectively. It can be

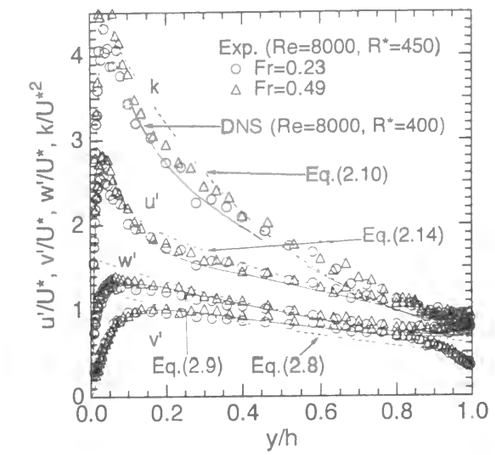

Fig.2.5 Turbulence intensities u'/U_*, v'/U_*, w'/U_* and turbulent kinetic energy k/U_*^2.

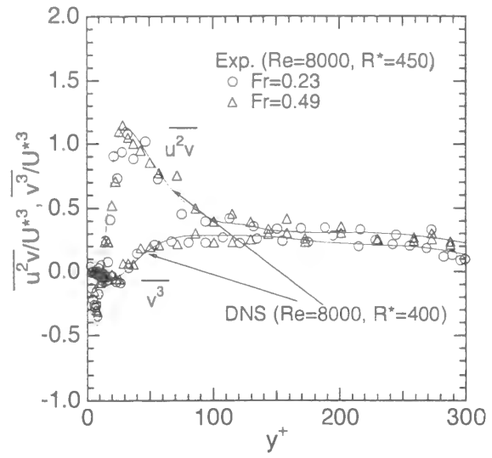

Fig.2.6 High-order correlation terms $\overline{u^2v}$ and $\overline{v^3}$.

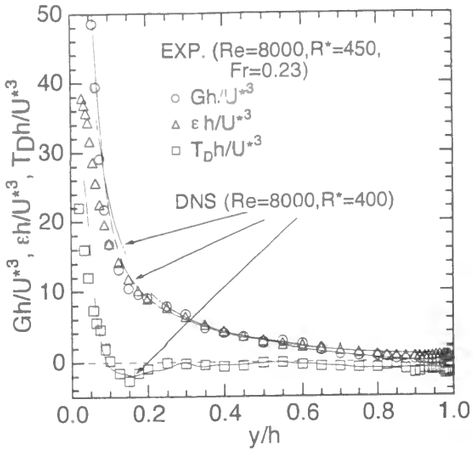

Fig.2.7 Turbulent energy budget.

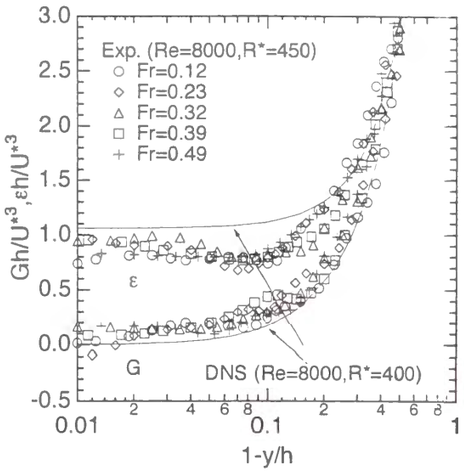

Fig.2.8 Turbulent generation Gh/U_*^3 and turbulent energy dissipation rate $\varepsilon h/U_*^3$ near the free surface in tranquil flow.

seen that turbulent energy is in surplus near the wall ($G>\varepsilon$), in equilibrium in the intermediate region ($G=\varepsilon$), and in deficit near the free surface ($G<\varepsilon$). The experimental data in open-channel flow is almost in coincidence with the computational data for a closed-channel, which means that the energy budget in open-channel flow at low Reynolds and Froude number is very similar to that for a closed-channel. In particular, near the free surface, ε is nearly balanced by T_D because G and P_D are negligibly small there, as pointed out by Nezu and Nakagawa (1993). Fig.2.8 shows the distributions of the turbulent generation Gh/U_*^3 and the turbulent energy dissipation rate $\varepsilon h/U_*^3$ near the free surface in tranquil flow. As with turbulence intensities, there seems to be no dependence on Froude number. This region is energy deficiency region, that is to say, $\varepsilon>G$, and it is very interesting that the energy deficiency (ε-G) in open-channel flow is smaller than that for closed-channel.

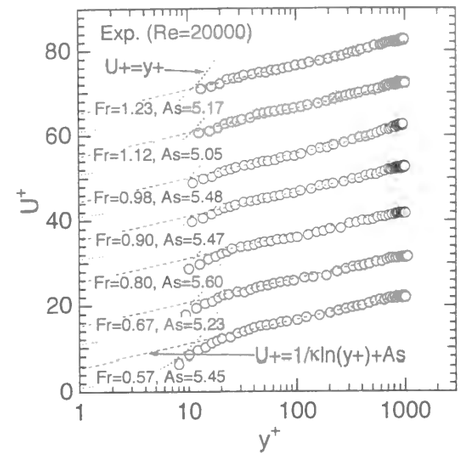

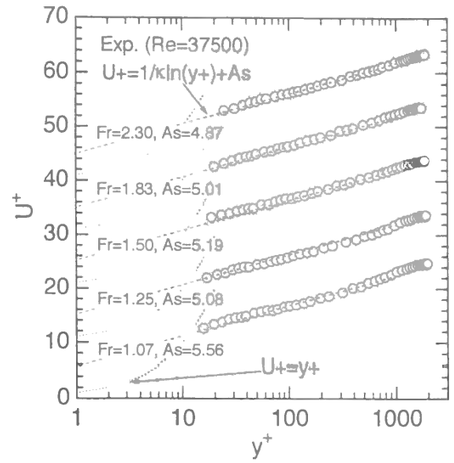

Fig.2.9 Primary mean velocity U^+ when the surface-wave fluctuations occur.

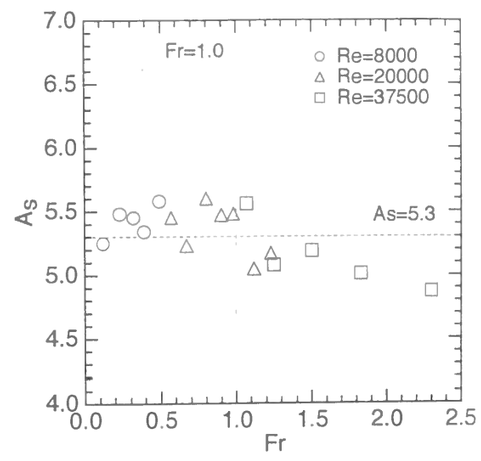

Fig.2.10 Integral constant A_s versus Froude number.

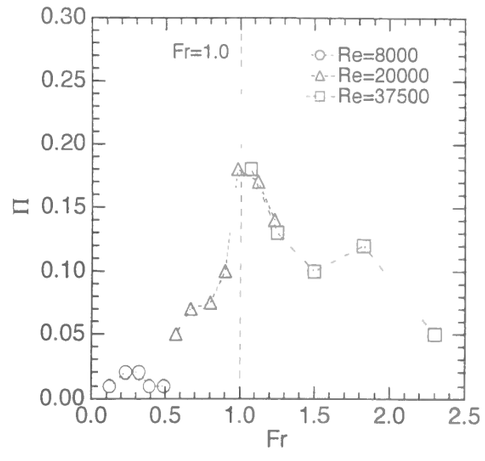

Fig.2.11 Wake strength parameter Π versus Froude number.

2.5 Relationship between Turbulence Structure near Free Surface and Surface-Wave Fluctuations

2.5.1 Variation of Turbulence Characteristics versus Froude Number

The difference between open-channel flows and closed-channel flows is clearly reflected in v', as mentioned previously. In open-channel flow, v' is damped near the free surface in tranquil flow, whereas v' increases as the Froude number increases and surface-wave fluctuations occur. Fig.2.9 shows the distributions of primary mean velocity when the surface-wave fluctuations occur. All the experimental data are in good agreement with the log law except near the free surface due to the increase of Reynolds number, and it becomes more difficult to measure near the wall as the Froude number increases due to the decrease of viscous sub-layer, as pointed out by Iwagaki (1955) and Tominaga and Nezu (1992). Fig.2.10 shows the variations of integral constant A_s evaluated from the linear regression of the log

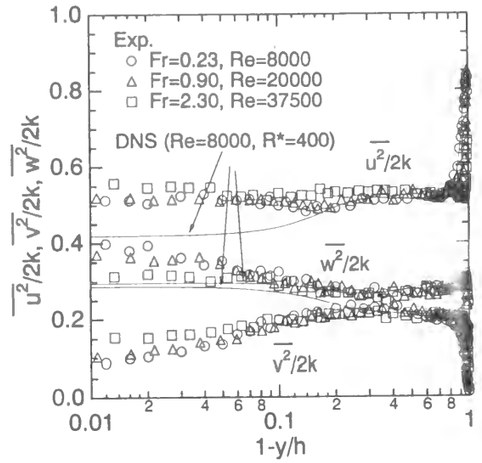

Fig.2.12 Turbulent energy redistribution near the free surface.

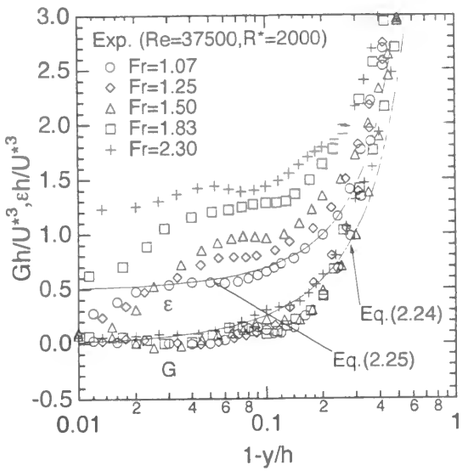

Fig.2.13 Turbulent generation Gh/U_*^3 and turbulent energy dissipation rate $\varepsilon h/U_*^3$ near the free surface in super-critica low.

law with the fixed value of κ=0.41. In sub-critical flow, the value attains almost a constant value A_s=5.5, whereas the value decreases as the Froude number increases in super-critical flow, which is the same characteristics as pointed out by Iwagaki (1955) and Prinos and Zeris (1995) due to the decrease of viscous sublayer. Fig.2.11 is the distribution of wake strength parameter Π versus Froude number. Nezu and Nakagawa (1993) suggested that Π is a function of Reynolds number. From this figure, Π is also found to depend on Froude number, and in particular, Π increases greatly near critical flow condition. This means that the primary velocity depends on the inactive component of surface-wave fluctuations near the critical flow, that is to say, the effect of instability.

Fig.2.12 shows the distribution of turbulent energy redistribution near the free surface, together with DNS data in duct flow, and these values never depend on U_*. It can be seen that the three components vary near the free surface, that is to say, y/h>0.8, due to the effect of Froude number. This means that the surface-wave fluctuations have an important role on the turbulent variation near the

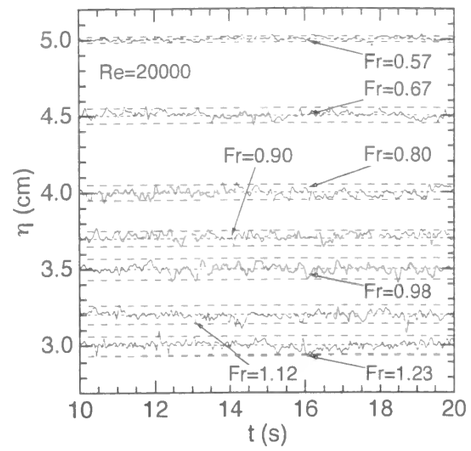

Fig.2.14 Time series of surface-wave fluctuations η.

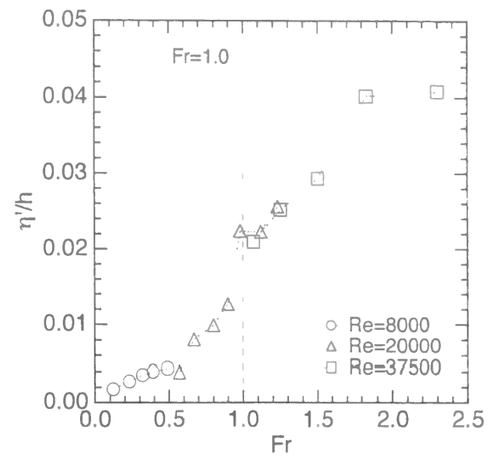

Fig.2.15 Intensity of surface-wave fluctuations η' normalized by the mean flow depth.

free surface. Fig.2.13 shows the distributions of the turbulent generation Gh/U_*^3 and the turbulent energy dissipation rate $\varepsilon h/U_*^3$ near the free surface in super-critical flow, together with Eqs.(2.24) and (2.25). G is similar to that in duct flow regardless of the Froude number (characteristics of self-consistency), whereas ε is dependent much on Froude number and generally increases as Froude number increases.

2.5.2 Relationship between Surface-Wave Fluctuations and Velocity Fluctuations

As mentioned before, the variation of turbulence intensity has a close relationship with the surface-wave fluctuations when Fr changes. However, Reynolds stress is almost constant regardless of Fr. It has been pointed out that this characteristic is related with the "*flow instability*" due to inactive motions, and therefore, the undulation of the free surface in the critical flow is related with the sudden increase of v'.

Fig.2.14 is the time series of surface-wave fluctuations η (cm). The amplitude has a maximum near the critical flow and the low-frequency component predominates, which was verified by the fact that the Flatness factor $F_\eta=\eta^4/\eta'^4$ had a maximum in the critical flow. Fig.2.15 shows the intensity of surface-wave fluctuations η' normalized by the mean flow depth h, *i.e.*, the value of η'/h. The value increases rapidly near the critical flow due to the effect of inactive component. This corresponds to the sudden increase of v', and therefore, η' and v' are related with each other. Fig.2.16 shows an example of the spectral distributions near the free surface in critical flow (Fr=0.98) by the FFT method $S_u(f)$, $S_v(f)$, $S_\eta(f)$, respectively. $S_\eta(f)$ has a clear peak at about f=2(Hz), which corresponds to the ripple of water wave near critical flow. $S_v(f)$ has also a peak at the same frequency, but $S_u(f)$ has no peak. This means that the wave and the vertical component of turbulence intensity have a very close and complicated relationship with each other near the free surface. For evaluating the effect of surface-wave fluctuations, it is very effective to examine the ratio Λ of the surface-wave fluctuation energy to the total kinetic energy per unit area. Fig.2.17 shows the distribution of Λ versus Froude number, together with Eq.(2.26). It can be seen that the ratio of surface-wave fluctuations increases greatly near the critical flow, which corresponds well to the distribution of η'/h in Fig.2.15. These characteristics are closely related to the predominance of low-frequency and inactive component near the critical

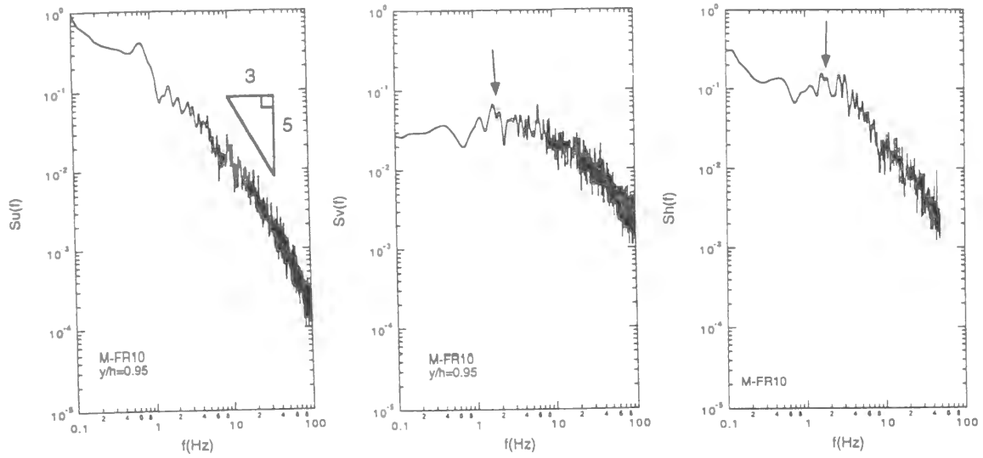

Fig.2.16 Spectral distributions near the free surface by the FFT method $S_u(f)$, $S_v(f)$, $S_\eta(f)$.

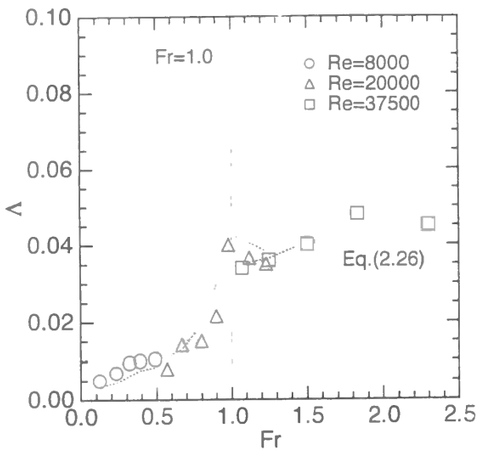

Fig.2.17 Ratio of the surface-wave fluctuation energy to the total kinetic energy per unit area Λ.

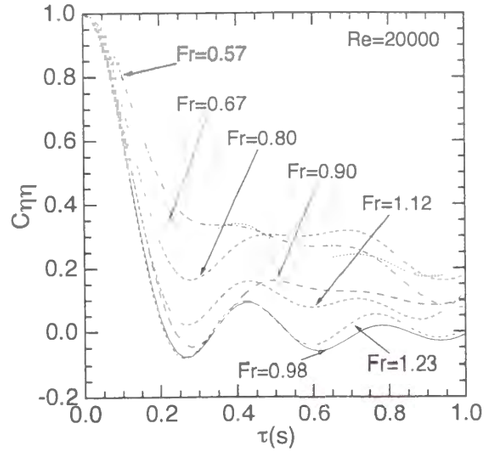

Fig.2.18 Auto-correlation coefficient $C_{\eta\eta}$.

flow, as mentioned before.

The cross-correlation coefficient C_{xy} of $x(t)$ and $y(t)$ is defined, as follows:

$$Cxy(\tau)=\overline{x(t)y(t+\tau)}/(x'y') \tag{2.42}$$

where x', y' are the corresponding turbulence intensities. Fig.2.18 is the auto-correlation coefficient $C_{\eta\eta}$ versus lag time τ(s). It can be seen that the correlation decreases as Fr becomes close to one, which implies the turbulence eddy becomes smaller and the flow may be more unstable near the critical flow. At the same time, the correlation of velocity components had a small value near the critical flow. This similarity can be verified by analyzing cross-correlation between the surface-wave fluctuations and the velocity fluctuations. Figs.2.19 and 20 show the cross-correlation coefficients $C_{u\eta}$ and $C_{v\eta}$ near the free surface. When the Froude number is small and free surface is flat, there is no

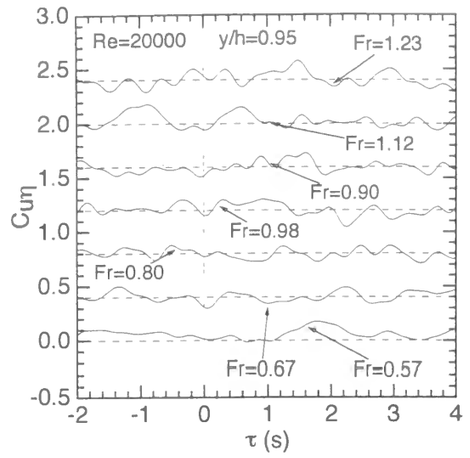

Fig.2.19 Cross-correlation coefficients $C_{u\eta}$ near the free surface.

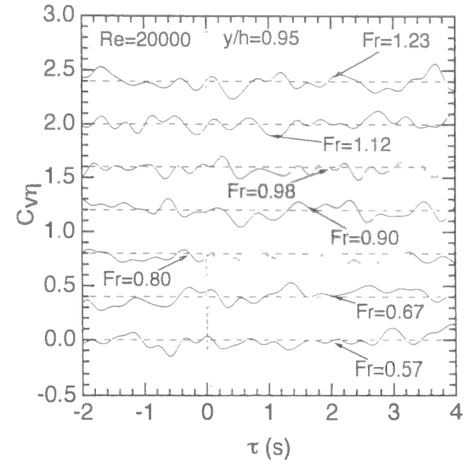

Fig.2.20 Cross-correlation coefficients $C_{v\eta}$ near the free surface.

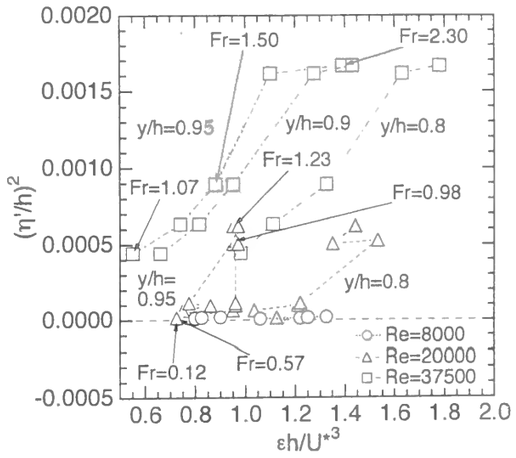

Fig.2.21 Square of η'/h versus turbulent energy dissipation rate.

tendency in both $C_{u\eta}$ and $C_{v\eta}$. However, the situation is different when the surface-wave fluctuations occur. As for $C_{u\eta}$, the coefficient takes a minimum value near τ=0(s) in wavy free surface, as implied by the continuity equation. On the other hand, $C_{v\eta}$ takes a maximum value near τ=0(s) in a stable flow, *i.e.*, away from the critical flow, which means that the water surface goes down when the local-accelerated flow goes downward (u>0, v<0) and that the water surface rises when the local-decelerated flow lifts up (u<0, v>0), as previously pointed out. However, the shift in a phase of $C_{v\eta}$ has a maximum near the critical flow, which means that this shift may cause the unstable flow and that turbulence intensities and surface-wave fluctuations change rapidly due to the predominance of inactive component. Furthermore, these systematic variations decrease rapidly away from the free surface and the effect of free surface is negligible for y/h<0.7.

As mentioned in Fig.2.13, the turbulent energy dissipation rate increases as the Froude number increases in super-critical flow, which suggests that there is a close relation between ε and the surface

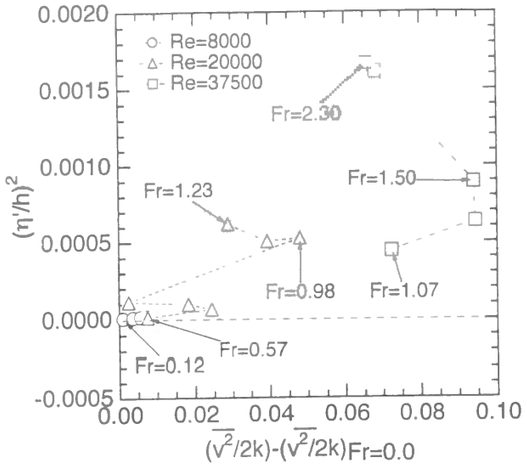

Fig.2.22 Square of η'/h versus the increasing rate of vertical component of turbulent energy redistributions.

waves. Fig.2.21 shows the square of η'/h versus ε near the free surface (y/h=0.8. 0.9 and 0.95). It can be seen that there exists a quasi-linear relationship between these two variables in the wavy flow. This means that the higher energy of surface-wave fluctuations results in the more energy dissipation near the free surface and that the surface waves affect greatly the energy budget near the free surface independent of the inactive component of turbulence. In this way, it has a possibility that the energy of surface-wave fluctuations has a close relationship with the change in turbulent energy redistributions from that in tranquil flow. Supposing that the increase of v' is due to the effect of surface-wave fluctuations as the Froude number increases, the following expression is valid.

$$\left[\left(\overline{v^2}/2k\right)-\left(\overline{v^2}/2k\right)_{Fr\to 0.0}\right]\propto E_\eta \tag{2.43}$$

Fig.2.22 shows the square of η'/h versus the increasing rate of vertical component of turbulent energy redistributions. It can be seen that there exists a linear relationship with each other at low Froude number. However, the surface-wave energy increases greatly in super-critical flow due to the effect of other component.

2.6 Space-Time Correlation Structures

2.6.1 Non-Conditional Space-Time Correlation

Figs.2.23(a)-(c) show some examples of non-conditional space-time correlation coefficients C_{uu} in the center of the channel evaluated from Eq.(2.35) in sub-critical flow (M-FR06), critical flow (M-FR10), and super-critical flow (S-FR31) versus the lag-time τ. At that time, fixed points × are near the wall (y/h=0.1) and the free surface (y/h=0.9). An evolution of correlation region can be seen clearly. Of particular significance is that the maximum correlation line fairly inclines downstream toward the wall due to the shear near the wall when the fixed point is near the wall, as pointed out by Nakagawa and Nezu (1981), regardless of Froude number and surface-wave fluctuations. This

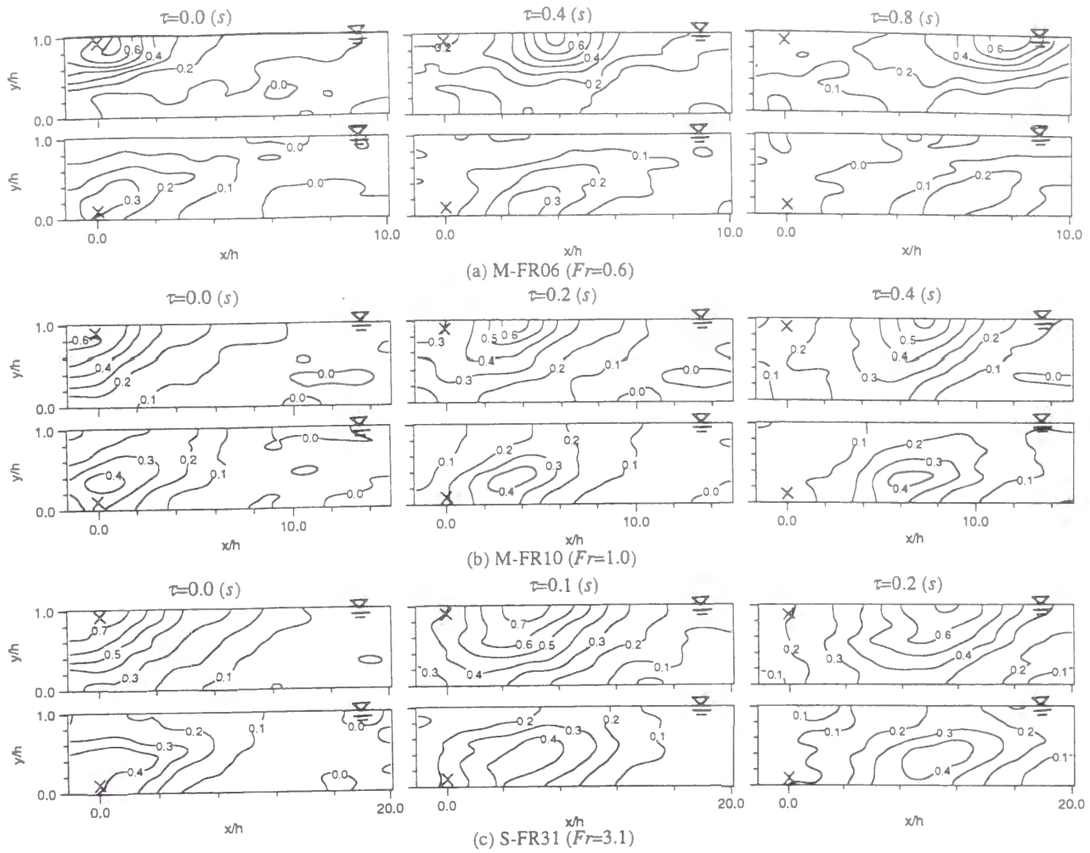

Fig.2.23 Non-conditional space-time correlation coefficients C_{uu} at the fixed point near the wall and near the free surface.

characteristic implies that the turbulence and coherent structures near the wall are related to the free surface region, as mentioned by Nakagawa and Nezu (1981), Komori *et al.* (1989) and Rashidi and Banerjee (1988).

On the other hand, the correlations at the fixed point near the free surface have little inclination and spread more widely below the free surface with the increase in Froude number. This phenomenon implies that the mixing in the bulk becomes more active in super-critical flow and that the large-scale vortices can be seen as boils near the free surface, which can be seen more clearly when the conditionally-averaged space-time correlation analyses are applied as mentioned in the next chapter. Furthermore, the coefficients C_{vv} did not have clearer phase difference as C_{uu} because there is no shear in the vertical velocity fluctuations. More detailed information about C_{vv} is shown in Nezu and Nakayama (1998b).

2.6.2 Macro-Scale

Fig.2.24 shows the distribution of macro-scales for the streamwise velocity component in the streamwise, vertical and spanwise directions L_{ux}, L_{uy}, L_{uz}, respectively, together with the DNS data of Handler *et al.* (1993) both in closed and open-channel flows. About the effect of velocity components (u, v and w) on the macro-scale, Nezu and Nakayama (1998b) have pointed out that the turbulence

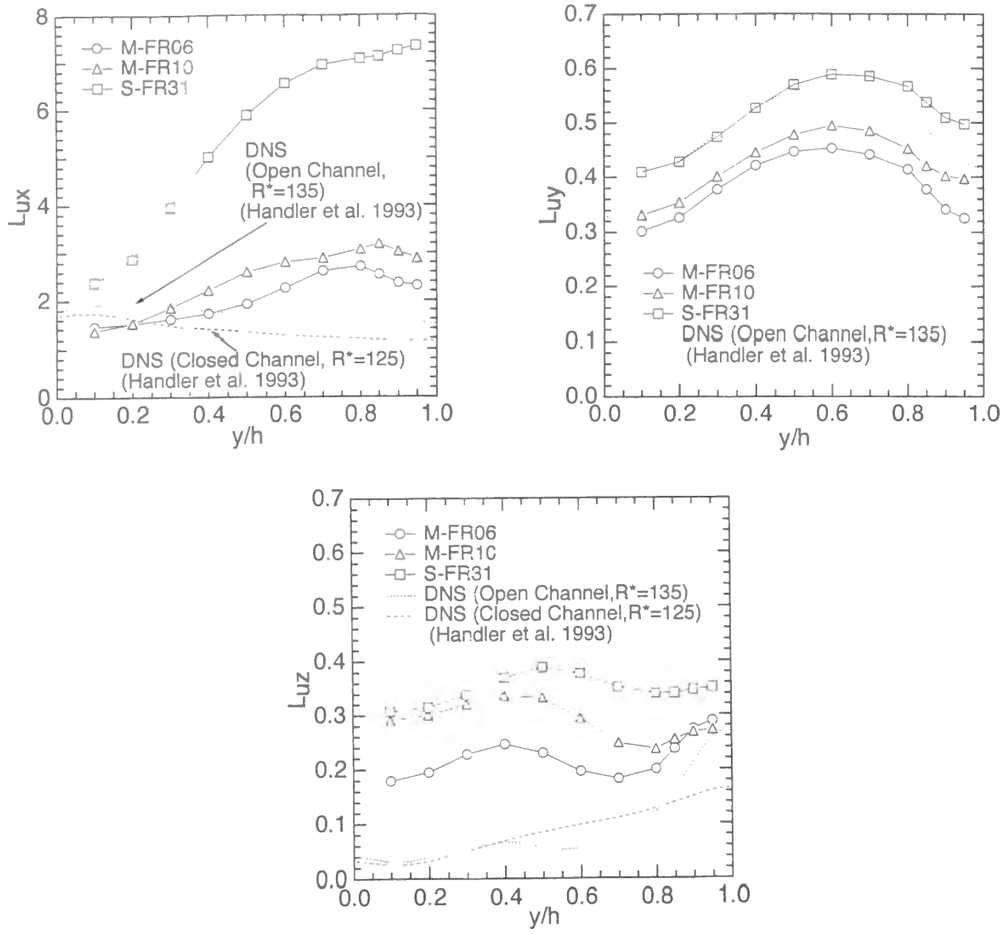

Fig.2.24 Macro-scales for the streamwise velocity component in the streamwise, vertical and spanwise directions L_{ux}, L_{uy}, L_{uz}.

scale in open-channel flow can be expressed by the correlation scales of the streamwise component because L_{ux}, L_{uy}, L_{uz} take the higher values. It can be seen that $L_{uz}<L_{uy}<L_{ux}$ independent of the vertical distance from the wall in the same way as Asano (1977). L_{ux} increases as the Froude number becomes greater. In a sub-critical flow (M-FR06), the value decreases at $y/h>0.8$, which is in agreement with the DNS data and attributes the damping characteristics of the free surface. The distribution of L_{uz} becomes flat in a super-critical flow (S-FR31). On the other hand, L_{uy} is quite different from L_{ux} and L_{uz} due to the great effects of the free surface. In particular, the value of L_{uy} decreases greatly at $y/h>0.6$. The peak position moves towards the free surface as the Froude number increases. This feature has a close relationship with an increase of the vertical turbulence intensity v' in a super-critical flow, as mentioned by Nezu and Nakagawa (1993). Therefore, in a tranquil flow, the coherent structure generated near the wall moves upward to the free surface and becomes a "*pancake-shaped*" (flat) structure as suggested by Banerjee (1992). However, the vortices are strongly stretched in the streamwise direction and go downwards into the bulk flow in a super-critical flow, which can be seen as boils near the free surface.

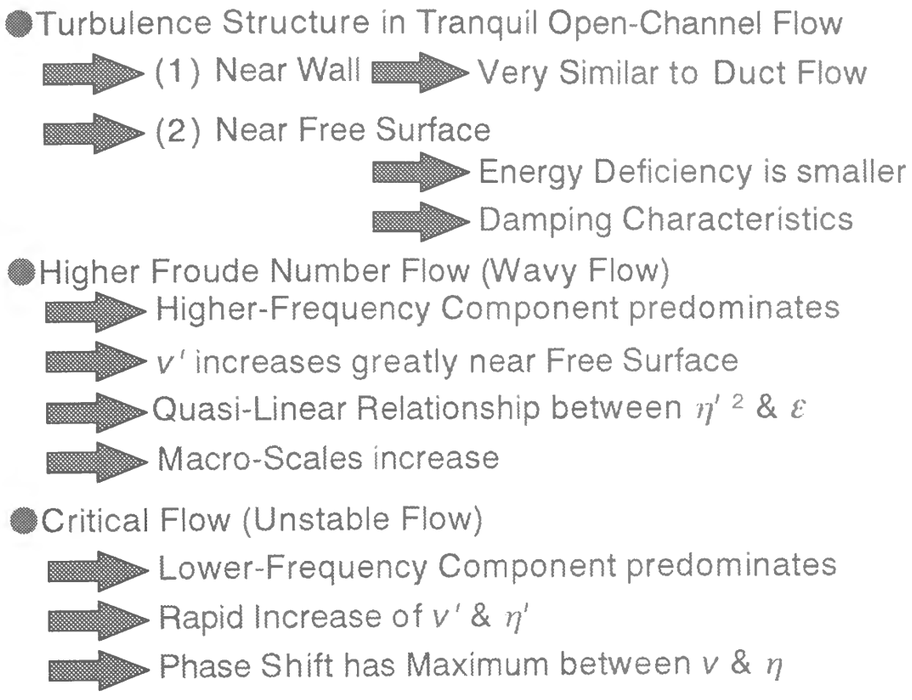

Fig.2.25 Conclusions of chapter 2.

2.7 Conclusions

In this study, turbulent characteristics and surface-wave fluctuations were simultaneously measured in open-channel flows by using two sets of fiber-optic LDA systems and the ultrasonic depth-meter instrument. Fig.2.25 shows the conclusions of chapter 2. It was found that the free surface affects the rate of turbulence redistributions. In particular, the turbulence intensity v' increases rapidly near the critical flow. This phenomenon is caused by the undulating and unstable nature of the flow. The waves and the turbulence have a close and complicated relationship with each other near the free surface. Consequently, the large phase shift between the wave and the turbulence causes the unstable flow, and turbulence intensities and surface-wave fluctuations change rapidly. Furthermore, by using two sets of LDA system simultaneously, the space-time correlation coefficient and macro-scale were evaluated, and related to the effect of free surface.

Notations

A : van Driest's damping coefficient (=26)
A' : van Driest's damping coefficient in u' (=10)
A_s : integration constant in log law
B : channel width
C : Kolmogoroff universal constant (about 0.5)
C_{uiuj} : non-conditional space-time correlation coefficient of velocity components u_i at a fixed point

P and u_j at an arbitrary point Q
C_{xy} : cross-correlation coefficient of x(t) and $y(t)$
$C_{\eta\eta}^{xy}$: auto-correlation coefficient of surface displacement
D : coefficient in u' of viscous term
f : frequency in Hz
$F(f)$: normalized FFT spectrum
Fr : Froude number ($=U_m/\sqrt{gh}$)
G : turbulent generation (or production)
g : acceleration due to gravity
h : flow depth
k : turbulent kinetic energy
k_w : wave number
L_{uixj} : macro-scale corresponding to velocity component u_i in the direction x_j
l : mixing length
l^+ : dimensionless mixing length ($=l^+=lU_*/\nu$)
N : hydraulic exponent ($=7/3+(1+2h/B)^{-1}$)
Re : Reynolds number ($=U_m h/\nu$)
R_* : turbulent Reynolds number ($=U_* h/\nu$)
S_b : channel slope
$S_u(f)$: spectrum of u-component
$S_v(f)$: spectrum of v-component
$S_\eta(f)$: spectrum of surface displacement
T_D : turbulent energy diffusion
U : primary mean velocity
U_m : bulk mean velocity
U^+ : U/U_* ; normalized mean velocity
U_* : friction velocity
u : instantaneous streamwise velocity component
u' : root-mean-square value of velocity fluctuations in x direction
$-\overline{uv}$: Reynolds stress
V_w : celerity of small-amplitude wave
v : instantaneous vertical velocity component
v' : root-mean-square value of velocity fluctuations in y direction
w : instantaneous spanwise velocity component
w' : root-mean-square value of velocity fluctuations in z direction
x : streamwise direction
$x_{j,max}$: separation distance up to the zero-cross of C_{uiuj}
y : vertical direction from the channel bed
y^+ : yU_*/ν ; vertical distance in law of the wall coordinates
z : spanwise direction from the center of the channel

Greek symbols
β : momentum collection coefficient
$(\Delta x, \Delta y, \Delta z)$: lag distance
ε : turbulent energy dissipation rate
η : instantaneous surface displacement with respect to the still water level
η' : intensity of surface-wave fluctuations ($\equiv\sqrt{\overline{\eta^2}}$)

κ : von Karman constant
Λ : ratio of surface-wave fluctuation energy to total kinetic energy per unit area
ν : kinetic viscosity
Π : wake strength parameter
τ : lag time
ω : angular frequency

References

[1] Asano, T. : Space-time correlation structure in open-channel flow, *Ph.D Thesis presented to Kyoto University*, 1977 (in Japanese).
[2] Banerjee, S. : Turbulence structures, *Chemical Engineering Science*, Vol.47, No.8, pp.1793-1817, 1992.
[3] Bradshaw, P. : 'Inactive' motion and pressure fluctuations in turbulent boundary layers, *J. Fluid Mech.*, Vol.28, pp.593-616, 1967.
[4] Brumley, B. H. and Jirka, G. H. : Near-surface turbulence in a grid-stirred tank, *J. Fluid Mech.*, Vol.183, pp.235-263, 1987.
[5] Coles, D. : The law of the wake in the turbulent boundary layer, *J. Fluid Mech.*, Vol.1, pp.191-226, 1956.
[6] Drayton, M.J. : Eulerian and lagrangian studies of inhomogeneous turbulence generated by an oscillating grid, *Ph.D Thesis presented to University of Cambridge*, 1993.
[7] Handler, R. A., Swean, T. F., Jr., Leighton, R. I., and Swearingen, J. D. : Large scales and the energy balance for turbulence near a free surface, *J. AIAA*, Vol.31, No.11, pp.1998-2007, 1993.
[8] Hunt, J. C. R. : Turbulence structure and turbulent diffusion near gas-liquid interfaces, *Gas Transfer at Water Surfaces*, W. Brutsaert and G. H. Jirka (eds.), Reidel Pub., pp.67-82, 1984.
[9] Hunt, J. C. R. and Graham, J. M. R. : Free-stream turbulence near plane boundaries, *J. Fluid Mech.*, Vol.84, pp.209-235, 1978.
[10] Iwagaki, Y. : Bed erosion mechanism by rainfall flow, *Ph.D Thesis presented to Kyoto University*, 1955 (in Japanese).
[11] Iwasa, Y. : Hydraulics, Asakura Press, 1967 (in Japanese).
[12] Kim, J., Moin, P. and Moser, R. : Turbulence statistics in fully developed channel flow at low Reynolds number, *J. Fluid Mech.*, Vol.177, pp.133-166, 1987.
[13] Komatsu, T., Shibata, T., Asai, K. and Takahara, K. : Turbulent characteristics near free surface of an oscillating-grid field, *Annual Journal of Hydraulic Engineering*, Vol.39, pp.819-826, 1995 (in Japanese).
[14] Komori, S., Hiraga, Y., Murakami, Y. and Ueda, H. : The generation of surface-renewal eddies in an open channel flow, *Proc. of 2nd. Int. Symp. on Transport Phenomena in Turbulent Flows*, Tokyo, pp.75-85, 1987.
[15] Komori, S., Murakami, Y. and Ueda, H. : The relationship between surface-renewal and bursting motions in an open-channel flow, *J. Fluid Mech.*, Vol.203, pp.103-123, 1989.
[16] Komori, S., Nagaosa, R., Murakami, Y., Chiba, S., Ishii, K. and Kuwahara, K. : Direct numerical simulation of three-dimensional open-channel flow with zero-shear gas-liquid interface, *Phys. Fluids A*, Vol.5, No.1, pp.115-125, 1993.
[17] Komori, S., Ueda, H., Ogino, F. and Mizushina, T. : Turbulence structure and transport mechanism at the free surface in an open channel flow, *Int. J. Heat Mass Transfer*, Vol.25, No.4, pp.513-521, 1982.

[18] Li, X., Dong, Z. and Chen, C. : Turbulent flows in smooth-wall open channels with different slope, *J. Hydraulic Research*, IAHR, Vol.33, No.3, pp.333-347, 1995.
[19] Nakagawa, H. and Nezu, I. : Structure of space-time correlations of bursting phenomena in an open-channel flow, *J. Fluid Mech.*, Vol.104, pp.1-43, 1981.
[20] Nakayama, T. : Turbulent structures and characteristics of coherent vortices near the free surface, *M.E. Thesis presented to Kyoto University*, 1997 (in Japanese).
[21] Nezu, I. : Turbulent structure in open-channel flows, *Ph.D Thesis presented to Kyoto University*, 1977 (in Japanese).
[22] Nezu, I. and Nakagawa, H. : Turbulence in open-channel flows, IAHR-Monograph, Balkema, 1993.
[23] Nezu, I., Nakayama, T. and Itoh, Y. : Turbulent structures in steep open-channel flows, *1st Symposium on Environmental Fluid Mechanics*, Vol.1, pp.323-324, 1996e (in Japanese).
[24] Nezu, I., Nakayama, T. and Itoh, Y. : Comparison of 3-D experimental database with direct numerical simulation, *Annual Journal of Hydraulic Engineering*, Vol.41, pp.1055-1060, 1997b (in Japanese).
[25] Nezu, I., Nakayama, T. and Kita, A. : Relationship between turbulence structures near the free-surface and surface-wave-fluctuations, *Annual Journal of Hydraulic Engineering*, Vol.41, pp.657-662, 1997c (in Japanese).
[26] Nezu, I. and Nakayama, T.: Relationship between turbulent structure near the free-surface and surface-wave-fluctuations, *Proc. of 27th IAHR Congress*, ASCE, IAHR, pp.245-250, 1997d.
[27] Nezu, I. and Nakayama, T. : Relationship between turbulent structures near the free-surface and surface-wave-fluctuations, *Journal of Hydraulic Engineering*, JSCE, No.593/II-43, pp.69-78, 1998a (in Japanese).
[28] Nezu, I. and Nakayama, T. : Space-time correlation structures of coherent vortices near the free surface, *Journal of Hydraulic Engineering*, JSCE, No.586/II-42, pp.51-60, 1998b (in Japanese).
[29] Nezu, I. and Nakayama, T.: Effect of the surface-wave fluctuations on coherent structures near the free surface, *11th Congress of the IAHR-APD*, pp.507-516, 1998g.
[30] Prandtl, L. : Uber die ausgebildete Turbulenz, ZAMM, Vol.5, 1925.
[31] Prinos, P. and Zeris, A. : Uniform flow in open channels with steep slopes, *J. Hydraulic Research*, IAHR, Vol.33, No.5, pp.705-719, 1995.
[32] Rashidi, M. and S. Banerjee : Turbulence structure in free surface channel flows, *Phys. Fluids*, Vol.31, No.9, pp.2491-2503, 1988.
[33] Rotta, J.C. : Turbulence stromungen, Teubner, Germany, 1972.
[34] Swean, T. F., Jr., Leighton, R. I., Handler, R. A., and Swearingen, J. D. : Turbulence modeling near the free surface in an open channel flow, *29th Aerospace Sciences Meeting*, Reno, Nevada, 1991.
[35] Tamburrino, A. and Gulliver, J. S. : Free surface turbulence measurements in an open-channel flow, *FED*, ASME, Vol.181, pp.103-112, 1994.
[36] Tamburrino, A. and Gulliver, J. S. : Large flow structures in a turbulent open channel flow, *J. Hydraulic Res.*, IAHR, Vol.37, No.3, 1999.
[37] Tominaga, A. and Nezu, I. : Velocity profiles in steep open-channel flows, *J. Hydraulic Eng.*, ASCE, Vol.118, No.1, pp.73-90, 1992.
[38] van Driest, E.R. : On turbulent flow near a wall, *J. Aero. Sci.*, No.23, pp.1007-1011, 1956.

CHAPTER 3

MUTUAL-INTERACTION BETWEEN BURSTS AND BOILS NEAR FREE SURFACE IN OPEN-CHANNEL FLOW

Abstract

In an open-channel flow, a free surface has a large effect on the turbulent energy redistribution near the free surface. When the Froude number increases and the surface-wave fluctuations occur, the damping effect is gradually lost out and the turbulent energy redistribution near the free surface changes largely. In this study, the damping characteristics are compared between the theoretical model and the experimental data. The effect of the surface-wave fluctuations is then considered by using a function of the Froude number. Furthermore, it has been pointed out that these characteristics are closely related to the coherent structures. So, PIV (Particle-Image Velocimetry) was used to measure evolutionary patterns of coherent vortices in the center of channel. Finally, a relationship between the "*bursting phenomenon*" generated near the wall and the "*surface renewal eddies*" near the free surface was evaluated in open-channel flows.

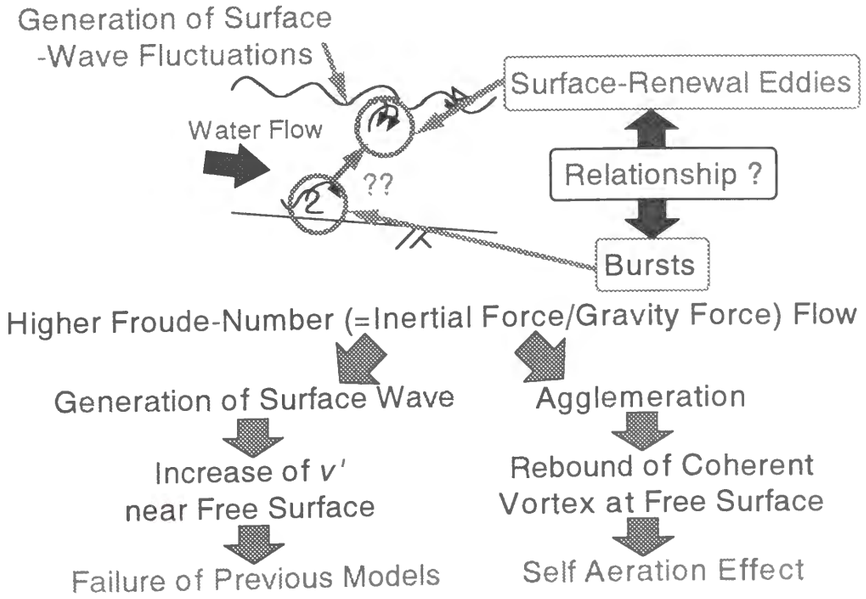

CHAPTER 3 MUTUAL-INTERACTION BETWEEN BURSTS AND BOILS NEAR FREE SURFACE IN OPEN-CHANNEL FLOW

Parts of this chapter were presented in the following papers.

[1] Nakayama, T. : Turbulent structures and characteristics of coherent vortices near the free surface, *M.E. Thesis presented to Kyoto University*, 1997 (in Japanese).
[2] Nezu, I., Abe, T., Shimura, T. and Nakayama, T. : Characteristics of compound open-channel flows with FLDA and PTV, *Proc. of 2nd Symposium on River Hydraulics and Environments*, pp.45-52, 1995 (in Japanese).
[3] Nezu, I., Shimura, T. and Nakayama, T. : Analyses of coherent vortices between main-channel and flood-plains by means of PTV, *Annual Journal of Hydraulic Engineering*, Vol.40, pp.1059-1064, 1996a (in Japanese).
[4] Nezu, I., Abe, T., Shimura, T. and Nakayama, T. : Space-time correlation analysis in compound open-channel flows by making use of Particle-Tracking Velocimetry, *Journal of Hydraulic Engineering*, JSCE, No.539/II-35, pp.89-98, 1996b (in Japanese).
[5] Nezu, I., Shimura, T., Nakayama, T. and Kamiya, H. : Hydraulic effects on secondary currents in compound open-channel flows, *1st Symposium on Environmental Fluid Mechanics*, Vol.1, pp.331-332, 1996c (in Japanese).
[6] Nezu, I. and Nakayama, T.: Measurements of horizontal coherent vortices between main-channel and flood-plains by using Particle-Tracking Velocimetry, *Flow Modeling and Turbulence Measurements VI*, Chen, Shih, Lienau and Kung (eds.), pp.229-236, 1996d.
[7] Nezu, I. and Nakayama, T. : Space-time correlation structures of horizontal coherent vortices in compound open-channel flows by using particle-tracking velocimetry, *J. Hydraulic Research*, IAHR, Vol.35, No.2, pp.191-208, 1997a.
[8] Nezu, I. and Nakayama, T. : Space-time correlation structures of coherent vortices near the free surface, *Journal of Hydraulic Engineering*, JSCE, No.586/II-42, pp.51-60, 1998b (in Japanese).
[9] Nezu, I. and Nakayama, T. : Effect of the surface-wave fluctuations on coherent structures near the free-surface, *Annual Journal of Hydraulic Engineering*, Vol.42, pp.853-858 1998c (in Japanese).
[10] Nezu, I. and Nakayama, T. : Characteristics of turbulent energy redistribution in an open-channel flow, *Proc. of 1998 Meeting of Japan Society of Fluid Mechanics*, pp.319-320, 1998d (in Japanese).
[11] Nezu, I. and Nakayama, T. : Relationship between bursts and boils in open-channel flows, *Journal of the Visualization Society of Japan*, Vol.18, No.1, pp.137-140, 1998e (in Japanese).
[12] Nezu, I. and Nakayama, T.: Effect of the surface-wave fluctuations on coherent structures near the free surface, *11th Congress of the IAHR-APD*, pp.507-516, 1998g.
[13] Nezu, I. and Nakayama, T.: Turbulent redistribution near the free surface by using numerical simulation, *11th Congress of the IAHR-APD*, pp.537-546, 1998h.
[14] Nezu, I. and Nakayama, T.: Mutual-interaction between bursts and boils very near the free surface in open-channel flows, *Environmental Hydraulics*, J.H.W.Lee *et al.* (eds), Balkema Pub., pp.297-303, 1998k.
[15] Nakayama, T. and Nezu, I. : Bursts near the free surface in open-channel flows and their relationship with turbulence structures, *Journal of Hydraulic Engineering*, JSCE, No.635/II-49, pp.31-40, 1999e (in Japanese).

3.1 Introduction

In an open-channel flow, a free surface has a large effect on the turbulent energy redistribution near the free surface. Davies (1972) and Hunt and Graham (1978) have evaluated theoretically the damping characteristics of the vertical component of turbulence intensity. These effects of the free surface are very important in an open-channel flow and therefore, these characteristics are quite different from those in a duct flow near the plane of symmetry. Furthermore, the turbulence structure becomes quite different from that in a quiet flow and a damping effect on the vertical motions is gradually lost out when the Froude number increases and surface-wave fluctuations occur. Consequently, "*Hunt's theory*" which was proposed in the flow of a smaller Froude number does not hold good near the free surface. At a higher Froude-number flow, a coherent structure, so-called the "*surface renewal eddies*", can be seen clearly at the free surface.

A closer interrelation between the wall region and the free surface region, *i.e.* the bursting and boil phenomena in open-channel flows, has been suggested by some researchers. Gulliver and Harverson (1989) have pointed out that the frequencies of the depth-scale coherent structure and the surface fluctuations due to the surface-renewal eddies have a linear relation with each other. Jackson (1976) described the features of boil vortices from field observations of boils in rivers. He speculated that the bursting motions generated in the wall region would move toward the free surface and form a boil there because the bursting period for boundary layers was roughly equal to the boil period. Komori *et al.* (1989) have related the surface renewal and the bursting motions with each other in view of their frequencies. It is very interesting that Banerjee (1992) has suggested two modes of the interaction between bursts and the free surface motions, *i.e.*, the "*splat pattern*" (pancake-shaped structure) and the "*attached vortex pattern*" (spinning structure), as shown in Fig.3.1. They have implied that both structures seem to occur and persist for some time at the free surface. Komori *et al.* (1993) have used the DNS adopting a boundary fitting condition of the free surface in open-channel flows and clarified the relationship between the generation of surface-renewal eddies and mass-transfer mechanism. Furthermore, Perot and Moin (1995) have estimated that there exist the surface renewal eddies due to the interaction between the splatting structure and the free surface, and that their structures promote the scalar transfer across the air-water interface. However, the situation may be quite different when the Froude number increases and surface-wave fluctuations occur.

In this study, the 3-D turbulence measurements have been conducted accurately with a laser Doppler anemometer (LDA) in order to evaluate the characteristics of turbulence redistribution near the free surface in open-channel flows. Furthermore, we evaluate the spatial scaling of bursts and boils by making use of PIV (Particle-Image Velocimetry) methods. We clarify then the mutual interaction between bursts near the wall and boils near the free surface by estimating the event contribution to the Reynolds shear stress and the period of bursts in the whole depth including the effect of Froude number.

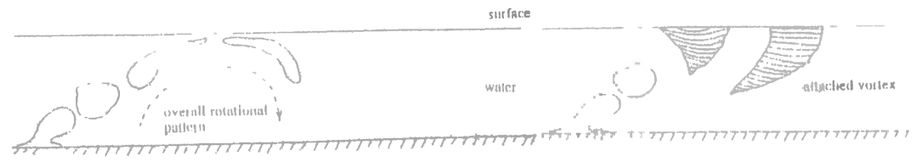

Fig.3.1 Schematic of two modes of the interaction of an ejection with the free surface by Banerjee (1992).

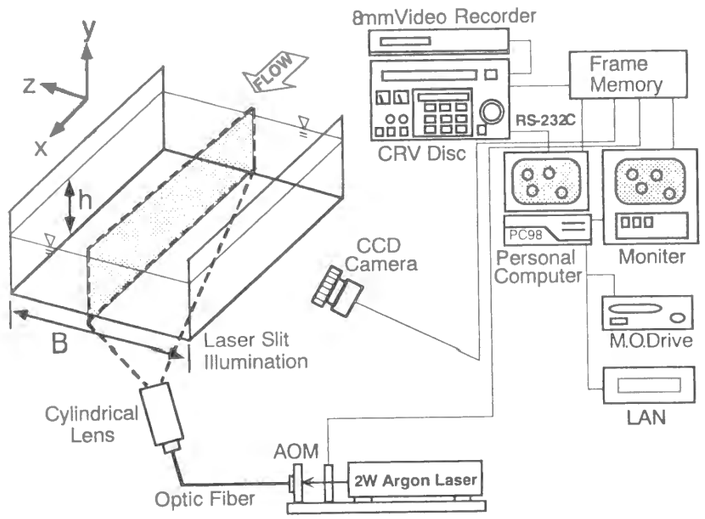

Fig.3.2 Schematic arrangements for the flow visualization and image analyses (PIV).

Table 3.1 Hydraulic conditions in PIV measurements of smooth-bed open-channel flow.

case	S_b	h (cm)	B/h	$A_m h$ ($\times 10^{-2}$)	U_m (cm/s)	U_* (cm/s)	Fr	Re ($\times 10^3$)
L-FR02	1/6000	5.0	8.0	0.0	16.0	0.99	0.23	8.0
M-FR06	1/1200	5.0	8.0	0.6	40.0	2.10	0.57	20.0
M-FR08	1/600	4.0	10.0	1.5	50.0	2.50	0.80	20.0
M-FR10	1/316	3.5	11.4	2.0	57.1	2.90	0.98	20.0
H-FR15	1/167	4.0	10.0	2.5	93.8	4.75	1.50	37.5
H-FR23	1/77	3.0	13.3	3.3	125.0	6.09	2.30	37.5
S-FR31	1/41	3.0	13.3	6.7	166.7	8.47	3.07	50.0

S_b=channel slope, h=flow depth, B=channel width,
A_m=wave height, $Fr=U_m/(gh)^{0.5}$, $Re=U_m h/\nu$

3.2 Experimental Set-Up and Procedures

Schematic arrangements for the present flow visualization and image analyses (PIV) are shown in Fig.3.2 The experiments were conducted in a 10m long, 40cm wide and 40cm deep tilting flume. The side walls of test section 6m downstream of the channel entrance were made of optical glass for LDA (DANTEC-made) and PIV (KANOMAX-made) measurements. Nylon 12 particles (50μm diameter and 1.01 specific gravity) were uniformly scattered in the circulating water of the flume. About 2mm thick laser-light sheet (LLS) was illuminated vertically into the bottom-wall and images of tracers were taken using a high-sensitive CCD camera that was placed beside the side-wall. In this study, one pixel of the image corresponds to the area of 0.4 × 0.4mm. These images were recorded in CRV disc (SONY-made) at the interval of 1/30s and analyzed by the PIV algorithm. Velocity vectors were obtained then at the fixed grid points in PIV, which is more accurate and convenient characteristic of PIV in comparison with PTV (Particle-Tracking Velocimetry) by Maas *et al.* (1993) and Malik *et al.* (1993). More detailed information on the present PIV system is available in Nezu and Nakayama (1998k, 1999e). At that time, 3-D measurements were made in the center of the channel by using a fiber-optic LDA in the same flume. The sampling time was 60sec and the sampling frequency was about 200Hz. Hydraulic conditions for PIV and LDA measurements are indicated in Table 3.1.

3.3 Theoretical Considerations

3.3.1 Turbulence Intensity of Vertical Component v' near Free Surface

Davies (1972) derived a linear expression (3.1) for the vertical intensity v' from continuity equation supposing that the streamwise intensity u' is independent of $y'=h-y$ near the free surface. In this expression, λ represents the thickness of the surface layer of damped turbulence and $v'=v_0$ at $y' \geqq \lambda$ near the free surface.

$$v'/v_0 = y'/\lambda ; y' < \lambda$$
$$v'/v_0 = 1 ; y' \geq \lambda \qquad (3.1)$$

Cowen *et al.* (1995) have confirmed the above equation by using PTV. Furthermore, Hunt and Graham (1978) have analyzed a grid turbulence above the moving bed by using a boundary layer theory and spectral methods and deduced the expression (3.2), where ε is the turbulent energy dissipation near the free surface.

$$v'/U_* = \gamma\left(\varepsilon \cdot h/U_*^3\right)^{1/3}(y'/h)^{1/3} ; \gamma = 1.34 \qquad (3.2)$$

Furthermore, Brumley and Jirka (1987) supposed the expression (3.3) by using Hunt's theory (where p=1.54, λ_2=1.4, g_2=0.558).

$$v'/v_0 = \left[\left(\lambda_2 (y'/h)^{2/3}\right)^{-p} \exp\left(-g_2^{1/2} y'/h\right) + 1\right]^{-1/2p} \qquad (3.3)$$

All these expressions are derived in a quiet flow and it has been pointed out that in particular the expressions (3.2) and (3.3) reproduce well the damping characteristics of v' near the free surface, as shown later.

3.3.2 Eddy Viscosity

The eddy viscosity ν_t for 2-D flow is defined as follows.

$$\nu_t \equiv -\overline{uv}/(\partial U/\partial y) \qquad (3.4)$$

Applying Eq.(2.6), (2.15) and (2.16) to the above equation (3.4), Eq.(3.4) can be transformed into the following equation.

$$\frac{\nu_t}{hU_*} = \frac{\kappa\left[(1-\xi) - V_t\right]}{\xi^{-1} + \pi\Pi \sin(\pi\xi)} \qquad (3.5)$$

This value is dependent on the wake parameter Π near the symmetrical axis of closed-channel flow and near the free surface. Furthermore, it is possible to estimate the following expression by using the concept of a phenomenological mixing-length model.

$$\nu_t \approx v \cdot L_y \qquad (3.6)$$

where L_y represents the vertical scale of macro-eddies.

3.3.3 Conditionally-Averaged Space-Time Correlation Analyses

The non-conditional space-time correlation analyses can be used to evaluate the convection process of turbulent eddy and the macro-scale as mentioned in the former chapter. However, it has a possibility that these space-time averaged correlation-coefficients of velocity fluctuations cancel the phase pattern and the transport phenomenon of coherent structures. For example, it is difficult to separate the sweep event and the ejection event of bursting phenomena by using the non-conditional space-time correlation analyses.

On the other hand, conditionally-averaged space-time correlation analyses are one of the methods to ensemble-average the velocity fluctuations only when there occurs the specific condition and the particular pattern of coherent vortices. Conditionally sampling ensemble-averaged space-time correlations $\langle u_i \rangle$ are defined in the same way as Nakagawa and Nezu (1981), as follows:

$$\langle u_i(x_0,y_0,z_0;\Delta x,\Delta y,\Delta z,\tau)\rangle = \frac{\int_T u_i(x_0+\Delta x,y_0+\Delta y,z_0+\Delta z,t_0+\tau)\cdot I(x_0,y_0,z_0,t_0)dt_0}{u_i'(x_0+\Delta x,y_0+\Delta y,z_0+\Delta z)\cdot\int_T I(x_0,y_0,z_0,t_0)dt_0}$$

$$= \frac{1}{u_i'\cdot M}\sum_{k=1}^{M} q_i(x_0+\Delta x,y_0+\Delta y,z_0+\Delta z,t_k+\tau) \tag{3.7}$$

in which, I : the detection function, τ : the lag time, T : the sampling time, and M : the sampling number, respectively. Lu and Willmarth (1973) have proposed the *u-v* quadrant threshold method, and when the threshold H is based on the Reynolds stress, the detection function I is defined as I=1 (the velocity fluctuations are greater than H) and I=0 (the velocity fluctuations are smaller than H), respectively.

The time fraction $T_i(H)$ and the contribution rate $RS_i(H)$ to the Reynolds stress can be defined as the following equations that are derived by Nezu and Nakagawa (1993).

$$T_i(H)=\int_{-\infty}^{H} p_i(w)dw \le 0,(i=1,3),\ T_i(H)=\int_{H}^{\infty} p_i(w)dw \ge 0,(i=2,4) \tag{3.8}$$

$$T_5(H)=\int_{-H}^{H} p_w(w)dw = 1-\{T_1(H)+T_2(H)+T_3(H)+T_4(H)\} \tag{3.9}$$

$$RS_i(H)=\int_{-\infty}^{H} w\cdot p_i(w)\,dw \le 0,(i=1,3),\ RS_i(H)=\int_{H}^{\infty} w\cdot p_i(w)\,dw \ge 0,(i=2,4) \tag{3.10}$$

$$RS_5(H)=\int_{-H}^{H} w\cdot p_w(w)dw = 1-\{RS_1(H)+RS_2(H)+RS_3(H)+RS_4(H)\} \tag{3.11}$$

where $p_i(w)$: a probability density function (p.d.f.) of instantaneous Reynolds stress, H : a threshold level of the contribution of each event to the Reynolds stress, and the hole event is labeled as event 5. Furthermore, the conventional Reynolds-stress p.d.f. $p_w(w)$ contributed from all events is obtained as follow:

$$p_w(w)=p_1(w)+p_2(w)+p_3(w)+p_4(w) \tag{3.12}$$

Several researchers have pointed out that ejection-line event (u<0, v>0) and sweep-like event (u>0, v<0) are important for evaluating coherent structures. So, in this study, the detection function is defined as follow:

$$I_2=1;\ u<0,v>0\ and\ |uv/(u'v')| \ge H_2$$
$$0;\ otherwise \tag{3.13}$$

$$I_4=1;\ u>0,v<0\ and\ |uv/(u'v')| \ge H_4$$
$$0;\ otherwise \tag{3.14}$$

where H_2 and H_4 are the "*half-value threshold level*" at RS_2=0.5RS_2 (H=0) and RS_4=0.5RS_4 (H=0) in the same way as Nakagawa and Nezu (1981).

3.3.4 Mean Bursting Period

Rao *et al.* (1971) have firstly estimated the mean bursting period in a boundary layer and proposed the following expressions.

$$T_B U_*^2/\nu = 0.65 R_\theta^{0.73} \tag{3.15}$$

$$T_B U_{max}/\delta^* \approx 32 \tag{3.16}$$

where $R_\theta=U_{max}\theta/\nu$, and δ^* and θ are the displacement thickness and momentum thickness, respectively. Laufer and Narayanan (1971) reduced Eq.(3.16) to Eq.(3.17).

$$T_B U_{max}/\delta \approx 5 \tag{3.17}$$

where δ is the boundary layer thickness. Furthermore, Nakagawa and Nezu (1978) have suggested the following expression in open-channel flow.

$$T_B U_{max}/h \approx T_e U_{max}/h \approx T_s U_{max}/h = (1.5-3.0) \tag{3.18}$$

In the above four equations, Eq.(3.15) is at inner-variable expression, whereas Eqs.(3.16)~(3.18) are at outer-variable expressions.

3.4 Characteristics of Turbulence Intensity v'

As mentioned in previous chapter, the turbulence intensity changes in a complicated manner near the free surface, and in particular, the vertical component v' is greatly affected by the free surface. Fig.3.3 shows the distribution of the vertical component of turbulence intensity v' near the free surface normalized by the friction velocity U_* for the case L-FR02 (Re=8000, R_*=450) of franquil flow and H-FR15 (Re=37500, R_*=1900) of the higher Froude number flow, where U_* was calculated by the log-law for primary mean velocity. In this figure, the expressions (Eqs.(3.1), (3.2) and (3.3)) and the DNS data in open-channel flow by Komori *et al.* (1993) are plotted together, where ε in Eq.(3.2) was the constant value near the free surface ($\varepsilon h/U_*^3$=0.8). It can be seen that Eqs.(3.2) and (3.3) coincide well with the experimental value in a tranquil flow (L-FR02). However, v' increases rapidly and Hunt's theory does not hold good when the Froude number increases. Fig.3.4 shows some examples of the

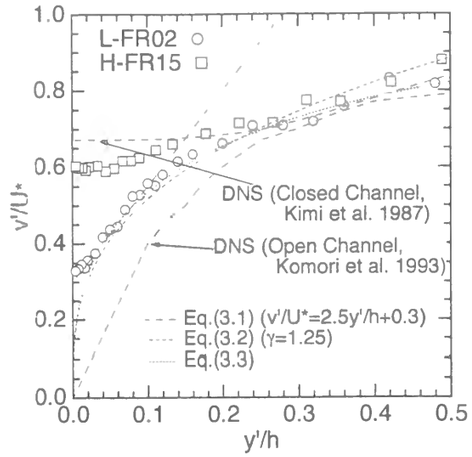

Fig.3.3 Vertical component of turbulence intensity v' near the free surface.

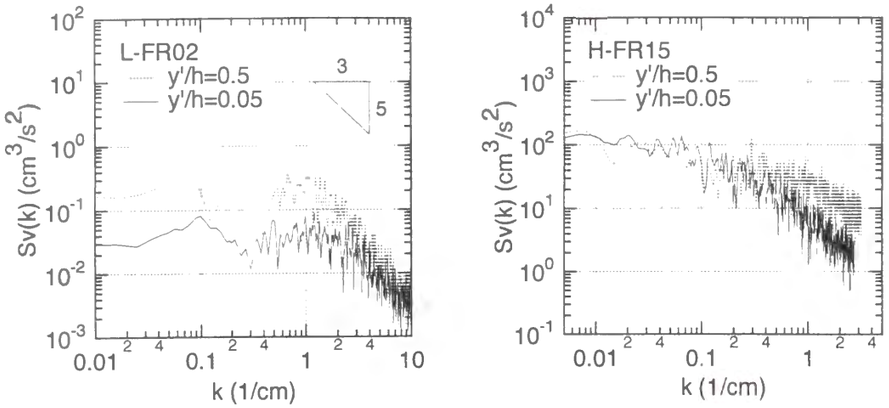

3.4 Spectral distributions $S_v(k)$.

spectral distributions $S_v(k)$ for the fluctuations $v(t)$ versus wave number k. The value of low wave-number near the free surface (y'/h=0.05) decreases in L-FR02, as has been pointed out by Hunt and Graham (1978). However, in a super-critical flow (H-FR15: Fr=1.50), the region of low wave-number does not decrease due to the turbulence eddies near the free surface, which is closely related to the increases of v' near the free surface.

Fig.3.5 is the distribution of experimental value of v' versus the value calculated from Eq.(3.2) by Hunt (1984). It can be seen that Hunt's theory is not applicable in y/h<0.9 because its theory assumes that eddies larger than the distance (h-y) from the free surface would not contribute much to the vertical fluctuations. In y/h>0.9, its theory reproduces well the damping effect in a tranquil flow (L-FR02). However, it is not applicable when Fr increases and the surface-wave fluctuations occur. So, it is necessary to modify its theory in a steep open-channel flow by considering the effect of surface-wave fluctuations.

Fig.3.6 shows the distribution of eddy viscosity ν_t, together with Eq.(3.5) and the DNS data in closed-channel by Kim *et al.* (1987). It can be seen that ν_t approaches zero near the free surface in open-channel flow, whereas ν_t takes a non-zero constant value at the symmetric surface in closed-

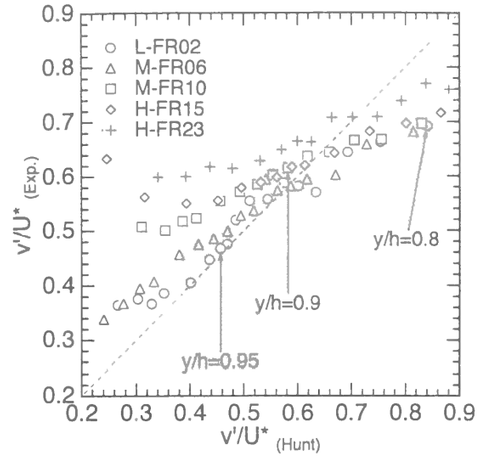

Fig.3.5 Evaluation of Hunt's theory.

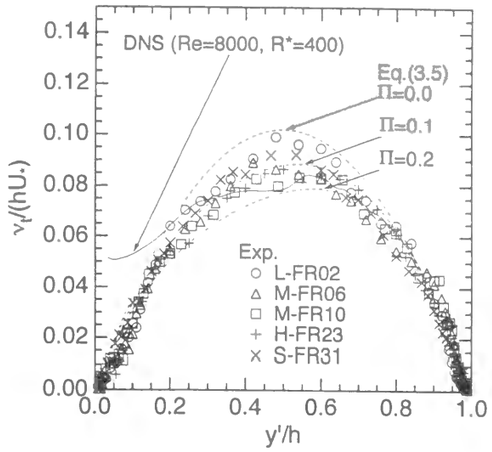

Fig.3.6 Eddy viscosity ν_t.

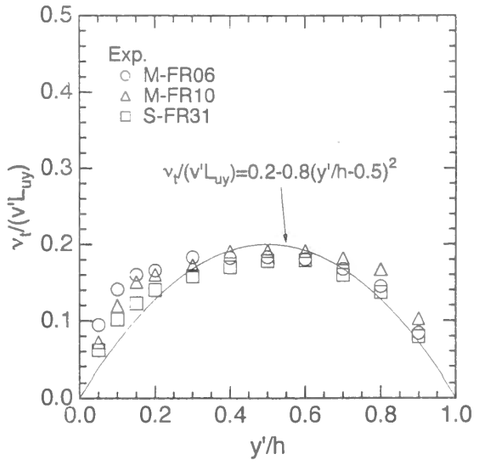

Fig.3.7 Ratio of ν_t to ($v'L_{uy}$).

channel flow. Furthermore, ν_t does not change so greatly in spite of the greater change of v' when the Froude number increases.

Fig.3.7 is the ratio of ν_t to ($v'L_{uy}$). The value of L_{uy} is the same as that in Fig.2.24. In this figure, it can be seen that the distribution is almost independent of the Froude number and Reynolds number. The value takes a maximum near the half of depth and decreases toward the wall and free surface. The approximate curve is also described in this figure. In this way, the value $\nu_t/v'L_{uy}$ is only dependent on the vertical direction, which means that Eq.(3.6) is effective regardless of Froude number.

3.5 Variation of Turbulent Energy Redistributions near Free Surface

For calculating the RSM, it is necessary to define the boundary conditions of turbulent energy redistributions at the free surface. The boundary conditions at the free surface in a tranquil flow are

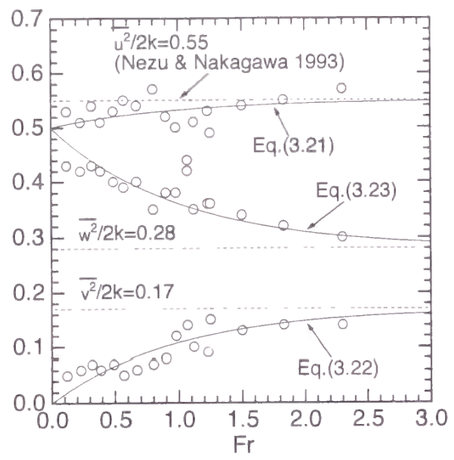

Fig.3.8 Turbulent energy redistributions near the free surface versus Froude number.

given explicitly by Eq.(3.19) and therefore, the turbulent redistributions at the free surface can be expressed by Eq.(3.20).

$$\partial U/\partial y=\partial W/\partial y=V=0;\ y/h=0 \tag{3.19}$$

$$\overline{u^2}/2k=a,\ \overline{v^2}/2k=0,\ \overline{w^2}/2k=b,\ a+b=1;\ y/h=0 \tag{3.20}$$

Furthermore, Davies (1972) has pointed out that the thickness where the damping characteristics are predominant becomes thinner as the vertical fluctuations increase. So, it is predictable that the turbulent redistributions near the free surface approach the constant ratio in an intermediate region derived by Nezu and Nakagawa (1993) with an increase of the Froude number due to the decrease of surface-influenced layer. Therefore, it is better to express the turbulent redistributions by the exponential function. Fig.3.8 shows the turbulent energy redistributions near the free surface (y'/h=0.02) versus Froude number, together with the constant values (dotted line) in Eq.(2.12) derived by Nezu and Nakagawa (1993). Furthermore, solid line is an approximate curve produced by the above-mentioned method ((3.21), (3.22), (3.23)).

$$\overline{u^2}/2k=0.55-0.05\exp(-Fr) \tag{3.21}$$

$$\overline{v^2}/2k=0.17(1-\exp(-Fr)) \tag{3.22}$$

$$\overline{w^2}/2k=0.28+0.22\exp(-Fr) \tag{3.23}$$

It can be seen that the streamwise redistribution almost equals the spanwise redistribution when the Froude number becomes close to zero, so called the "*hydrostatic*". Furthermore, the turbulent redistributions approach the constant ratio in Eq.(2.12), with an increase of the Froude number. In this way, it is because the thickness of the damping predominance becomes thinner than y'/h=0.05 that the region of low wave-number does not decrease in a super-critical flow in Fig.3.4.

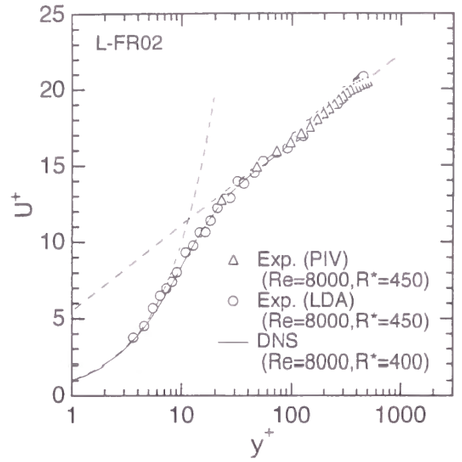

Fig.3.9 Primary mean velocity U^+ (PIV data and DNS data).

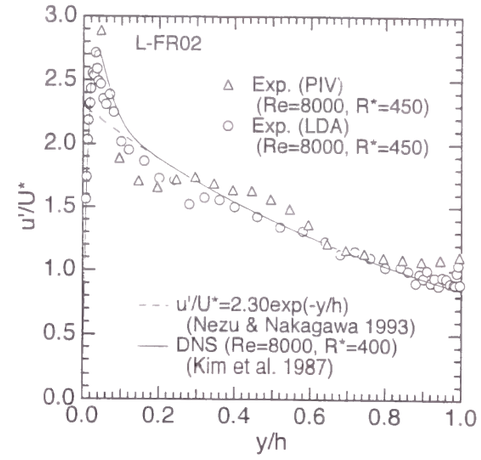

Fig.3.10 Turbulence intensity u'/U_* (PIV data and DNS data)

3.6 Accuracy of PIV Measurements

For the first time, it is necessary to examine the accuracy of the present PIV measurements due to the study of coherent structures. So, some comparisons were made between PIV data and LDA data for the case L-FR02 (Fr=0.23). The distribution of primary mean velocity U normalized by the friction velocity U_*, *i.e.*, $U^+=U/U_*$, is shown in Fig.3.9, together with DNS data of Kim *et al.* (1987) in a closed channel. PIV data agrees very well with LDA data in the log-law region, and consequently PIV is a very powerful and accurate method. Fig.3.10 is the turbulence intensity u' normalized by U_*. The PIV value is a little scattered near the wall and the free surface due to the decrease of mask and search regions. And the PIV value is greater near the free surface (y/h>0.9) due to the lower algorithm of image boundaries. However, even the result of turbulence intensity agrees reasonably well with the LDA data and the advantage of the PIV method is that the instantaneous velocities of an arbitrary points in the LLS can be obtained. The present PIV may be more accurate than the PTV (Particle-Tracking Velocimetry), which Nezu and Nakayama (1997a, 1998b) have used in a compound open-channel flow.

3.7 Instantaneous Velocity Vectors

In this way, the turbulence structure in a steep open-channel flow is closely related with the mutual interaction between the surface-renewal eddies and bursting motions. It is possible that these relations may change when the Froude number increases.

3.7.1 Instantaneous Structures in a Tranquil Flow

In general, the free surface acts as a kind of weak wall in a tranquil flow and the vertical component of turbulence intensity is largely damped near the free surface. Figs.3.11(a)-(b) are the primary component of the instantaneous velocity fluctuations in the center of channel for L-FR02. Fig.3.11(a) is about the various points from the bottom of the wall (y/h=0.1, 0.5 and 0.9), and Fig.3.11(b) is about

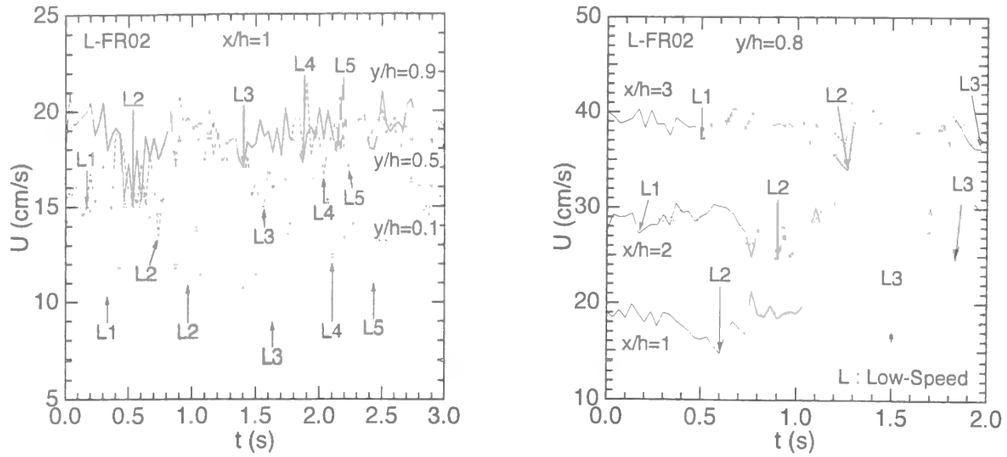

(a) Various points from the bottom of the wall (b) Various points in the streamwise direction

Fig.3.11 Instantaneous velocity fluctuations.

the various points in the streamwise direction (x/h=1, 2 and 3), respectively. In Fig.3.11(b), the velocity values are shifted by 10cm/s at x/h=2 and 3, together with the dotted lines which are shifted from x/h=1 at the convection time.

From Fig.3.11(a), regular fluctuations are shown (L1～L5) due to the generation of the "*bursting phenomena*" and the mean period of vortex generation attains TU_{max}/h=2.2 (U_{max} is a maximum velocity), which is almost coincidence with the mean bursting period (TU_{max}/h=1.5～3.0), as pointed out by Nezu and Nakagawa (1993). Furthermore, the occurrence of peak values (for example, L3) is earlier as the free surface is approached, which implies that the coherent structure is football-shaped as mentioned in the former chapter. The periods near the wall and the free surface take almost the same values, and almost all the burstings generated near the wall lift up to the free surface, as pointed out by Komori *et al.* (1989). Fig.3.11(b) indicates that "*Taylor's frozen-turbulence hypothesis*" is effective.

Fig.3.12 shows an example of velocity vector fields that are viewed in movable coordinates of the bulk mean velocity in the center of channel in the same way as Utami and Ueno (1987). When the Froude number is small in a tranquil flow, the coherent structures generated near the wall about twice the depth as mentioned by Utami and Ueno (1987) are quasi-periodically convected to the streamwise direction, and some of the coherent structures lift up greatly near the free surfa (A and B), which correspond to the regions of low velocity (L) in Fig.3.11. In contrast, due to the damping effect of the free surface, the coherent structures diminish the size and power near the free surface.

The spanwise vorticities Ω ($=\partial u/\partial y-\partial v/\partial x$, clockwise direction is positive) are shown in Fig.3.13, which are normalized by the maximum velocity U_{max} and the flow depth h. The front parts of upward region (A-1 and B-1) attain negative values and back parts (A-2 and B-2) attain positive values. These characteristics agree well with a conceptual model of Nakagawa and Nezu (1981). The coherent regions indicate an inclined angle toward the wall. The contour of instantaneous Reynolds stress $-uv$ at t=0.6s is shown in Fig.3.14, which is normalized by U_*^2. It can be seen that the regions of "*ejection*" (A and B) attain greater value and generate a greater energy than the other regions.

3.7.2 Instantaneous Structures in a Super-Critical Flow

On the other hand, the greater coherent structures can be seen to the streamwise direction when the Froude number is larger than one in a super-critical flow and the surface-wave fluctuations occur.

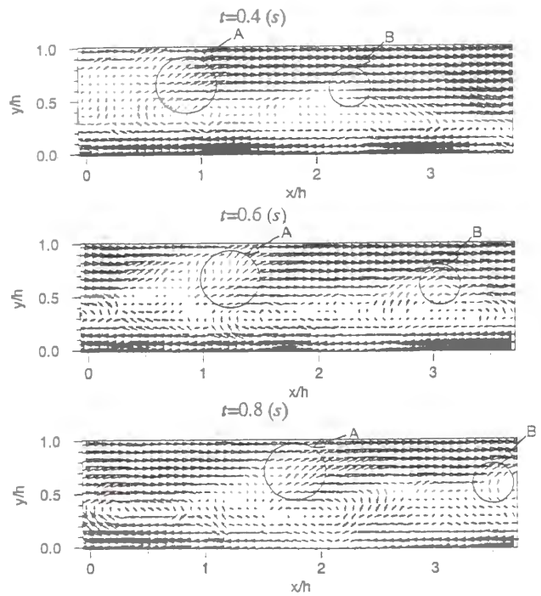

Fig.3.12 Velocity vector fields in tranquil flow (L-FR02).

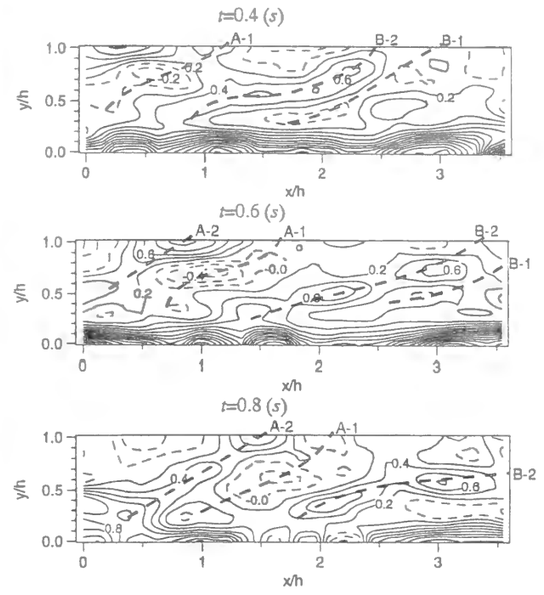

Fig.3.13 Contours of instantaneous spanwise vorticities (L-FR02).

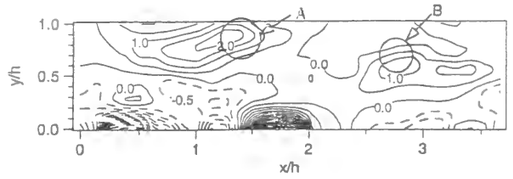

Fig.3.14 Contour of instantaneous Reynolds stress (L-FR02).

Rashidi and Banerjee (1988) have pointed out that the coherent structures bound near the free surface and go back to the wall in such a flow, and Nezu and Nakayama (1998b) have confirmed the bounding phenomena by using simultaneously two sets of LDA. Fig.3.15 is instantaneous velocity vector fields for the case S-FR31 (Fr=3.07). It can be seen that the two coherent vortices (C and D) are generated at the interval of TU_{max}/h=3.3, which coincides well with the mean bursting period by Nakagawa and Nezu (1978) in the same way as L-FR02 in a tranquil flow. Of particular significance is the agglemeration (E) of the coherent vortices at t=0.0s. The period of this vortex is quite larger (TU_{max}/h=9.0) and represents the near value of "*boils* (*surface renewal eddies*)" in rivers, proposed by Jackson (1976). Nezu and Nakagawa (1993) have pointed out that the third kind of boils due to the bursting phenomena predominates on smooth open-channel flow, which means that the agglemeration may occur in steep open-channel flow.

Fig.3.16 shows the spanwise vorticities Ω with respect to Fig.3.15. Some shapes of contours are similar to those for L-FR02 (C and D), but the others are very different and attain a negative value near the free surface due to (E). The region of positive value near the wall (G) is blocked by the generation of negative vorticities near the free surface. In this way, the agglemeration is predominant when the surface-wave fluctuations occur, and therefore boils can be seen clearly on the free surface. Furthermore,

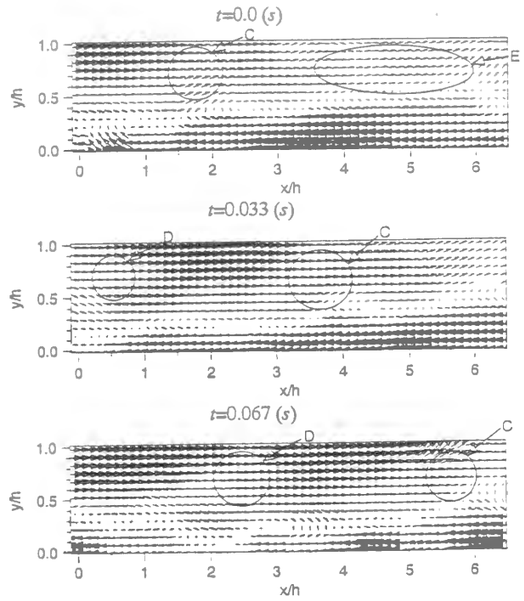

Fig.3.15 Velocity vector fields in super-critical flow (S-FR31).

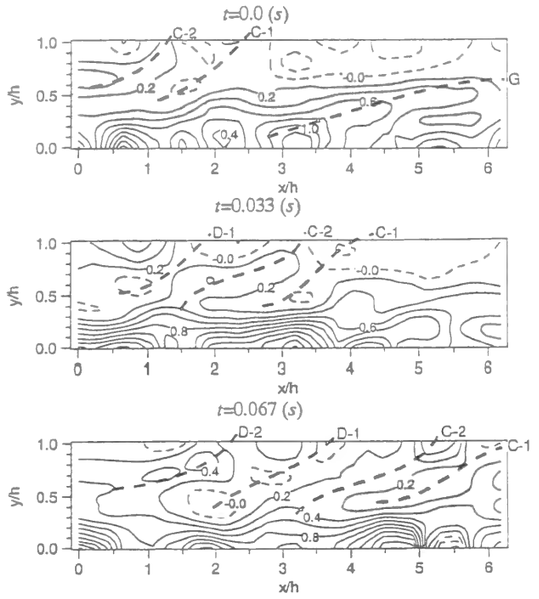

Fig.3.16 Contours of instantaneous spanwise vorticities (S-FR31).

it has a possibility that this agglemeration is closely related to the decrease of the surface-influenced layer (the thickness of the damping predominance).

3.8 Relationship between Bursting Phenomena and Surface-Renewal Eddies

3.8.1 Mean Bursting Period in Open-Channel Flows

As mentioned before, the surface-renewal eddies and bursting motions have a close relationship with each other. Komori *et al.* (1989) have related these coherent structures with each other in view of their frequencies. It is possible that these relations may change when the Froude number increases.

Fig.3.17 is the ratio of the sweep magnitude to the ejection magnitude RS_4/RS_2 in Eq.(3.10), and Fig.3.18 shows the ratio of fraction time T_4/T_2 in Eq.(3.8) at H=0 when the Froude number changes. The value of RS_4/RS_2 decreases with an increase of y/h and then increases at y/h>0.8. On the other hand, the value of T_4/T_2 indicates the opposite characteristics. However, RS_4/RS_2 and T_4/T_2 do not vary with the Froude numbers and they are not affected by the generation of surface-wave fluctuations.

The mean bursting periods normalized by the maximum velocity U_{max} and the flow depth h are shown in Figs.3.19(a)-(b), where T_e and T_s are the ejection and sweep periods in the Quadrant techniques, so-called the "*half-value threshold levels*" by Nezu and Nakagawa (1993). It can be seen that T_e increases with y/h at about y/h<0.7, regardless of the Froude number, but T_s is almost constant in the same region. This indicates that the upward eddies that are generated by bursting in the buffer region near the wall become greater to the extent, but the outer (high-speed) flow goes downward with little deformation. On the other hand, the distributions of T_e and T_s change largely at about y/h>0.7. The value decreases near the free surface when the Froude number is small in a tranquil flow. However, the value increases with an increase of the Froude number. This is closely related with the effect of free surface and the agglemeration occurs in a super-critical flow, and therefore, the period increases

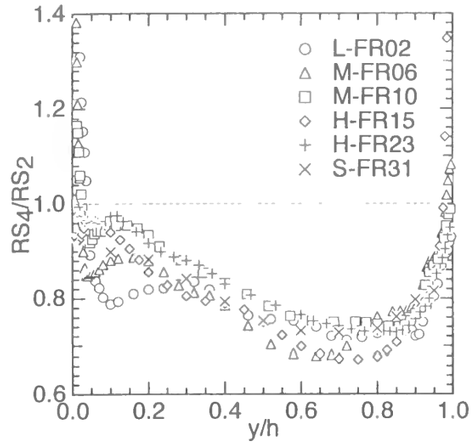

Fig.3.17 Ratio of the sweep magnitude to the ejection magnitude RS_4/RS_2.

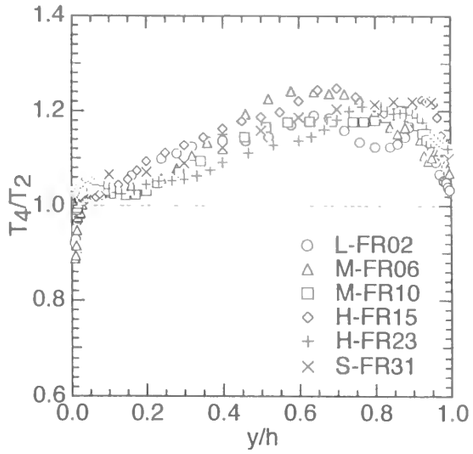

Fig.3.18 Ratio of fraction time T_4/T_2.

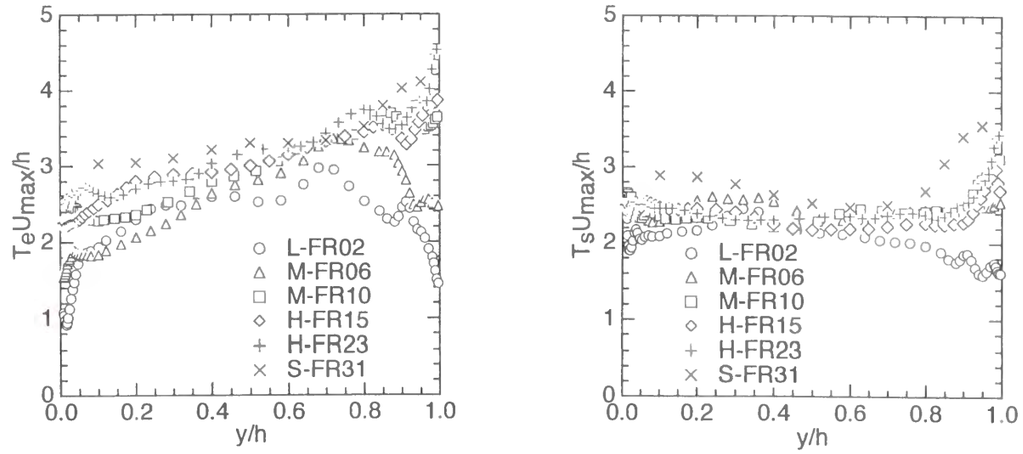

(a) Distribution of T_e (b) Distribution of T_s

Fig.3.19 Mean bursting period.

greatly.

3.8.2 Sampling of Coherent Vortices by Conditionally-Averaged Space-Time Correlation Analyses

Fig.3.20 shows the conditionally-averaged space-time correlation structure <u> in Eq.(3.7) normalized by the turbulence intensity u' in M-FR06 (sub-critical flow), M-FR10 (critical flow) and S-FR31 (super-critical flow) for the fixed point near the wall (y/h=0.1) when the second quadrant (u<0, v>0) is sampled (I_2=1); ejection event. The maximum correlation line fairly inclines downstream toward the wall in the same way as in non-conditional space-time correlation coefficients C_{uu} in Fig.2.23. Furthermore, the peak of ejection increases more greatly than that of sweep as the Froude number increases, which implies that the enlargement of bursting phenomena in the increase of Froude number is mainly due to the enlargement of ejection, that is to say, the upward flow from the wall toward the

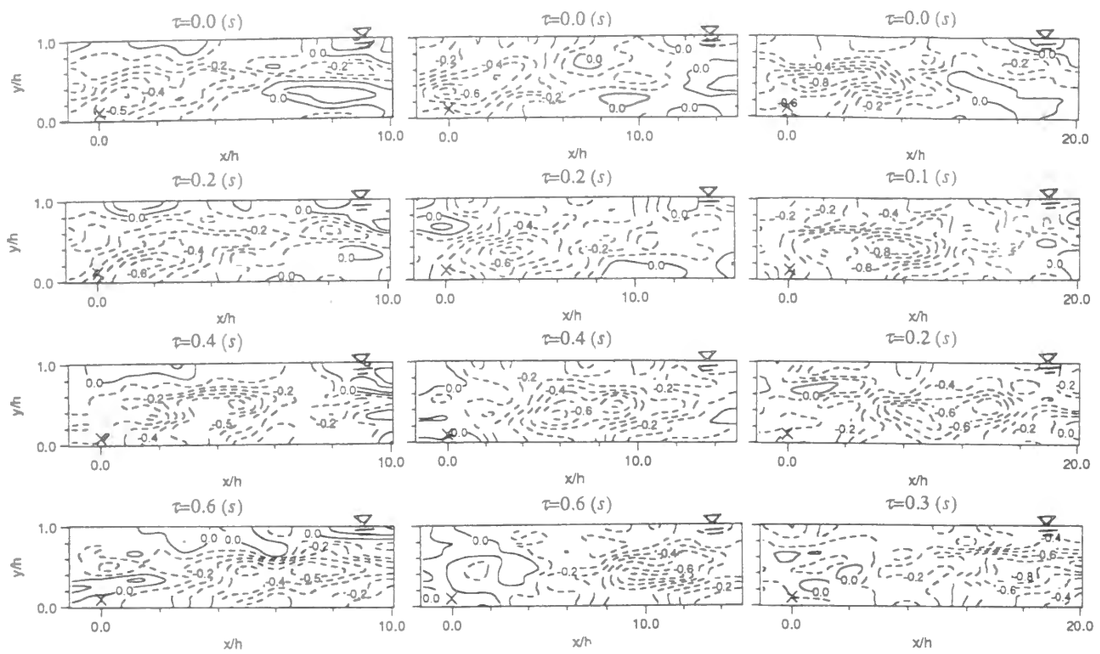

Fig.3.20 Conditionally-averaged space-time correlation structure <u> for the fixed point near the wall (y/h=0.1) when the second quadrant (u<0, v>0) is sampled (I_2=1).

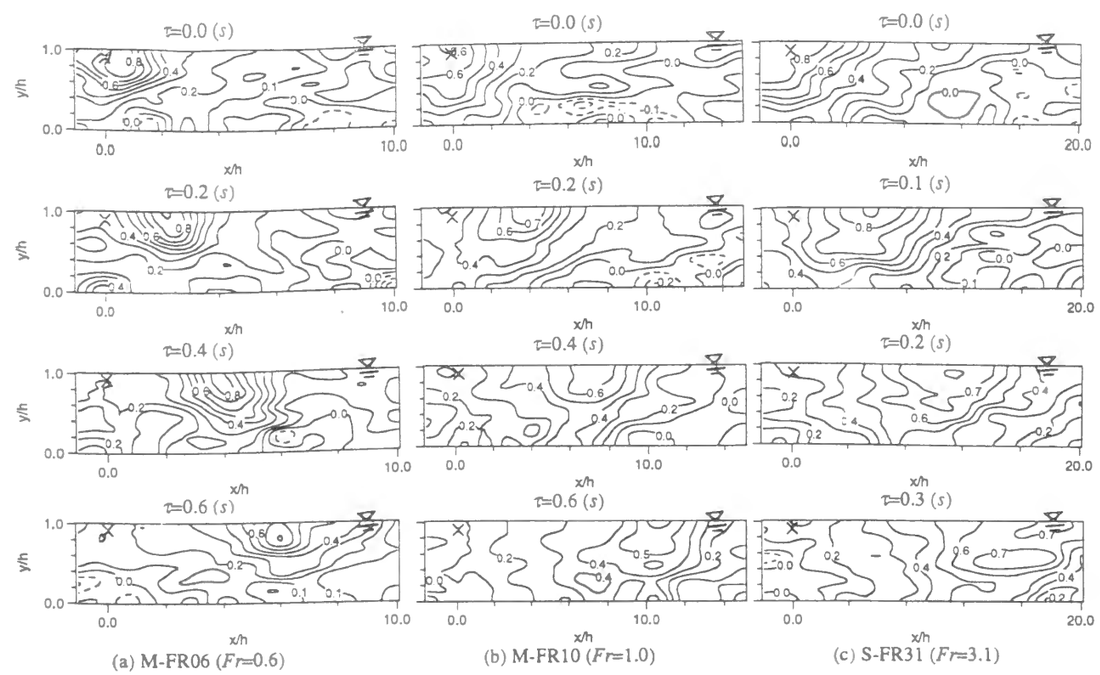

(a) M-FR06 (Fr=0.6) (b) M-FR10 (Fr=1.0) (c) S-FR31 (Fr=3.1)

Fig.3.21 Conditionally-averaged space-time correlation structure <u> for the fixed point near the free surface (y/h=0.9) when the fourth quadrant (u>0, v<0) is sampled (I_4=1).

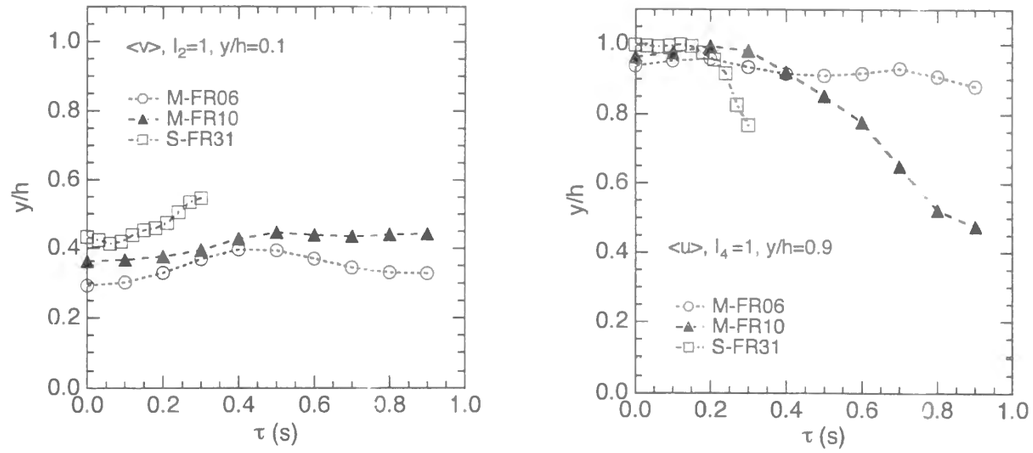

(a) Near the wall (b) Near the free surface

Fig.3.22 Convection process of the peak position of <u> and <v> to the vertical direction.

free surface. The spacial scale of ejection spreads more widely in the streamwise direction than that of sweep, as pointed out by Nakagawa and Nezu (1981) and Krogstad *et al.* (1993).

Fig.3.21 shows the conditionally-averaged space-time correlation structure <u> normalized by the turbulence intensity u' in the same cases as Fig.3.20 for the fixed point near the free surface (y/h=0.9) when the fourth quadrant (u>0, v<0) is sampled (I_4=1); sweep event. In M-FR06, it can be seen that the high correlation region near the free surface is convected to the streamwise direction without moving downward. On the contrary, as the Froude number increases, a vortex with strong correlations (that is to say, a comparatively high-speed flow) moves downward into the wall. This indicates that the coherent structure lifted up from the wall bounds near the free surface and go back into the bulk in a super-critical flow. These phenomena can be seen clearly in Figs.3.22(a)-(b). These figures show the convection process of the peak position of <u> and <v> to the vertical direction versus lag time. As the Froude number increases, the high-correlation region near the wall lifts up more greatly and the region near the free surface goes downward greatly. In this way, the coherent structure near the wall is closely related to that near the free surface, and the mixture of both coherent structures is promoted in super-critical flow.

3.9 Conclusions

In this study, an effect of the surface-wave fluctuations on coherent structures near the free surface was evaluated by using PIV method and LDA. At that time, the boundary conditions at the free surface were defined as the function of Froude number on the basis of LDA data. It is clear that the bursting phenomena are comparatively related with the surface renewal eddies near the free surface and also that the agglemeration is predominant in a super-critical flow. These phenomena have a close relationship with the complexity of the turbulence redistribution near the free surface and it is necessary to evaluate these relations. Fig.3.23 shows the physical model of coherent vortices near the free surface predicted from the chapters 2 and 3, and Fig.3.24 shows the conclusions of chapter 3. When the bursting generated near the wall approaches to the free surface, the damping characteristics of turbulence change greatly depending on whether or not the surface-wave fluctuations occur and the similarity formula does not

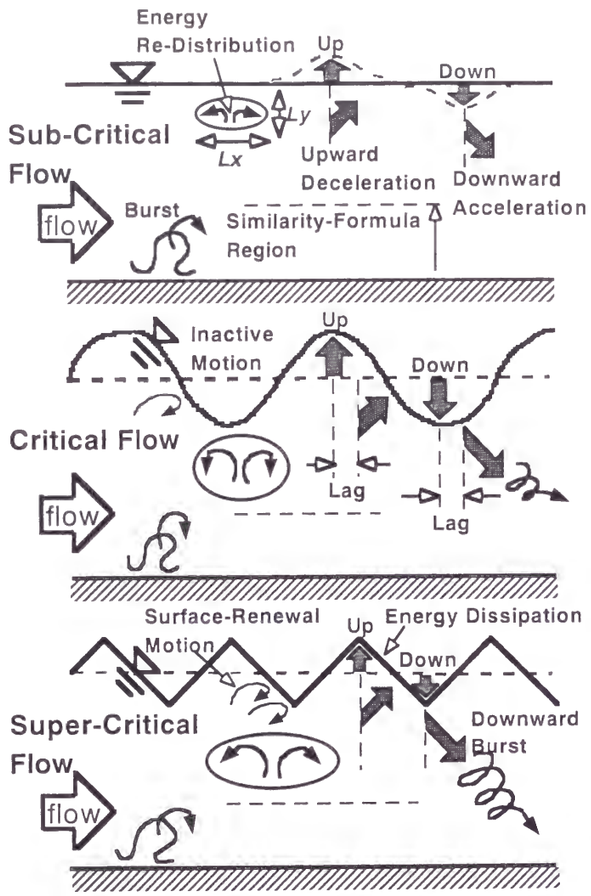

Fig.3.23 Physical model of coherent vortices near the free surface.

become effective. In a sub-critical flow without waves, the energy is mainly redistributed from the vertical component of velocity fluctuations to the streamwise and spanwise components, which results in the decrease of the vertical component of macro-scale. Near the critical flow, the flow becomes unstable due to the predominance of inactive component, and the turbulence characteristics and the surface-wave fluctuations increase rapidly. At that time, the shift in phase between the velocities and waves has a maximum and the macro-scale increases vertically due to the decrease of downward flow near the free surface. In a super-critical flow, the surface-renewal eddies predominate and the energy dissipation becomes greater near the free surface, and the higher-speed downward flow occurs. In this situation, there is little shift in phase and the flow becomes stable again. The macro-scale increases greatly, in particular, to the streamwise direction. In this way, the turbulence and coherent structures near the free surfac in open-channel flow are closely related to the surface-waves, which has an important role on the mass transfer across the air-water interfaces.

Notations

A_m : wave amplitude

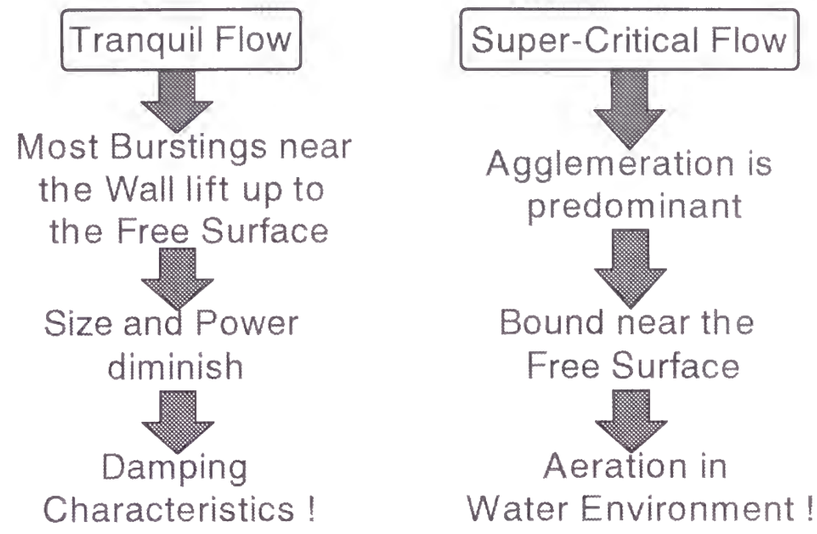

Fig.3.24 Conclusions of chapter 3.

B : channel width
Fr : Froude number ($=U_m/\sqrt{gh}$)
G : turbulent generation (or production)
g : acceleration due to gravity
H : threshold level of the contribution of each event to the Reynolds stress
H_2, H_4 : half-value threshold level
h : flow depth
I : detection function
k : turbulent kinetic energy, wave number
L_y : vertical scale of macro-eddies
M : sampling number
$p_i(w)$: probability density function of instantaneous Reynolds stress
Re : Reynolds number ($=U_m h/\nu$)
$RS_i(H)$: contribution rate of i-th event
S_b : channel slope
T : sampling time
T_B : mean bursting period
T_e : ejection period in the Quadrant techniques
$T_i(H)$: time fraction of i-th event
T_s : sweep period in the Quadrant techniques
U_m : bulk mean velocity
U_{max} : maximum velocity
U_* : friction velocity
u : instantaneous streamwise velocity component
u' : root-mean-square value of velocity fluctuations in x direction
$<u_i>$: conditionally-averaged space-time correlation

$-\overline{uv}$: Reynolds stress
$\overline{u^2}/2k$, $\overline{v^2}/2k$, $\overline{w^2}/2k$: turbulent energy redistributions
v : instantaneous vertical velocity component
v' : root-mean-square value of velocity fluctuations in y direction
w : instantaneous spanwise velocity component
w' : root-mean-square value of velocity fluctuations in z direction
x : streamwise direction
y : vertical direction from the channel bed
y' : distance from the free surface ($=h-y$)

Greek symbols
(Δx, Δy, Δz) : lag distance
ε : turbulent energy dissipation rate
λ : thickness of the surface layer of damped turbulence
ν : kinetic viscosity
ν_t : eddy viscosity
η : instantaneous surface displacement with respect to the still water level
η' : intensity of surface-wave fluctuations ($=\sqrt{\overline{\eta^2}}$)
τ : lag time
Ω : instantaneous spanwise vorticity ($=\partial u/\partial y-\partial v/\partial x$, clockwise direction is positive)

References

[1] Ashworth, P.J., Bennett, S.J., Best, J.L. and McLelland, S.J. : Coherent flow structures in open channels, John Wiley and Sons Ltd., 1996.
[2] Antonia, R.A., Bisset, D.K. and Browne, L.W.B. : Effect of Reynolds number on the topology of the organized motion in a turbulent boundary layer, *J. Fluid Mech.*, Vol.213, pp.267-286, 1990.
[3] Banerjee, S. : Turbulence structures, *Chemical Engineering Science*, Vol.47, No.8, pp.1793-1817, 1992.
[4] Brumley, B. H. and Jirka, G. H. : Near-surface turbulence in a grid-stirred tank, *J. Fluid Mech.*, Vol.183, pp.235-263, 1987.
[5] Cowen, E.A., Monismith, S.G. and Koseff, J.R. : Digital particle tracking velocimetry measurements very near a free-surface, *Air-Water Gas Transfer*, B. Jahne and E.C. Monahan (eds.), AEON Verlag, pp.135-144, 1995.
[6] Davies, J. T. : Turbulence Phenomena, Academic Press, San Francisco, 1972.
[7] Gulliver, J. S. and Halverson, M. J. : Air-water gas transfer in open channels, *Water Resources Res.*, Vol.25, No.8, pp.1783-1793, 1989.
[8] Hunt, J. C. R. : Turbulence structure and turbulent diffusion near gas-liquid interfaces, *Gas Transfer at Water Surfaces*, W. Brutsaert and G. H. Jirka (eds.), Reidel Pub., pp.67-82, 1984.
[9] Hunt, J. C. R. and Graham, J. M. R. : Free-stream turbulence near plane boundaries, *J. Fluid Mech.*, Vol.84, pp.209-235, 1978.
[10] Jackson, R. G. : Sedimentological and fluid-dynamic implications of the turbulent bursting phenomenon in geophysical flows, *J. Fluid Mech.*, Vol.77, pp.531-560, 1976.
[11] Kim, J., Moin, P. and Moser, R. : Turbulence statistics in fully developed channel flow at low Reynolds number, *J. Fluid Mech.*, Vol.177, pp.133-166, 1987.
[12] Komori, S., Murakami, Y. and Ueda, H. : The relationship between surface renewal and bursting

motions in an open-channel flow, *J. Fluid Mech.*, Vol.203, pp.103-123, 1989.
[13] Komori, S., Nagaosa, R., Murakami, Y., Chiba, S., Ishii, K. and Kuwahara, K. : Direct numerical simulation of three-dimensional open-channel flow with zero-shear gas-liquid interface, *Phys. Fluids A*, Vol.5, No.1, pp.115-125, 1993.
[14] Krogstad, P.-A., Antonia, R.A. and Browne, L.W.B. : The use of orthogonal X-wire arrays for structure investigation in a turbulent boundary layer, *Experiments in Fluids*, Vol.15, pp.231-239, 1993.
[15] Krogstad, P.-A., Antonia, R.A. and Browne, L.W.B. : Comparison between rough- and smooth-wall turbulent boundary layers, *J. Fluid Mech.*, Vol.245, pp.599-617, 1992.
[16] Maas, H.G., Gruen, A. and Papantoniou, D.A. : Particle tracking velocimetry in three-dimensional flows ; Part 1. Photogrammetric determination of particle coordinates, *Experiments in Fluids*, Vol.15, pp.133-146, 1993.
[17] Laufer, J. and Narayanan, M.A.B. : Mean period of the turbulent production mechanism in a boundary layer, *Phys. Fluids*, Vol.14, pp.182-183, 1971.
[18] Lu, S.S. and Willmarth, W.W. : Measurements of the structure of the Reynolds stress in a turbulent boundary layer, *J. Fluid Mech.*, Vol.60, pp.481-511, 1973.
[19] Malik, N.A., Dracos, Th. and Papantoniou, D.A. : Particle tracking velocimetry in three-dimensional flows ; Part 2. Particle tracking, *Experiments in Fluids*, Vol.15, pp.279-294, 1993.
[20] Nakagawa, H. and Nezu, I. : Bursting phenomenon near the wall in open-channel flows and its simple mathematical model, *Memoirs, Faculty of Eng.*, Kyoto University, Vol.40, pp.213-240, 1978.
[21] Nakagawa, H. and Nezu, I. : Structure of space-time correlations of bursting phenomena in an open-channel flow, *J. Fluid Mech.*, Vol.104, pp.1-43, 1981.
[22] Nakayama, T. : Turbulent structures and characteristics of coherent vortices near the free surface, *M.E. Thesis presented to Kyoto University*, 1997 (in Japanese).
[23] Nezu, I. and Nakagawa, H. : Turbulence in open-channel flows, IAHR Monograph, Balkema, 1993.
[24] Nezu, I., Abe, T., Shimura, T. and Nakayama, T. : Characteristics of compound open-channel flows with FLDA and PTV, *Proc. of 2nd Symposium on River Hydraulics and Environments*, pp.45-52, 1995 (in Japanese).
[25] Nezu, I., Shimura, T. and Nakayama, T. : Analyses of coherent vortices between main-channel and flood-plains by means of PTV, *Annual Journal of Hydraulic Engineering*, Vol.40, pp.1059-1064, 1996a (in Japanese).
[26] Nezu, I., Abe, T., Shimura, T. and Nakayama, T. : Space-time correlation analysis in compound open-channel flows by making use of Particle-Tracking Velocimetry, *Journal of Hydraulic Engineering*, JSCE, No.539/II-35, pp.89-98, 1996b (in Japanese).
[27] Nezu, I., Shimura, T., Nakayama, T. and Kamiya, H. : Hydraulic effects on secondary currents in compound open-channel flows, *1st Symposium on Environmental Fluid Mechanics*, Vol.1, pp.331-332, 1996c (in Japanese).
[28] Nezu, I. and Nakayama, T.: Measurements of horizontal coherent vortices between main-channel and flood-plains by using Particle-Tracking Velocimetry, *Flow Modeling and Turbulence Measurements VI*, Chen, Shih, Lienau and Kung (eds.), pp.229-236, 1996d.
[29] Nezu, I. and Nakayama, T. : Space-time correlation structures of horizontal coherent vortices in compound open-channel flows by using particle-tracking velocimetry, *J. Hydraulic Research*, IAHR, Vol.35, No.2, pp.191-208, 1997a.
[30] Nezu, I. and Nakayama, T. : Space-time correlation structures of coherent vortices near the free surface, *Journal of Hydraulic Engineering*, JSCE, No.586/II-42, pp.51-60, 1998b (in Japanese).
[31] Nezu, I. and Nakayama, T. : Effect of the surface-wave fluctuations on coherent structures near the free-surface, *Annual Journal of Hydraulic Engineering*, Vol.42, pp.853-858, 1998c (in Japanese).

[32] Nezu, I. and Nakayama, T. : Characteristics of turbulent energy redistribution in an open-channel flow, *Proc. of 1998 Meeting of Japan Society of Fluid Mechanics*, pp.319-320, 1998d (in Japanese).
[33] Nezu, I. and Nakayama, T. : Relationship between bursts and boils in open-channel flows, *Journal of the Visualization Society of Japan*, Vol.18, No.1, pp.137-140, 1998e (in Japanese).
[34] Nezu, I. and Nakayama, T.: Effect of the surface-wave fluctuations on coherent structures near the free surface, *11th Congress of the IAHR-APD*, pp.507-516, 1998g.
[35] Nezu, I. and Nakayama, T.: Turbulent redistribution near the free surface by using numerical simulation, *11th Congress of the IAHR-APD*, pp.537-546, 1998h.
[36] Nezu, I. and Nakayama, T.: Mutual-interaction between bursts and boils very near the free surface in open-channel flows, *Environmental Hydraulics*, J.H.W.Lee *et al.* (eds), Balkema Pub., pp.297-303, 1998k.
[37] Nakayama, T. and Nezu, I. : Bursts near the free surface in open-channel flows and their relationship with turbulence structures, *Journal of Hydraulic Engineering*, JSCE, No.635/II-49, pp.31-40, 1999e (in Japanese).
[38] Perot, B. and Moin, P. : Shear-free turbulent boundary layers. Part 1. Physical insights into near-wall turbulence, *J. Fluid Mech.*, Vol.295, pp.199-227, 1995.
[39] Rashidi, M. and S. Banerjee : Turbulence structure in free-surface channel flows, *Phys. Fluids*, Vol.31, No.9, pp.2491-2503, 1988.
[40] Rao, K.N., Narasimha, R. and Rarayanan, M.A.B. : The 'bursting' phenomenon in a turbulent boundary layer, *J. Fluid Mech.*, Vol.48, pp.339-352, 1971.
[41] Utami, T. and Ueno, T. : Experimental study on the coherent structure of turbulent open-channel flow using visualization and picture processing, *J. Fluid Mech.*, Vol.174, pp.399-440, 1987.

CHAPTER 4

TURBULENT REDISTRIBUTION NEAR FREE SURFACE BY USING NUMERICAL SIMULATION INCLUDING EFFECT OF ANISOTROPY

Abstract

Numerical simulation was conducted by using Reynolds stress model (RSM) at a new boundary condition of the free surface including the effect of Froude number. The pressure-strain terms were corrected in steep open-channel flows, and as a result, the turbulent redistributions were more accurately reproduced. This means that the turbulent redistributions near the free surface are greatly affected by the pressure-strain terms.

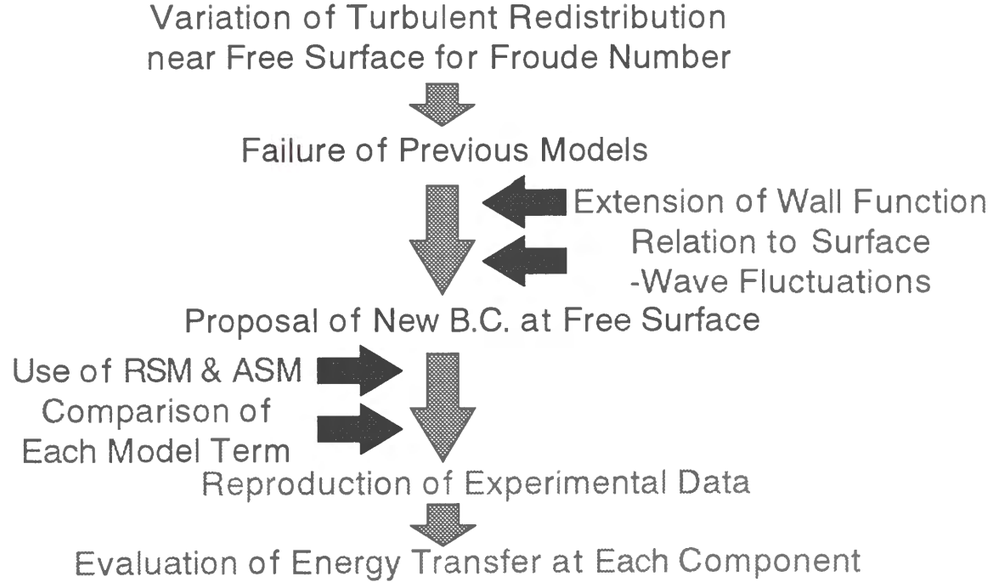

CHAPTER 4 TURBULENT REDISTRIBUTION NEAR FREE SURFACE BY USING NUMERICAL SIMULATION INCLUDING EFFECT OF ANISOTROPY

Parts of this chapter were presented and submitted in the following papers.

[1] Nezu, I. and Nakayama, T. : Relationship between turbulent structures near the free-surface and surface-wave-fluctuations, *J. Hydraulic Engrg.*, JSCE, No.593/II-43, pp.69-78, 1998a (in Japanese).
[2] Nezu, I. and Nakayama, T.: Turbulent redistribution near the free surface by using numerical simulation, *11th Congress of the IAHR-APD*, pp.537-546, 1998h.
[3] Nezu, I. and Nakayama, T.: Mutual-interaction between bursts and boils very near the free surface in open-channel flows, *Environmental Hydraulics*, J.H.W.Lee *et al.* (eds.), Balkema Pub., pp.297-303, 1998k.
[4] Nakayama, T. and Nezu, I. : Bursts near the free surface in open-channel flows and their relationship with turbulence structures, *Journal of Hydraulic Engineering*, JSCE, No.635/II-49, pp.31-40, 1999e (in Japanese).
[5] Nakayama, T. and Nezu, I. : Numerical simulation of turbulence structures near the free surface by using Reynolds Stress Model, *Journal of Hydraulic Engineering*, JSCE, 1999g (in Japanese, to be accepted).
[6] Nezu, I. and Nakayama, T : Numerical calculation of steep open-channel flows by considering effects of surface-wave fluctuations, *Proc. of Water, Environment, Ecology, Socio-Economics, and Health Engineering*, pp.33-48, 1999j.
[7] Nezu, I. and Nakayama, T. : Numerical simulation of steep open-channel flows by using RSM, *Proc. of 1999 Meeting of Japan Society of Fluid Mechanics*, pp.383-384, 1999k (in Japanese).

4.1 Introduction

In an open-channel flow, a free surface has a significant effect on the turbulent energy redistribution near the free surface. In particular, the turbulence structure of a steep open-channel flow is quite different from that of a quiet flow and a damping effect on the vertical motions is gradually lost out when the Froude number increases and the surface-wave fluctuations occur, as pointed out by Nezu and Nakayama (1998a). Recently, some researchers, for example, Komori *et al.* (1993), Handler *et al.* (1993), and Nagaosa and Saito (1997) have conducted a direct numerical simulation (DNS) in open-channel flow due to the development of computers, and clarified the relationship between turbulent energy redistribution and coherent structure near the free surface. Perot and Moin (1995) have studied the structure of "*splats*" and "*antisplats*" near the free surface and evaluated the relation between these structures and the pressure-strain terms. However, these calculations were conducted in low-Reynolds-number flows. It is, however, still difficult to calculate a steep open-channel flow with larger surface-wave fluctuations. In this situation, it is still convenient to use the Reynolds stress model (RSM) in order to calculate steep open-channel flows because of a short calculation time and a low capacity of computer, as compared with large-eddy simulation (LES) and DNS.

Demuren and Sarkar (1993) investigated the roles of pressure-strain and turbulent diffusion models in the numerical calculation of closed-channel flow using the RSM. They pointed out that the Speziale-Sarkar-Gastki model (SSG) for pressure-strain terms reproduces the experiment very well. On the other hand, Naot *et al.* (1993) have calculated an argebraic stress model (ASM) in open-channel flows. They compared Hossain and Rodi (1980) model and Naot-Yacoub-Moalem (1989) model of the free-surface boundary condition for the turbulent energy dissipation rate ε. They pointed out that both models are very effective in open-channel flows, and that the former is identified as the special case of the latter.

Furthermore, Nezu and Nakayama (1998k) have compared the experimental data with the previous turbulence model considering the effect of damping characteristics near the free surface in open-channel flows, so called, the "*Hunt's theory*" (Hunt and Graham, 1978). They pointed out that this model which was proposed in the flow at a smaller Froude number does not hold good at all near the free surface in steep open-channel flows. They suggested the exponential function of the turbulent redistributions as free-surface boundary conditions because the thickness where the damping characteristics are predominant becomes thinner as the vertical fluctuations increase, as pointed out by Davies (1972). Therefore, the turbulent redistributions near the free surface approach a constant ratio in an intermediate region ($50<y^+<0.6R_*$) derived by Nezu and Nakagawa (1993) with an increase of the Froude number due to the decrease of the "*surface-influenced layer*". They calculated the RSM by using these boundary conditions at the free surface and showed the coincidence between the measured data and the calculated ones.

Nakayama and Yokojima (1999) have considered the intermittency of the large-eddy structure which interacts with the free surface and conducted a modelling of the equations for the mean free-surface position and the fluctuations of the free surface by using k-ω model. They showed a predictive accuracy of this model for a step flow accompanying the local surface variation. Borue *et al.* (1995) have conducted the DNS in the flow with small-amplitude gravity waves by assuming linearization of the boundary conditions at the free surface. Tsai (1998) also computed the DNS by considering the pressure variations due to the surface-wave fluctuations and considered the relationship between the coherent structures ("*surface renewal eddies*"), so called, the "*splatting*" and "*swirling*" events. However, these models are only applicable to sub-critical flows with small surface-wave fluctuations.

In this study, a numerical simulation was conducted by using Reynolds stress model (RSM) at a new boundary condition of the free surface including the effect of Froude number. The turbulent

Table 4.1 Hydraulic conditions in RSM of smooth-bed open-channel flow.

case	S_b	h (cm)	B/h	A_m/h (x10^{-2})	U_m (cm/s)	U_* (cm/s)	Fr	Re (x10^3)
run1	1/6000	5.0	8.0	0.0	16.0	0.99	0.23	8.0
run2	1/600	4.0	10.0	1.5	50.0	2.50	0.80	20.0
run3	1/167	4.0	10.0	2.5	93.8	4.75	1.50	37.5

S_b=channel slope, h=water depth, B=channel width,
A_m=wave height, $Fr=U_m/(gh)^{0.5}$, $Re=U_m h/\nu$

redistributions were well reproduced by correcting the pressure-strain terms in a steep open-channel flow. It was concluded that the pressure-strain term affects greatly the turbulent redistributions near the free surface.

4.2 Experimental Conditions and Calculation Procedures

4.2.1 Experimental Procedures

The experiments were conducted in a 10m long, 40cm wide and 40cm deep tilting flume, the same flume in the former chapter. The side and bed walls of the test section 6m downstream of the channel entrance were made of optical glass for LDA (DANTEC-made) measurements. The 3-D measurements were made in the center of the channel by using a fiber-optic LDA. The sampling time was 60sec and the sampling frequency was about 200Hz. At that time, an ultrasonic depth-meter instrument (KEYENCE-made, 1/10mm accuracy) was set above the free surface and synchronized with the LDA. Hydraulic conditions for the experiments are shown in Table 4.1. The parameters are defined as follows, h : the flow depth, A_m : the wave amplitude, U_m : the bulk mean velocity and U_* : the friction velocity, respectively. In this study, the aspect ratio was greater, *i.e.*, $B/h>5$, for two dimensional (2-D) flow with smooth bed, and the Froude number Fr ($=U_m/\sqrt{gh}$) was changed for several stages, so called, run1 : a sub-critical flow with flat surface, run2 : near a critical flow, and run3 : a super-critical flow with large surface-wave fluctuations, respectively.

4.2.2 Fundamental Equations of Reynolds Stress Model

Calculation was conducted in a 2-D fully-developed open-channel flow (the aspect ratio was greater than 5 in the experiment as pointed out by Nezu and Nakagawa (1993)) by using Reynolds stress model (RSM). Coordinate axes in a streamwise, vertical and spanwise directions are defined as x, y and z, and the corresponding velocity fluctuations are u, v and w, respectively. The basic equations are given by a continuity equation (4.1), a momentum equation (4.2), Reynolds stress equations (4.3) and a dissipation equation (4.4), as follows:

$$\frac{\partial U_i}{\partial x_i}=0 \tag{4.1}$$

$$\frac{DU_i}{Dt}=g_i-\frac{1}{\rho}\frac{\partial P}{\partial x_i}-\frac{\partial \overline{u_i u_j}}{\partial x_j}+\nu\frac{\partial^2 U_i}{\partial x_j \partial x_j} \tag{4.2}$$

$$\frac{D\overline{u_i u_j}}{Dt}=D_{ij}+G_{ij}+\phi_{ij}-\varepsilon_{ij} \tag{4.3}$$

$$\frac{D\varepsilon}{Dt}=c_\varepsilon\frac{\partial}{\partial y}\left(\frac{k}{\varepsilon}\overline{v^2}\frac{\partial \varepsilon}{\partial y}\right)-c_{\varepsilon 1}\frac{k}{\varepsilon}\overline{uv}\frac{\partial U}{\partial y}-c_{\varepsilon 2}\frac{k^2}{\varepsilon} \tag{4.4}$$

where u_i, k and ε are the components of velocity fluctuations, turbulent kinetic energy and turbulent energy dissipation rate, respectively. C_ε(=0.15), $C_{\varepsilon 1}$(=1.44) and $C_{\varepsilon 2}$(=1.92) are model parameters, and D_{ij} : the diffusion term for Daly-Harlow model (GGDH) (Eq.(4.5)), G_{ij} : the generation term (Eq.(4.6)), ϕ_{ij} : the pressure-strain term for Speziale-Sarkar-Gastki model (SSG, 1991) (Eq.(4.7)) superior to Launder-Reece-Rodi model (LRR, 1975) as have been pointed out by many researchers, and ε_{ij} : the dissipation term for Hallback model (1990) (Eq.(4.8)), respectively.

$$D_{ij}=c_s\frac{\partial}{\partial y}\left(\frac{k}{\varepsilon}\overline{v^2}\frac{\partial \overline{u_i u_j}}{\partial y}\right) \tag{4.5}$$

$$G_{ij}=-\overline{u_i v}\frac{\partial U_j}{\partial y}-\overline{u_j v}\frac{\partial U_i}{\partial y} \tag{4.6}$$

$$\phi_{ij}=\beta_0\varepsilon b_{ij}+\beta_1\varepsilon\left(b_{ik}b_{jk}-\frac{1}{3}b_{mn}b_{mn}\delta_{ij}\right)+\beta_2 k S_{ij}+\beta_3 G_k b_{ij}$$
$$+\beta_4 k\left(b_{ik}S_{jk}+b_{jk}S_{ik}-\frac{2}{3}b_{mn}S_{mn}\delta_{ij}\right)+\beta_5 k\left(b_{ik}W_{jk}+b_{jk}W_{ik}\right)$$
$$+c_3\frac{k}{\varepsilon}\left(\overline{v^2}\delta_{ij}-\frac{3}{2}\overline{u_i v}\delta_{j2}-\frac{3}{2}\overline{u_j v}\delta_{i2}\right)f_s \tag{4.7}$$

$$\varepsilon_{ij}=\varepsilon e_{ij}+\frac{2}{3}\varepsilon\delta_{ij},\ e_{ij}=2\left[1+2\alpha\left(b_{mn}b_{mn}-\frac{1}{3}\right)\right]b_{ij}-4\alpha\left(b_{ik}b_{jk}-\frac{1}{3}b_{mn}S_{mn}\delta_{ij}\right) \tag{4.8}$$

$$b_{ij}=\frac{\overline{u_i u_j}}{2k}-\frac{1}{3}\delta_{ij},\ S_{ij}=\frac{1}{2}\left(\frac{\partial U_i}{\partial x_j}+\frac{\partial U_j}{\partial x_i}\right),\ W_{ij}=\frac{1}{2}\left(\frac{\partial U_i}{\partial x_j}-\frac{\partial U_j}{\partial x_i}\right),$$

$$f_s=\left[\frac{L}{(h-y)+c_f L}\right]^2,\ L=\frac{C_\mu^{3/4}k^{3/2}}{\kappa\varepsilon} \tag{4.9}$$

where b_{ij} : the anisotropy tensor, S_{ij} : the rate of strain tensor, W_{ij} : the rotation tensor, and G_k : the rate of production of turbulent kinetic energy, respectively. c_s (=0.18), α (=0.75), c_3 (=0.05), c_f(=0.01), β_0 (=-3.4), β_1 (=4.2), β_2 (=0.8-$\Pi^{1/2}$), β_3 (=-1.8), β_4 (=1.25), and β_5 (=0.4) are model parameters, respectively. The first line in Eq.(4.7) contains a mixture of terms representing both "*slow*" and "*rapid*" contributions to the pressure-strain correlation. The first term is the usual Rotta term for the return to isotropy, and the second term is a non-linear contributions to the return to isotropy. The last two terms on the first line are contributions to the rapid part, the first of these is a linear term and the second is quadratic in b_{ij}, since G_k itself is linear in b_{ij}. The two terms of second line are linear terms of b_{ij} containing S_{ij} and W_{ij}, respectively. The third line shows Shir model (1973) reflecting the effect of free surface, where f_s is the free-surface damping function in the same manner as Celik and Rodi (1984), Gibson and Rodi (1989) and Naot *et al.* (1993). e_{ij} in Eq.(4.8) is the algebraic dissipation model that relates the anisotropies of the dissipation rate tensor to those of the Reynolds stress tensor.

4.2.3 Boundary Conditions at the Free Surface

There exist various boundary conditions at the free surface in open-channel flow. Hossain and Rodi (1980) have supposed the following boundary condition of ε at the free surface on the assumption that the length scale l is proportional to the distance from some virtual origin above the free surface and that $l=0.07h$ at the free surface.

$$\varepsilon_s = \frac{C_\mu^{3/4} k^{3/2}}{\kappa y'} \tag{4.10}$$

where C_μ (=0.09) is a model parameter and κ is the von Karman constant. Naot-Yacoub-Moalem (1989) extended Hossain and Rodi model on assuming that the inward energy flux is equal to the outward energy flux near the free surface, as follows:

$$\frac{dl}{dy} = -C_{lf}\,; C_{lf} = \frac{1}{3}\left(\frac{\overline{v^2}}{k}\right)^2 \frac{\sigma_\varepsilon}{C_\mu} \tag{4.11}$$

where σ_ε (=1.225) is a model parameter. So, Hossain and Rodi model is interpreted as $l=0.07h$ at $y=h$ (free surface) in Eq.(4.11).

$$l = 1.07h - y \tag{4.12}$$

If both the boundary conditions, Eqs.(4.11) and (4.12) are equal to each other, then $dl/dy=-1$, identified as the special case with $C_f=1.0$ in Eq.(4.11) ; $\overline{v^2}/2k=0.456$. However, attempts to get better agreement with the data of Ueda *et al.* (1977) suggested $C_f=1.44$ and $\overline{v^2}/2k=0.546$. Though Eqs.(4.11) and (4.12) are the boundary conditions at the flat free surface in a low Froude number, it has a possibility that Eq.(4.11) can be expanded to the wavy flow in a higher Froude number through the variation of $\overline{v^2}/2k$.

By the way, Davies (1972) has pointed out that the surface-influenced layer where the damping characteristics are predominant becomes thinner as the vertical fluctuations increase. On the basis of his study, Nezu and Nakayama (1998h) have experimentally suggested the exponential function of the turbulent redistributions as free-surface boundary conditions as follows (see Fig.3.8) :

$$\overline{u^2}/2k = 0.55 - 0.05\exp(-Fr) \tag{4.13}$$

$$\overline{v^2}/2k = 0.17(1 - \exp(-Fr)) \tag{4.14}$$

$$\overline{w^2}/2k = 0.28 + 0.22\exp(-Fr) \tag{4.15}$$

The above equations show that three components of turbulent redistributions approach constant values in intermediate region proposed by Nezu and Nakagawa (1993) when Froude number increases due to an increase of the ratio of the inertia force to the gravity force.

4.2.4 Calculation Procedures

In this study, the wall function was applied as the wall boundary conditions of k and ε due to the high Reynolds-number turbulence-model. Initial conditions for the mean flow, the turbulent energy

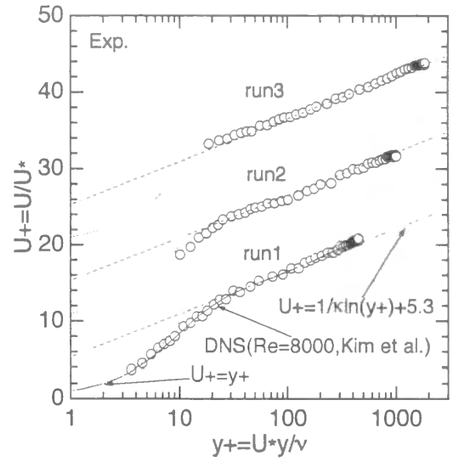

Fig.4.1 Primary mean velocity U^+ (Exp.).

and the dissipation rate were taken as an uniform flow U_m, $k=0.01U_m^2$ and $\varepsilon=k^{3/2}/(0.8h)$, respectively. The governing equations were differentiated by the control volume method, and the converged solution was obtained by SIMPLE algorithm. The calculations used 50 grid points in the vertical direction. The value of normalized distance from the wall $y^+=U_*y/\nu$ at the node nearest to the wall was about $y^+=40$. Along the line of nodes nearest to the walls, the local equilibrium is assumed: The streamwise velocity component is specified based on the logarithmic velocity of the wall, and the turbulent energy redistributions attain constant values in intermediate region ($\overline{u^2}/2k=0.55$, $\overline{v^2}/2k=0.17$, $\overline{w^2}/2k=0.28$).

4.3 Experimental Results

4.3.1 Distribution of Primary Mean Velocity and Turbulence Intensities

Fig.4.1 shows the distribution of primary mean velocity $U^+=U/U_*$ normalized by the friction velocity U_* versus the inner variable $y^+=U_*y/\nu$. U_* was calculated by the log-law formula (the viscous-sublayer formula $U^+=y^+$ was also used for run1). In this figure, DNS database in duct flow (Re=8000, R_*=400, which are almost same as run1) by Kim *et al.* (1987), the viscous-sublayer formula and the log-law formula are also plotted together. It can be seen that the experimental data in run1 coincides well with the DNS data. In particular, the viscous-sublayer formula holds well in run1. Near the free surface, wake phenomena can be seen as the Reynolds number increases as pointed out by Nezu and Nakagawa (1993). In this way, the turbulence structure near the wall in open-channel flow is similar to that in duct flow, and the free-surface effect does not reach the wall region. Fig.4.2 shows the distribution of turbulence intensities u'/U_*, v'/U_*, w'/U_* versus the outer variable y'/h ($y'=h-y$ is the distance from the free surface), together with the DNS data in duct flow by Kim *et al.* (1987), the DNS data in open-channel flow by Komori *et al.* (1993) and the semi-theoretical curve derived by Nezu and Nakagawa (1993). Of particular significance is that v' decreases greatly near the free surface in run1, which is closely related to the decrease of low wavenumber in the vertical-component spectrum of velocity fluctuations as pointed out by Nakayama and Nezu (1999f). However, the value increases near the free surface as the Froude number increases. u' and w' do not change so greatly (u' increases a little and w' decreases a little).

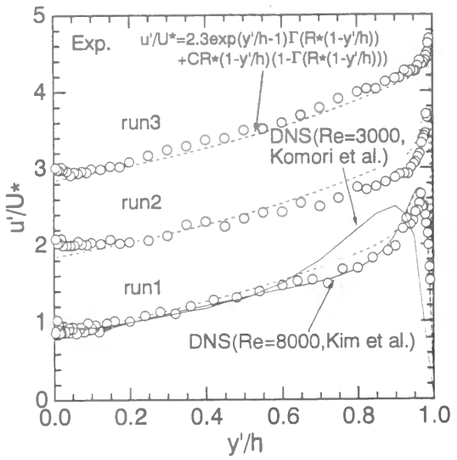

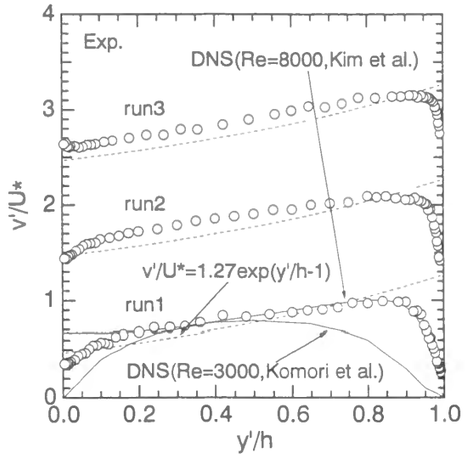

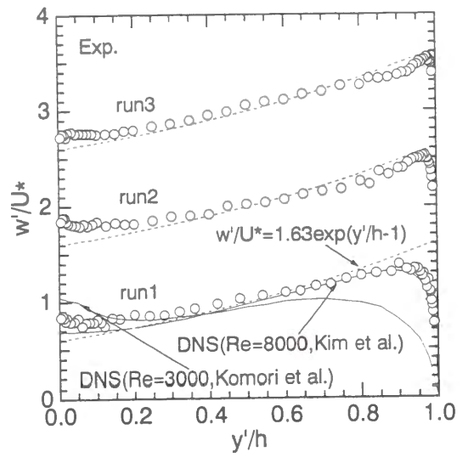

Fig.4.2 Turbulence intensities u'/U_*, v'/U_*, w'/U_* (Exp.).

4.3.2 Reynolds Stress and Turbulent Energy

Fig.4.3 is the distribution of Reynolds stress $-\overline{uv}/U_*^2$, together with the DNS data by Kim *et al.* (1987) and the semi-theoretical curve by Nezu and Nakagawa (1993). The value of $-\overline{uv}/U_*^2$ in open-channel flow coincides well with that in duct flow even near the free surface, which means that the symmetry condition at the free surface is appropriate even in open-channel flow. The distribution of turbulent kinetic energy k/U_*^2 is shown in Fig.4.4. It can be seen that the value in open-channel flow is similar to that in duct flow in spite of a great discrepancy of turbulence intensities with each other. Therefore, the boundary conditions of $-\overline{uv}$ and k at the free surface are symmetrical hereafter.

4.3.3 Turbulent Generation and Dissipation Rate

Fig.4.5 shows the distributions of the turbulent generation Gh/U_*^3 and the turbulent energy dissipation rate $\varepsilon h/U_*^3$. Both values were evaluated in the same way as Nezu and Nakayama (1998a). In this figure, the DNS data by Kim *et al.* (1987) and the semi-theoretical curve by Nezu and Nakagawa (1993) were also plotted together. The value of G is similar to that in duct flow regardless of the

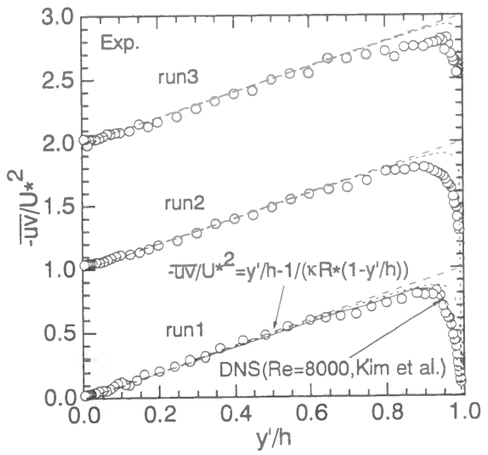

Fig.4.3 Reynolds stress $-\overline{uv}/U_*^2$ (Exp.).

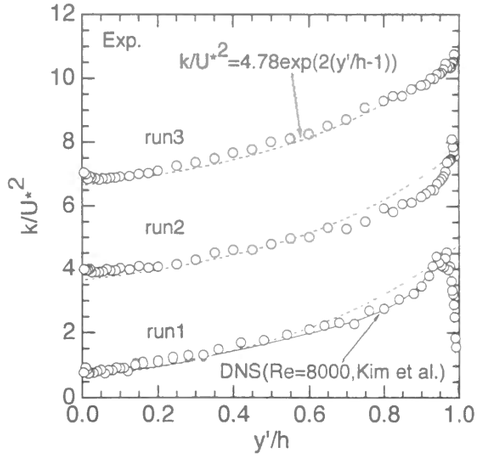

Fig.4.4 Turbulent kinetic energy k/U_*^2 (Exp.).

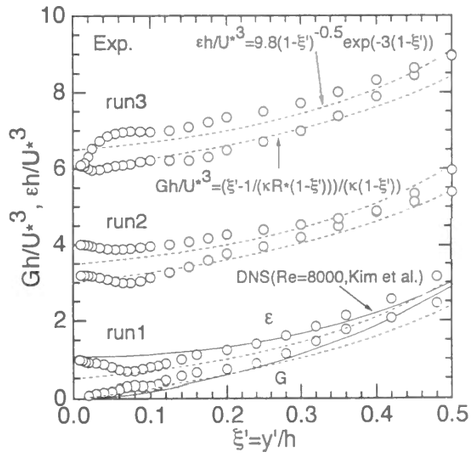

Fig.4.5 Turbulent generation Gh/U_*^3 and turbulent energy dissipation rate $\varepsilon h/U_*^3$ (Exp.).

Froude number, whereas the values of ε are quite different with each other. When the Froude number is small in run1, ε decreases around y'/h=0.1 (the edge of surface-influenced layer) and increases toward the free surface. These phenomena have a close relationship with the decrease of length scale due to the effect of free surface, as have been firstly pointed out by Hossain and Rodi (1980). On the other hand, in run3, the value increases a little around y'/h=0.1 and decreases toward the free surface. The same characteristics can be seen in the experimental data of oscillating grid generated flow by Brumley and Jirka (1987), which is closely related to the generation of surface-renewal eddies.

4.4 Calculation Methods including Effects of Froude Number

4.4.1 Limit of Boundary Condition for ε at Free Surface

4.4.1a Boundary Conditions of Dissipation Rate ε at Free Surface

As can be seen in the experimental data in Fig.4.5, the value of ε increases greatly near the free

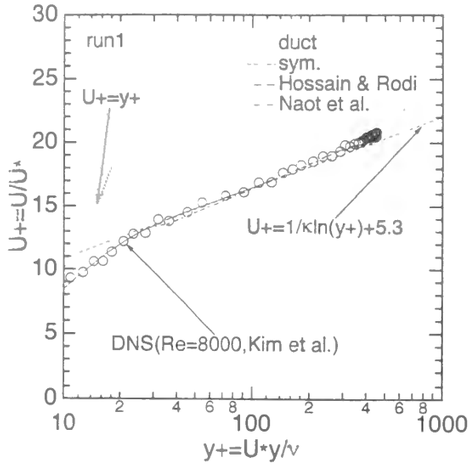

Fig.4.6 Primary mean velocity U^+ (Cal. run1).

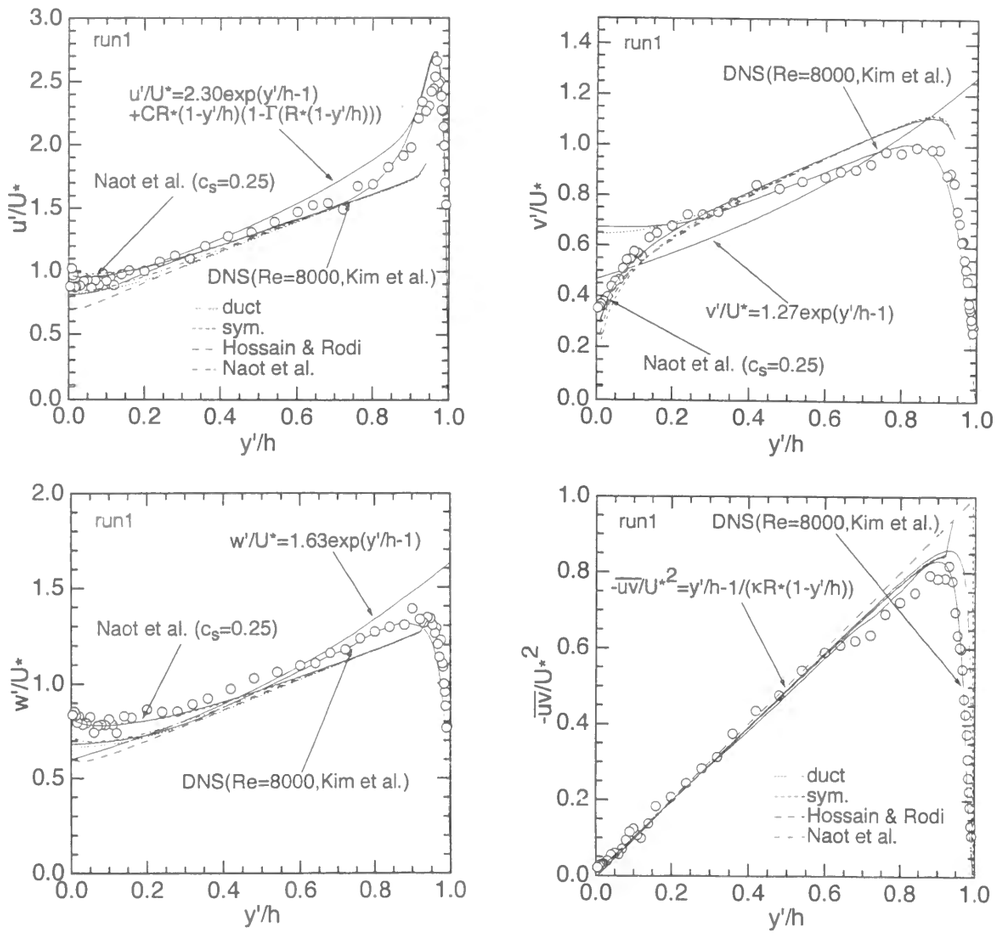

Fig.4.7 Turbulence intensities u'/U_*, v'/U_*, w'/U_* and Reynolds stress $-\overline{uv}/U_*^2$ (Cal. run1).

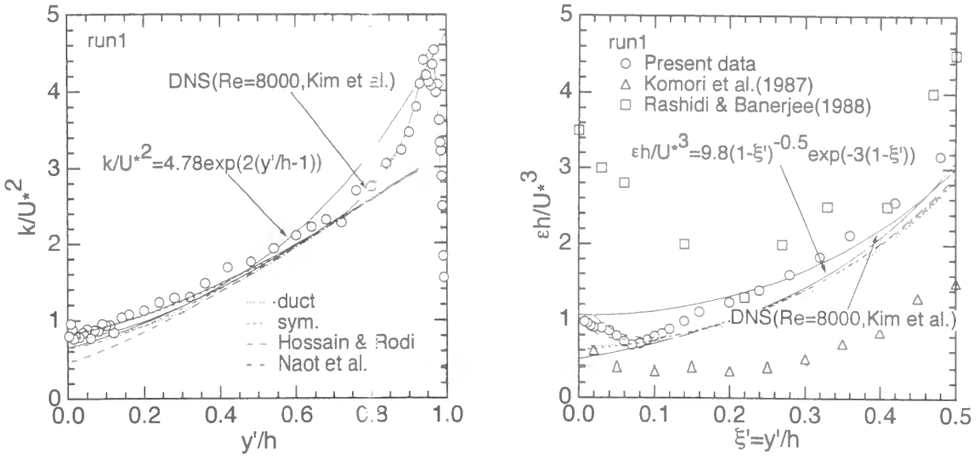

Fig.4.8 Turbulent kinetic energy k/U_*^2 and dissipation rate $\varepsilon h/U_*^3$ (Cal. run1).

surface in tranquil flow. There have been suggested several boundary conditions at the free surface about these characteristics. Fig.4.6 shows the distribution of U^+ in run1 when the symmetry condition, Hossain and Rodi model, and Naot-Yacoub-Moalem model (C_{lf}=1.44) of ε were used at the boundary condition of free surface. The other variables were symmetrical at the free surface. In this figure, the calculation result in duct flow (c_3=0 in Eq.(4.7)) was also described. It can be seen that all the models reproduce comparatively well the experimental data.

Fig.4.7 shows the distribution of turbulence intensities u'/U_*, v'/U_*, w'/U_* and $-\overline{uv}/U_*^2$ near the free surface. The calculated values of v' and $-\overline{uv}$ coincide well with the experimental values, and the damping characteristics are well reproduced near the free surface. On the other hand, the calculated values of u' and w' are quite smaller in Hossain and Rodi model. This is because these values are greatly affected by the boundary condition of ε, as mentioned later. In this figure, the calculation data at c_s=0.25 is also described when Naot-Yacoub-Moalem model was applied to the calculation. In this situation, the values of u' and w' increase slightly, which coincides well with the experimental value.

Fig.4.8 shows k/U_*^2 and $\varepsilon h/U_*^3$. The experimental data by Komori *et al.* (1987) and Rashidi and Banerjee (1988) are also plotted in the figure of ε. The calculated value of k reproduces well the experimental value except Hossain and Rodi model. As for ε, Hossain and Rodi model and Naot-Yacoub-Moalem model reproduce well the increasing characteristics of ε near the free surface. However, these calculations do not quite change regardless of Froude number or Reynolds number, which means that it is necessary to apply a new model including the effect of Froude number in run3.

4.4.1b Boundary Conditions of ε for Steep Open-Channel Flow

As mentioned before, Naot-Yacoub-Moalem model reproduces well the experimental value of ε near the free surface, and it has the possibility of reproducing the effect of Froude number by changing the parameter C_{lf}. Fig.4.9 is the distribution of C_{lf} versus Froude number when Eq.(4.14) was substituted for Eq.(4.11). It can be seen that C_{lf} increases and approaches the constant value as Froude number increases. On the other hand, Fig.4.10 shows the distribution of $\varepsilon h/U_*^3$ near the free surface when C_{lf} changes. In this figure, the calculated value at the symmetrical boundary condition of ε was also described. The calculation value of C_{lf}=1.44 reproduces well the experimental value in run1. However, the value of C_{lf} has to attain a negative value (C_{lf}<0) if the experimental value in run3 is reproduced. This means that the increase of length scale in steep open-channel flow cannot be reproduced by

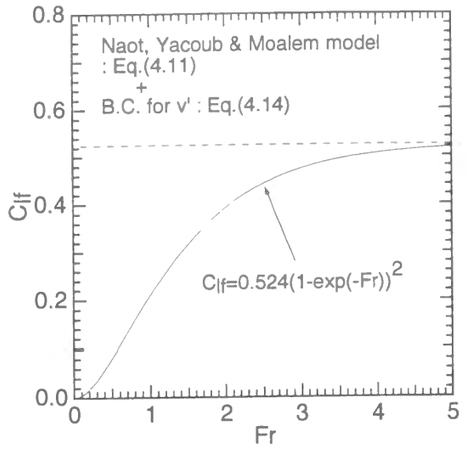

Fig.4.9 Coefficient C_{lf} versus Froude number.

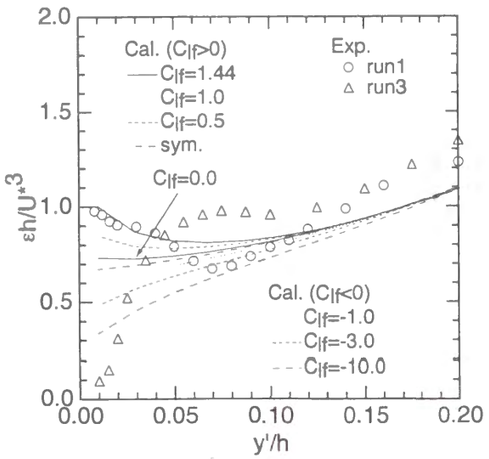

Fig.4.10 Dissipation rate $\varepsilon h/U_*^3$ when C_{lf} changes.

applying Naot-Yacoub-Moalem model. Therefore, ε cannot be evaluated only by the vertical component of turbulence intensity v' near the free surface.

In this way, the effect of Froude number on the variation of the turbulent redistributions near the free surface cannot be reproduced even if the effect of Froude number on ε may be considered. Therefore, it is necessary to apply the boundary conditions of turbulent redistributions at the free surface, or improve the pressure-strain term.

4.4.2 Effect of Froude Number on Turbulent Redistributions

4.4.2a Revision of Shir Model in Pressure-Strain Term

As mentioned before, Froude number has a great influence on the turbulent redistributions near the free surface. When these effects are considered in the turbulence modeling, there are two ways, as follows: (a) giving the boundary conditions of the turbulent redistributions at the free surface, and (b) including the effect of Froude number in the pressure-strain term ϕ_{ij}. In particular, as for (b), Perot and Moin (1995) have pointed out that the coherent structures near the free surface, so called, the "*splats*" and "*antisplats*" are closely related to the pressure-strain term. Sugihara and Matsunaga (1998) conducted a numerical simulation by using LRR model in oscillating grid generated flow, and pointed out that the thickness of surface-influenced layer becomes larger as the coefficient of pressure-strain term c_3 increases. Furthermore, Nezu and Nakayama (1998h) clarified the decrease features of surface-influenced layer witn an increase of Froude number (Eqs.(4.13)-(4.15)). Considering the above mentioned, c_3 can be expressed, as follows:

$$c_3 = c_{30}\exp(-Fr) \tag{4.16}$$

where c_{30} is the utmost limit of c_3 at $Fr \to 0$ (ideally flat mirror surface).

4.4.2b Primary Mean Velocity and Turbulence Intensities

Fig.4.11 shows the distribution of U^+ when (a) the before-mentioned boundary conditions of the turbulent redistributions (Eqs.(4.13)-(4.15)) were used at the free surface (cal-1), and when (b) the above equation (4.16) was used in the computation (cal-2). All the other variables were symmetrical at

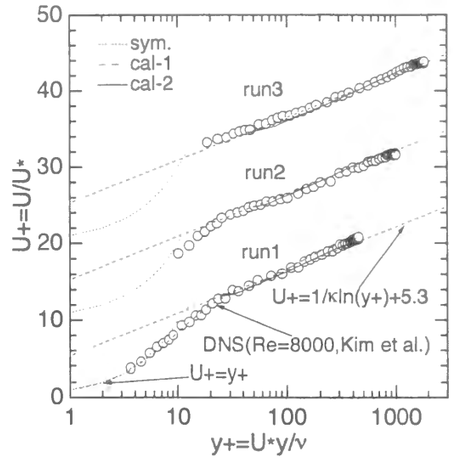

Fig.4.11 Primary mean velocity U^+ (cal-1 and cal-2).

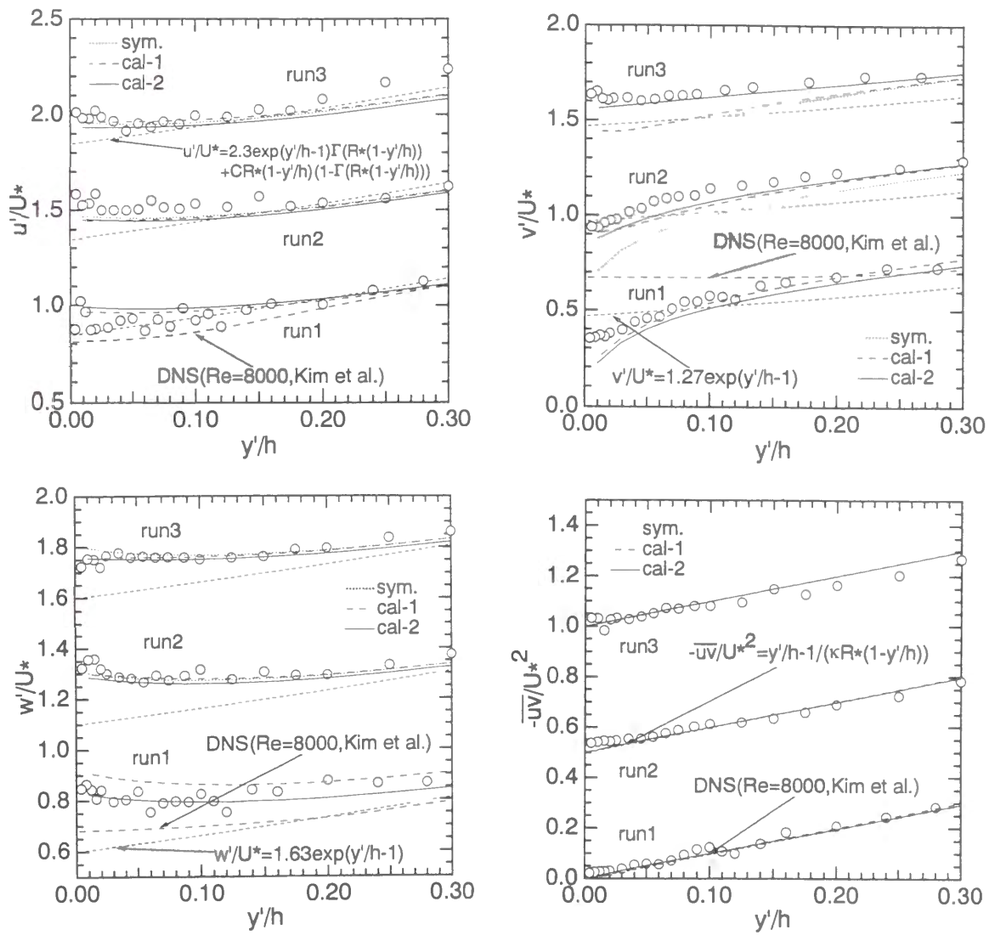

Fig.4.12 Turbulence intensities u'/U_*, v'/U_*, w'/U_* and Reynolds stress $-\overline{uv}/U_*^2$ (cal-1 and cal-2).

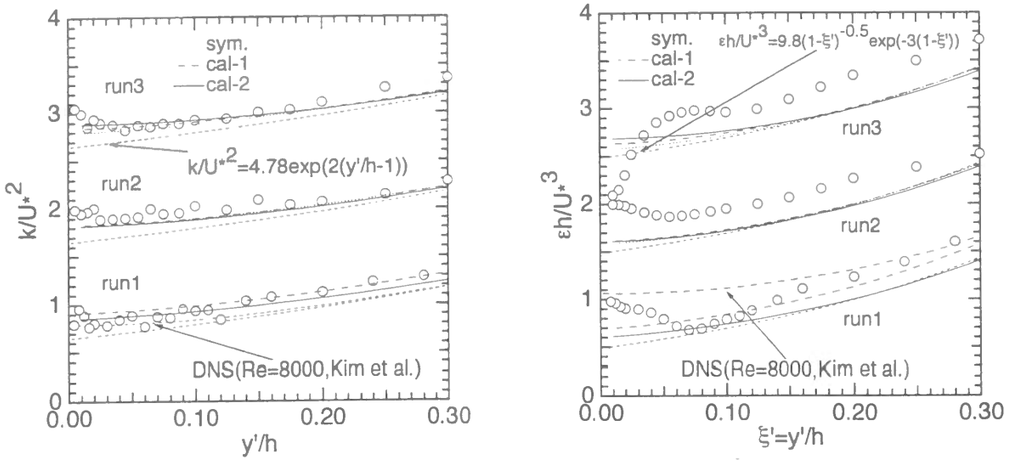

Fig.4.13 Turbulent kinetic energy k/U_*^2 and dissipation rate $\varepsilon h/U_*^3$(cal-1 and cal-2).

the free surface. In this figure, the calculation data are also plotted when all the variables are symmetrical (sym.). It can be seen that both calculations (cal-1 and cal-2) coincide well with the experimental data regardless of both Reynolds number and Froude number.

Fig.4.12 shows the distribution of u'/U_*, v'/U_*, w'/U_* and $-\overline{uv}/U_*^2$ near the free surface. Of particular significance is that v' increases greatly near the free surface with an increase of the Froude number. Though the symmetric condition cannot reproduce these characteristics, the cal-1 and cal-2 reproduce roughly these characteristics, and in particular, the cal-2 reproduces them very well. However, the cal-1 underestimates the experimental data near the free surface as Froude number increases. This means that the boundary conditions Eqs.(4.13)-(4.15) reproduce roughly the effect of Froude number, but it is difficult to reproduce the decrease of surface-influenced layer with an increase of Froude number. And w' decreases slightly as Froude number increases and both the calculations are in good agreement with each other. On the other hand, u' increases a little and the cal-1 coincides with the experimental value, whereas the cal-2 decreases slightly when Froude number increases. This difference greatly depends on the redistribution rates of Shir model, which implies that it is necessary to revise Shir model in open-channel flow.

4.4.2c Turbulent Energy and Dissipation Rate

The distribution of k/U_*^2 and $\varepsilon h/U_*^3$ is shown in Fig.4.13. The both calculated values of k reproduce well the experimental data in this figure. On the other hand, the value of ε in the calculation is almost far from a good reproduction of the experimental data. This means that it is impossible to reproduce the distribution of ε only with the boundary conditions of the turbulent redistributions at the free surface or the pressure-strain term including the effect of Froude number.

4.4.2d Turbulent Energy Budget in Reynolds Stress Equation

As mentioned before, the pressure-strain terms are closely related to the turbulent redistributions near the free surface. Fig.4.14 shows the distributions of the pressure-strain term ϕ_{ij} near the free surface for the cal-1 and cal-2 when the Froude number increases. In this figure, the calculated value of duct flow (duct) is also plotted. Of particular significance is that the values of ϕ_{22} are quite different between open-channel flow and duct flow in the region of $y'/h<0.1$. The value of open-channel flow changes from the positive value to the negative one near the free surface, as pointed out by Handler *et*

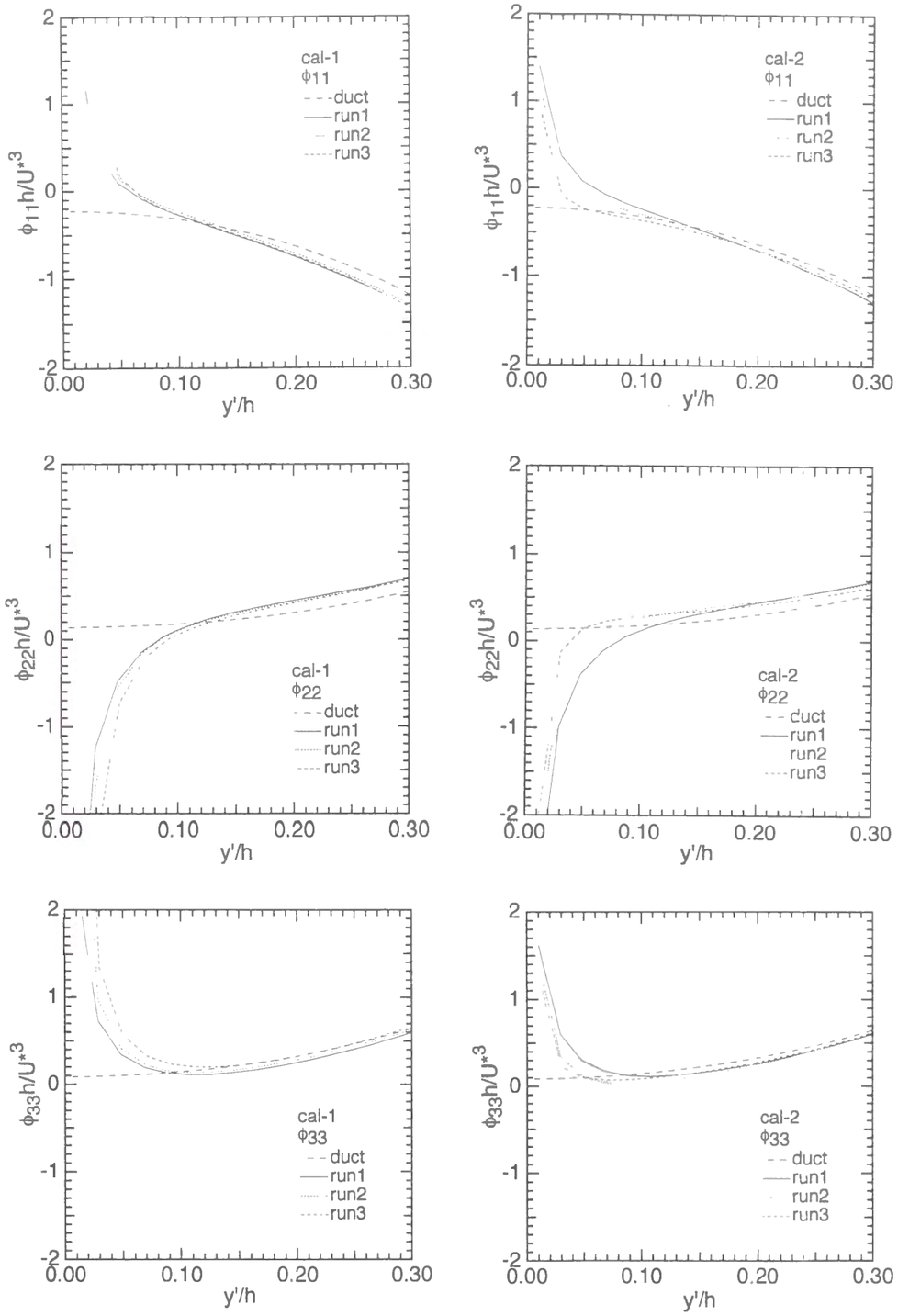

Fig.4.14 Pressure-strain term ϕ_{ij} near the free surface (cal-1 and cal-2).

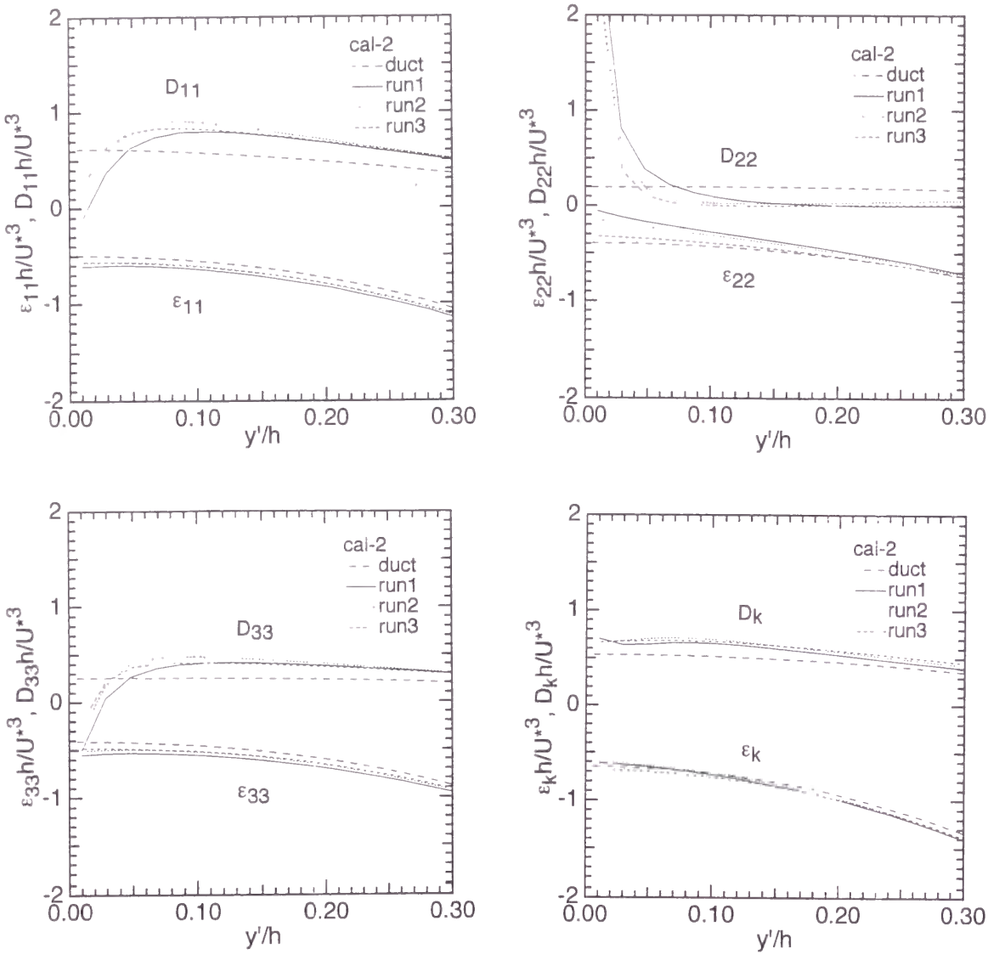

Fig.4.15 Dissipation term ε_{ij} and the diffusion term D_{ij} (cal-2).

al. (1993) and Nagaosa and Saito (1997). ϕ_{22} decreases greatly and ϕ_{33} increases significantly in the cal-1 with an increase of Froude number, whereas these values approach the values of duct flow in cal-2. The cal-2 is better than the cal-1 because the turbulent redistributions approach the constant value in the intermediate region (the same as in duct flow).

Fig.4.15 shows the distributions of the dissipation term ε_{ij} and the diffusion term D_{ij} in the cal-2. Near the free surface, the total dissipation rate ε_k is almost equal to the total diffusion rate D_k regardless of Froude number. Furthermore, the streamwise and spanwise components of D_{ij} and ε_{ij} are almost independent of Froude number, whereas D_{22} and ε_{22} approach the curve of duct flow with an increase of Froude number. In this way, the vertical components in Reynolds stress equation depend greatly on Froude number, which affects the vertical component of turbulence intensity near the free surface.

- Conventional Model (Davies, Hunt & Graham, Brumley & Jirka)
  - ⇒ Applicable only in Tranquil Flow
- Super-Critical Flow (Surface-Wave Fluctuations occur)
  - ⇒ Great Effect of Froude Number (*Fr*)
  - ⇒ Decrease of Surface-Influenced Layer
  - ⇒ Turbulent Redistributions approach the Constant Ratio in Intermediate Region.
- Two Methods for Considering Effect of Froude Number
  - (1) Giving B.C. of Turbulent Redistributions at Free Surface
  - (2) Extension of Shir Model
  - ⇒ Reproduce well Experimental Values !

Fig.4.16 Conclusions of chapter 4.

4.5 Conclusions

In this study, a numerical simulation was conducted in smooth open-channel flow by using Reynolds stress model including the effect of Froude number in comparison with the experimental data. Fig.4.16 shows the conclusions of chapter 4. At that time, two methods, that is to say, (1) giving the boundary conditions of the turbulent redistributions at the free surface, and (2) the extension of Shir model, were used for considering the effect of Froude number, and these calculations reproduce well the experimental values.

Notations

A_m : wave amplitude
B : channel width
b_{ij} : anisotropy tensor
C_ε, $C_{\varepsilon 1}$, $C_{\varepsilon 2}$: model parameters in dissipation equation
C_μ, σ_ε : model parameters
c_s : model parameters in diffusion term
D_{ij} : diffusion term
e_{ij} : algebraic dissipation model that relates the anisotropies of the dissipation rate tensor to those of the Reynolds stress tensor
Fr : Froude number ($=U_m/\sqrt{gh}$)
f_s : free-surface damping function
G : turbulent generation (or production)
G_{ij} : generation term

G_k : rate of production of turbulent kinetic energy
g : acceleration due to gravity
h : flow depth
k : turbulent kinetic energy
l : length scale
P : pressure fluctuation
Re : Reynolds number ($=U_m h/\nu$)
R_* : turbulent Reynolds number ($=U_* h/\nu$)
S_b : channel slope
S_{ij} : rate of strain tensor
$\overline{u^2}/2k$, $\overline{v^2}/2k$, $\overline{w^2}/2k$: turbulent energy redistributions
W_{ij} : rotation tensor
U_m : bulk mean velocity
U^+ : U/U_* ; normalized mean velocity
U_* : friction velocity
u : instantaneous streamwise velocity component
u' : root-mean-square value of velocity fluctuations in x direction
$-\overline{uv}$: Reynolds stress
v : instantaneous vertical velocity component
v' : root-mean-square value of velocity fluctuations in y direction
w : instantaneous spanwise velocity component
w' : root-mean-square value of velocity fluctuations in z direction
x : streamwise direction
y : vertical direction from the channel bed
y^+ : yU_*/ν ; vertical distance in lawof the wall coordinates
y' : distance from the free surface ($=h-y$)

Greek symbols
α : model parameters in dissipation term
β_0, β_1, β_2, β_3, β_4, β_5 ,c_3 : model parameters in pressure-strain term
ε : turbulent energy dissipation rate
ε_{ij} : dissipation term
ε_s : dissipation rate at the free surface
ϕ_{ij} : pressure-strain term
η' : intensity of surface-wave fluctuations ($\equiv\sqrt{\overline{\eta^2}}$)
ν : kinetic viscosity

References

[1] Arakawa, C. : Computational fluid dynamics for engineering, University of Tokyo Press, 1994 (in Japanese).
[2] Borue, V., Orszag, S. and Staroselsky, I. : Interaction of surface waves with turbulence : Direct numerical simulations of turbulent open-channel flow, *J. Fluid Mech.*, Vol.286, pp.1-23, 1995.
[3] Brumley, B. H. and Jirka, G. H. : Near-surface turbulence in a grid-stirred tank, *J. Fluid Mech.*, Vol.183, pp.235-263, 1987.
[4] Celik, I. and Rodi, W. : Simulation of free surface effects in turbulent channel flows, *Physico*

Chemical Hydrodynamics, Vol.5, pp.217-227, 1984.
[5] Chen, C.J. and Tanaka, N. : Fundamentals and applications of turbulence models, Structual and Planning Institute Press, 1992 (in Japanese).
[6] Davies, J. T. : Turbulence Phenomena, Academic Press, San Francisco, 1972.
[7] Demuren, A.O. and Sarkar, S. : Perspective: Systematic study of Reynolds stress closure methods in the computations of plane channel flows, *J. Fluids Engineering*, Vol.115, pp.5-12, 1993.
[8] Gibson, M.M. and Rodi, W. : Simulation of free surface effects on turbulence with a Reynolds stress model, *J. Hydraulic Research*, IAHR, Vol.27, No.2, pp.233-244, 1989.
[9] Hallback, M., Groth, J. and Johansson A.,V. : An algebraic model for nonisotropic turbulent dissipation rate in Reynolds stress closures, *Phys. Fluids, A*, Vol.2, No.10, pp.1859-1866, 1990.
[10] Handler, R. A., Swean, T. F., Jr., Leighton, R. I., and Swearingen, J. D. : Large scales and the energy balance for turbulence near a free surface, *J. AIAA*, Vol.31, No.11, pp.1998-2007, 1993.
[11] Hossain, M.S. and Rodi, W. : Mathematical modelling of vertical mixing in stratified channel flow, *Proc. of the 2nd Symposium on Stratified Flows*, 1980.
[12] Hunt, J. C. R. and Graham, J. M. R. : Free-stream turbulence near plane boundaries, *J. Fluid Mech.*, Vol.84, pp.209-235, 1978.
[13] Kim, J., Moin, P. and Moser, R. : Turbulence statistics in fully developed channel flow at low Reynolds number, *J. Fluid Mech.*, Vol.177, pp.133-166, 1987.
[14] Komori, S., Hiraga, Y., Murakami, Y. and Ueda, H. : The generation of surface-renewal eddies in an open-channel flow, *Proc. of 2nd. Int. Symp. on Transport Phenomena in Turbulent Flows*, Tokyo, pp.75-85, 1987.
[15] Komori, S., Nagaosa, R., Murakami, Y., Chiba, S., Ishii, K. and Kuwahara, K. : Direct numerical simulation of three-dimensional open-channel flow with zero-shear gas-liquid interface, *Phys. Fluids A*, Vol.5, No.1, pp.115-125, 1993.
[16] Launder, B.E., Reece, G.J. and Rodi, W. : Progress in the development of a Reynolds-stress turbulent closure, *J. Fluid Mech.*, Vol.68, pp.537-566, 1975.
[17] Nagaosa, R. and Saito, T. : Turbulence structure and scalar transfer in stratified free-surface flows, *AIChE J.*, Vol.43, No.10, pp.2393-2404, 1997.
[18] Nakayama, A. and Yokojima, S. : Turbulence model with free-surface fluctuation effects for the calculation of open-channel flows", *Annual J. Hydraulic Engrg.*, JSCE, Vol.43, pp.389-394 ,1999 (in Japanese).
[19] Naot, D., Nezu, I. and Nakagawa, H. : Hydrodynamic behavior of compound rectangular open-channels, *J. Hydraulic Engineering*, ASCE, Vol.119, No.3, pp.390-408, 1993.
[20] Naot, D., Yacoub, N. and Maron Moalem, D. : Open surface renewal boundary conditions for the k-ε turbulence model, *the 23rd IAHR Conference*, 1989.
[21] Nezu, I. and Nakagawa, H. : Turbulence in open-channel flows, IAHR-Monograph, Balkema, 1993.
[22] Nezu, I. and Nakayama, T. : Relationship between turbulent structures near the free-surface and surface-wave-fluctuations, *J. Hydraulic Engrg.*, JSCE, No.593/II-43, pp.69-78, 1998a (in Japanese).
[23] Nezu, I. and Nakayama, T.: Turbulent redistribution near the free surface by using numerical simulation, *11th Congress of the IAHR-APD*, pp.537-546, 1998h.
[24] Nezu, I. and Nakayama, T.: Mutual-interaction between bursts and boils very near the free surface in open-channel flows, *Environmental Hydraulics*, J.H.W.Lee *et al.* (eds.), Balkema Pub., pp.297-303, 1998k.
[25] Nakayama, T. and Nezu, I. : Bursts near the free surface in open-channel flows and their relationship with turbulence structures, *Journal of Hydraulic Engineering*, JSCE, No.635/II-49, pp.31-40, 1999e (in Japanese).

[26] Nakayama, T. and Nezu, I. : Numerical simulation of turbulence structures near the free surface by using Reynolds Stress Model, *Journal of Hydraulic Engineering*, JSCE, 1999g (in Japanese, to be accepted).
[27] Nezu, I. and Nakayama, T : Numerical calculation of steep open-channel flows by considering effects of surface-wave fluctuations, *Proc. of Water, Environment, Ecology, Socio-Economics, and Health Engineering*, pp.33-48, 1999j.
[28] Nezu, I. and Nakayama, T. : Numerical simulation of steep open-channel flows by using RSM, *Proc. of 1999 Meeting of Japan Society of Fluid Mechanics*, pp.383-384, 1999k (in Japanese).
[29] Ooka, R. : Numerical study on air flow and heat transfer in building and urban space by means of differential stress model, *Ph.D Thesis presented to University of Tokyo*, 1997 (in Japanese).
[30] Patankar, S.V. : Numerical heat transfer and fluid flow, Hemisphere, 1980.
[31] Perot, B. and Moin, P. : Shear-free turbulent boundary layers. Part 1. Physical insights into near-wall turbulence, *J. Fluid Mech.*, Vol.295, pp.199-227, 1995.
[32] Rashidi, M. and Banerjee, S. : Turbulence structure in free-surface channel flows, *Phys. Fluids*, Vol.31, No.9, pp.2491-2503, 1988.
[33] Roache, P.J. : Computational fluid dynamics, Hermosa, 1976.
[34] Rodi, W. : Turbulence models and their application in hydraulics, IAHR-Monograph, Balkema, 1993.
[35] Shir, C. C. : A preliminary numerical study of atmospheric turbulent flows in the idealized planetary layer, *J. Atmos. Sci.*, Vol.30, pp.233-244, 1973.
[36] Speziale, C. G., Sarkar, S. and Gastki, T. B. : Modeling the pressure-strain correlation of turbulence: An invariant dynamical systems approach, *J. Fluid Mech.*, Vol.227, pp.245-272, 1991.
[37] Sugihara, Y. and Matsunaga, N. Application of a Reynolds stress model for turbulence near a free surface, *Annual J. Hydraulic Engrg.*, JSCE, Vol.42, pp.613-618, 1998 (in Japanese).
[38] Tsai, W.-T. : A numerical study of the evolution and structure of a turbulent shear layer under a free surface, *J. Fluid Mech.*, Vol.354, pp.239-276, 1998.
[39] Ueda, H., Moller, R., Komori, S. and Mizushina, T. : Eddy diffusivity near the free surface of open channel flow, *Int. J. Heat and Mass Transfer*, Vol.20, pp.1127-1136, 1977.

CHAPTER 5

EFFECT OF MACRO-ROUGHNESS AND WAVE ON TURBULENCE STRUCTURE NEAR FREE SURFACE

Abstract

Recently, there are many researches of experiments and calculations about the coherent structure over smooth bed, and it is revealed that the turbulence structure is closely related to the coherent structure. In an open-channel flow, turbulent energy redistributions change variously within a "*surface-influenced layer*" which is roughly ten per cent of the flow depth, and a damping effect on the vertical motions is gradually lost out as the Froude number and the surface-wave fluctuations are increasing, as mentioned before.

As for the rough flow, it has been pointed out that boils become stronger and larger as the bed roughness increases. However, the upper part (free-surface side) of the velocity profile over a rough bed resembles that over a smooth bed, even though a wake zone may appear above the roughness elements. On the other hand, these characteristics are quite different from those in a wave-induced flow that can be seen in the sea.

In this study, the turbulence structure and the coherent structure over large-roughness were evaluated by making use of LDA and PIV (Particle-Image Velocimetry) methods in comparison with a wave-induced (periodic sine-wave) flow. At that time, space-time correlation analyses were conducted with a laser Doppler anemometer (LDA) and an ultrasonic depth-meter instrument. Finally, the effect of such macro-roughness on coherent structures was investigated by distinguishing the "*turbulence effect*" and the "*wave-induced effect*" in open-channel flows.

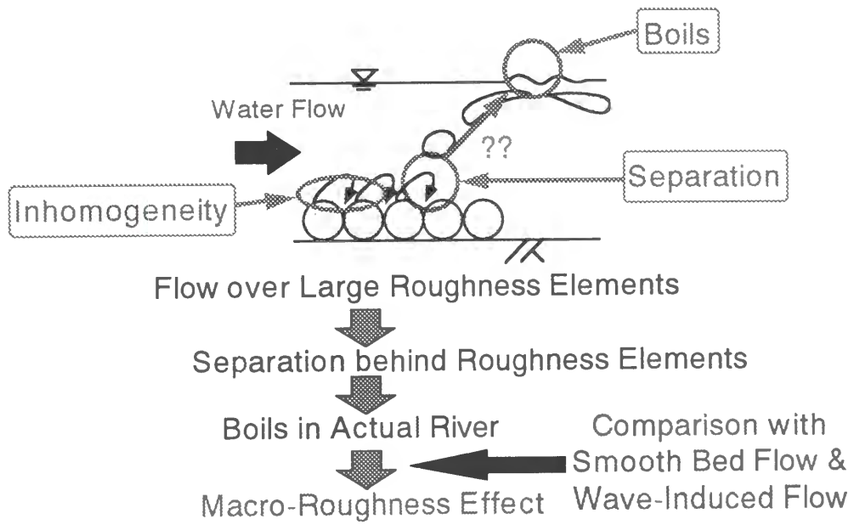

CHAPTER 5 EFFECT OF MACRO-ROUGHNESS AND WAVE ON TURBULENCE STRUCTURE NEAR FREE SURFACE

Parts of this chapter were presented in the following papers.

[1] Nezu, I., Nakayama, T. and Fujita, M. : Turbulence and free-surface fluctuations in open channel flows over macro-roughness, *Journal of Applied Mechanics*, JSCE, Vol.1, pp.709-718, 1998f (in Japanese).
[2] Nezu, I. and Nakayama, T.: Separation between turbulence and water-wave effects in an open-channel flow, *Flow Modeling and Turbulence Measurements VII*, pp.67-76, 1998i.
[3] Nezu, I. and Nakayama, T.: Effect of macro-roughness on coherent structures by using PIV methods, *Flow Modeling and Turbulence Measurements VII*, pp.617-626, 1998j.

5.1 Introduction

There have been many researches about the coherent structure over smooth bed in an open-channel flow. Nakagawa and Nezu (1981) have firstly investigated the structure of space-time correlations of bursting motions in an open-channel flow by a new conditional sampling analysis of the instantaneous velocity and Reynolds-stress signals measured simultaneously by two sets of dual-sensor hot-film anemometers. They have proposed then a phenomenological model of bursting phenomenon as shown in Fig.5.1. Recently, Myose and Blackwelder (1994) have experimentally emulated both the dynamics and the interaction of turbulent boundary-layer eddy structures by using "*Gortler vortex*", and evaluated the relationship between the bursting phenomenon and the structure of outer region. They have suggested then that the outer region of turbulent boundary layer plays an important role in the bursting process.

Nakagawa *et al.* (1975) have compared the small roughness flow and the smooth flow and mentioned that away from the roughness elements, the distributions of turbulence intensities are very similar with each other and that the same similarity law is effective. Bayazit (1976) evaluated the theoretical origin of rough flow and how far the effect of roughness elements spreads from the top of roughness. Kironoto (1993) and Kironoto and Graf (1994) have measured accurately the turbulence structures in rough bed flow and suggested the semi-empirical formula in rough flow in the same way as Nezu and Nakagawa (1993) in smooth flow. They evaluated the mixing length and macro-scale in rough flow in comparison with smooth flow.

If the roughness elements are comparatively large over the bed as compared with the flow depth, some motions of separation may occur in the dead zone behind the roughness elements and the surface-wave fluctuations may increase due to such motions. Kanda and Doi (1980) have evaluated the effect of roughness pattern on the flow resistance and the turbulence characteristics near the free surface in large roughness flow. In the same roughened flow with spheres, Kanda and Suzuki (1985) have considered the effect of Froude number on flow resistance and pointed out that its effect is correspondent to the effect of Reynolds number and relative depth. Furthermore, Herbich and Shulits (1964) have evaluated the roughness coefficients for flows in which the roughness size protrudes through the water surface. In this boulder-strewn flow, the log law is not effective.

On the other hand, Jackson (1976) described the features of boil vortices from field observations of boils in rivers. He speculated that the bursting motions generated in the wall region would move toward the free surface and form a boil there because the bursting period for boundary layers was roughly equal to the boil period. Furthermore, he has mentioned that rough beds and entrained sediment

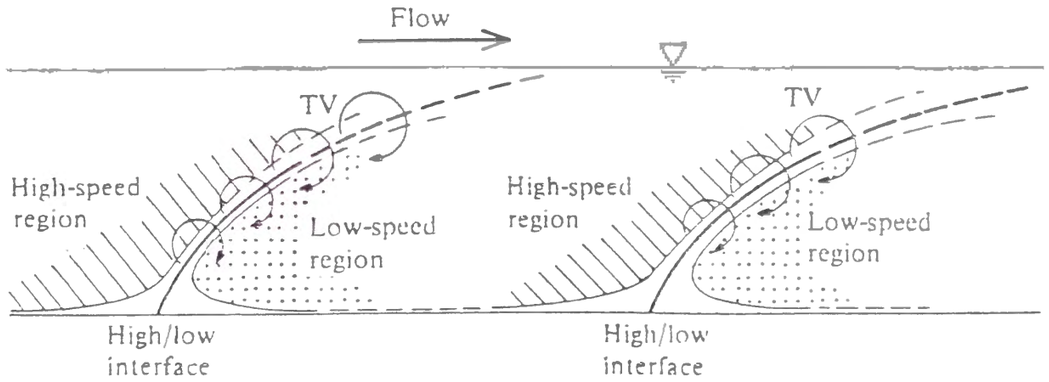

Fig.5.1 Conceptual model of high-speed and low-speed regions in open-channel flow by Nakagawa and Nezu (1981).

may modify the intensity of bursting but do not alter the basic burst cycle. It has, however, the possibility that the coherent structures over rough bed become different from those over smooth bed when the roughness is comparatively large. Nakagawa *et al.* (1975) and Nezu and Nakagawa (1993) have mentioned that the tendency toward isotropy becomes stronger as the roughness size increases and that the vertical intensity of the turbulence increases slightly within the inner region. Raupach (1981) has used the quadrant analysis to investigate the events contributing to the Reynolds shear stress over regularly arrayed rough surfaces of several different densities and over a smooth surface. He has shown that sweeps are stronger than ejections close to rough surfaces and account for fairly most of the stress. He called such layer as "*roughness sublayer*". Krogstad, *et al.* (1992) have used the quadrant analysis in the same way as Raupach (1981), and suggested that the strength of the "*active motion*" depends on the nature of the surface by comparing between smooth- and rough-wall spectra of the normal velocity fluctuations. Furthermore, Nakagawa *et al.* (1989) have evaluated the effect of vortex sheddings from the roughness elements on the turbulence structure around roughness in the flow with small relative submergence. Therefore, the coherent structures over rough bed may be quite different from those over smooth bed, and the surface-wave fluctuations may become larger. Moog and Jirka (1995) have studied the "*macro-roughness effect*" on the turbulent energy dissipation rate near the free surface. They have related a gas transfer coefficient with the turbulent dissipation rate near the surface, and evaluated the macro-roughness enhancement over rough bed. This fact implies that macro-roughness may have an important role on the coherent structures in open-channel flow.

By the way, it is possible to increase the turbulence intensity in a wave-induced flow as seen in the surf zone, which is a little different from the wave-current coexisting flow, for example, longshore current and rip current, *etc.* due to inhomogeneity of radiation stress. Asano (1986) has evaluated the vertical distribution of mean flow and turbulence intensity and the effect of wave-phase to the turbulent variation in the wave-induced current. Tanaka (1987) has measured the mean velocity and the bed shear stress in the wave-induced current. He has presented the linear expression of velocity-defect near the free surface and evaluated the energy transfer between the mean flow and the wave. Nevertheless, its turbulence structure might be very different from that in a steep open-channel flow because wave heights were considerably large in the surf zone. So, it is necessary to consider the "*wave effect*" on the turbulence structure in a small amplitude wave.

In this study, we deal with open-channel flows over rough beds in comparison with smooth bed. We evaluate an instantaneous and space-time correlation mechanism of coherent structures by using PIV (Particle-Image Velocimetry) methods. Next, we have measured the turbulent characteristics in an open-channel flow with a wave-induced (periodic sine-wave) flow at several types of wave periods and wave heights for separating the "*turbulence effect*" and the "*wave effect*" in open-channel flows. Finally, we reveal the effect of macro-roughness on coherent structures over rough beds.

5.2 Experimental Apparatus and Procedures

The experiments were conducted in a 10m long, 40cm wide and 40cm deep tilting flume. The side walls of the test section 6m downstream of the channel entrance were made of optical glass for LDA (DANTEC-made) and PIV (KANOMAX-made) measurements. Hydraulic conditions for the experiments are shown in Table 5.1. In this study, the flows over smooth bed and rough bed were compared with each other and the effect of roughness elements on turbulence structures was considered. In rough flow, the bottom of the flume was covered by spherical glass beads of k_s=1.7cm diameter, arranged in the most compact configuration. On the other hand, in a wave-induced (periodic sine-wave) flow, several types of wave periods and wave heights were generated.

Table 5.1 Hydraulic conditions of rough-bed flow and wave-induced flow.

case	condition	S_b	h (cm)	B/h	h/k_s	A_m/h (x10^{-2})	U_m (cm/s)	U_* (cm/s)	Fr	Re (x10^3)
L02S	S	1/6000	5.0	8.0	-	0.0	16.0	0.99	0.23	8.0
L02R	R	1/1400	5.0	8.0	2.94	0.0	16.0	1.58	0.23	8.0
LA1S	W	1/6000	5.0	8.0	-	1.0	16.0	0.95	0.23	8.0
LA2S	W	1/6000	5.0	8.0	-	2.5	16.0	0.94	0.23	8.0
M06S	S	1/1200	5.0	8.0	-	0.6	40.0	2.10	0.57	20.0
M10S	S	1/316	3.5	11.4	-	2.0	57.1	2.90	0.98	20.0
H15S	S	1/167	4.0	10.0	-	2.5	93.8	4.75	1.50	37.5
H15R	R	1/34	4.0	10.0	2.35	5.0	93.8	10.72	1.50	37.5
H23S	S	1/77	3.0	13.3	-	3.3	125.0	6.09	2.30	37.5
S31S	S	1/41	3.0	13.3	-	6.7	166.7	8.47	3.07	50.0

S:smooth, R:rough, W:wave-induced, A_m=amplitude
k_S=1.7(cm), $Fr=U_m/(gh)^{0.5}$, $Re=U_m h/\nu$

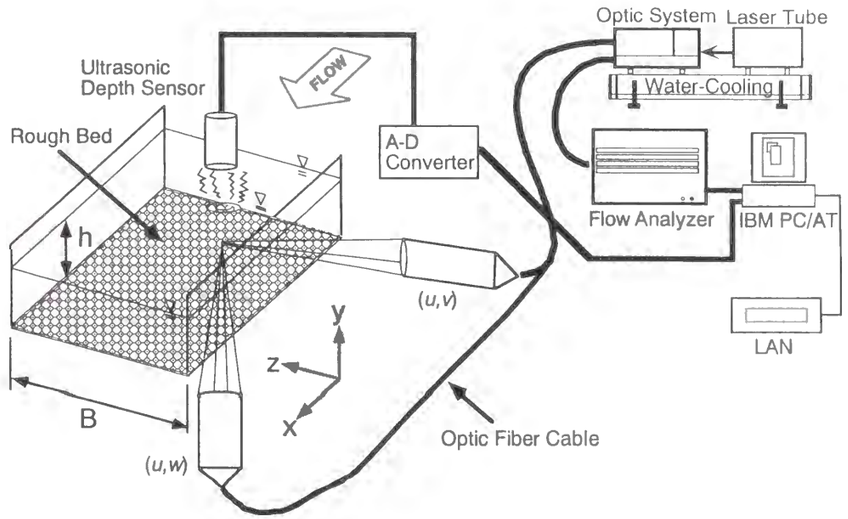

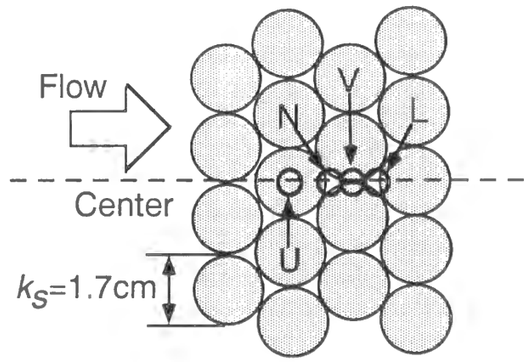

Fig.5.2 Experimental flume and LDA system of rough bed flow

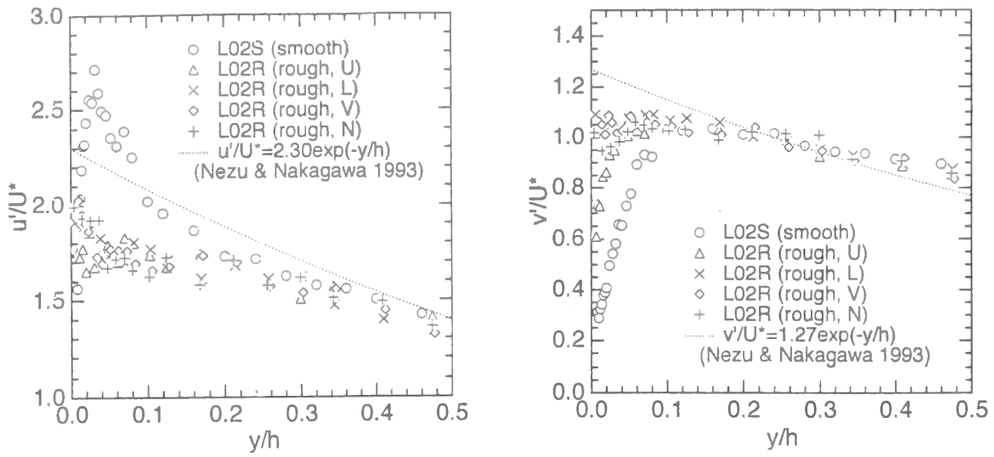

Fig.5.3 Turbulence intensities u'/U_* and v'/U_* for various measuring points around roughness elements.

Flow visualization was conducted by using PIV (KANOMAX-made) methods. Nylon 12 particles (50μm diameter and 1.01 specific gravity) stirred into the alcohol were uniformly scattered in the circulating water of the flume. About 2mm thick laser-light sheet (LLS) was illuminated vertically and images of tracers were taken using a high-sensitive CCD camera (1800 frames of image) that was placed beside the side-wall. In this study, one pixel of the image corresponds to the area of 0.4 × 0.4mm. These images were recorded in CRV disc (SONY-made) at the interval of 1/30sec and analyzed by the PIV algorithm.

Furthermore, LDA (DANTEC-made) measurements were conducted at the same flow conditions. The sampling time was 60sec and the sampling frequency was about 200Hz. At that time, an ultrasonic depth-meter instrument (KEYENCE-made) was set above the free surface, and synchronized with LDA of movable point, as depicted in Fig.5.2. Cross-correlation between the velocity fluctuations and the surface-wave fluctuations was calculated then.

5.3 Long-Time Averaged Turbulence Characteristics

5.3.1 Difference of Turbulence Intensity around Roughness Elements

Firstly, it is necessary to evaluate how far the roughness effect spreads from the roughness elements. Some researchers have studied the effect of vortex-sheddings from individual roughness elements on the turbulence structure of flow with small relative submergence. Kikkawa *et al.* (1988) have investigated the distributions of velocity and Reynolds stress around roughness elements and mentioned that the upward flow occurs in the upstream of roughness and the downward flow occurs in the downstream of roughness elements, which implies that the homogeneity does not hold good near roughness elements. Fig.5.3 shows the distribution of turbulence intensities u'/U_* and v'/U_* for various measuring points around roughness elements, together with the data for L02S (smooth bed). Herein, the origin of vertical direction (y=0) was set at the top of the roughness elements. It can be seen clearly that the distribution v' at point U (top of roughness element) is quite different from the others around roughness elements (L, V and N) near the bed. The distribution v' at U is similar to the distribution for smooth bed, and the value decreases near the wall. Furthermore, the vertical intensity v' increases slightly but the streamwise

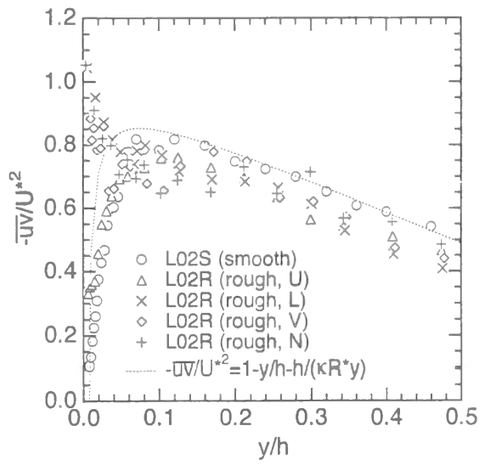

Fig.5.4 Reynolds stress $-\overline{uv}/U_*^2$ for various measuring points around roughness elements.

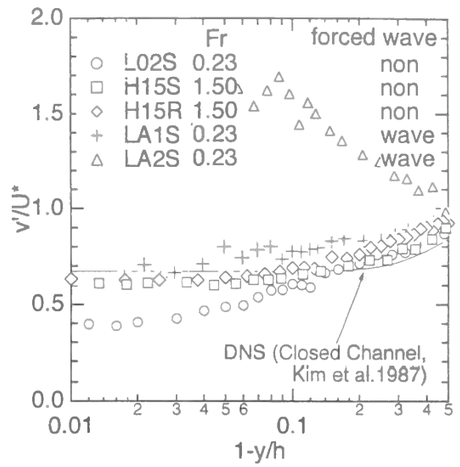

Fig.5.5 Vertical component of turbulence intensity v'/U_* near the free surface.

intensity u' decreases near the wall (y/h<0.3; roughness sublayer) for L02R, which shows that the tendency toward isotropy becomes stronger for rough bed, as pointed out by Nezu and Nakagawa (1993). Fig.5.4 shows the distribution of Reynolds stress $-\overline{uv}/U_*^2$ at various measuring points around roughness elements, together with the data for L02S. The characteristic at U is similar to that of v'. The distribution of $-\overline{uv}$ for rough bed is similar to that for smooth bed away from the wall (y/h>0.3), which is the same characteristics for u' and v'. Therefore, the effect of roughness element on the turbulence intensity is weaker away from the wall, that is to say, out of the roughness sublayer.

5.3.2 Turbulence Intensity in Wave-Induced Flow

It has been pointed out that the turbulence intensity changes greatly near the free surface, and in particular, the vertical component v' is greatly affected by the free surface. Fig.5.5 shows the distribution of the vertical component of turbulence intensity v'/U_* near the free surface. Furthermore, DNS database in duct flow (Re=8000, R_*=400) by Kim *et al.* (1987) and the semi-empirical formula in an open-channel flow derived by Nezu and Nakagawa (1993) are plotted together in this figure. It can be seen that v' is damped near the free surface, that is to say, y/h>0.9 in a tranquil flow (L02S) in comparison with the DNS data of duct flow. However, when the surface-wave fluctuations occur, the value of v' increases rapidly (H15S, H15R, LA1S and LA2S). This means that the damping effect is lost out as the surface-wave fluctuations increase and that the surface-wave fluctuations play an important role on the turbulent variations near the free surface.

5.3.3 Spectral Distribution of Velocity Fluctuations

Hunt and Graham (1978) and Hunt (1984) have related the damping characteristics of v' with the spectrum. Fig.5.6 shows some examples of the spectral distributions $S_v(k)$ for the fluctuations $v(t)$ for L02S, H15R and LA2S (see Fig.3.4), respectively. The value of low wave-number near the free surface (y/h=0.95) decreases in L02S, as has been pointed out by Hunt and Graham (1978). However, in a super-critical flow (H15R: Fr=1.50), the region of low wave-number does not decrease with an increase of y/h due to the turbulence eddies near the free surface. On the other hand, in a wave-induced flow (LA2S), $S_v(k)$ has distinguishable peaks at k=1.2 (1/cm) (corresponds to the period of the induced-wave) and k=2.2 (1/cm). Nevertheless, $S_v(k)$ decreases in the region of low wave-number as is the

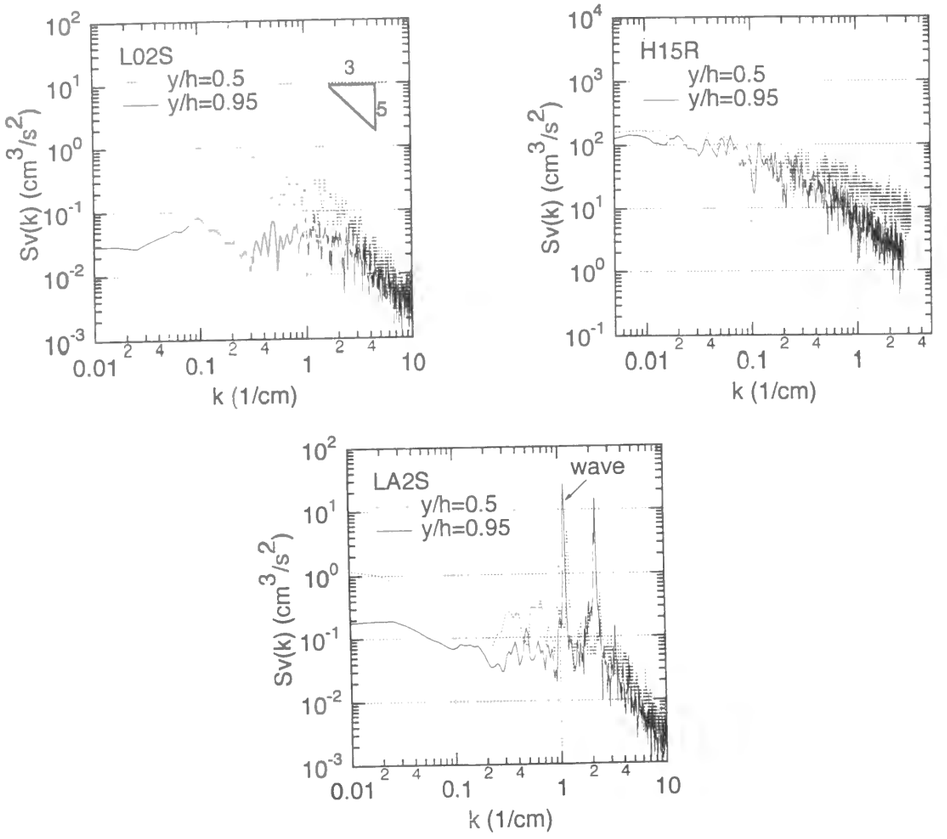

Fig.5.6 Spectral distributions $S_v(k)$.

same with L02S. This implies that the turbulence structures in H15R is quite different from those in LA2S. That is to say, the induced wave of small amplitude affects only the particular frequency region of velocity fluctuations and has less effect on the energy cascade-process, which differs quite from those in a super-critical flow.

5.3.4 Turbulent Energy Budget near Free Surface

The turbulent generation (or production) G, the turbulent energy diffusion T_D and ε are defined in the same manner as in the chapter 2.

Fig.5.7 is the turbulent energy budget near the free surface, together with DNS data of Kim *et al.* (1987). As for G, the values of L02S, H15S and H15R coincide well with the semi-empirical formula in open-channel flow derived by Nezu and Nakagawa (1993), whereas the value of LA2S increases significantly near the free surface. This implies that the energy is not generated near the free surface even in a super-critical flow. On the contrary, ε increases in H15S and H15R with an increase of the Froude number, in spite of little increase in LA2S. As for T_D, the value of LA2S increases quite greatly near the free surface. In this way, the turbulent energy is convected without any deformations in a wave-induced flow of small amplitude (without breaking wave), whereas the energy of water waves is added to the turbulent energy in a super-critical flow of steep open-channel.

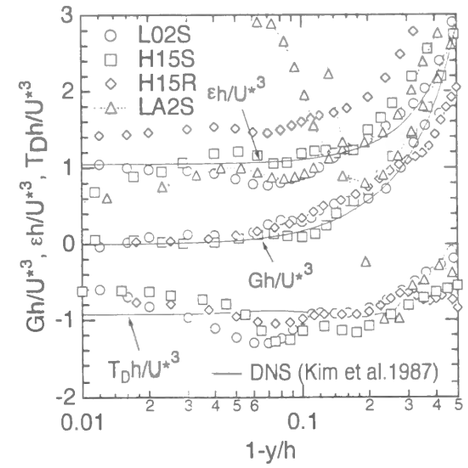

Fig.5.7 Turbulent energy budget near the free surface.

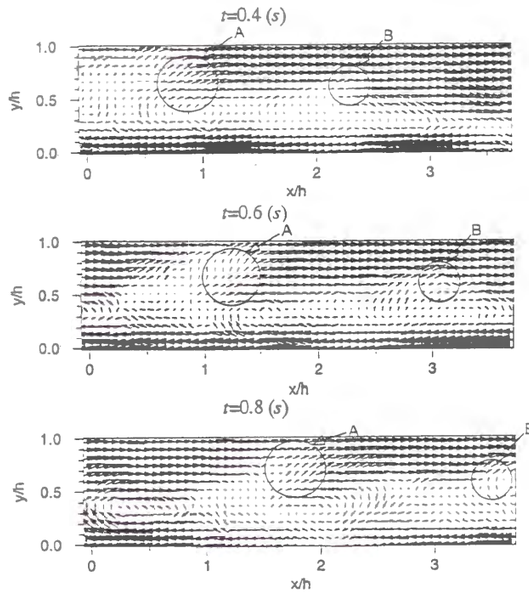

Fig.5.8 Velocity vector fields in tranquil flow over smooth bed (L02S).

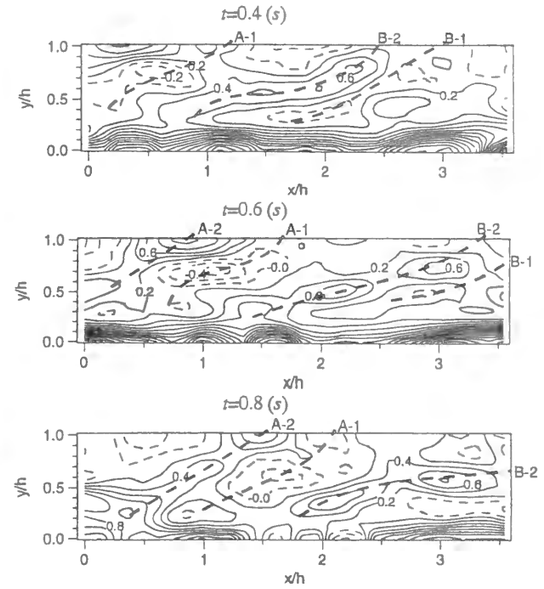

Fig.5.9 Contours of instantaneous spanwise vorticities over smooth bed (L02S).

5.4 Instantaneous Flow Structures over Rough Bed

5.4.1 Instantaneous Structures in Quiet Free Surface

Fig.5.8 shows an example of velocity vector fields that are viewed in movable coordinates of the bulk mean velocity in the center of channel for L02S (over smooth bed) when the free surface is quiet in the same figure as Fig.3.12 (Froude number Fr is small. This figure is again shown here for comparison with rough bed flow.). It can be seen that there exist quasi-periodical patterns of a high-speed region and a low-speed region alternately (about twice the depth as mentioned by Utami and Ueno (1987)).

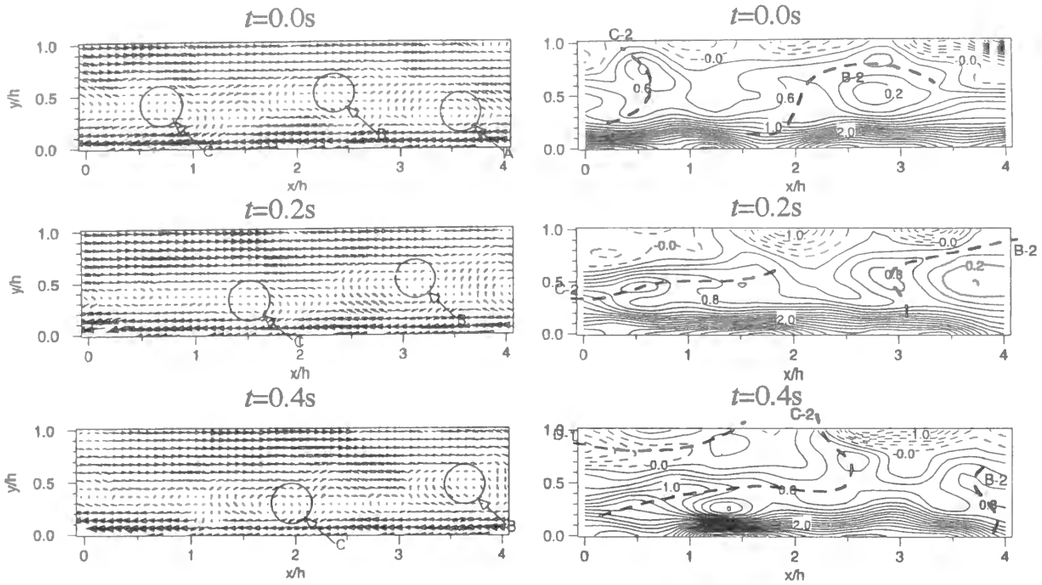

Fig.5.10 Velocity vector fields in tranquil flow over rough bed (L02R).

Fig.5.11 Contours of instantaneous spanwise vorticities over rough bed (L02R).

The spanwise vorticities Ω are shown in Fig.5.9, which are normalized by the maximum velocity and the flow depth (the same figure as Fig.3.13). The dotted line is the valley (negative peak : A-1 and B-1) and the ridge (positive peak : A-2 and B-2) of vorticities. The front parts of upward-motion region (A-1 and B-1) attain negative values and back parts (A-2 and B-2) attain positive values. These characteristics agree fairly well with a conceptual model of Nakagawa and Nezu (1981), as shown in Fig.5.1. The coherent regions indicate an inclined angle toward the wall.

On the other hand, it has a possibility that this quasi-periodic structure may become weaker or diminish over rough bed due to the macro-roughness. Fig.5.10 is the velocity vector fields for L02R (over rough bed, the same *Fr* as L02S). It can be seen that some of the smaller-scale coherent structures are generated near the bed and the quasi-periodic structures become weaker. Near the free surface, the coherent structures diminish the size and power due to the damping effect of the free surface, which is the same as L02S. This characteristic can be seen clearly in the spanwise vorticities Ω, as shown in Fig.5.11. The value of vorticities takes a greater value near the rough wall than over smooth bed due to the wake effect of roughness elements. Furthermore, the periodicity of coherent vortices becomes weaker over the whole depth and the inclination of the greater value region (dotted line) changes variously depending on the roughness elements.

5.4.2 Generation of Boil Vortices near Free Surface

As mentioned previously, some researchers have pointed out that boils become stronger and larger as the bed roughness increases. Furthermore, it is presumable that boils can be seen more clearly as the velocity increases. Fig.5.12 is the velocity vector fields for H15R in super-critical flow when the surface-wave fluctuations occur. The coherent vortices are generated near the roughness elements, and then convected to the streamwise direction and become larger as they lift up toward the free surface. These large-scale coherent structures are generated quasi-periodically and the larger vortices are lost out at t=0.1s. Therefore, the boil period is greater in river, as pointed out by Jackson (1976).

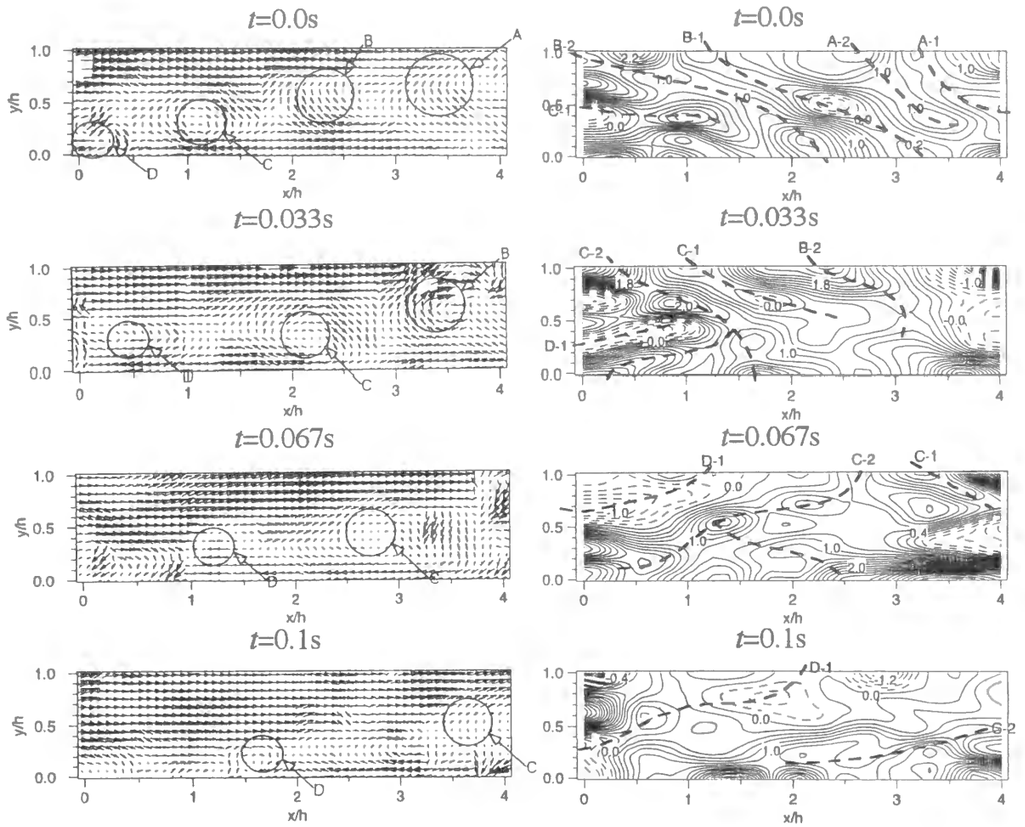

Fig.5.12 Velocity vector fields in super-critical flow over rough bed (H15R).

Fig.5.13 Contours of instantaneous spanwise vorticities over rough bed (H15R).

The spanwise vorticities Ω are shown in Fig.5.13. The regions of greater value are inclined in the upstream direction when the large-scale coherent structures occur frequently (A and B, t=0.0～0.033s). When the larger vortices disappear (t=0.1s), the shape of contours becomes similar to that for L02R as seen in Fig.5.11.

5.4.3 Instantaneous Structures in Wave-Induced Flow

In contrast, Fig.5.14 is an example of instantaneous velocity vector fields for LA2S (wave period ; T=0.3s, wave amplitude ; A_m=1.25mm) in a wave-induced flow. It was revealed that the streamwise velocity became maximum when the flow was deepest (wave crest) (t=0.0s, x/h=1.2) and that the streamwise velocity became minimum when the flow was shallowest (wave trough) (t=0.2s, x/h=2.0), which implies that the flow was really three-dimensional (3-D). The vertical velocity moves downwards at the upstream of the wave crest (t=0.0s, x/h=0.5) and goes upwards at the downstream (t=0.0s, x/h=2.0). It can be seen that the coherent structures near the wall are prevented from lifting upwards by the periodic wave near the free surface. Fig.5.15 shows the spanwise vorticities Ω with respect to Fig.5.14. The lower-value region is generated near the wave trough and the higher-value region generated near the wall is disturbed. In this way, it is evident that the coherent structures in a steep open-channel flow are much different from those in a wave-induced flow.

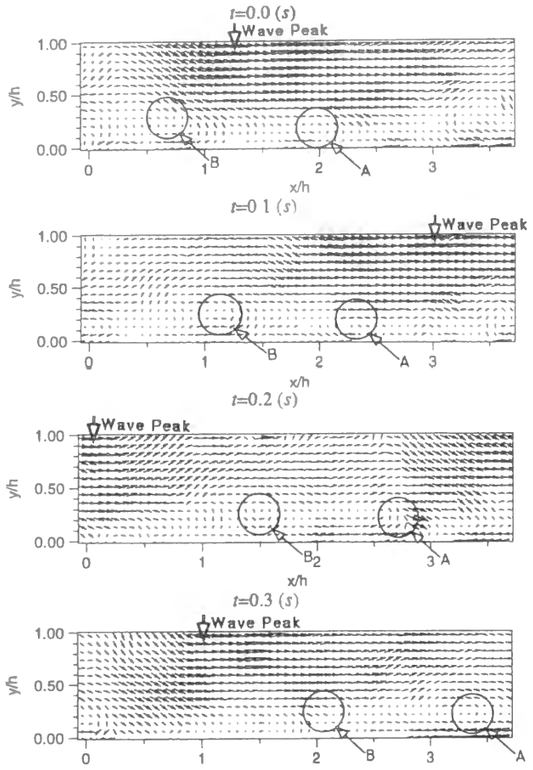

Fig.5.14 Velocity vector fields in wave-induced flow (LA2S).

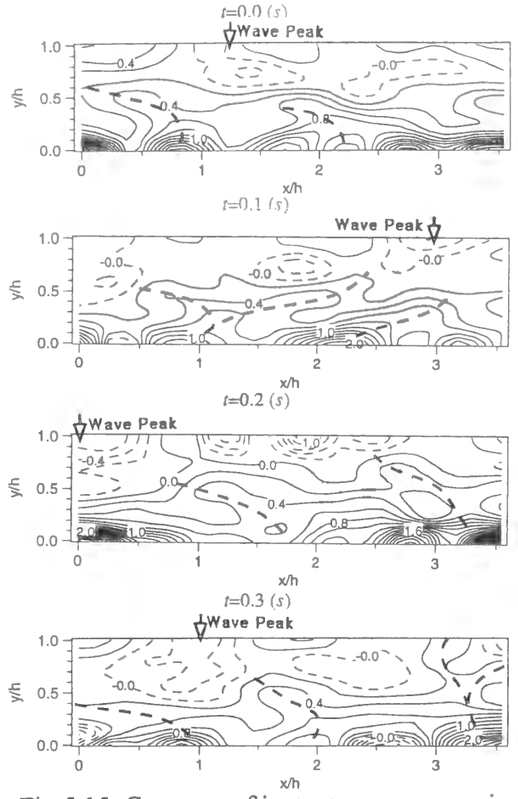

Fig.5.15 Contours of instantaneous spanwise vorticities in wave-induced flow (LA2S).

5.5 Effect of Roughness Elements on Coherent Structures and Surface-Wave Fluctuations

5.5.1 Difference of Correlation Structures around Roughness Elements

Non-conditional space-time correlation coefficient C_{uiuj} of velocity components u_i at a fixed point P and u_j at arbitrary point Q is defined in the same manner as in the chapter 2.

Fig.5.16 shows some examples of non-conditional space-time correlation coefficients C_{uu} over smooth bed (L02S) for fixed points × near the wall (y/h=0.05) versus the lag-time τ. The maximum correlation line fairly inclines downstream and the large-eddy structure is convected downstream without any remarkable deformation, as mentioned by Nakagawa and Nezu (1981).

In contrast, the horizontal inhomogeneity of the flow dominates greatly near the rough bed, as pointed by Raupach *et al.* (1980). Figs.5.17 and 18 are the contours of C_{uu} over rough bed (L02R) for two fixed points × near the wall (y/h=0.05), the downstream (point N) and upstream (point L) of the top of roughness, respectively. Dotted lines mean the negative values. There exists the different and complex correlation structure over rough bed. It can be seen clearly that the negative value spreads widely in Fig.5.17. On the other hand, the positive value spreads intermittently downstream from the fixed point L in Fig.5.18. The contours of this positive value is a little different from that for L02S in Fig.5.16, and the great value spreads intermittently. This fact coincides well with the measurement by Kikkawa *et al.* (1988) as mentioned before, and implies that the inhomogeneity of the coherent structure

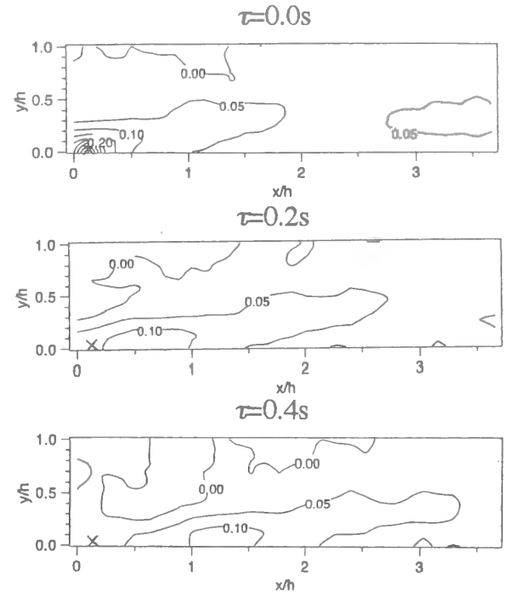

Fig.5.16 Non-conditional space-time correlation coefficients C_{uu} over smooth bed (L02S).

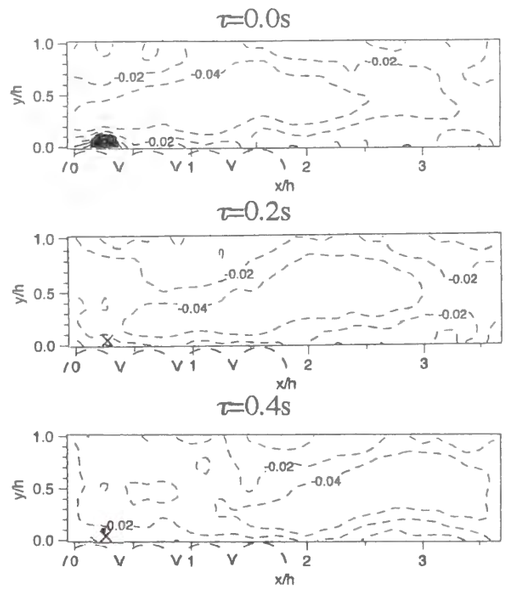

Fig.5.17 Non-conditional space-time correlation coefficients C_{uu} over rough bed at the downstream of the top of roughness (L02R).

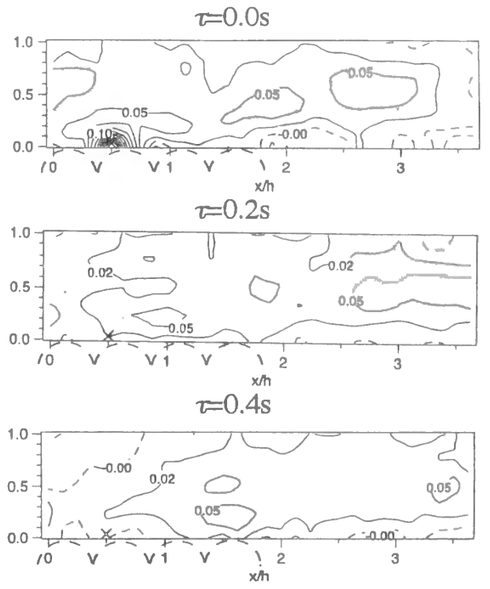

Fig.5.18 Non-conditional space-time correlation coefficients C_{uu} over rough bed at the upstream of the top of roughness (L02R).

predominates near the rough bed. The work of separation occurs more intensively in the dead zone behind the roughness elements as Fr increases, which may have a great and important effect on the formation of boil vortices near the free surface.

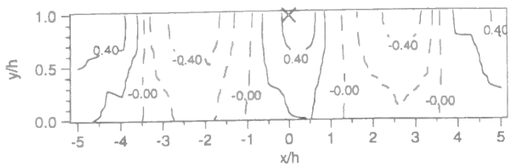

(a) LA2S (wind-induced flow)

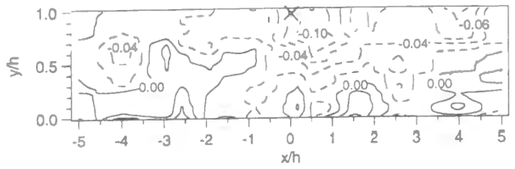

(b) H15S (smooth flow)

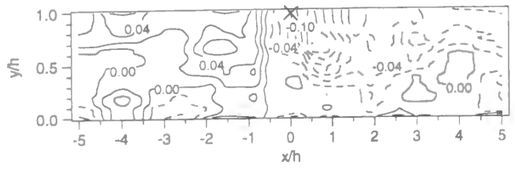

(c) H15R (rough flow)

Fig.5.19 Cross-correlation coefficient $C_{\eta u}$.

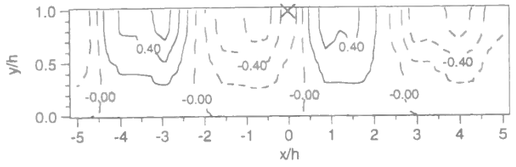

(a) LA2S (wind-induced flow)

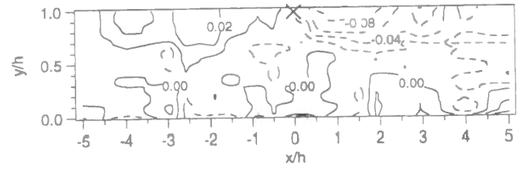

(b) H15S (smooth flow)

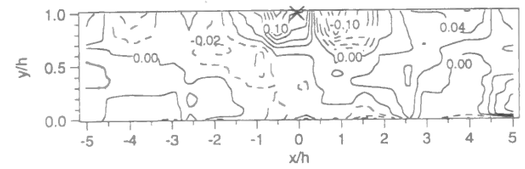

(c) H15R (rough flow)

Fig.5.20 Cross-correlation coefficient $C_{\eta v}$.

5.5.2 Relation between Velocity and Surface-Wave Fluctuations

The surface-wave fluctuations become greater as Fr increases, which indicates that the coherent structures generated near the wall have an important effect on the turbulence structure near the free surface, as pointed by Rashidi and Banerjee (1988). Figs.5.19(a)-(c) show the cross-correlation coefficient $C_{\eta u}$ normalized by η' and u' for H15S (smooth flow), H15R (rough flow) and LA2S (wave-induced flow), respectively. Herein, the fixed point of the surface-wave fluctuations η is x=0. Figs.5.20(a)-(c) show the cross-correlation coefficient $C_{\eta v}$ normalized by η' and v' in the same cases as Figs.5.19(a)-(c). From Fig.5.19(a) and Fig.5.20(a), it can be seen that the correlation structures in wave-induced flow (LA2S) are very different from those in steep open-channel flow (H15S and H15R) and the values of correlation are quasi-periodically and much greater. On the other hand, the values in steep open-channel flow (H15S and H15R) are much smaller than those in wave-induced flow (LA2S), as shown in Figs.5.19(b)-(c) and Figs.5.20(b)-(c). Furthermore, it can be seen that the negative peak-value of correlation near x=0 for H15R is greater than that for H15S. The contours for H15S and H15R have a clear difference with each other. The surface-wave fluctuations at the fixed point are closely related to the downstream velocity fluctuations for smooth flow (H15S). On the contrary, the correlation takes a positive value at x/h<0 for rough flow (H15R), and these positive regions spread more widely as the lag time τ passes. This means that the roughness elements have an important role on the generation of boil near the free surface, as mentioned by Jackson (1976), and that the instantaneous structures in Fig.5.12 generate a larger-scale boils, as we can observe in rivers. So, the structure of a steep open-channel flow differs significantly from that of a wave-induced flow and it is very important to mutually compare with each other in order to separate the "*turbulence effect*" and the "*wave effect*" in open-channel flows.

Figs.5.21(a)-(c) are the contours of lag time τ(s) when $C_{\eta u}$ takes a sub-peak value. The values near

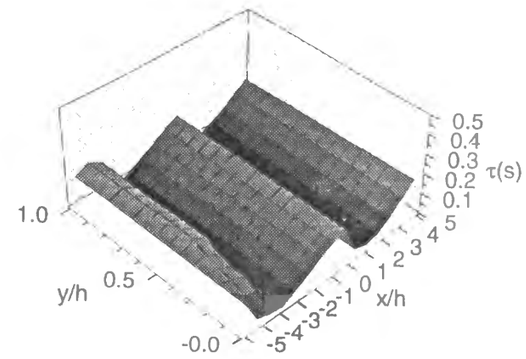

(a) LA2S (wave-induced flow)

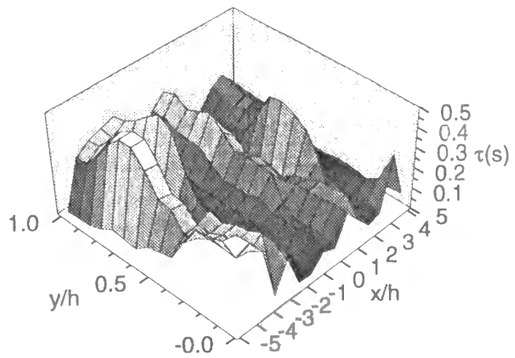

(b) H15S (smooth flow)

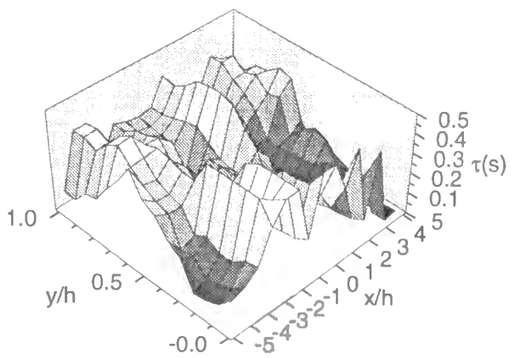

(c) H15R (rough flow)

Fig.5.21 Contour of lag time τ(s) when $C_{\eta u}$ takes a sub-peak value.

the wall and the free surface for LA2S take the same due to the effect of periodic wave. In this way, the "*wave effect*" relates to the pressure gradient, which affects the bulk flow widely. On the contrary, the "*turbulence effect*" disappears away from the free surface ("*isotropization*") and the correlation between velocity fluctuations and surface-wave fluctuations is very small for H15S.

5.6 Conclusions

In this chapter, the effect of macro-roughness on coherent structures over rough beds was investigated. At that time, space-time correlation analyses were used, and the relation between boils and surface-wave fluctuations was evaluated by using PIV methods and simultaneous measurements of both LDA and ultrasonic depth-meter instrument. Fig.5.22 shows the conclusions of chapter 5. The results we got are as follows,

(1) The vertical intensity v' increases slightly but the streamwise intensity u' decreases near the rough bed. This characteristic shows that the tendency toward isotropy becomes stronger near the roughness elements.

(2) The coherent vortices are quasi-periodically generated near the roughness elements. These vortices are convected to the streamwise direction and become larger as they lift up toward the free surface in

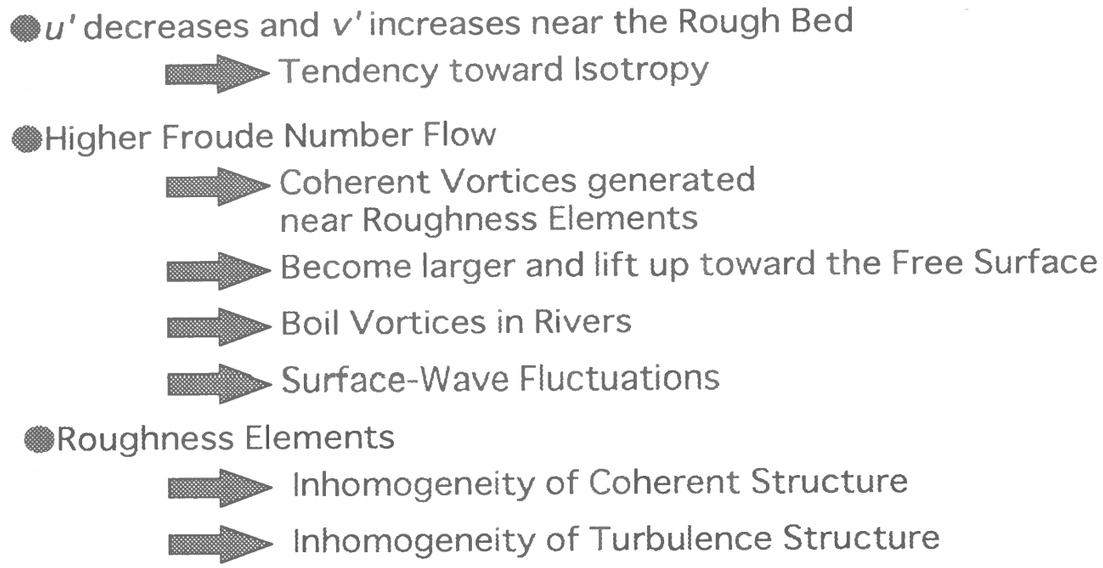

Fig.5.22 Conclusions of chapter 5.

a higher Froude number flow, which can be seen as boil vortices in rivers.
(3) The correlation structure varies near the rough bed due to the roughness elements. This fact implies that the inhomogeneity of the coherent structure predominates near the rough bed.
(4) The surface-wave fluctuation at the fixed point is closely related to the upstream velocity fluctuation for rough flow. This means that the roughness elements have an important role on the generation of boil near the free surface.
(5) The turbulence structure in a steep open-channel flow was compared with that in a wave-induced flow in order to separate the "*turbulence effect*" and the "*wave effect*" in open-channel flows.

Notations

A_m : wave amplitude
B : channel width
C_{uiuj} : non-conditional space-time correlation coefficient of velocity components u_i at a fixed point P and u_j at an arbitrary point Q
$F(f)$: normalized FFT spectrum
Fr : Froude number ($=U_m/\sqrt{gh}$)
G : turbulent generation (or production)
g : acceleration due to gravity
h : flow depth
k : turbulent kinetic energy, wave number
k_s : equivalent sand-grain diameter
Re : Reynolds number ($=U_m h/\nu$)
R_* : turbulent Reynolds number ($=U_* h/\nu$)
S_b : channel slope

$S_v(k)$: spectrum of v-component in a wave number k
T : wave period
T_D : turbulent energy diffusion
U_m : bulk mean velocity
U_* : friction velocity
u : instantaneous streamwise velocity component
u' : root-mean-square value of velocity fluctuations in x direction
$-\overline{uv}$: Reynolds stress
v : instantaneous vertical velocity component
v' : root-mean-square value of velocity fluctuations in y direction
w : instantaneous spanwise velocity component
w' : root-mean-square value of velocity fluctuations in z direction
x : streamwise direction
y : vertical direction from the channel bed

Greek symbols
$(\Delta x, \Delta y, \Delta z)$: lag distance
ε : turbulent energy dissipation rate
η : instantaneous surface displacement with respect to the still water level
η' : intensity of surface-wave fluctuations
ν : kinetic viscosity
τ : lag time
Ω : instantaneous spanwise vorticity ($=\partial u/\partial y - \partial v/\partial x$, clockwise direction is positive)

References

[1] Asano, T. : Hydrodynamics in wave-current co-existing fields, *Ph.D Thesis presented to Kyoto University*, 1986 (in Japanese).
[2] Ashworth, P.J., Bennett, S.J., Best, J.L. and McLelland, S.J. : Coherent flow structures in open channels, John Wiley and Sons Ltd., 1996.
[3] Bayazit, M. : Free surface flow in a channel of large relative roughness, *J. Hydraulic Research*, IAHR, Vol.14, No.2, pp.115-125, 1976.
[4] Herbich, J.B. and Shulits, S. : Large-scale roughness in open-channel flow, *Proc. of ASCE*, HY6, pp.203-230, 1964.
[5] Hunt, J. C. R. : Turbulence structure and turbulent diffusion near gas-liquid interfaces, *Gas Transfer at Water Surfaces*, W. Brutsaert and G. H. Jirka (eds.), Reidel Pub., pp.67-82, 1984.
[6] Hunt, J. C. R. and Graham, J. M. R. : Free-stream turbulence near plane boundaries, *J. Fluid Mech.*, Vol.84, pp.209-235, 1978.
[7] Jackson, R. G. : Sedimentological and fluid-dynamic implications of the turbulent bursting phenomenon in geophysical flows, *J. Fluid Mech.*, Vol.77, pp.531-560, 1976.
[8] Kanda, T. and Doi, K. : Characteristics of flow resistance of large relative roughness, *Research Report of Construction Engineering Research Institute*, Vol.22, pp.217-234, 1980 (in Japanese).
[9] Kanda, T. and Suzuki, K. : Characteristics of resistance to shallow water flows over bed roughened with spheres, *Journal of Hydraulic Engineering*, JSCE, No.357/II-3, pp.65-74, 1985 (in Japanese).
[10] Kikkawa, H., Uematsu, R., Jyo, M. and Sekine, M. : An experimental study on velocity profiles over the bed roughened with spheres or hemispheres and fluid forces exerted on them, *Journal of*

Hydraulic Engineering, JSCE, No.399/II-10, pp.47-54, 1988 (in Japanese).
[11] Kim, J., Moin, P. and Moser, R. : Turbulence statistics in fully developed channel flow at low Reynolds number, *J. Fluid Mech.*, Vol.177, pp.133-166, 1987.
[12] Kironoto, B.A. : Turbulence characteristics of uniform and non-uniform rough open-channel flow, *Ph.D Thesis presented to Lausanne University*, 1993.
[13] Kironoto, B.A. and Graf, W.H. : Turbulence characteristics in rough uniform open-channel flow, *Proc. of Inst. Civ. Engrs., Wat. Marit. and Energy*, Vol.98, pp.1-20, 1994.
[14] Krogstad, P.-A., Antonia, R.A. and Browne, L.W.B. : Comparison between rough- and smooth-wall turbulent boundary layers, *J. Fluid Mech.*, Vol.245, pp.599-617, 1992.
[15] Moog, D. B. : Stream reaeration and the effects of large-scale roughness and bedforms, *Ph.D Thesis presented to Cornell University*, 1995.
[16] Moog, D. B. and Jirka, G. H. : Macroroughness effects on stream reaeration, *Air-Water Gas Transfer*, B. Jahne and E.C. Monahan (eds.), AEON Verlag, pp.89-99, 1995.
[17] Myose, R. Y. and Blackwelder, R. F. : On the role of the outer region in the turbulent-boundary-layer bursting process, *J. Fluid Mech.*, Vol.259, pp.345-373, 1994.
[18] Nakagawa, H. and Nezu, I. : Structure of space-time correlations of bursting phenomena in an open-channel flow, *J. Fluid Mech.*, Vol.104, pp.1-43, 1981.
[19] Nakagawa, H., Nezu, I. and Ueda, H. : Turbulence of open channel flow over smooth and rough beds, *Journal of Hydraulic Engineering*, JSCE, No.241, pp.155-168, 1975.
[20] Nakagawa, H., Tsujimoto, T. and Shimizu, Y. : Turbulent structure of flow with small relative submergence affected by organized fluctuation due to vortex-sheddings from roughness elements, *Annual Journal of Hydraulic Engineering*, Vol.33, pp.487-492, 1989 (in Japanese).
[21] Nezu, I. and Nakagawa, H. : Turbulence in open-channel flows, IAHR Monograph, Balkema, 1993.
[22] Nezu, I., Nakayama, T. and Fujita, M. : Turbulence and free-surface sluctuations in open channel flows over macro-roughness, *Journal of Applied Mechanics*, JSCE, Vol.1, pp.709-718, 1998f (in Japanese).
[23] Nezu, I. and Nakayama, T.: Separation between turbulence and water-wave effects in an open-channel flow, *Flow Modeling and Turbulence Measurements VII*, pp.67-76, 1998i.
[24] Nezu, I. and Nakayama, T.: Effect of macro-roughness on coherent structures by using PIV methods, *Flow Modeling and Turbulence Measurements VII*, pp.617-626, 1998j.
[25] Rashidi, M. and S. Banerjee : Turbulence structure in free-surface channel flows, *Phys.Fluids*, Vol.31, No.9, pp.2491-2503, 1988.
[26] Raupach, M. R. : Conditional statistics of Reynolds stress in rough-wall and smooth-wall turbulent boundary layers, *J. Fluid Mech.*, Vol.108, pp.363-382, 1981.
[27] Raupach, M. R., Thom, A. S. and Edwards, I. : A wind-tunnel study of turbulent flow close to regularly arrayed rough surfaces, *Boundary-Layer Meteorology*, Vol.18, pp.373-397, 1980.
[28] Tanaka, H. : Studies on water particle velocity and bottom shear stress under non-linear wave with an arbitrary profile, *Proc. of Hydraulic Engineering*, JSCE, Vol.381, pp.181-187, 1987 (in Japanese).
[29] Utami, T. and Ueno, T. : Experimental study on the coherent structure of turbulent open-channel flow using visualization and picture processing, *J. Fluid Mech.*, Vol.174, pp.399-440, 1987.

CHAPTER 6

TURBULENCE STRUCTURE AT AIR-WATER INTERFACE WITH WIND SHEAR

Abstract

When the wind blows over the water, there occur drift currents and wind waves due to the wind shear across an air-water interface. At that time, mass transfer across a gas/liquid interface is of fundamental importance to environmental and geophysical sciences. Some studies about the wind-induced currents have been conducted in the field of coastal engineering and geophysical sciences. However, there are few studies about the wind-shear induced turbulence. So, the turbulence fields on both sides of an air-water interface were examined experimentally in wind-water tunnel. The turbulence quantities in the air behave similarly to those in flows over flat plates in open-channels. As for the water side, wave component and turbulence component were separated by a spectral separation method. Turbulence component has universal characteristics on a 2-D gravity wave. It became clear that turbulence structure and energy budget on both sides are closely related with each other and also that energy transfer through the air-water interface increases when the wind becomes faster. The present study was undertaken with the goal of evaluating the relationship between the wind waves and the turbulence structures across the air-water interface in a laboratory wind tunnel.

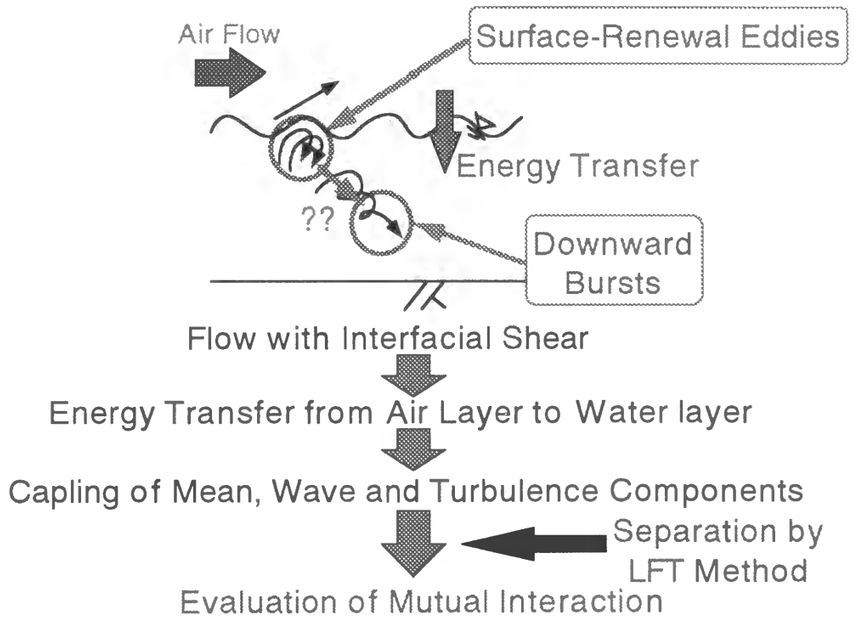

CHAPTER 6 TURBULENCE STRUCTURE AT AIR-WATER INTERFACE WITH WIND SHEAR

Parts of this chapter were presented in the following papers.

[1] Nezu, I., Nakayama, T. and Inoue, R. : Turbulence structures in air-water interface with wind shear, *Annual Journal of Hydraulic Engineering*, Vol.43, pp.413-418, 1999a (in Japanese).
[2] Nezu, I. and Nakayama, T. : Effect of turbulence components below wind water waves, *Annual Journal of Hydraulic Engineering*, Vol.43, pp.407-412, 1999b (in Japanese).
[3] Nezu, I. and Nakayama, T. : Fundamental study at air-water interfaces with wind shear, *28th IAHR Congress*, IAHR, 1999c.
[4] Nezu, I. and Nakayama, T.: Effect of turbulence components below wind water waves, *28th IAHR Congress*, IAHR, 1999d.
[5] Nakayama, T. and Nezu, I. : Turbulence structures of wind water waves, *Journal of Hydraulic Engineering*, JSCE, No.642/II-50, 2000a (in Japanese).

6.1 Introduction

So far, there have been a lot of researches about wind wave in the branch of coastal engineering and geophysical science. These researches are mainly divided into two categories; the one is about the drift current, wind velocity and momentum transport across the interface, *etc*., and the other is about the turbulence characteristics in a detailed level.

As for the former research, Wu (1981) has confirmed the logarithmic distribution of wind velocity over a water surface and suggested a criterion to separate roughness conditions of the water surface into three regimes: aerodynamically smooth, moderately rough and fully rough. By the way, it is very important to make clear whether or not the momentum flux from the air side takes the same value to that into the bulk of water at the interface. There have been many but different researches about momentum transfer across the interface. For example, Shemdin (1972) has pointed out that almost all the momentum from the air side is transferred to the bulk of the water, Wu (1975) about 70% and Mitsuyasu (1985) about the half, *etc*. Though Wu (1988) has supposed two principal non-dimensional parameters relating the roughness height and the friction velocity of wind, it is not yet clear about the relationship between the structure of wind wave and the surface-wave fluctuations. Therefore, it is necessary to carry out further examinations about these points.

On the other hand, most of the latter researches have been conducted in laboratory experiments and are closely related to a gas transfer across the interface. When the wind blows over the water, the energy is transferred to the mean and wave fields. At that time, there occurs the energy transport from the wave field to the mean field and from the mean field to the turbulent field. So, the coupling and the interaction among the mean, wave and turbulent fields exist, as pointed out by Cheung (1985) and Cheung and Street (1988). So, it is very important how to separate the wave-induced component and turbulence-induced component from velocity fluctuations. There are several methods for separating these two components. The first method (a) derived by Benilov *et al*. (1974) is called the "*linear filtration technique* (LFT)". In this method, the orbital motion of surface waves is assumed to be linearly related to the surface displacement, while turbulence and orbital motion are assumed to be uncorrelated at first order. Howe *et al*. (1982) pointed out that the wave component affects the mean velocity near the interface by using this method. The second method (b) derived by Dean (1965) is a nonlinear least squares resolution, which assumes that wave-induced motions and turbulence interact each other. Jiang *et al*. (1990) have used this method and pointed out that the wave-turbulence interaction does cause the energy transfer. The third method (c) derived by Thais and Magnaudet (1995, 1996) is called the "*nonlinear triple decomposition method* (TDM)", by which the fluctuating water velocity is split into three contributions; that is to say, the potential, rotational wave-related and remaining turbulent components. They proposed that the wave-turbulence interactions scale with the ratio between the wave kinetic energy at the surface and the wind shear. Except the above-mentioned three methods, there are a few methods to separate the wave component. Bliven *et al*. (1984) have evaluated the first and the second order velocity spectra due to the surface elevation by using the deep water-wave theory, and Plate and Friedrich (1984) have used the simpler method to regard only the peak region of velocity spectrum as the wave component.

In this way, there have been few comprehensive studies of detailed phenomena about wind waves. So, we compare the experimental data with the existing studies and reveal the structure of wind-induced waves and the relation to the surface-wave fluctuations. Furthermore, each decomposing method has some advantage and disadvantage, and it is difficult to decide immediately which is the best method. In this study, we used the most simple method, so called, LFT, and revealed the turbulence structure and coherent vortices in wind waves.

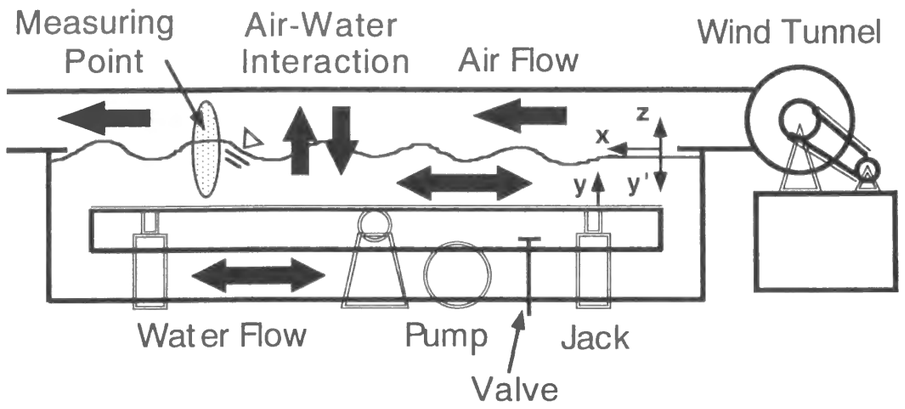

Fig.6.1 Schematic diagram of tilting wind-water tunnel.

Table 6.1 Hydraulic conditions of wind wave.

	$U_{a,max}$ (m/s)	U_{*a} (cm/s)	z_a (cm)	η' (cm)	H/λ	R_r
d2wa	0.94	3.84	0.00321	0.0292	3.200	0.08
d2wb	1.79	7.56	0.00402	0.0145	2.667	0.19
d2wc	2.63	12.01	0.00617	0.0130	1.333	0.47
d2wd	3.63	17.51	0.00796	0.0855	1.143	0.88
d2we	4.56	21.79	0.00978	0.4812	0.571	1.35
d2wf	5.46	28.67	0.01145	0.7085	0.286	2.06
d2wg	6.76	38.98	0.01410	0.8559	0.235	3.45
d2wh	8.30	50.29	0.01981	0.8157	0.200	6.25

6.2 Experimental Apparatus and Procedures

The experiments were conducted in a 16m long, 40cm wide and 50cm deep tilting wind-water tunnel, as shown in Fig.6.1. The wind tunnel is composed of a recirculating tilting water flume and an open-ended wind tunnel. The side and bottom walls of the measuring point 9m downstream of the channel entrance were made of optical glass for LDA measurements. Coordinate axes in the streamwise, vertical and spanwise directions were defined as x, y and z', respectively, and z was in the vertical direction from the water surface. And the corresponding velocity components are u, v, and w, respectively. Hydraulic conditions for the experiments are shown in Table 6.1. The parameters are defined as follows, $U_{a,max}$: the maximum wind velocity, U_{*a} : the friction velocity in the air layer calculated from the log-law, z_a : roughness height, η' : the intensity of surface-wave fluctuations, H : the flow depth, λ : wave length, $Rr=U_{*a}z_a/\nu_a$: roughness Reynolds number, and ν_a : kinetic viscosity of air, respectively. In all the experimental cases, the flow depth was fixed to be 8cm. Winds of several speeds were blown over a stable water in recirculating flume by valve in the same way as Reid (1957) and Baines and Knapp (1965), and the measurements were made in the center of channel by using a 500mW fiber-optic two-component LDA system (DANTEC-made). The sampling time was 60sec and the sampling frequency was about 200Hz. At that time, an ultrasonic depth-measuring instrument (0.1mm accuracy, KEYENCE-made) was set above the free surface, and synchronized with the LDA,

and wave component and turbulence component were separated by a spectral separation method. Wind velocity was accurately measured with the LDA and a fog generator. Furthermore, the surface drift velocity U_s was determined by measuring the time for a floating cube of about 2mm side to travel a fixed distance (50cm) by video recorder (0.01sec) and averaging more than 30 samples.

6.3 Theoretical Consideration and LFT Method

6.3.1 Theoretical Consideration

The distribution of wind mean velocity over a water surface can be expressed by a log-law in a same manner as boundary layer over a fixed wall, as follows:

$$\frac{U_a - U_s}{U_{*a}} = \frac{1}{\kappa}\ln\frac{z}{z_a} \tag{6.1}$$

where U_s is a surface drift velocity, z_a is a roughness height of water surface, and U_* is the friction velocity. From now on, subscript "a" means air side and "w" means the water side. Wu (1981) has proposed three regimes dependent on the roughness of water surface, as follows:
(a) Aerodynamically smooth : $Rr=U_{*a}z_a/\nu_a<0.5$
(b) Incompletely rough : $0.5<Rr<2$
(c) Aerodynamically rough : $Rr>2$

Shemdin (1972) and Wu (1975) have pointed out that the log-law is effective near the free surface even in the water side.

$$\frac{U_s - U_w}{U_{*w}} = \frac{1}{\kappa}\ln\frac{y'}{y_w} + 8.5 \tag{6.2}$$

where $y'=H-y$ is the distance from the free surface into the bulk of water, and H is the flow depth of channel.

The dispersion relation of linear wave (small-amplitude waves theory) is given as follows;

$$c^2 = \left(\frac{g\lambda}{2\pi} + \frac{2\pi\sigma}{\rho\lambda}\right)\tanh\frac{2\pi h}{\lambda} \tag{6.3}$$

where c : wave celerity and σ : surface tension. Given f_p (primary frequency of wind wave), c and λ are uniquely defined due to the relation $c=\lambda f_p$.

Wu (1988) has supposed two principal non-dimensional parameters characterizing wind-wave interaction in a local equilibrium and pointed out that these parameters are universal in a laboratory flume and field level, as follows:

$$\frac{gz_a}{U_{*a}^2} = \alpha \tag{6.4}$$

$$\frac{\omega_p z_a}{U_{*a}} = \gamma \tag{6.5}$$

where ω_p ($=2\pi f_p$) is the angular frequency of dominant waves. Eq.(6.4) describes the growth of roughness length with wind proposed by Charnock (1955), and corresponds to the inverse of square of Froude number (α=0.0185). Eq.(6.5) is the relation describing the influence of dominant waves on wind-

wave interacting processes proposed by Toba (1979).

6.3.2 LFT (Linear Filtration Technique) Method

Any flow field quantities $F(x,t)$ can be decomposed into three parts, *i.e.*,

$$F(x,t)=\overline{F}(x)+\tilde{F}(x,t)+F'(x,t) \tag{6.6}$$

where $\overline{F}(x)$, $\tilde{F}(x,t)$ and $F'(x,t)$ are the mean, wave-induced and turbulence-induced components, respectively. Straightforward time averaging of F can determine the mean value $\overline{F}$, as follows:

$$\overline{F}(x)=\lim_{T\to\infty}\frac{1}{T}\int_0^T F(x,t)dt \tag{6.7}$$

Benilov *et al.* (1974) proposed a spectral separation method (LFT) on the following assumption.
(i) The wave-induced component is linearly correlated with surface displacement η:

$$\tilde{F}(x,t)=L\eta(r,t) \tag{6.8}$$

(ii) The wave-induced motions and turbulence are not correlated with each other:

$$\overline{\tilde{F}F'}=0 \tag{6.9}$$

where L is some linear operator and r is the horizontal vector. In this way, the second moments of $\tilde{F}$ and F' can be computed by LFT:

$$S_{\alpha\beta}(f)=S_{\tilde{\alpha}\tilde{\beta}}(f)+S_{\alpha'\beta'}(f) \tag{6.10}$$

$$S_{\tilde{\alpha}\tilde{\beta}}(f)=\frac{S_{\alpha\eta}(f)S_{\beta\eta}{}^{*}(f)}{S_{\eta\eta}(f)} \tag{6.11}$$

where $S_{\alpha\beta}$ is the cross spectrum of function α and β, $S_{\eta\eta}$ the power spectrum of η, $S_{\beta\eta}{}^{*}$ the conjugate of the cross spectrum $S_{\beta\eta}$, and f the frequency, respectively. By using the above equations, the power spectra of total velocity fluctuation and of wave-induced component are correlated with each other.

6.4 Fundamental Characteristic of Wind Wave

6.4.1 Momentum Transfer

When the wind blows over the water, the drift current occurs in the water side. Wu (1975) has evaluated the relation between the wind velocity and the surface drift velocity, and suggested the following relation.

$$U_s=0.55U_{*a} \tag{6.12}$$

Fig.6.2 shows the ratio of drift current to friction velocity U_s/U_{*a} versus the maximum wind velocity $U_{a,max}$. It can be seen that the value approaches a constant value derived by Wu (1975) when the wind velocity becomes faster and the surface-wave fluctuations occur. However, the value decreases in a lower wind velocity and tranquil surface. This phenomenon may be closely related with a momentum transfer, as mentioned later. Figs.6.3 and 6.4 show the primary mean velocity both in the air side and

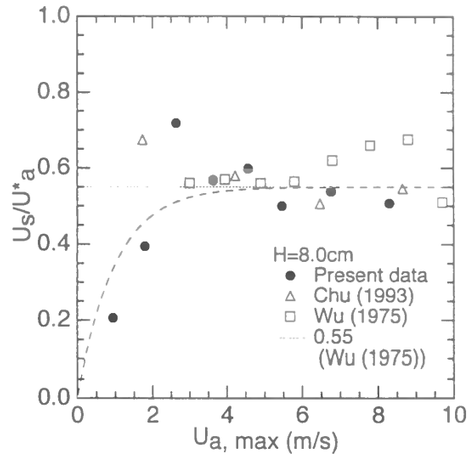

Fig.6.2 Ratio of drift current to friction velocity U_s/U_{*a} in wind wave.

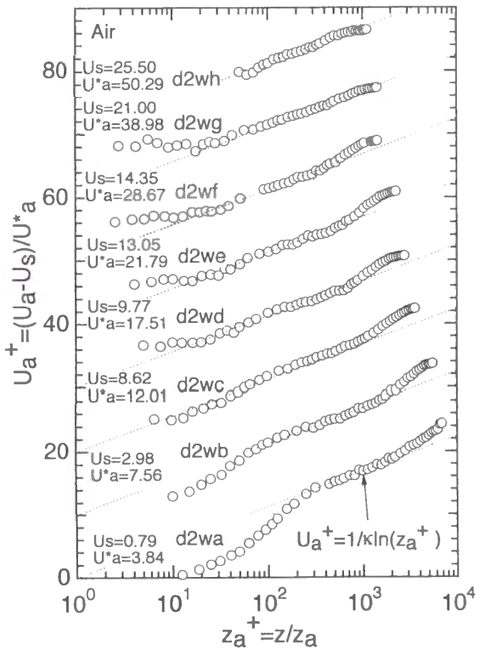

Fig.6.3 Primary mean velocity in air side U_a^+.

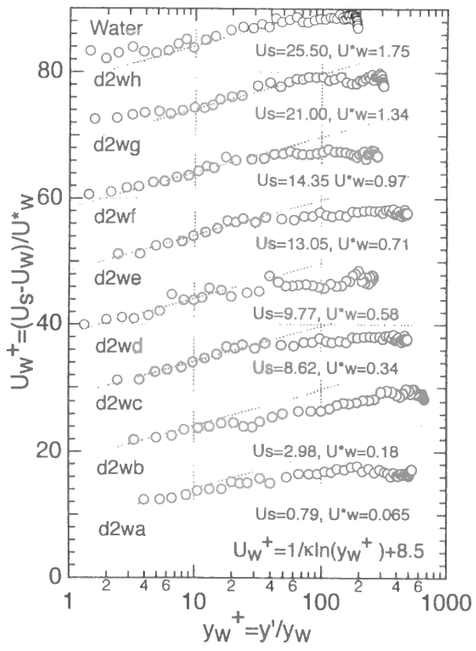

Fig.6.4 Primary mean velocity in water side U_w^+.

the water side from the interface, where z is the distance to the upward-vertical direction from the interface (air side) and y' is downward-vertical direction (water side). In Fig.6.3, there exists a viscous sublayer near the interface in the case of d2wa and d2wb. Furthermore, the value of U_a^+ becomes larger than the log-law near the interface when the wind becomes stronger, which implies that a roughness sublayer develops in the same manner as rough bed flow over a fixed boundary. On the other hand, the log-law also holds good in the water side in Fig.6.4, in the same way as Shemdin (1972), Wu (1975) and Wu and Tsanis (1995). The increasing characteristic near the interface in rough situation is similar to that in the air side. In this way, the primary mean velocities on both sides

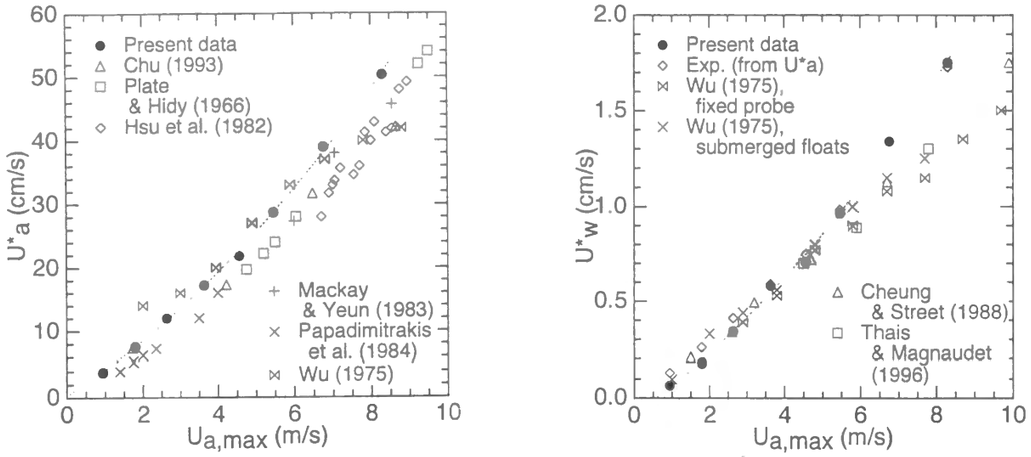

(a) Air layer (b) Water layer

Fig.6.5 Friction velocities both in air side and water side evaluated from the log-law.

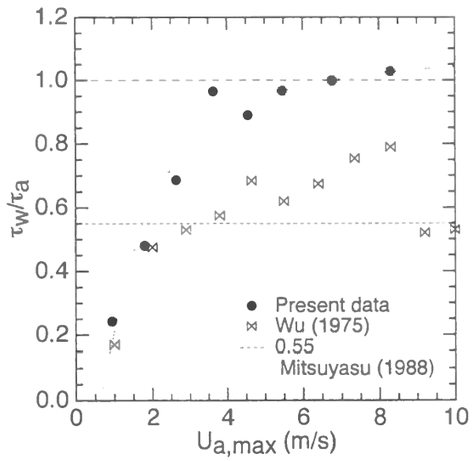

Fig.6.6 Ratio of shear stress τ_w/τ_a.

have similar characteristics due to a close relationship across the interface.

Figs.6.5(a)-(b) show the friction velocities both in air side and water side evaluated from the log-law. Dotted curve is the two-order approximate one calculated from the experimental data. It can be seen that the present data are in a good agreement to the former values, which implies that U_{*a} and U_{*w} have an unique relation to the maximum wind velocity. Furthermore, the increasing rate of friction velocity becomes greater as the wind increases due to the change into the rough turbulence flow in the same way as Ocampo-Torres and Donelan (1995).

Fig.6.6 shows the ratio of shear stress τ_w/τ_a, in which $\tau_a=\rho_a U_{*a}^2$ and $\tau_w=\rho_w U_{*w}^2$. It has been pointed out that the momentum transport by waves is at most 7% of the momentum from the air side, which implies that the shear stresses of both sides coincide with each other except for the case that the momentum varies in the streamwise direction. In this figure, the momentum is continuous, *i.e.*, $\tau_w=\tau_a$, when the wind velocity becomes faster and the surface-wave fluctuations occur. However, the value of τ_w/τ_a is smaller in a lower wind velocity. This is because the shear stress is transferred through the

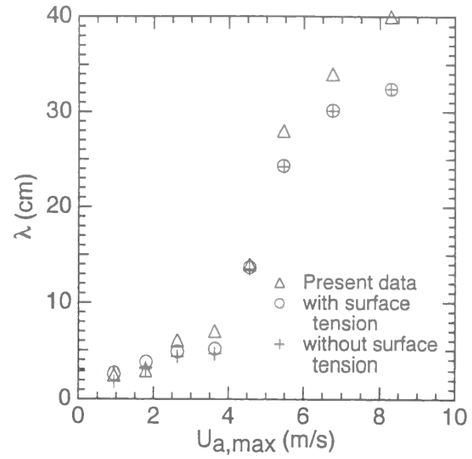

Fig.6.7 Wave length of wind wave.

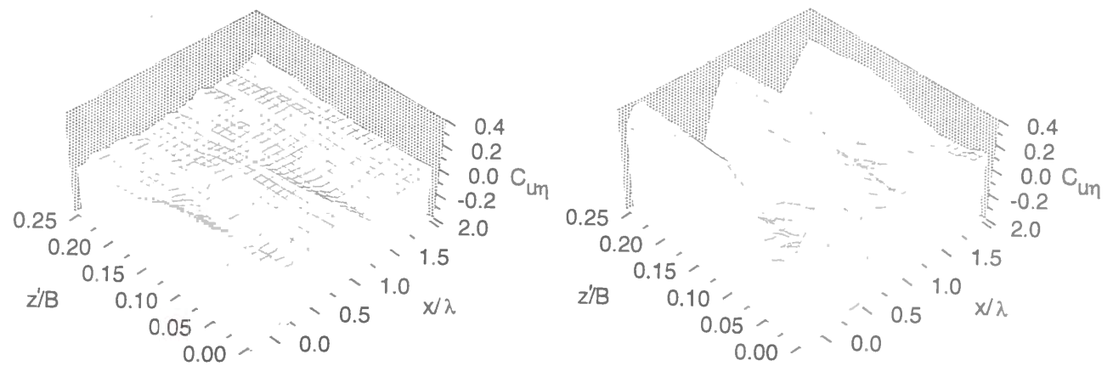

(a) d2wd (Incompletely rough region) (b) d2wf (Rough region)

Fig.6.8 Water surface plot of cross-correlation coefficient $C_{u\eta}$.

molecular viscosity of air in aerodynamically smooth conditions, whereas the drag on the water surface would be closely related to the roughness elements formed by the surface wave field in rough regime.

6.4.2 Developing Process of Wind Wave

When the wind blows over the water, the wind wave occurs at the free surface and changes considerably at various wind speeds, and the developing process of wind wave is closely related to the shape of free surface. From the flow visualization and the time-series of instantaneous surface-wave fluctuations, it became clear that there occurs the 3-D capillary wave in an incompletely rough region and that then it changes into the regular 2-D gravity wave in a rough region, as pointed out by Wu (1975). Fig.6.7 is the wave length of wind wave evaluated from the periodicity of cross-correlation coefficient between the velocity fluctuations at the fixed point and the surface-wave fluctuations at the movable point, together with Eq.(6.3). It can be seen that the experimental value deviates from the linear relation when the wind increases, which means that the non-linear component occurs in a rough region.

Figs.6.8(a)-(b) show the water surface plot of cross-correlation coefficient $C_{u\eta}$ when LDA (u) was

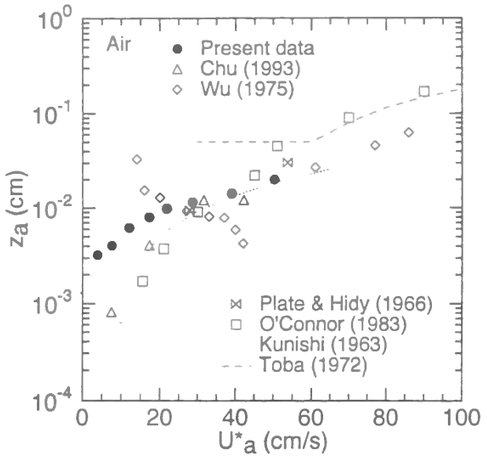

Fig.6.9 Roughness height of air side z_a.

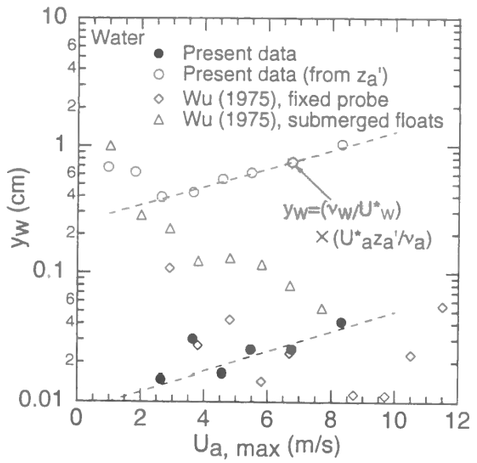

Fig.6.10 Roughness height of water side y_w.

fixed at the center of the channel below the trough of waves (x=0, z'=0) and the depth-measuring instrument (η) was moved around the horizontal plane. It can be seen that the peak position of correlation attains like a chessboard in d2wd (incompletely rough situation). On the other hand, in d2wf, the value shows the occurrence of 2-D wave (rough situation). These wave shapes have a close relationship with the roughness height as mentioned later.

6.4.3 Relation between Roughness Height and Surface Wave

Figs.6.9 and 6.10 show the roughness height of both the air and water sides. As for the roughness height of air side z_a, the present data coincides reasonably with the existing results except for the data of Wu (1968, 1975). The difference from Wu's data may be because he has applied some detergent to the water in order to suppress the generation of wind waves. Fig.6.10 is the roughness height of water side y_w (the present data are shown by solid circle), together with the value calculated from z_a' (open circle, the value calculated from Eq.(6.1) at A_r=8.5) on the assumption that the roughness Reynolds numbers of both sides equal to each other, *i.e.*, $y_w U_{*w}/\nu_w = z_a' U_{*a}/\nu_a$. It can be seen that distribution of two values is very similar. However, the value from z_a' is much larger, which means the roughness Reynolds number of water side is smaller and thus the difference from log-law near the interface in water side is smaller than that in air side, as shown in Figs.6.3 and 6.4.

Fig.6.11 shows the distribution of Charnock number α in Eq.(6.4) versus roughness Reynolds number Rr. The value approaches a constant value as the wind increases, and coincides well with the former value in rough region. On the other hand, Toba's (1979) relation γ in Eq.(6.5) is shown in Fig.6.12, which value decreases and approaches the experimental value by Chu (1993) as the wind increases. Chu (1993) has conducted an experiment in a laboratory and Toba's (1979) data were attained in a field, which implies that the constant value by Toba (1979) depends greatly on whether the data are obtained in a laboratory or a field.

Kitaigorodskii (1984) has pointed out that there exists a linear relation between the intensity of surface-wave fluctuations and roughness height in a higher wind velocity. Fig.6.13 shows the relation between the intensity of surface-wave fluctuations $\eta'=\sqrt{\overline{\eta^2}}$ and roughness height z_a. It can be seen that the intensity η' takes almost a constant value in smooth situation and increases rapidly in incompletely rough situation (3-D capillary wave), and that there exists a linear relation in rough region (2-D gravity wave).

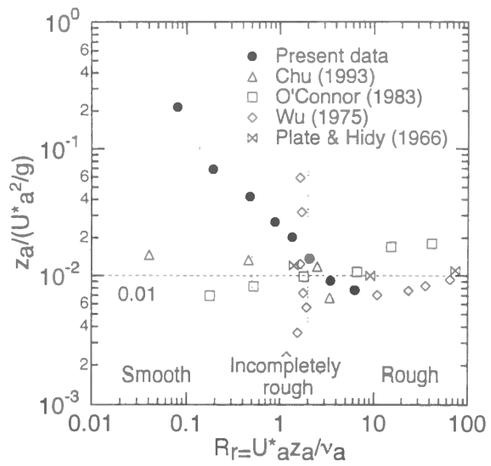

Fig.6.11 Charnock number α versus roughness Reynolds number Rr.

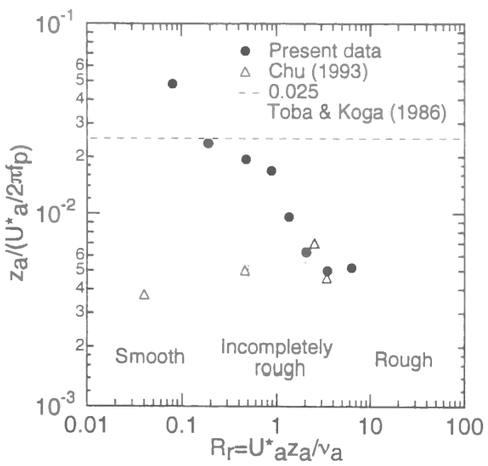

Fig.6.12 Toba's relation γ versus roughness Reynolds number Rr.

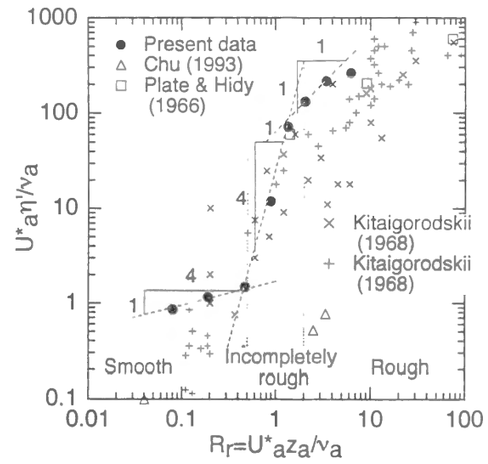

Fig.6.13 Relation between the intensity of surface-wave fluctuations $\eta'=\sqrt{\overline{\eta^2}}$ and roughness height z_a.

6.5 Turbulence Structure across Air-Water Interface

6.5.1 Turbulence Structure on Air Side

6.5.1a Turbulence Intensity and Reynolds Stress on Air Side

The great difference of wind waves from usual boundary layers over fixed wall is that the roughness height (surface-wave fluctuations) becomes larger as the wind velocity becomes faster. Nakayama and Nezu (2000a) have revealed an unique relation between the intensity of surface-wave fluctuations and roughness height; the shape of surface waves depending on the roughness Reynolds number, *i.e.*, aerodynamically smooth, incompletely rough and rough. Fig.6.14 shows the distribution of turbulence intensities u'/U_{*a} and v'/U_{*a} on the air side, together with DNS data of Kim *et al.* (1987) and semi-theoretical curve derived by Nezu and Nakagawa (1993), where d is the half height of air channel. It can be seen that the distributions of u'/U_{*a} and v'/U_{*a} in d2wa are the almost same as those over a

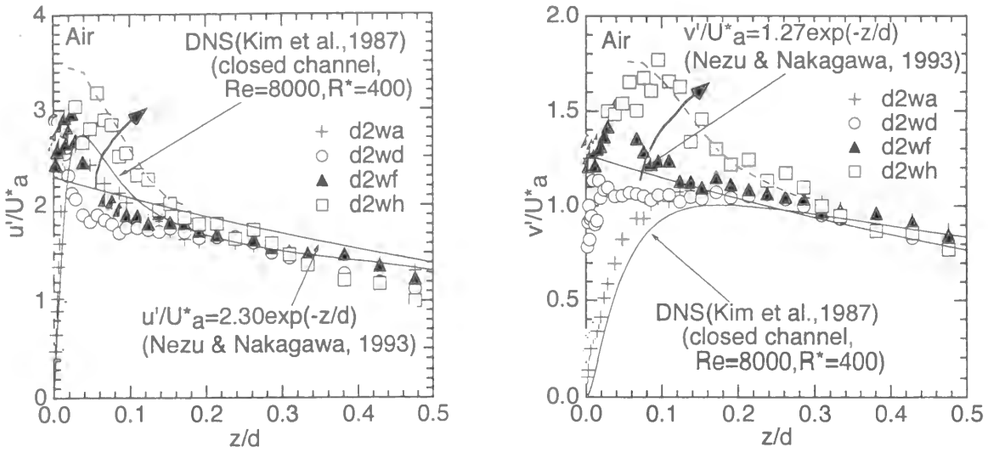

Fig.6.14 Turbulence intensities u'/U_* and v'/U_* on air side.

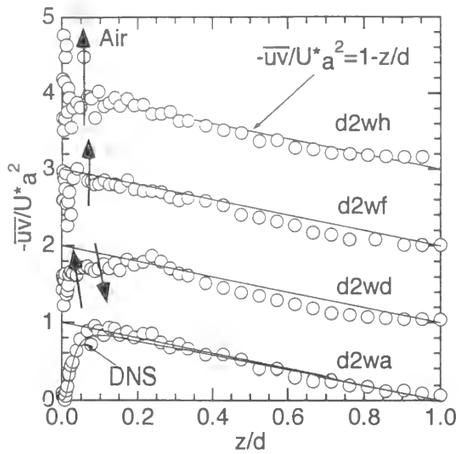

Fig.6.15 Reynolds stress $-\overline{uv}/U_{*a}^2$ on air side.

smooth fixed bed, and that the distributions in d2wd are similar to those in a rough bed (tendency toward isotropy) when 3-D capillary wave occurs. Furthermore, these values become greater than the semi-theoretical curves when 2-D gravity wave occurs in d2wf and d2wh. The distribution of Reynolds stress $-\overline{uv}/U_{*a}^2$ is shown in Fig.6.15. There appears a similar distribution as in smooth bed in d2wa, and there exists a constant stress layer peculiar to rough flow in d2wd. When the wind becomes greater in rough region, Reynolds stress approaches a triangular distribution and increases greatly near the interface, which causes a large energy transport to the generation of surface wave.

6.5.1b Energy Budget on Air Side

Figs.6.16(a)-(c) show the distributions of turbulent generation Gd/U_{*a}^3, turbulent energy dissipation rate $\varepsilon d/U_{*a}^3$ and turbulent energy diffusion $T_D d/U_{*a}^3$ on air side, respectively. The value of ε was evaluated from the -5/3 power law of FFT spectrum, as pointed out by Nezu and Nakagawa (1993). It can be seen that G decreases slightly near the interface and ε decreases considerably when wind waves

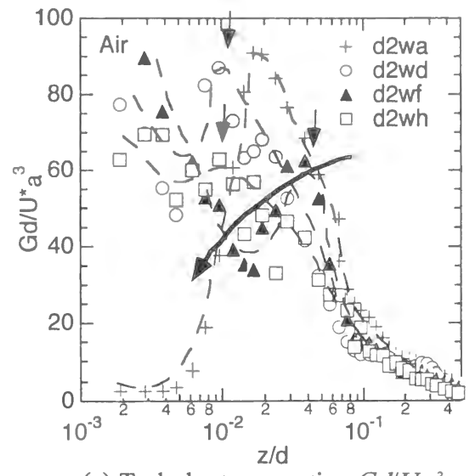

(a) Turbulent generation Gd/U_{*a}^3

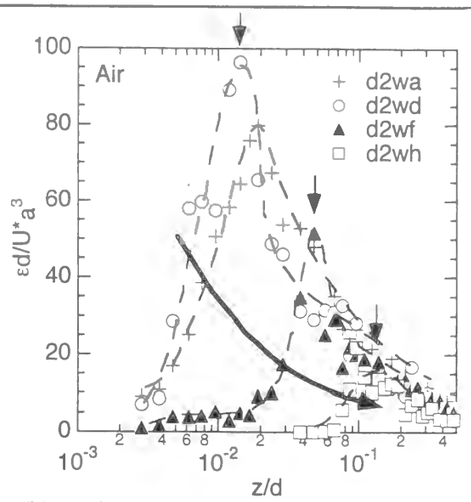

(b) Turbulent energy dissipation rate $\varepsilon d/U_{*a}^3$

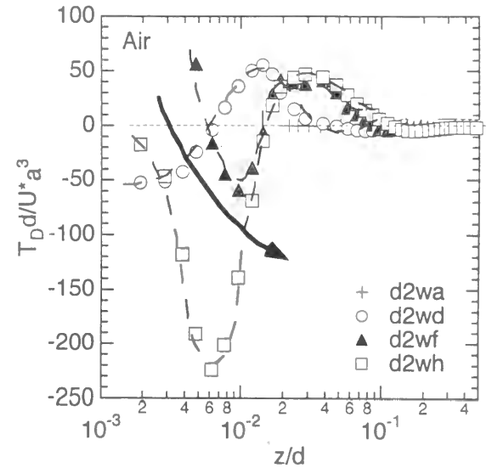

(c) Turbulent energy diffusion $T_D d/U_{*a}^3$

Fig.6.16 Turbulent generation Gd/U_{*a}^3, turbulent energy dissipation rate $\varepsilon d/U_{*a}^3$ and turbulent energy diffusion $T_D d/U_{*a}^3$ on air side.

occur. The value of T_D decreases greatly as wind increases, which is closely related to the energy transfer into water side, as mentioned later. When the wind blows over the water, the energy of wind is transferred to the mean-flow and wave fields in the water. At that time, there occur the energy transfers from mean-flow field to wave field and from mean field to turbulence field, and thus the mean-flow, wave and turbulence fields are closely coupled.

6.5.2 Turbulence Structure on Water Side

6.5.2a Decomposition on Wave-Component and Turbulence-Component by LFT

Fig.6.17 shows an example of spectral decomposition by LFT on the water side. It can be seen clearly that the wave-induced component (indicated as w) is centered around a narrow band of frequency, which corresponds to the frequency of dominant waves. Outside this band, the kinetic energy caused

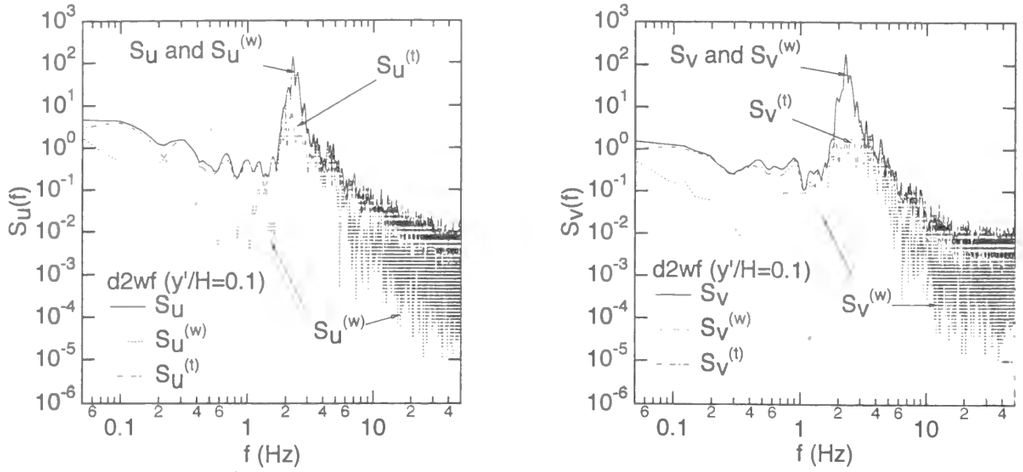

Fig.6.17 Spectral decomposition by LFT on water side.

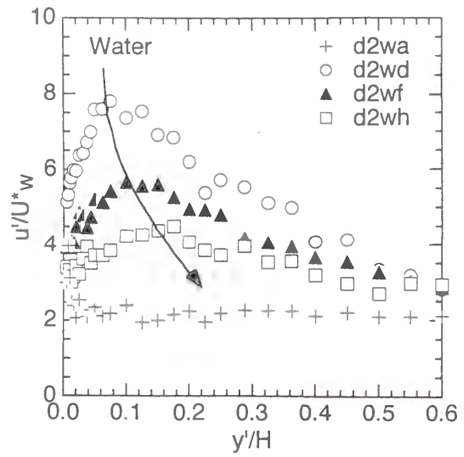

(a) Total turbulence intensity u'

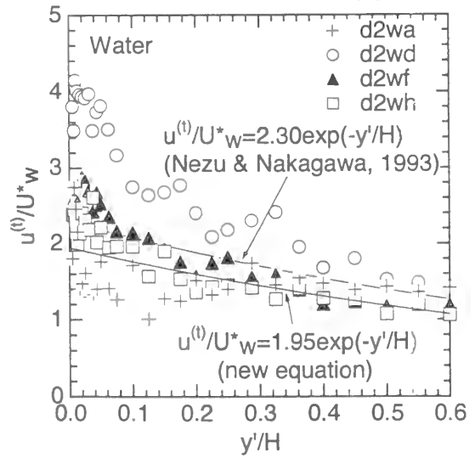

(b) Turbulence-induced r.m.s. $u^{(t)}$

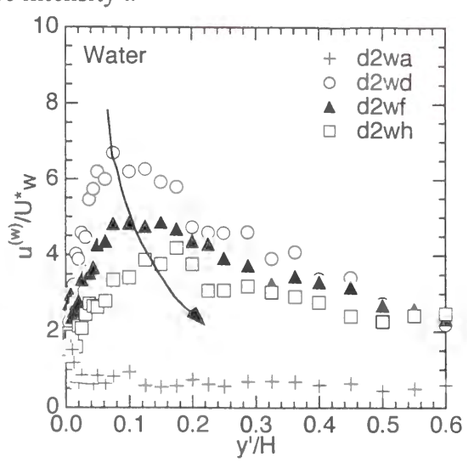

(c) Wave-induced r.m.s. $u^{(w)}$

Fig.6.18 Streamwise components of turbulence intensities u', $u^{(t)}$ and $u^{(w)}$.

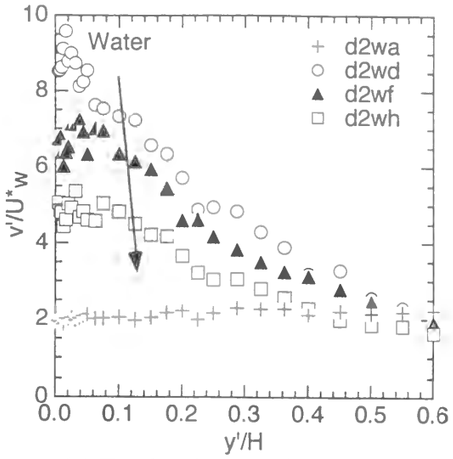

(a) Total turbulence intensity v'

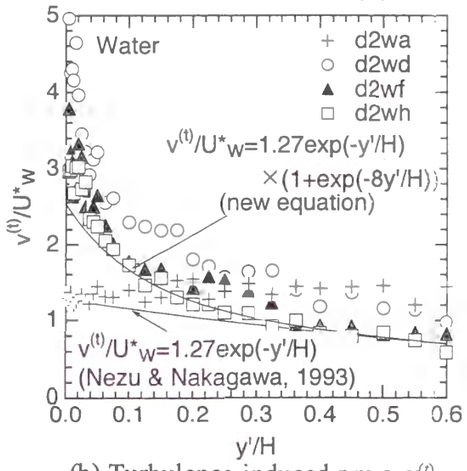

(b) Turbulence-induced r.m.s. $v^{(t)}$

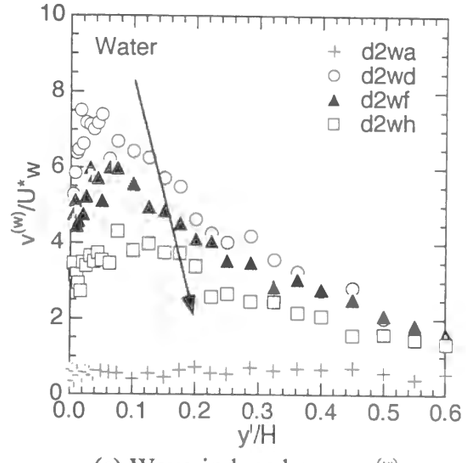

(c) Wave-induced r.m.s. $v^{(w)}$

Fig.6.19 Vertical components of turbulence intensities v', $v^{(t)}$ and $v^{(w)}$.

by the wave-induced component is negligibly small and thus the turbulence component (indicated as *t*) is predominant, which implies that the wave component and turbulence component are well decomposed.

6.5.2b Turbulence Intensity and Reynolds Stress on Water Side

Figs.6.18 and 6.19 show the total turbulence intensities u' and v', turbulence-induced r.m.s. $u^{(t)}$ and $v^{(t)}$ and wave-induced r.m.s. $u^{(w)}$ and $v^{(w)}$, respectively. Howe *et al.* (1982) pointed out that the total turbulence intensity decreases and finally approaches a constant value as the wind speed increases and 2-D gravity wave occurs. The same characteristic can be seen in this figure. The distribution in d2wa (smooth) is quite different from the others and takes a constant value over the depth, that is to say, like a laminar distribution. It can be seen that the wave component is predominant under wind waves, whereas the turbulence component takes a greater part in smooth situation, as pointed out by Howe *et al.* (1982). Furthermore, the turbulence component has a stronger universality under 2-D gravity wave in the case of d2wf and d2wh, as shown in the revised semi-theoretical formula.

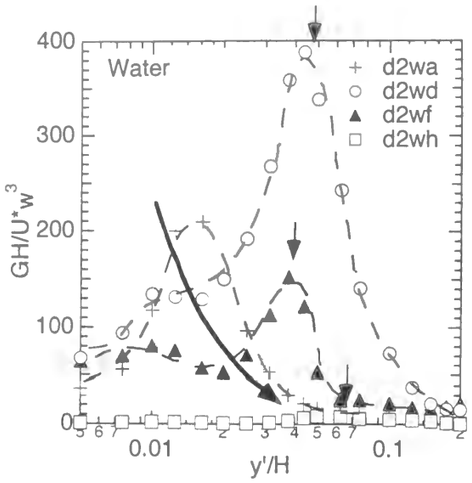

(a) Turbulent generation GH/U_{*w}^3

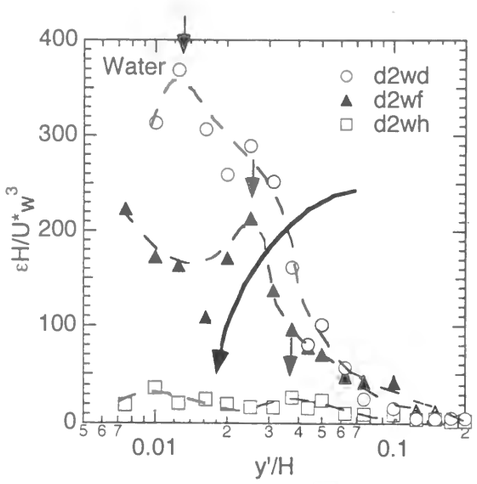

(b) Turbulent energy dissipation rate $\varepsilon H/U_{*w}^3$

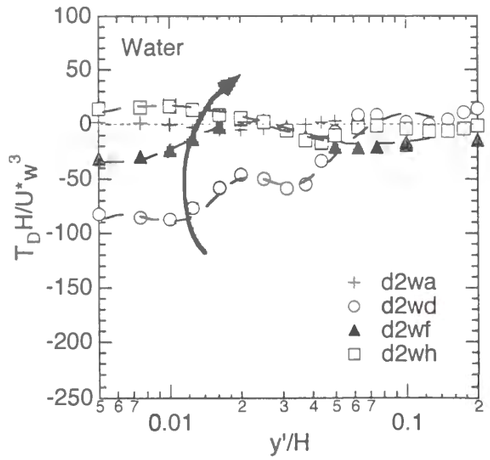

(c) Turbulent energy diffusion T_DH/U_{*w}^3

Fig.6.20 Turbulent generation GH/U_{*w}^3, turbulent energy dissipation rate $\varepsilon H/U_{*w}^3$ and turbulent energy diffusion T_DH/U_{*w}^3 on water side.

6.5.2c Energy Budget on Water Side

As mentioned before, when the wind blows over the water, the energy is transferred to the mean and wave fields and there occurs the energy transport from the wave field to the mean field and from the mean field to the turbulence field. So, the coupling among these three fields exist, as pointed out by Cheung (1985) and Cheung and Street (1988). Jiang *et al.* (1990) pointed out that the wave-turbulence interaction contributes to momentum and energy transfer.

Figs.6.20(a)-(c) show the distributions of GH/U_{*w}^3, $\varepsilon H/U_{*w}^3$ and T_DH/U_{*w}^3 on water side. The distributions of G and ε are comparatively similar to those on air side. However, the situation becomes a little different very near the interface in 2-D gravity wave. Firstly, there appears $G>\varepsilon$ on air side (an excess energy is transferred to water side), whereas $G<\varepsilon$ on water side (energy deficiency). Secondly, the peak position (indicated by arrow) of G is closer to the interface than that of ε on air side, whereas

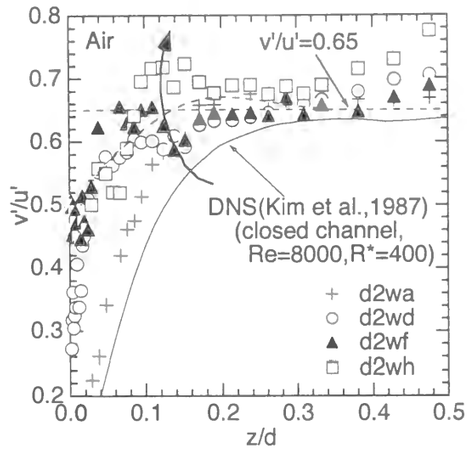

(a) Air layer

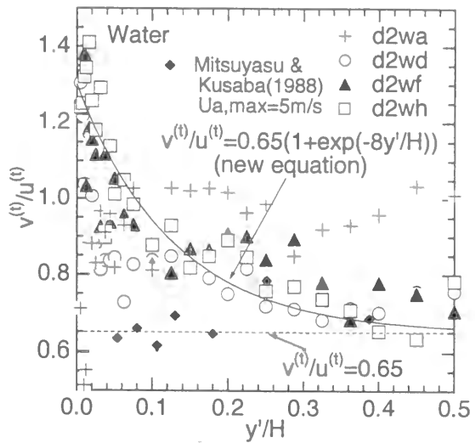

(b) Water layer

Fig.6.21 Turbulence intensity ratio v'/u' on both air and water sides.

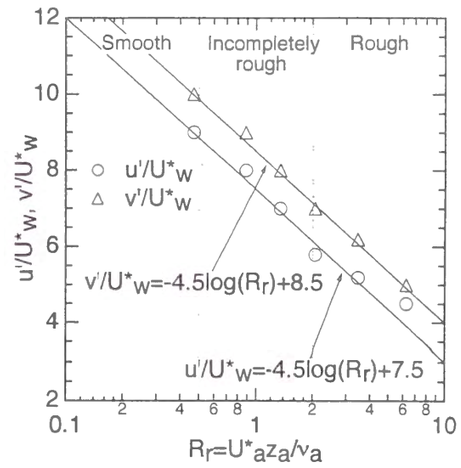

(a) Peak value

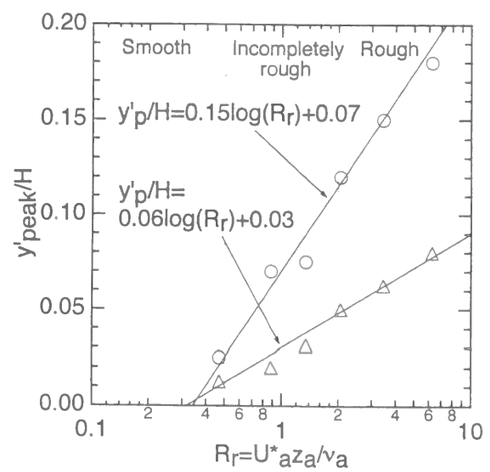

(b) Peak position

Fig.6.22 Peak value and peak position of turbulence intensity on water side against roughness Reynolds number Rr.

the situation is contrary on water side. The value of T_D in water increases as wind increases, which implies the energy transfer becomes greater as wind velocity increases and corresponds well to the energy transfer on air side.

6.5.3 Relationship of Turbulence Structures on Both Sides

6.5.3a Relation of Turbulence Structures

Figs.6.21(a)-(b) show the distributions of turbulence intensity ratio v'/u' on both air and water sides. It can be seen that both data approach the same value $v'/u'=0.65$ away from the interface, that is to say, an "*equilibrium state*". On air side, the value decreases near the interface in smooth situation, and the value becomes greater (toward isotropy) as wind increases, which is similar to rough bed flow.

In contrast, the value increases greatly near the interface on water side. Mitsuyasu and Kusaba (1988) added some detergent into the water in order to suppress the generation of wind waves and their data take the equilibrium value. In this way, the increase of v'/u' near the free surface on water layer is peculiar to the flow field below the wind wave.

6.5.3b Forecasting Turbulence Intensities in Water Layer

It may be very useful to forecast the turbulence (in particular, the peak value) in wind wave by measuring the wind velocity. From Figs.6.18 and 6.19, it became clear that the total turbulence intensities near the free surface decrease as the wind increases. Figs.6.22(a)-(b) show the peak value and peak position of turbulence intensity on water side against roughness Reynolds number Rr in the semi-logarithmic plot. It can be seen that the peak value is well approximated by the logarithmic decreasing-function from the incompletely rough region to the rough region and that the peak position by the logarithmic increasing-function. By using these functions, the turbulence intensities on water side can be evaluated only by measuring the wind velocity.

6.6 Conclusions

In this study, fundamental characteristics in wind waves were investigated as a first step. Fig.6.23 shows the conclusions of chapter 6. It was found that the logarithmic law of mean velocity is effective on both air and water sides. The momentum transfer in smooth situation is very different from that in rough situation, and the momentum flux is continuous across the interface in rough situation. Roughness heights on both sides are closely related with each other, and the former is generally greater than the latter. Finally, there has a close relationship between the roughness height and the surface-wave fluctuations, and in particular, there has a linear relation in fully rough situation.

Furthermore, the characteristics of turbulence component and wave component were evaluated by using LFT in wind waves. The turbulence quantities in the air behave similarly to those in flows over flat plates. In the water, the total turbulence intensity decreases as an increase of wind velocity, whereas the turbulence component has a stronger universality. Furthermore, energy budget on both sides has a close relationship with each other and energy transfer through the air-water interface increases when the wind velocity increases.

Notations

B : channel width
c : wave celerity
d : half height of air channel
F : any flow field quantities
Fr : Froude number in water layer ($=U_m/\sqrt{gH}$)
f_p : primary frequency of wind wave
G : turbulent generation (or production)
g : acceleration due to gravity
H : flow depth
L : some linear operator
Rr : roughness Reynolds number ($=U_{*a}z_a/\nu_a$)
r : horizontal vector

- Log-Law of Mean Velocity
  - ⇒ Effective in Both Air and Water Layers
- Momentum Transfer
  - ⇒ Smooth Situation : $\tau_w/\tau_a<1.0$: Rough Situation : $\tau_w/\tau_a=1.0$
- Roughness Heights
  - ⇒ Values Increase as Wind Increases
  - ⇒ z_a' (Air Side) >> y_w (Water Side)
- Intensity of Surface-Wave Fluctuations
  - ⇒ Closely Related to Roughness Height
  - ⇒ Linear Relation ($\eta'\sim z_a$) in Rough Region
- Turbulence characteristics in Air Layer
  - ⇒ Similar to Those over Flat Plates
- Turbulence characteristics in Water Layer
  - ⇒ Total Turbulence Intensities ↓ : Universal Characteristics of Turbulence Component
- Increase of Wind Velocity
  - ⇒ $G\uparrow$, $\varepsilon\downarrow$, $T_D\downarrow$ (Air Layer): $G\downarrow$, $\varepsilon\downarrow$, $T_D\uparrow$ (Water Layer)
  - ⇒ Energy Transfer from Air to Water Layer ↑

Fig.6.23 Conclusions of chapter 6.

$S_{\alpha\beta}$: cross spectrum of function α and β
$S_{\eta\eta}$: power spectrum of η
$S_{\beta\eta}^*$: conjugate of the cross spectrum $S_{\beta\eta}$
T_D : turbulent energy diffusion
U_a : wind velocity
$U_{a,max}$: maximum wind velocity
U_m : bulk mean velocity
U_s : surface drift velocity
U_{*a} : friction velocity in air layer
U_{*b} : friction velocity in water layer
U_{*w} : friction velocity at the interface
u : instantaneous streamwise velocity component
u', v' : total turbulence intensities
$u^{(t)}$, $v^{(t)}$: turbulence-induced r.m.s.
$u^{(w)}$, $v^{(w)}$: wave-induced r.m.s.
$-\overline{uv}$: Reynolds stress
v : instantaneous vertical velocity component
x : streamwise direction
y : vertical direction from the channel bed
y_w : roughness height in water layer
y' : distance from the free surface ($=H-y$)

y'_{peak} : peak position of turbulence intensity from the free surface (=H-y)
z : vertical direction from water surface
z' : spanwise direction from the center of the channel
z_a : roughness height in air layer

Greek symbols
α : Charnock constant
ε : turbulent energy dissipation rate
γ : Toba's relation
η' : intensity of surface-wave fluctuations ($\equiv\sqrt{\overline{\eta^2}}$)
λ : wave length
ν_a : kinetic viscosity of air
ν_w : kinetic viscosity of water
ρ_a : density of air
ρ_w : density of water
σ : surface tension
τ_a : shear stress in air layer (=$\rho_a U_{*a}^2$)
τ_w : interfacial shear stress in water layer (=$\rho_w U_{*w}^2$)
ω_p : angular frequency of dominant waves (=$2\pi f_p$)

References

[1] Baines, W.D. and Knapp, D.J. : Wind driven water currents, *J. Hydraulic Eng.*, ASCE, Vol.91, HY2, pp.205-221, 1965.
[2] Benilov, A.Y., Kouznetsov, O.A. and Panin, G.N. : On the analysis of wind wave-induced disturbances in the atmospheric turbulent surface layer, *Boundary Layer Meteo.*, Vol.6, pp.269-285, 1974.
[3] Bliven, L.F., Huang, N.E. and Long, S.R. : A laboratory study of the velocity field below surface gravity waves, *Gas Transfer at Air-Water Interfaces*, W. Brutsaert and G.H. Jirka (eds.), pp.181-190, 1984.
[4] Charnock, H. : Wind stress on a water surface, *Quart. J. Roy. Meteor. Soc.*, No.81, pp.639-640, 1955.
[5] Cheung, T.K. : A study of the turbulent layer in the water at an air-water interface, *Ph.D Thesis presented to Stanford University*, 1985.
[6] Cheung, T.K. and Street, R.L. : Turbulent layers in the water at an air-water interfaces, *J. Fluid Mech.*, Vol.194, pp.133-151, 1988.
[7] Chu, C.R. : Experiments on gas transfer and turbulence structure in free surface flows with combined wind/bottom shear, *Ph.D Thesis presented to Cornell University*, 1993.
[8] Dean, R.G. : Stream function representation of non linear ocean waves, *J. Geophys. Res.*, Vol.70, No.18, pp.4561-4572, 1965.
[9] Hidy, G.M. and Plate, E.J. : Wind action on water standing in a laboratory channel, *J. Fluid Mech.*, Vol.26, pp.651-687, 1966.
[10] Howe, B.M., Chambers, A.J., Klotz, S.P., Cheung, T.K. and Street, R.L. : Comparison of profiles and fluxes of heat and momentum above and below an air-water interface, *Trans. ASME C: J. Heat Transfer*, Vol.104, pp.34-39, 1982.
[11] Jiang, J.Y., Street, R.L. and Klotz, S.P. : A study of wave-turbulence interaction by use of a

nonlinear water wave decomposition technique, *J. Geophys. Res.*, Vol.95, No.C9, pp.16037-16054, 1990.
[12] Kim, J., Moin, P. and Moser, R. : Turbulence statistics in fully developed channel flow at low Reynolds number, *J. Fluid Mech.*, Vol.177, pp.133-166, 1987.
[13] Kitaigorodskii, S.A. : On the calculation of the aerodynamic roughness of the sea surface, *Bull., Acad. Sci. USSR, Atmospheric and Oceanic Physics*, Vol.4, No.8, 1968.
[14] Kitaigorodskii, S.A. and Donelan, M.A. : Wind-wave effects on gas transfer, *Gas Transfer at Air-Water Interfaces*, W. Brutsaert and G.H. Jirka (eds.), pp.147-170, 1984.
[15] Mitsuyasu, H. : A note on the momentum transfer from wind to waves, *J. Geophys. Res.*, Vol.90, No.C2, pp.3343-3345, 1985.
[16] Mitsuyasu, H. and Kusaba, T. : Wind waves and wind-generated turbulence in the water, *The Ocean Surface*, Y. Toba and H. Mitsuyasu (eds.), Reidel, pp.389-394, 1985.
[17] Nezu, I. and Nakagawa, H. : Turbulence in open-channel flows, IAHR-Monograph, Balkema, 1993.
[18] Nezu, I., Nakayama, T. and Inoue, R. : Turbulence structures in air-water interface with wind shear, *Annual Journal of Hydraulic Engineering*, Vol.43, pp.413-418, 1999a (in Japanese).
[19] Nezu, I. and Nakayama, T. : Effect of turbulence components below wind water waves, *Annual Journal of Hydraulic Engineering*, Vol.43, pp.407-412, 1999b (in Japanese).
[20] Nezu, I. and Nakayama, T. : Fundamental study at air-water interfaces with wind shear, *28th IAHR Congress*, IAHR, 1999c.
[21] Nezu, I. and Nakayama, T.: Effect of turbulence components below wind water waves, *28th IAHR Congress*, IAHR, 1999d.
[22] Nakayama, T. and Nezu, I. : Turbulence structures of wind water waves, *Journal of Hydraulic Engineering*, JSCE, No.642/II-50, 2000a (in Japanese).
[23] Ocampo-Torres, F.J. and Donelan, M.A. : On the influence of fetch and the wave field on the CO2 transfer process : Laboratory measurements, *Air-Water Gas Transfer*, B. Jahne and E.C. Monahan (eds.), AEON Verlag, pp.543-552, 1995.
[24] Phillips, O.M. : The dynamics of the upper ocean, Cambridge University Press, 1977.
[25] Plate, E.J. and Friedrich, R. : Reaeration of open channel flow, *Gas Transfer at Air-Water Interfaces*, W. Brutsaert and G.H. Jirka (eds.), pp.333-346, 1984.
[26] Reid, R.O. : Modification of the quadratic bottom-stress law for turbulent channel flow in the presence of surface wind-stress, *Tech. Memo.*, No.93, Beach Erosion Board, U.S. Corps of Engineers, 1957.
[27] Shemdin, O.H. : Wind-generated current and phase speed of wind waves, *J. Physical Ocean.*, No.2, pp.411-419, 1972.
[28] Thais, L. and Magnaudet, J. : A triple decomposition of the fluctuating motion below laboratory wind water waves, *J. Geophys. Res.*, Vol.100, No.C1, pp.741-755, 1995.
[29] Thais, L. and Magnaudet, J. : A triple decomposition of the fluctuating motion below laboratory wind water waves, *J. Fluid Mech.*, Vol.328, pp.313-344, 1996.
[30] Toba, Y. : Study on wind waves as a strongly nonlinear phenomenon, *12th Symp. on Naval Hydrodynamics*, Natl. Acad. of Sci., Washington, D.C., pp.529-540, 1979.
[31] Toba, Y. : Atmosphere-Ocean Interactions, University of Tokyo Press, 1996 (in Japanese).
[32] Wu, J. : Laboratory studies of wind-wave interactions, *J. Fluid Mech.*, Vol.34, pp.91-111, 1968.
[33] Wu, J. : Wind-induced drift currents, *J. Fluid Mech.*, Vol.68, pp.49-70, 1975.
[34] Wu, J. : On critical roughness Reynolds number of the atmospheric surface layer, *J. Geophys. Res.*, Vol.86, No.C7, pp.6661-6665, 1981.
[35] Wu, J. : On nondimensional correlation between roughness length and wind-friction velocity, *J.*

Oceanogr. Soc. Japan, Vol.44, pp.254-260, 1988.
[36] Wu, J. and Tsanis, I.K. : Numerical study of wind-induced water currents, *J. Hydraulic Eng.*, ASCE, Vol.121, No.5, pp.388-395, 1995.

CHAPTER 7

TURBULENCE STRUCTURE IN WIND-STREAM COMBINED FLOWS

Abstract

In actual rivers, a wind blows over the flowing water, so called, a condition that the bed shear and the interfacial shear coexist. The mean velocity and turbulence intensity distribution were experimentally investigated for both liquid phase and air phase of air-water stratified two-phase flows. As a result, the mixing-length model in wind wave was extended in the air flow of two-phase flows. As for water layer, it was clarified that the shear stress does not vary linearly which adds interfacial shear to the bed shear when there exist both the bed shear and the interfacial shear and that the distribution is parabolic. Furthermore, the non-linearity increases as the ratio of friction velocities in both layers increases. In this way, it was found that the relative velocity between the air flow and the water flow is closely related to the turbulence structure near the free surface in two-phase flows.

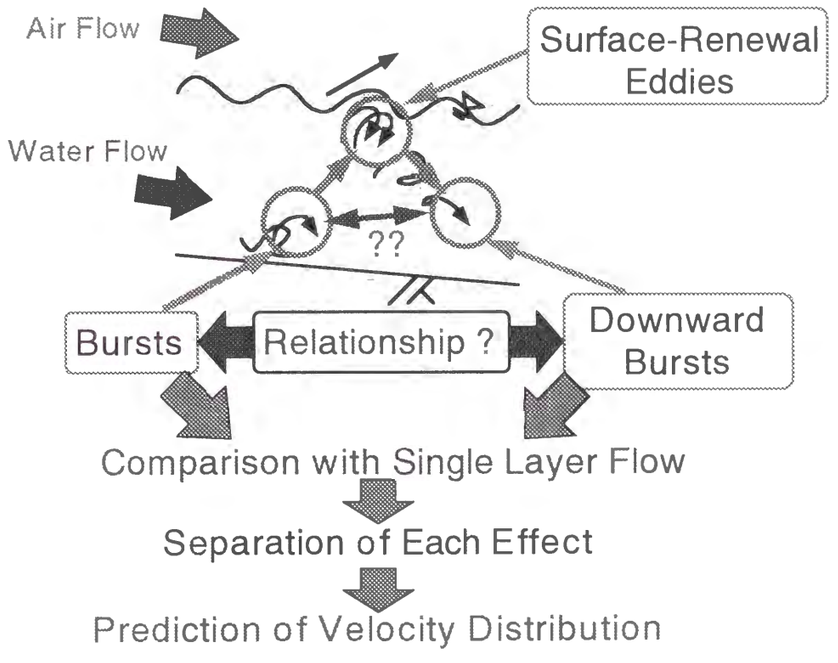

Parts of this chapter were presented and submitted in the following papers.

[1] Nezu, I., Nakayama, T. and Inoue, R. : Turbulence structures in air-water interface with wind shear, *Annual Journal of Hydraulic Engineering*, Vol.43, pp.413-418, 1999a (in Japanese).
[2] Nezu, I. and Nakayama, T. : Fundamental study at air-water interfaces with wind shear, *28th IAHR Congress*, IAHR, 1999c.
[3] Nezu, I. and Nakayama, T.: Effect of turbulence components below wind water waves, *28th IAHR Congress*, IAHR, 1999d.
[4] Nezu, I., Nakayama, T. and Inoue, R. : Influence of turbulence structure on gas transfer across air-water interface, *Journal of Applied Mechanics*, JSCE, Vol.2, pp.673-684, 1999h (in Japanese).
[5] Nakayama, T. and Nezu, I. : Turbulence structures of wind/stream combined flow, *Journal of Hydraulic Engineering*, JSCE, 1999m (in Japanese, to be accepted).
[6] Nakayama, T. and Nezu, I. : Turbulence structures of wind water waves, *Journal of Hydraulic Engineering*, JSCE, No.642/II-50, 2000a (in Japanese).

7.1 Introduction

Up to the former chapters, the turbulence structure and coherent structure were evaluated in open-channel flow and wind wave. However, in actual rivers, a wind blows over the flowing water and the bed shear and the interfacial shear coexist, as shown in Fig.7.1. In chemical, mechanical and nuclear engineering, the flow characteristics and the interfacial heat transfer coefficients have been investigated experimentally for the need to estimate accurately the heat transfer rate at the liquid surface of cooling reactors.

Hanratty and Engen (1957), Cohen and Hanratty (1965) and Hanratty (1983) classified the surface wave into smooth surface, 2-D waves, 3-D waves, roll waves, and dispersed waves in terms of a liquid and a gas Reynolds number in two-layer flows, and analytically solved the initiation of atomization in comparison with Kelvin-Helmholtz theory. About these waves, Akai *et al.* (1977, 1980) have evaluated the variations of auto-correlation function of surface-wave fluctuations. They pointed out that a large amount of momentum transfer occurs in the vicinity of the disturbed interfaces because the eddy viscosities obtained in the vicinity of the wave interface exhibit a much larger value than those obtained for the region close to a smooth wall in the single-phase flow. Furthermore, it was clarified that the asymmetric behavior of the total eddy viscosity introduced by the wave-induced shear stress causes a significant distortion of the velocity profile in the gas phase.

In order to evaluate the turbulence structure of these two-layer flows, the prediction of the distributions of water and wind velocities has mainly been conducted so far. As for the wind velocity, there have been a lot of researches about the relation between the wind velocity and the roughness height in view of the disagreement of the Miles' (1957) inviscid theory with experimental data. Because

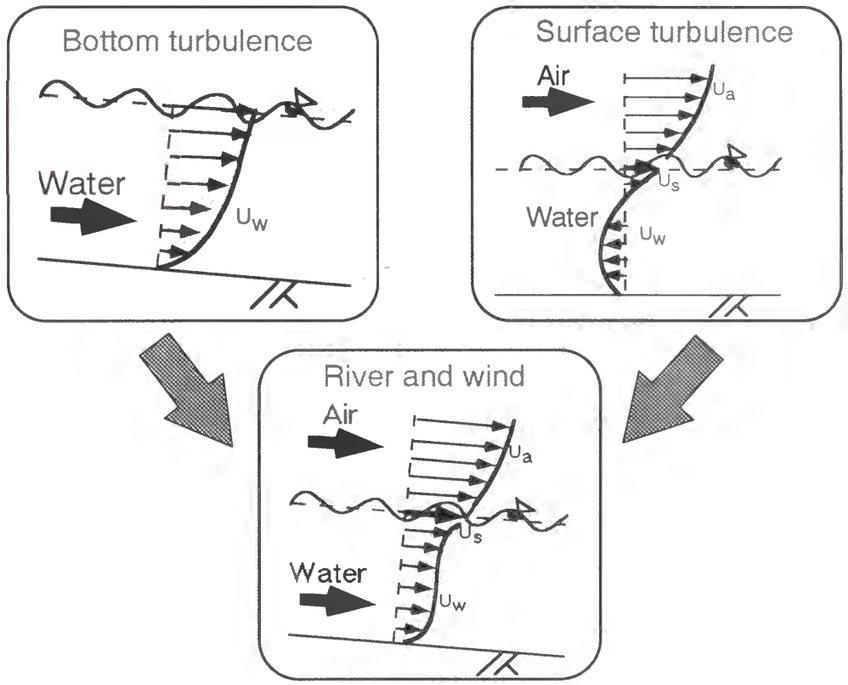

Fig.7.1 Schematic representation of flow conditions.

it is important how to model the mixing length for defining the velocity distribution, Riley *et al.* (1982) have suggested the new mixing-length model in wind wave in comparison with the mixing-length model in smooth flow by van Driest (1956) and the model in rough flow by Rotta (1962). On the other hand, about the water flow, Henstock and Hanratty (1976) have evaluated the interfacial drag and the height of water layer in annular flow on the assumption that the shear stress is given by a weighted average of bed shear and interfacial shear suggested by Hughmark (1973). Furthermore, Reid (1957) has led the distribution of primary mean velocity depending on the ratio of the bed shear to the interfacial shear in two-layer flows on the assumption that the distribution of shear stress is linear and that the mixing length is parabolic. However, errors are unavoidable when the distribution of primary velocity is calculated supposing the unknown distribution of mixing length and the shear stress. Tsuruya (1987) connected the log-law from the bed wall and that from the interface by using the continuity equation and the boundary condition, and verified the coincidence of this calculated value with the experimental value. Furthermore, Hughes and Duffey (1991) have extended Reid's (1957) equation to integrate the expression for the dimensionless velocity gradient and compared the velocity distribution depending on the relative magnitude of bed shear and interfacial shear and on the eddy viscosity at the interface.

Tsuraya (1987) has suggested an empirical formula of turbulence intensity on the assumption that the turbulence energies generated at the wall and at the interface can be added linearly. However, though the turbulence intensity in open-channel flow has the universally semi-theoretical relations as pointed out by Nezu and Nakagawa (1993), the turbulence intensity in wind wave decreases as the wind increases as suggested by Nakayama and Nezu (2000a). So, it may be impossible to express universally the turbulence intensity in two-layer flow in the same way as Tsuraya (1987). Furthermore, Fabre *et al.* (1984) examined the occurrence of secondary currents and the non-linearity of shear stress in two-layer flows. Banat (1992) pointed out that the Boussinesq law is not suitable to the momentum equation in the interfacial layer and that the secondary currents play an important role in the transfer of the excess energy in the interfacial layer toward the bulk of the liquid phase though it is applicable in the lower layer of water flow. Therefore, the linearity does not generally hold good in two-layer flows and it has a possibility that there occurs the interaction of both shears.

In this way, there have been almost no researches about the relationship of turbulence structures between on the air and water layers. In this study, the turbulence structures in two-layer flows and the relationship between both layers were examined by using LDA.

7.2 Experimental Apparatus and Procedures

The experiments were conducted in a tilting wind-water tunnel of 16m long, 40cm wide and 50cm deep in the same flume as in the chapter 6. In this chapter, there exist both the air and the water flows as shown in Fig.7.2. The present air/water tunnel is composed of a recirculating tilting water flume and an open-ended wind tunnel. Coordinate axis in the streamwise direction is defined as x. The direction of air and water flows is defined as positive, as shown in Fig.7.2. In this study, only co-current case was evaluated because fully-developed flow could be easily generated. As for the vertical direction, the upward direction from the bottom is defined as y. The upward and downward directions from the interface are defined as z and y' ($=H-y$, H is the flow depth), respectively. Instantaneous velocities for the streamwise and vertical components are $u(t)$ and $v(t)$, respectively.

In order to measure the instantaneous velocity for both air and water, 500mW LDA system (DANTEC-made) was used at the center of channel 9m downstream of the channel entrance. About water flow, sampling time was 60sec, and sampling frequency was about 150Hz. An ultrasonic depth-

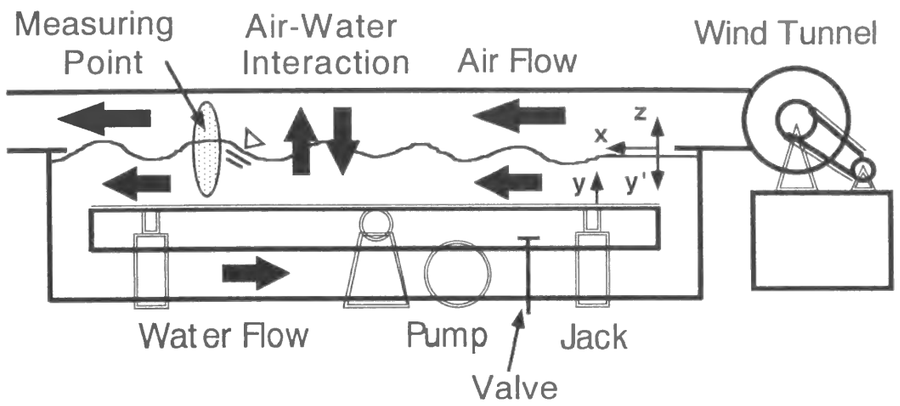

Fig.7.2 Schematic diagram of tilting wind-water tunnel.

Table 7.1 Hydraulic conditions of two-layer flows.

	$U_{a,max}$ (m/s)	Q (l/s)	Fr	U^*a (cm/s)	U^*b (cm/s)
w1f0	1.49	0.0	0.01	5.34	0.05
w2f0	4.39	0.0	0.09	21.37	0.43
w3f0	8.41	0.0	0.15	37.99	0.58
w0f1	0.00	3.2	0.32	0.00	1.22
w1f1	1.49	3.2	0.32	4.52	1.25
w2f1	4.39	3.2	0.32	18.45	1.20
w3f1	8.41	3.2	0.33	40.20	1.22
w0f2	0.00	8.0	0.80	0.00	2.53
w1f2	1.49	8.0	0.81	3.20	2.57
w2f2	4.39	8.0	0.83	13.66	2.61
w3f2	8.41	8.0	0.95	38.57	2.61
w0f3	0.00	15.0	1.50	0.00	4.64
w1f3	1.49	15.0	1.57	1.82	4.67
w2f3	4.39	15.0	1.58	12.49	4.77
w3f3	8.41	15.0	1.63	32.19	4.93

measuring instrument (KEYENCE-made) was set above the free-surface and synchronized with the LDA. Wind velocity was accurately measured with a fog generator (sampling number was 10,000, and sampling frequency was about 1kHz).

Hydraulic conditions for the experiments are shown in Table 7.1. Experiments are divided into three conditions; (A) bottom-shear generated flow (open-channel flow), (B) wind-shear generated flow and (C) combined wind/stream flows. The parameters are defined as follows, Q : flow discharge, H : the flow depth, $U_{a,max}$: the maximum wind velocity, U_{*a} : the friction velocity in the air layer calculated from the log-law, U_{*b} : the friction velocity in the water layer, Fr ($=U_m/\sqrt{gH}$) : Froude number, and η' ($\equiv\sqrt{\overline{\eta^2}}$) : the intensity of surface-wave fluctuations, respectively. Flow depth was fixed at H=4.0cm in all cases. As for (B) wind-induced flow, winds of several speeds were blown over a still water in recirculating flume (valve-closed : wind-tank) and non-recirculating flume (valve-open

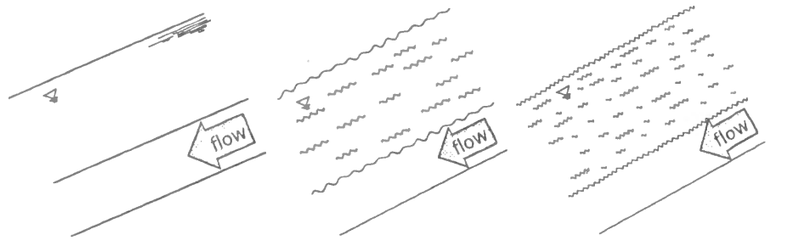

Sub-Critical Flow　Near-Critical Flow　Super-Critical Flow

(A) Open-Channel Flow

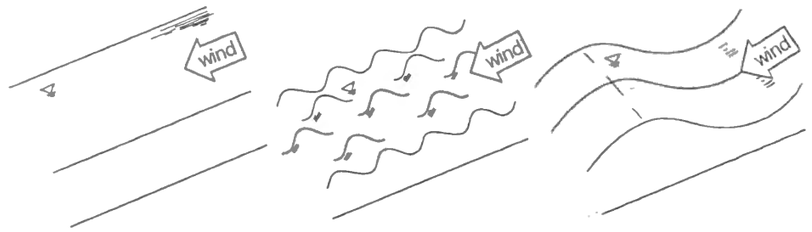

Smooth Region　Incompletely Rough Region (3-D Wave)　Rough Region (2-D Wave)

(B) Wind-Water Wave

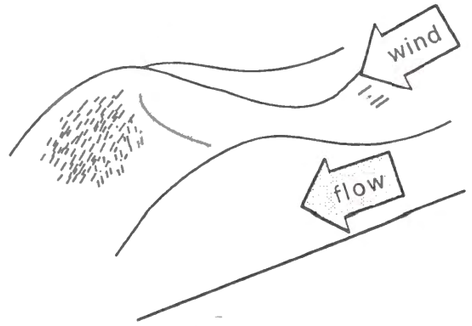

(C) Combined Wind/Stream Flow

Fig.7.3 Free surface situations.

: wind-open). As for (C) combined wind/stream flows, only co-current case was evaluated. The stream condition was changed to three patterns, so called, Fr=0.32 (sub-critical flow), 0.80 (near-critical flow) and 1.50 (super-critical flow). The wind condition was changed to three patterns, that is to say, $U_{a,max}$(m/s)=1.49 (smooth region), 4.39 (incompletely rough region) and 8.41 (rough region). These situations are depicted in Fig.7.3.

7.3 Previous Mixing-Length Models

7.3.1 Mixing-Length Model in Air Layer

The great difference between the boundary layer over the wavy interface and that over the flat plate is that the roughness height at the interface increases as the wind velocity increases. At that time, it is

very important how better the mixing length l is modeled for deciding the distribution of wind velocity. Here, three types of previous mixing-length model are shown;

(1) van Driest's (1956) Model

$$l=\kappa z\left[1-\exp\left(-\frac{zU_{*a}}{\nu_a A}\right)\right] \tag{7.1}$$

where κ : von Karman constant (=0.41), U_{*a} : friction velocity in air layer, and ν_a : kinetic viscosity of air, respectively. This model is for the flow over flat plate (A=26).

(2) Rotta's (1962) Model

$$l=l_0+\kappa z \tag{7.2}$$

This model is applicable only for the rough bed flow because l_0 means the turbulent mixing over the roughness element and takes non-zero value at the wall.

(3) Riley *et al.*'s (1982) Model

$$l=l_0+\kappa z\left[1-\exp\left(-\frac{zU_{*a}}{\nu_a B}\right)\right]^2 \tag{7.3}$$

where l_0=0 and B=13 in smooth bed flow.

7.3.2 Mixing-Length Model in Water Layer

Hughes and Duffey (1991) have extended the Reid's (1957) idea to lead into the velocity distribution in water layer. They obtained the velocity distribution in Eq.(7.7) from the momentum balance on the assumption that the shear stress varies linearly and that the mixing length is parabolic.

$$\frac{\tau(y)}{\rho_w}\equiv-\overline{uv}+\nu_w\frac{\partial U}{\partial y}=\frac{\tau_b}{\rho_w}\left(1-\frac{y}{H}\right)+\frac{\tau_w}{\rho_w}\frac{y}{H} \tag{7.4}$$

$$l=k_b y\left[1+\left(\frac{k_w}{k_b}-1\right)\frac{y}{H}\right] \tag{7.5}$$

$$D=1-\exp\left(-\frac{yU_{*b}}{\nu_w A}\right) \tag{7.6}$$

$$U^+=\int_0^{y^+}\frac{2\tau^+}{1+(1+4l^{+2}D^2\tau^+)^{1/2}}dy^+ \tag{7.7}$$

where D : the van Driest damping function, U_{*b} : friction velocity in water layer, ρ_w : density of water, ν_w : kinetic viscosity of water, k_b ($=\kappa$=0.41), k_w ($l=k_w H$ at $y=H$), and τ_b and τ_w are wall shear and interfacial shear, respectively. For $\tau_w=k_w=0$, Eq.(7.7) reduces to the open-channel flow without interfacial shear. Superscript "+" means non-dimensional value in Eq.(7.7).

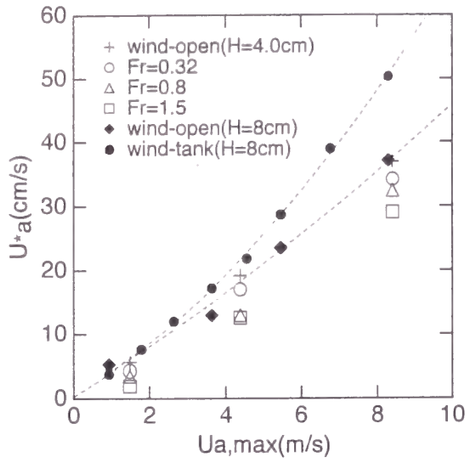

Fig.7.4 Friction velocity in air side U_{*a} evaluated from the log-law in two-layer flows.

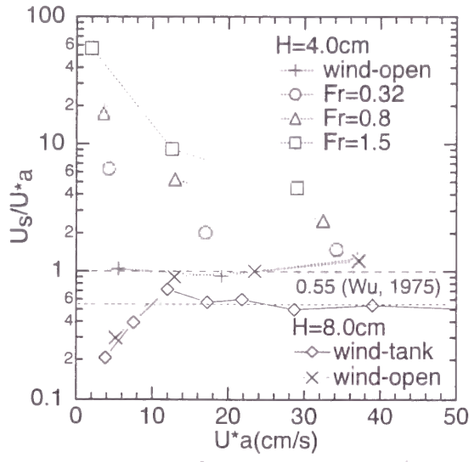

Fig.7.5 Ratio of drift current to friction velocity U_s/U_{*a} in two-layer flows.

7.4 Turbulence Structure of Air Flow

7.4.1 Turbulence Structure of Air Flow

7.4.1a Friction Velocity and Drift Current

Fig.7.4 shows the distribution of friction velocity in air side U_{*a} evaluated from the log-law versus the maximum wind velocity $U_{a,max}$, together with the value of wind wave in recirculating flume by valve (wind-tank) by Nakayama and Nezu (2000a) and in non-recirculating flume without valve (wind-open). Dotted curve is the two-order approximate one calculated from the experimental data. It can be seen that the discrepancy between wind-tank and wind-open increases as the wing velocity increases and that the values of wind-open are little dependent on the flow depth. Furthermore, the friction velocity U_{*a} decreases as the water velocity increases, which means that U_{*a} increases as the relative velocity of air flow and water flow is larger.

Fig.7.5 shows the ratio of drift current to friction velocity U_s/U_{*a} versus U_{*a}. The value in recirculating flume (H=8.0cm, wind-tank) corresponds well to the previous value (U_s/U_{*a}=0.55) at the rough situation in the faster wind velocity (U_{*a}>10cm/s), whereas the value in non-recirculating flume takes a little larger value than that in recirculating flume (U_s/U_{*a}=1.0). In the two-layer flows, U_s/U_{*a} takes a larger value than one, which increases as the relative velocity increases. The relative drift current $(U_s-U_{s,flow})/U_{*a}$ is shown in Fig.7.6, where $U_{s,flow}$ is the drift current in open-channel flow. The value approaches the value in wind wave with the increase in wind velocity, which implies that the relative drift current takes the universal value even in two-layer flows.

7.4.1b Primary Mean Velocity and Roughness Height

Fig.7.7 shows the distribution of primary mean velocity in air layer U_a^+, together with the log law and the value in wind wave (wind-open). In this figure, z_a is roughness height evaluated by the log law. Measurement in the vertical direction was conducted up to the point $z \fallingdotseq d$ (half height of air channel) in order to include the maximum wind velocity. The log law holds good even in two-layer flows. Fig.7.8 shows the distribution of roughness height z_a versus U_{*a}. It can be seen that z_a increases as U_{*a} increases in wind-open and Fr=0.32. In Fr=0.80, z_a takes a minimum value at the intermediate

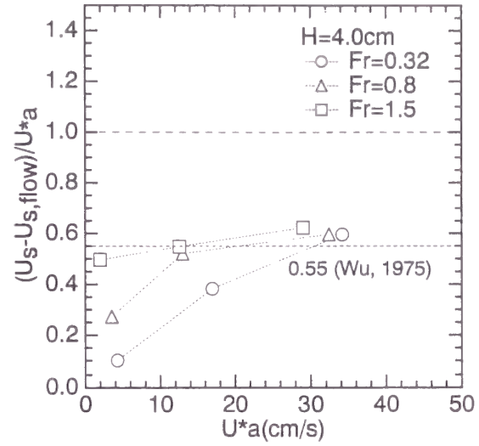

Fig.7.6 Relative drift current $(U_s-U_{s,flow})/U_{*a}$.

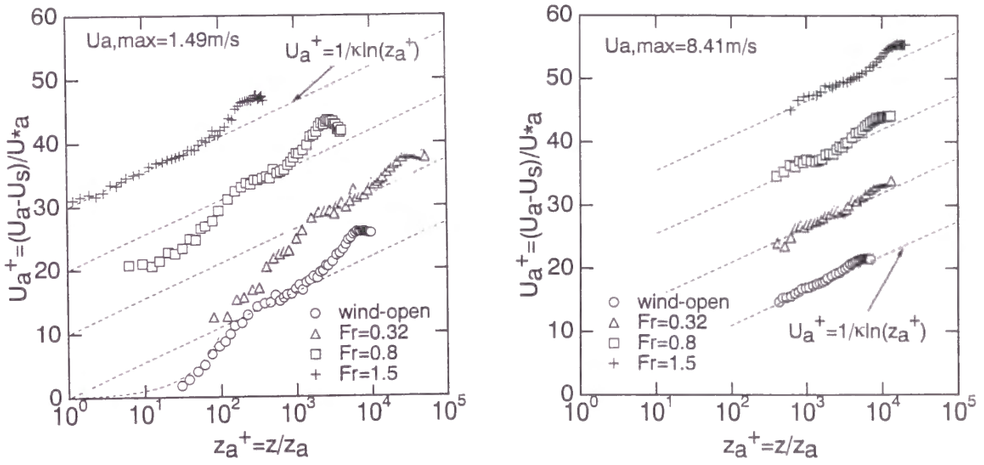

Fig.7.7 Primary mean velocity in air side U_a^+.

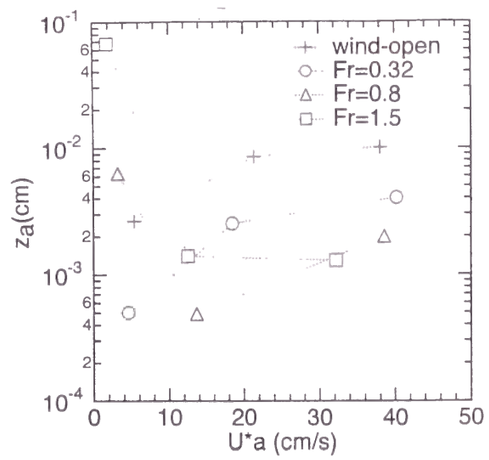

Fig.7.8 Roughness height of air side z_a versus U_{*a}.

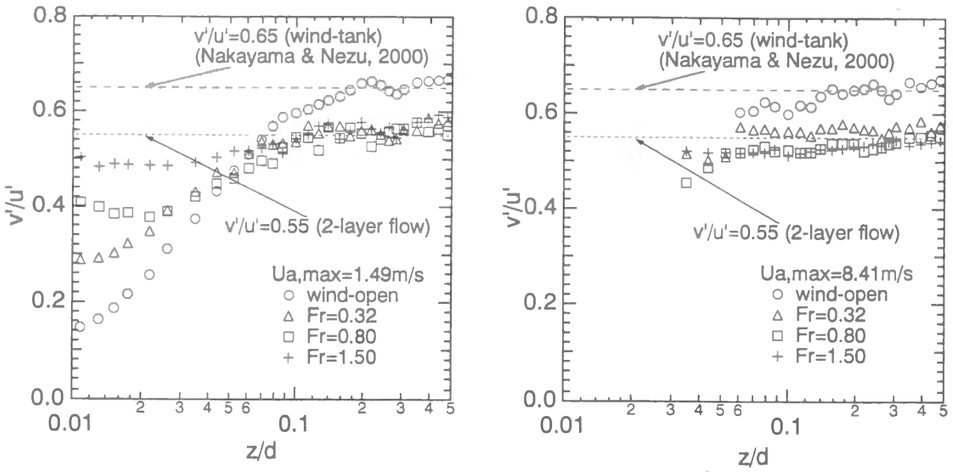

Fig.7.9 Turbulence intensity ratio v'/u' on air side.

wind velocity. In Fr=1.50, z_a monotonically decreases as U_{*a} increases. In this way, z_a depends greatly on the relative velocity of air and water, and there always exists the condition that z_a takes a minimum value, so-called condition that the relative velocity takes a minimum value, when the wind velocity changes at the fixed water velocity in two-layer flows.

7.4.1c Turbulence Intensity Ratio

Fig.7.9 shows the ratio of turbulence intensities v'/u'. In this figure, the equilibrium value (v'/u'=0.65) at the log-law region in wind wave (wind-tank) proposed by Nakayama and Nezu (2000a) is also plotted. In wind-open, v'/u' approaches the constant value (v'/u'=0.65) away from the interface at the log-law region regardless of the wind velocity. On the other hand, in two-layer flows, v'/u' takes a little smaller value (v'/u'=0.55) than that in wind wave, whereas v'/u' approaches the same value as in wind wave toward the upper wall. This means that the non-isotropy of turbulence takes a larger value in two-layer flows than in wind wave. Furthermore, in the case of smaller wind velocity ($U_{a,max}$=1.49m/s), the return to isotropy increases near the interface as the water velocity increases, which is mainly caused by the increase of roughness height and separation behind the wave crest due to the surface-wave fluctuations.

7.4.2 Extension of Mixing-Length Model to Two-Layer Flows

Fig.7.10 shows the mixing length l normalized by U_{*a} and ν_a in the smaller wind case, together with van Driest's (1956) model (A=26) in Eq.(7.1) and Riley *et al.*'s (1982) model (l_0=0, B=13) in Eq.(7.3). It can be seen that Riley *et al.*'s model reproduces well the experimental value in the point that the mixing length near the interface is a little smaller than that near the flat plate.

The ratio of l_0 to z_a is shown in Fig.7.11, where l_0 is the coefficient in Eq.(7.3) at the fixed value B=13 decided from the least square method between the experimental data and Eq.(7.3). In this figure, the empirical formula by Riley *et al.* (1982) and the boundary values between smooth region, incompletely rough region and rough region (Rr=0.137, 2.2) are also plotted together. The data in wind wave coincide well with the curve by Riley *et al.* and l_0 is in proportion to z_a in rough region. On the other hand, l_0/z_a increases remarkably in smooth and incompletely rough region as Froude number increases. Therefore, in two-layer flows, as the water velocity increases, roughness Reynolds number decreases due to the decrease of relative wind velocity and mixing length increases greatly in smooth

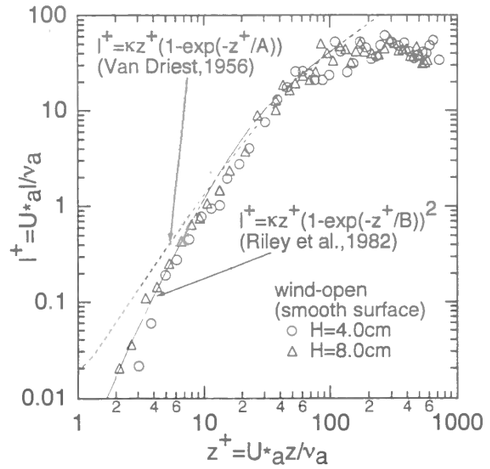

Fig.7.10 Mixing length l normalized by U_{*a} and ν_a in smaller wind case.

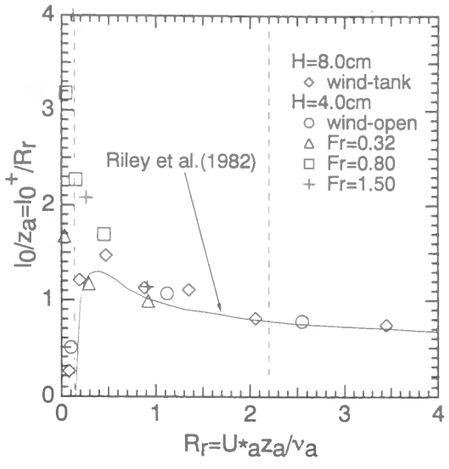

Fig.7.11 Ratio of l_0 to z_a versus roughness Reynolds number Rr.

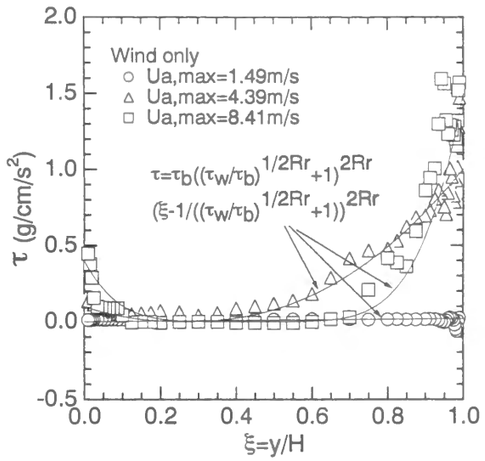

Fig.7.12 Shear stress $\tau(y)$ in wind wave.

and incompletely rough region.

7.5 Turbulence Structure of Water Flow

7.5.1 Shear Stress in Water Layer

So far, many researchers, for example, Reid (1957), Hughes and Duffey (1991) and Taniguchi *et al.* (1996), have evaluated the velocity distribution in water layer on the assumption that the shear stress varies linearly (it is not clarified that the shear stress distribution is linear even in wind wave.) and that the mixing length is parabolic. However, there have been less verifications any more.

Fig.7.12 shows the distribution of shear stress $\tau(y)$ (g/cm/s^2) in wind wave. The shear changes from linear to parabolic distribution as the wind increases. Considering that there exists a small bed shear in non-recirculating flow due to the non-zero bulk mean velocity, the shear stress distributions can

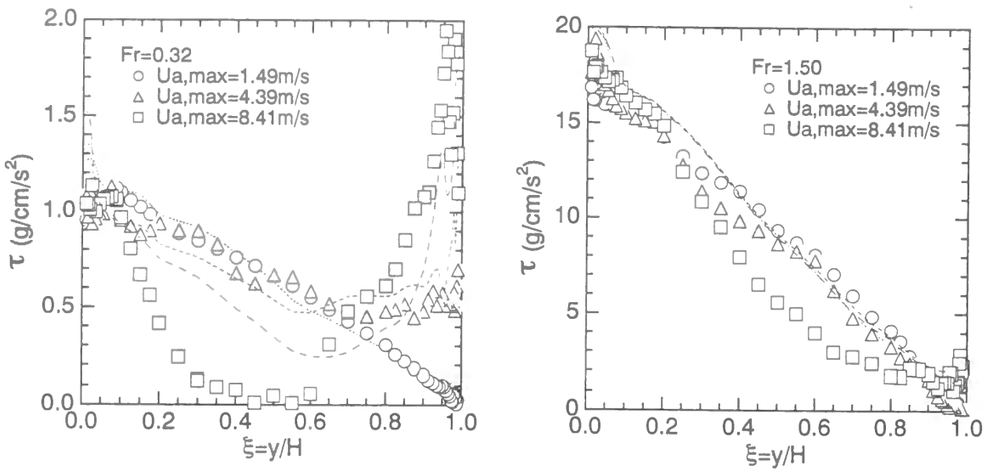

Fig.7.13 Shear stress $\tau(y)$ in two-layer flows.

approximate to be parabolic as follows;

$$\frac{\tau(y)}{\tau_b}=\left\{\left(\frac{\tau_w}{\tau_b}\right)^{1/2Rr}+1\right\}^{2Rr}\left\{\frac{y}{H}-\frac{1}{(\tau_w/\tau_b)^{1/2Rr}+1}\right\}^{2Rr} \tag{7.8}$$

In this way, in wind wave, the linear distribution of shear stress does not generally hold good as in open-channel flow, which may be closely related to the occurrence of secondary currents (upflow at the center of the channel) as mentioned by Banat (1992).

Fig.7.13 shows the distribution of shear stress $\tau(y)$ in two-layer flows, together with the dotted curve that only water flow and air flow's data added linearly. When the Froude number is smaller, the effect of air flow to the shear stress is greater. Furthermore, as the wind velocity is faster, the linear solution overestimates the shear stress in an intermediate region. This is because the secondary currents are greater in two-layer flows than in wind wave. Therefore, the shear stress in two-layer flows is refined from Eq.(7.4) to Eq.(7.9).

$$\frac{\tau(y)}{\tau_b}=1-\frac{y}{H}+\left\{\left(\frac{\tau_w}{\tau_b}\right)^{1/2Rr}+1\right\}^{2Rr}\left\{\frac{y}{H}-\frac{1}{(\tau_w/\tau_b)^{1/2Rr}+1}\right\}^{2Rr} \tag{7.9}$$

7.5.2 Primary Mean Velocity

Fig.7.14 shows the distribution of primary mean velocity on water layer $U^+=U/U_{*_b}$ in wind wave, normalized by the friction velocity at the bed wall U_{*_b} and the kinetic viscosity of water ν_w, where $y^+=U_{*_b}y/\nu_w$ is the normalized distance from the bed wall. In this figure, the semi-theoretical curve using Eq.(7.7) evaluated from Eqs.(7.5) and (7.8) is also described (k_w=0.01). It can be seen that the distribution varies from the laminar distribution in smooth region to logarithmic distribution in rough region, which differs a little from Eloubaidy and Plate (1972) in the point that they pointed out the log law is effective near the bed in wind wave regardless of wind velocity. Furthermore, the curve reproduces well the experimental data, which means that the shear stress distribution in Eq.(7.8) is effective.

Fig.7.15 shows the distribution of water velocity U^+ in two-layer flows, together with the semi-

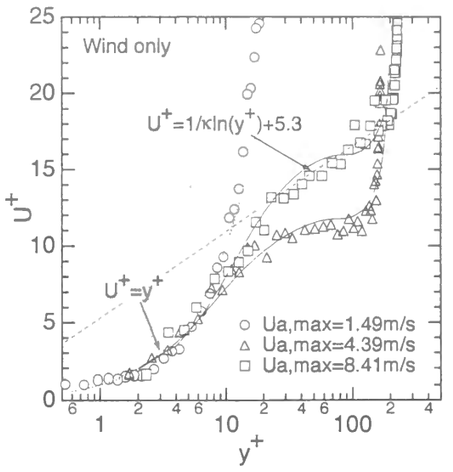

Fig.7.14 Primary mean velocity on water layer U^+ in wind wave.

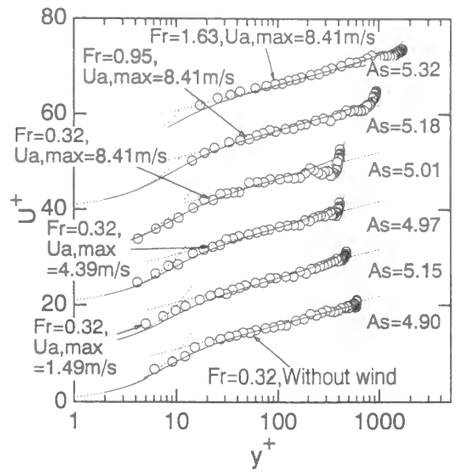

Fig.7.15 Primary mean velocity on water layer U^+ in two-layer flows.

theoretical curve using Eq.(7.7) evaluated from Eqs.(7.5) and (7.9) (k_w=0.01). In this figure, A_s means integration constant in log law. The log law is effective near the wall even in two-layer flows. The curve calculated from Eq.(7.7) is well coincident with the experimental data except the case in Fr=0.32 and $U_{a,max}$=8.41 (m/s), which is due to the fact that the calculated curve does not contain the effect of secondary currents in shear stress distribution. Taniguchi *et al.* (1996) pointed out that the semi-theoretical curve calculated from Eqs.(7.4) and (7.5) coincides very well with the experimental data and this may be because their experiment was conducted in smaller wind velocity (Reynolds number equals about 20,000.). Furthermore, the water velocity increases rapidly near the free surface as the wind velocity increases, which implies that the relative velocity between water and air affects greatly the velocity distribution in water layer.

7.5.3 Turbulence Intensity and Dissipation Rate

7.5.3a Non-Linearity of Turbulence Intensity

Tsuraya (1987) has suggested an empirical formula of turbulence intensity on the assumption that the turbulence energies generated at the wall and at the interface can be added linearly, as follows;

$$u'=\sqrt{u'^2_{water}+u'^2_{wind}}$$
$$v'=\sqrt{v'^2_{water}+v'^2_{wind}} \tag{7.10}$$

He suggested the empirical formula by using the above assumption and pointed out that this empirical formula coincides well with the experimental data. However, in the modeling of atmospheric and oceanic mixing layer, it is usual to evaluate the mutual effect of wind and convection by the sum of energy flux, as follows :

$$u'=\left(u'^3_{water}+u'^3_{wind}\right)^{1/3}$$
$$v'=\left(v'^3_{water}+v'^3_{wind}\right)^{1/3} \tag{7.11}$$

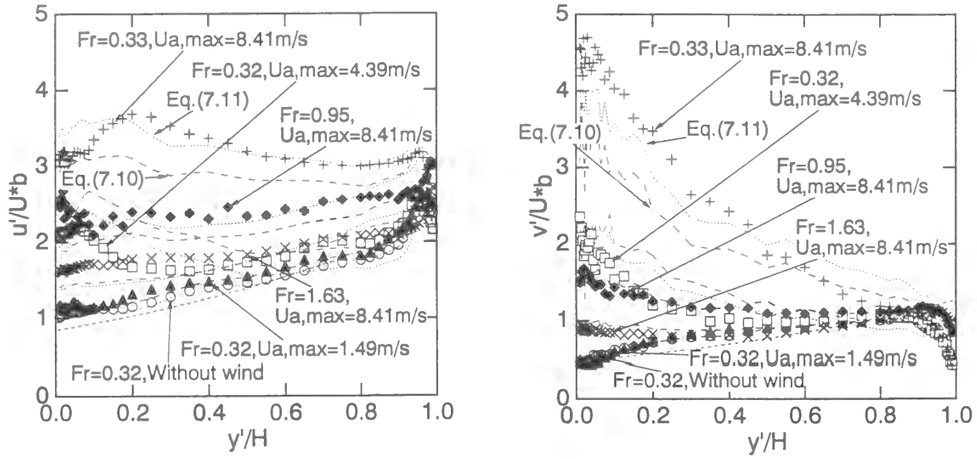

Fig.7.16 Turbulence intensities u'/U_{*b} and v'/U_{*b} on water side.

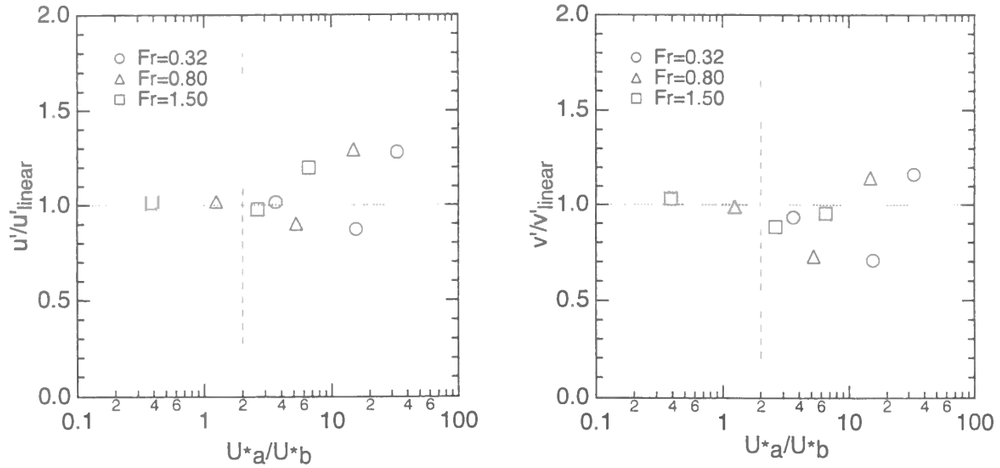

Fig.7.17 Ratio of the experimental values to the linear values u'/u'_{linear} and v'/v'_{linear}.

The turbulence intensities u'/U_{*b} and v'/U_{*b} are shown in Fig.7.16 versus the distance from the free surface $y'=H-y$. In the same way as in Fig.7.15, the value increases near the free surface as the relative velocity is larger. Furthermore, Eqs.(7.10) and (7.11) are also described in this figure. Both calculated values reproduce well the experiment in $u'/U_{*b}<2.0$ or $v'/U_{*b}<2.0$. However, Eqs.(7.10) and (7.11) become scattered from the experimental values at the higher values and Eq.(7.11) is better than Eq.(7.10), which implies that the mutual effect in two-layer flows can be well reproduced by the sum of energy flux. So, the turbulence intensities in two-layer flows are not expressed by the universal formula in the same way as open-channel flow because u'_{wind}/U_{*a} and v'_{wind}/U_{*a} wind decrease as the wind velocity increases.

The depth-averaged values of the ratio of the experimental values (u', v') to the linear values $(u'_{linear}, v'_{linear})$ evaluated by Eq.(7.11) are shown in Fig.7.17. The non-linearity increases as U_{*a}/U_{*b} becomes greater than 2 or 3, which is closely related to the generation of secondary currents. In this way, it is from now on needed to forecast the turbulence considering the effect of non-linearity in two-

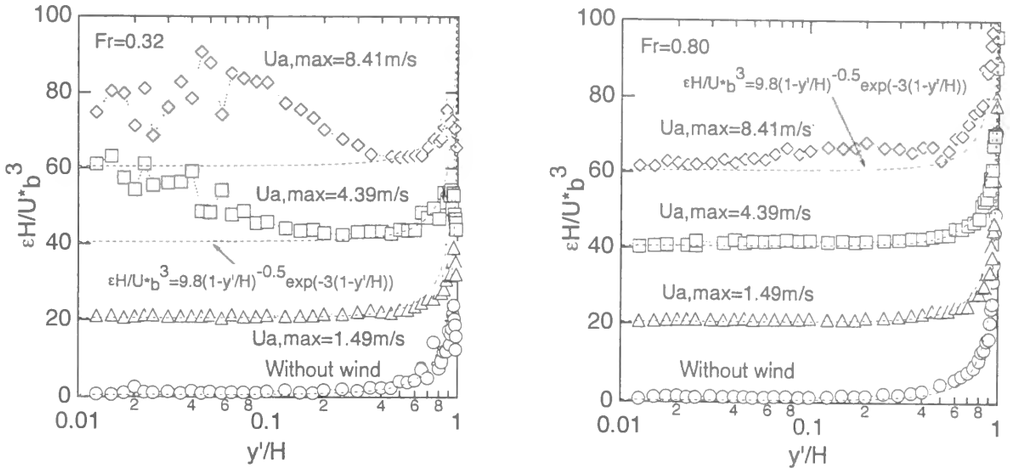

(a) Fr=0.32 (b) Fr=0.80

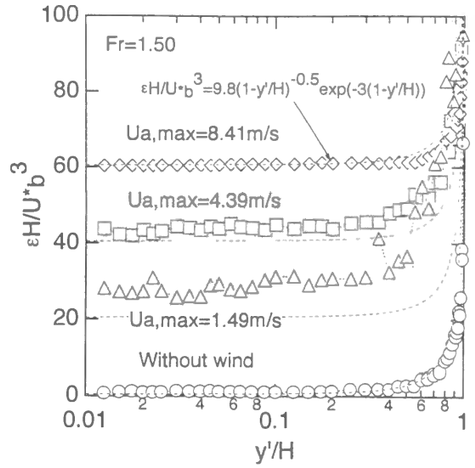

(c) Fr=1.50

Fig.7.18 Turbulent dissipation rate $\varepsilon H/U_{*b}^3$ near free surface.

layer flows.

7.5.3b Distribution of Dissipation Rate

Figs.7.18(a)-(c) show the distributions of the turbulent dissipation rate $\varepsilon H/U_{*b}^3$ near the free surface evaluated from the –5/3 power law of spectrum when the Froude number changes. In this figure, the semi-empirical formula in open-channel flow by Nezu and Nakagawa (1993) is also plotted together. As the wind velocity increases, ε increases near the free surface in Fr=0.32, whereas ε decreases near the free surface in Fr=1.50. This is because in Fr=1.50, the relative velocity decreases as the wind velocity increases. In this way, in order to evaluate the turbulence structure in two-layer flows, it is necessary to consider both the friction velocities or the bulk mean friction velocity in the same way as Eloubaidy and Plate (1972).

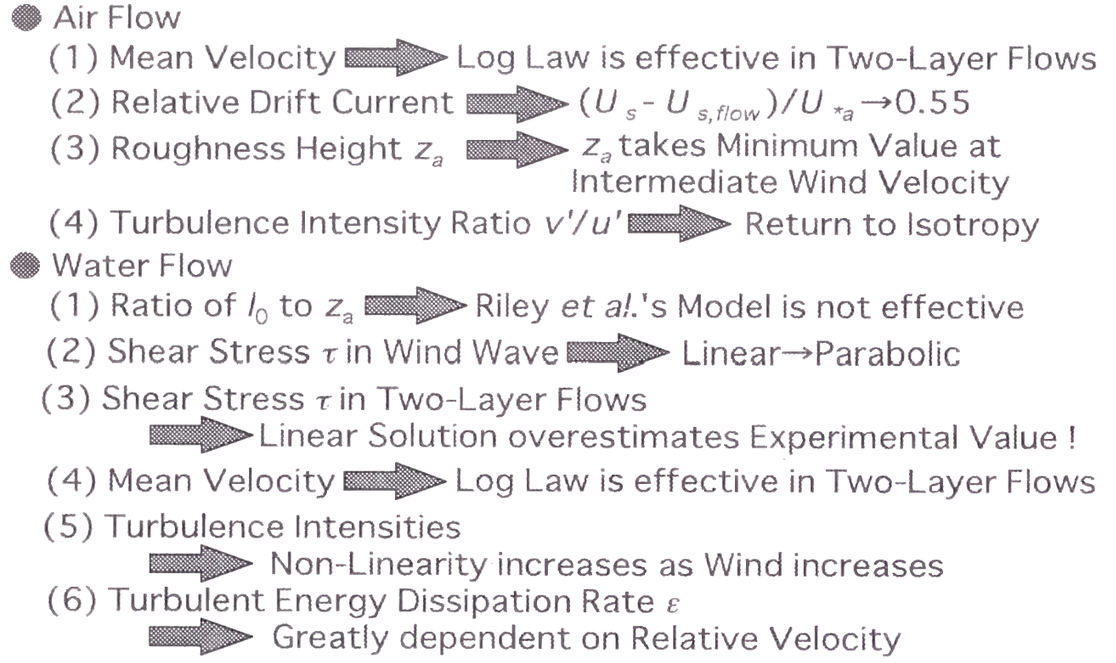

Fig.7.19 Conclusions of chapter 7.

7.6 Conclusions

In this study, the turbulence structure in two-layer flows was conducted. Fig.7.19 shows the conclusions of chapter 7. The log law is effective both in air and water layer near the interface. And the roughness height is closely related to the relative velocity of both layers. Furthermore, the relative drift current takes the universal value even in two-layer flows. About the air layer, the mixing-length model in wind wave was extended in the air flow of two-phase flows.

In the water layer, it was clarified that the shear stress does not vary linearly which adds interfacial shear to the bed shear due to the generation of secondary currents. Furthermore, the non-linearity increases with the increase in the ratio of friction velocities in both layers. In this way, the turbulence intensities and the dissipation rate have a close relationship with the relative velocity of both layers.

Notations

A, B : parameters in damping function
A_s : integration constant in log law
B : channel width
D : van Driest damping function
d : half height of air channel
Fr : Froude number in water layer ($=U_m/\sqrt{gH}$)
g : acceleration due to gravity
H : flow depth

k_w : constants of mixing length at the interface
k_b : von Karman constant ($=\kappa=0.41$)
l : mixing length
l_0 : turbulent mixing over the roughness element
l^+ : dimensionless mixing length ($=U_{*a}l/\nu_a$)
Rr : roughness Reynolds number ($=U_{*a}z_a/\nu_a$)
U_a : wind velocity
$U_{a,max}$: maximum wind velocity
U_m : bulk mean velocity
U_s : surface drift velocity
$U_{s,flow}$: drift current in open-channel flow
U_{*a} : friction velocity in air layer
U_{*b} : friction velocity in water layer
U_{*w} : friction velocity at the interface
u : instantaneous streamwise velocity component
u'_{linear}, v'_{linear} : linear values of turbulence intensities
v : instantaneous vertical velocity component
x : streamwise direction
y : vertical direction from the channel bed
y^+ : yU_{*b}/ν_w ; vertical distance in law of the wall coordinates
y' : distance from the free surface ($=H-y$)
z : vertical direction from water surface

Greek symbols
ε : turbulent energy dissipation rate
η' : intensity of surface-wave fluctuations ($\equiv\sqrt{\overline{\eta^2}}$)
κ : von Karman constant ($=0.41$)
λ : wave length
ν_a : kinetic viscosity of air
ν_w : kinetic viscosity of water
ρ_a : density of air
ρ_w : density of water
$\tau(y)$: distribution of shear stress in water flow
τ_w : interfacial shear stress ($=\rho_w U_{*w}^2$)
τ_b : wall shear stress ($=\rho_w U_{*b}^2$)
τ^+ : dimensionless shear stress ($=\tau/\tau_b$)

References

[1] Akai, M., Inoue, A. and Aoki, S. : Structure of a co-current stratified two-phase flow with wavy surface, *Theor. Appl. Mech.*, Vol.25, pp.445-456, 1977.
[2] Akai, M., Inoue, A., Aoki, S. and Endo, K. : A co-current stratified air-mercury flow with wavy interface, *Int. J. Multiphase Flow*, Vol.6, pp.173-190, 1980.
[3] Banat, M. : Two-phase stratified gas-water fully developed wavy flow, *Int. J. Engineering Fluid Mech.*, Vol.5, No.3, pp.329-372, 1992.
[4] Cohen, L.S. and Hanratty, T.J. : Generation of waves in the concurrent flow of air and a liquid,

AIChE J., Vol.11, No.1, pp.138-144, 1965.
[5] Eloubaidy, A.F. and Plate, E.J. : Wind shear-turbulence and reaeration coefficient, *J. Hydraulic Eng.*, ASCE, Vol.98, HY1, pp153-170, 1972.
[6] Fabre, J., Marodon, D., Masbernat, L. and Suzanne, C. : Turbulent structure of wavy stratified air-water flow, *Gas Transfer at Air-Water Interfaces*, W. Brutsaert and G.H. Jirka (eds.), pp.113-123, 1984.
[7] Hanratty, T.J. : Interfacial instabilities caused by air flow over a thin liquid layer, *Waves on fluid interfaces*, R.E. Meyer (eds.), 1983.
[8] Hanratty, T.J. and Engen, J.M. : Interaction between a turbulent air stream and a moving surface, *AIChE J.*, Vol.3, No.3, pp.299-304, 1957.
[9] Henstock, W.H. and Hanratty, T.J. : The interfacial drag and the height of the wall layer in annular flows, *AIChE J.*, Vol.22, No.6, pp.990-1000, 1976.
[10] Hughes, E.D. and Duffey, R.B. : Direct contact condensation and momentum transfer in turbulent separated flows, *J. Multiphase Flow*, Vol.17, No.5, pp.599-619, 1991.
[11] Hugemark, G.A. : Film thickness, entrainment, and pressure drop in upward annular and dispersed flow, *AIChE J.*, Vol.19, No.5, pp.1062-1065, 1973.
[12] Miles, J.W. : On the generation of surface waves by shear flow, *J. Fluid Mech.*, Vol.3, pp.185-204, 1957.
[13] Nezu, I. and Nakagawa, H. : Turbulence in open-channel flows, IAHR-Monograph, Balkema, 1993.
[14] Nezu, I., Nakayama, T. and Inoue, R. : Turbulence structures in air-water interface with wind shear, *Annual Journal of Hydraulic Engineering*, Vol.43, pp.413-418, 1999a (in Japanese).
[15] Nezu, I. and Nakayama, T. : Fundamental study at air-water interfaces with wind shear, *28th IAHR Congress*, IAHR, 1999c.
[16] Nezu, I. and Nakayama, T.: Effect of turbulence components below wind water waves, *28th IAHR Congress*, IAHR, 1999d.
[17] Nezu, I., Nakayama, T. and Inoue, R. : Influence of turbulence structure on gas transfer across air-water interface, *Journal of Applied Mechanics*, JSCE, Vol.2, pp.673-684, 1999h (in Japanese).
[18] Nakayama, T. and Nezu, I. : Turbulence structures of wind/stream combined flow, *Journal of Hydraulic Engineering*, JSCE, 1999m (in Japanese, to be accepted).
[19] Nakayama, T. and Nezu, I. : Turbulence structures of wind water waves, *Journal of Hydraulic Engineering*, JSCE, No.642/II-50, 2000a (in Japanese).
[20] Plate, E.J. and Friedrich, R. : Reaeration of open channel flow, *Gas Transfer at Air-Water Interfaces*, W. Brutsaert and G.H. Jirka (eds.), pp.333-346, 1984.
[21] Reid, R.O. : Modification of the quadratic bottom-stress law for turbulent channel flow in the presence of surface wind-stress, *Tech. Memo.*, No.93, Beach Erosion Board, U.S. Corps of Engineers, 1957.
[22] Riley, D.S., Donelan, M.A. and Hui, W.H. : An extended Miles' theory for wave generation by wind, *Boundary Layer Meteo.*, No.22, pp.209-225, 1982.
[23] Rotta, J.C. : Turbulent boundary layers in incompressible flow, *Progresses in Aerospace Sci.*, No.2, pp.1-219, 1962.
[24] Taniguchi, H., Ueno, K., Aritomi, M. and Takahashi, M. : Turbulence structure in liquid phase of air-water stratified flow, *Flow Modeling and Turbulence Measurements VI*, Chen, Shih, Lienau and Kung (eds.), Balkema, pp.771-778, 1996.
[25] Tsuruya, H. : Influence of Wind to Turbulence Structure and Mass Transport near the Ocean Surface, *Ph.D Thesis presented to Tokyo Institute of Technology*, 1987 (in Japanese).
[26] van Driest, E.R. : On turbulent flow near a wall, *J. Aero. Sci.*, No.23, pp.1007-1011, 1956.

CHAPTER 8

CHARACTERISTIC OF GAS TRANSFER COEFFICIENT ACROSS AIR-WATER INTERFACE

Abstract

Mass transfer across an air-water interface is a fundamental and very important process in environmental and geophysical problems. The relation between the turbulence structure near the interface and the gas transfer process across the air-water interface was experimentally evaluated. At that time, three different turbulent conditions were considered; namely, the bottom shear driven turbulence, the wind shear driven turbulence, and the combined wind/stream driven turbulence. As a result, the mechanism of gas transfer across the air-water interface is well explained by a small-eddy model of turbulence.

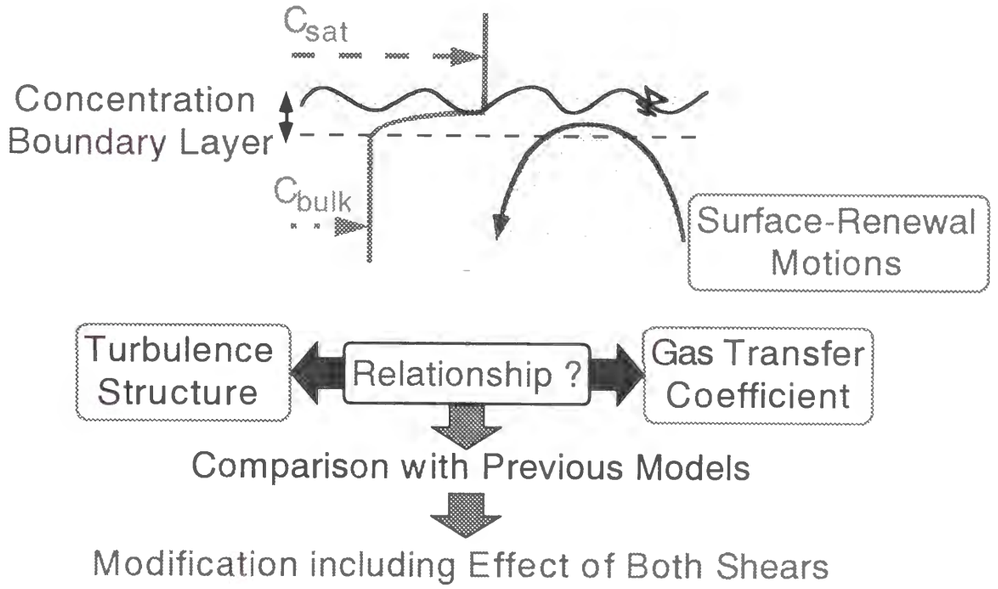

CHAPTER 8 CHARACTERISTIC OF GAS TRANSFER COEFFICIENT ACROSS AIR-WATER INTERFACE

Parts of this chapter were presented in the following papers.

[1] Nezu, I. and Nakayama, T. : Fundamental study at air-water interfaces with wind shear, *28th IAHR Congress*, IAHR, 1999c.
[2] Nakayama, T. and Nezu, I. : Relationship between turbulence structures and gas transfer across air-water interface, *Journal of Hydraulic Engineering*, JSCE, No.635/II-49, pp.85-95, 1999f (in Japanese).
[3] Nezu, I., Nakayama, T. and Inoue, R. : Influence of turbulence structure on gas transfer across air-water interface, *Journal of Applied Mechanics*, JSCE, Vol.2, pp.673-684, 1999h (in Japanese).
[4] Nezu, I., Nakayama, T. and Inoue, R. : Relation between turbulence structure and gas transfer coefficient near the free surface, *Proc. of Water, Environment, Ecology, Socio-Economics, and Health Engineering*, pp.203-216, 1999i.
[5] Nakayama, T. and Nezu, I. : Turbulence structures of wind water waves, *Journal of Hydraulic Engineering*, JSCE, No.642/II-50, 2000a (in Japanese).

8.1 Introduction

Mass transfer across a gas-liquid interface is of fundamental importance to environmental and geophysical sciences. In most cases of practical importance, the majority of environmentally important gases have low solubility (or high Henry's constant : for example, O_2, N_2, CO_2, CO and CH_4) and the liquid flow is turbulent, and therefore the gas transport across the interface is governed by the hydrodynamic conditions of liquid side. Recently, Jirka and Ho (1990) and Chu and Jirka (1992) have used a finished oxygen microprobe, and measured very accurately the instantaneous gas concentration fluctuations very near the free surface. They evaluated the co-spectra of vertical velocity and concentration and clarified that both fluctuations are closely related with each other.

By the way, the previous model of gas transfer coefficient K_L is mainly classified into two models, that is to say, (1) conceptual model and (2) hydrodynamic model. Conceptual model is simple solution of a vertically one-dimensional diffusion equation without any explicit advective flow field. Lewis and Whitman (1924) have proposed a "*film model*" on the assumption that there exist two stagnant thin films on each side of gas-liquid interface and that the gas molecules pass through these two films by molecular diffusion.

$$K_L = \frac{D_m}{\delta_l} \tag{8.1}$$

where D_m (cm²/s) is the molecular diffusivity of the gas in the liquid, δ_l (cm) is the thickness of the film. On the other hand, Danckwerts (1951) modified the Higbie's (1935) model and derived a "*surface-renewal model*", as follows:

$$K_L = \sqrt{D_m \cdot r} \tag{8.2}$$

where r (1/s) is the mean frequency of surface renewal. Furthermore, O'Connor and Dobbins (1956) have suggested the combined model of film model (r=0) and surface-renewal model (r= ∞) depending on r.

In hydrodynamic model, the advective diffusion equation is solved under the imposed assumption of a simple, single-scale flow pattern. This model is mainly divided into the "*large-eddy model*" by Fortescue and Pearson (1967) and the "*small-eddy model*" by Lamont and Scott (1970). The integral length scale is used for time scale in the large-eddy model, and Kolmogorov scale (the dissipation rate of turbulent energy ε) is considered to be an important parameter in the small-eddy model, as follows:

$$K_L^+ \equiv \frac{K_L}{U_*} \propto Sc^{-1/2} R_*^{-1/2} : LargeEddyModel \tag{8.3}$$

$$K_L^+ \propto Sc^{-1/2} R_*^{-1/4} : SmallEddyModel \tag{8.4}$$

where $Sc(=\nu/D_m)$ is the Schmidt number, and R_* is the turbulent Reynolds number. Furthermore, Theofanous *et al.* (1976) proposed a two-regime model combining the large-eddy model for low Reynolds number with the small-eddy model for high Reynolds number. Furthermore, Brumley and Jirka (1988) have suggested the newer model different from the above-mentioned two models. They considered the surface divergence fluctuations as an important force of gas transport across the Kolmogorov sublayer into the bulk water and combined the stagnation flow model by Chan and Scriven (1970) and the random eddy model by Harriott (1962).

In order to evaluate the relation between the turbulence structure and gas transfer across an air-

water interface, it is necessary to consider the following three different turbulent conditions for the first time, as pointed out by Plate and Friedrich (1984) ; (A) bottom-shear generated turbulence (open-channel flow), (B) wind-shear generated turbulence and (C) combined wind/stream turbulent conditions. As for (A) open-channel flow, there have been various discussions whether the large-eddy model or the small-eddy model is effective, and this is not clear yet. Hirayama *et al.* (1995) have pointed out that the large-eddy model is more effective based on turbulence intensities by examining the former experimental data comprehensively. On the other hand, Moog (1995) and Moog and Jirka (1995) conducted some experiments in the newest Tilting Wind-Water Tunnel (TWWT) and concluded that the small eddies are more active in the surface renewal. Furthermore, Dobbins (1964, 1965) and Thackston and Krenkel (1969) have applied the renewal model and proposed a formula including the effect of Froude number to account for enhanced surface area due to surface distortions in open-channel flow.

As for (B) wind-induced flow, Nezu and Nakayama (1999c) showed the relation between the intensity of surface-wave fluctuations and roughness height of water surface. They pointed out that the intensity takes almost a constant value in a smooth situation and increases rapidly in an incompletely rough situation (3-D capillary wave), and also that there exists a linear relation in a rough region (2-D gravity wave). O'Connor (1983) has applied the film model in the smooth situation and the renewal model in the rough situation, and expanded semi-theoretically the relation between K_L and the friction velocity U_{*a} in the air flow by using the continuity of momentum across the interface. Broecker and Siems (1984), Liss and Merlivat (1986) and Chu and Jirka (1995) also pointed out the discontinuity of K_L around a particular friction velocity and the value of K_L increases rapidly due to the change of surface roughness conditions.

Finally, as for (C) combined wind/stream flow, Mattingly (1977) has proposed the equation of K_L in the bottom-shear flow and applied the expression into the two-layer flows. Eloubaidy and Plate (1972) have developed the theoretical equation to predict K_L based on the concept that K_L is controlled by an effective turbulent diffusion coefficient at the free surface in the combined flow. On the other hand, Jirka and Brutsaert (1984) suggested a simple relationship for the relative importance of streamflow generated turbulence and of wind turbulence on gas exchange on the basis of estimation for the near-surface turbulent energy dissipation rates. Chu (1993) has expanded this idea and related the turbulence structure near the free surface with the gas transfer across an air-water interface. However, there is not a clear relation between their suggestion and the previous models. Consequently, it is necessary to correlate these models with each other.

In this way, there remain a lot of questions unanswered concerning the turbulence structure near the free surface and its role in the interfacial gas transfer process. The aim of this study is to relate the turbulence structure near the free surface with the gas transfer coefficient each other.

8.2 Experimental Apparatus and Procedures

The experiments were conducted in a tilting wind-water tunnel of 16m long, 40cm wide and 50cm deep, as shown in Fig.8.1 in the same way as in the chapters 6 and 7. The present air/water tunnel is composed of a recirculating tilting water flume and an open-ended wind tunnel. Coordinate axis in the streamwise direction is defined as x. As for the vertical direction, the upward direction from the bottom is defined as y. The upward and downward directions from the interface are defined as z and y' ($=H-y$, H is the flow depth), respectively. Instantaneous velocities for the streamwise and vertical components are $u(t)$ and $v(t)$, respectively.

In order to measure the instantaneous velocity for both air and water, 500mW LDA system

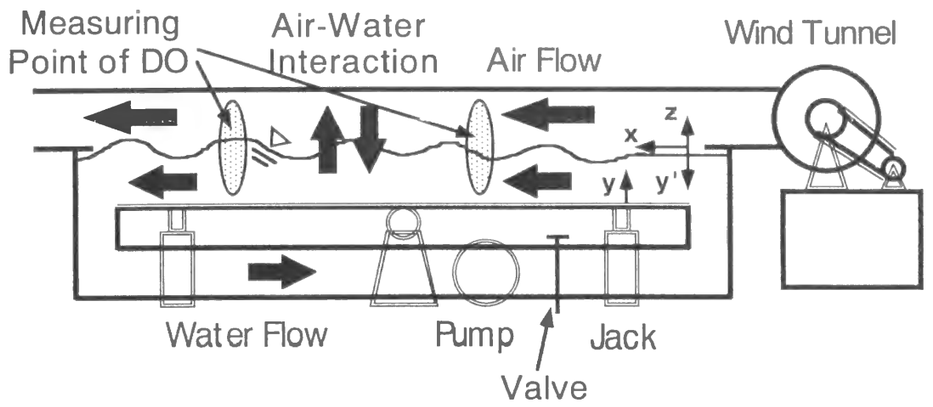

Fig.8.1 Schematic diagram of tilting wind-water tunnel.

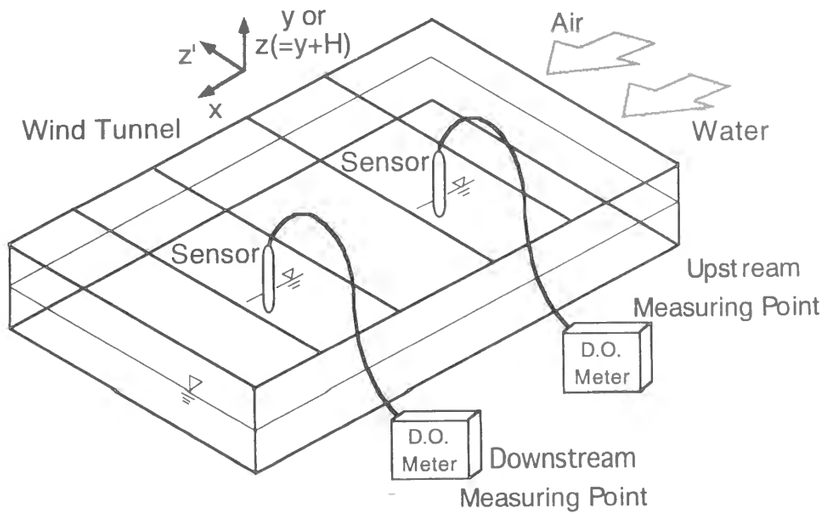

Fig.8.2 Schematic representation of dissolved oxygen (DO) measurement.

(DANTEC-made) was used at the center of channel 9m downstream of the channel entrance. About water flow, sampling time was 60sec, and sampling frequency was about 150Hz. An ultrasonic depth-measuring instrument (KEYENCE-made) was set above the free surface and synchronized with the LDA. Wind velocity was accurately measured with a fog generator (sampling number was 10,000, and sampling frequency was about 1kHz). By applying the log law both in the air flow and the water flow, the friction velocities were evaluated.

Dissolved oxygen meter (0.1 mg/l accuracy, CENTRAL SCIENCE-made) was used for the measurement of dissolved oxygen (DO) concentrations, as shown in Fig.8.2. Water was deoxygenated by putting enough sodium sulfite(Na_2SO_3) in the following equation.

$$O_2 + 2Na_2SO_3 \rightarrow 2Na_2SO_4 \tag{8.5}$$

Table 8.1 Hydraulic conditions in DO measurements.

Wind-Water Wave (Valve-Closed)

case	H (cm)	$U_{a,max}$ (m/s)	$U_{w,mean}$ (cm/s)	U^*a (cm/s)
d2wa	8.0	0.94	0.0	3.84
d2wb	8.0	1.79	0.0	7.56
d2wd	8.0	3.63	0.0	17.51
d2wf	8.0	5.46	0.0	28.67
d2wh	8.0	8.30	0.0	50.29
d3wi	20.0	11.20	0.0	107.80

Open-Channel Flow

case	H (cm)	$U_{w,mean}$ (cm/s)	Fr	U^*b (cm/s)
d1f1	4.0	6.8	0.10	0.44
d1f2	4.0	20.2	0.32	1.22
d1f3	4.0	50.2	0.80	2.53
d1f4	4.0	92.9	1.50	4.64
d1f5	4.0	123.5	2.00	6.06
d2f1	8.0	11.2	0.32	0.56

Wind-Water Wave (Valve-Open)

case	H (cm)	$U_{a,max}$ (m/s)	$U_{w,mean}$ (cm/s)	U^*a (cm/s)
d2wa	8.0	0.94	0.004	5.20
d2wd	8.0	3.63	0.017	12.92
d2wf	8.0	5.46	0.051	23.45
d2wh	8.0	8.30	0.074	37.13
d1wh	4.0	5.42	0.054	24.0

Wind/Stream Combined Flow

case	H (cm)	$U_{a,max}$ (m/s)	$U_{w,mean}$ (cm/s)	Fr	U^*a (cm/s)	U^*b (cm/s)
w1f1	4.0	1.49	20.30	0.32	4.52	1.25
w2f1	4.0	4.39	20.26	0.32	18.45	1.20
w3f1	4.0	8.41	20.59	0.33	40.20	1.22
w1f2	4.0	1.49	50.47	0.81	3.20	2.57
w2f2	4.0	4.39	51.83	0.83	13.66	2.61
w3f2	4.0	8.41	59.24	0.95	38.57	2.61
w1f3	4.0	1.49	98.27	1.57	1.82	4.67
w2f3	4.0	4.39	98.64	1.58	12.49	4.77
w3f3	4.0	8.41	101.84	1.63	32.19	4.93

Then DO measurement was conducted by this instrument. K_L was calculated by the time-gradient of the measured value of DO concentration, which was corrected to 20℃ value K_{L0} by the empirical temperature-correction, as follow:

$$K_L = K_{L0} \cdot \theta^{T-20} \tag{8.6}$$

where θ is the temperature collection coefficient (=1.0241) as suggested by Elmore and West (1961).

Hydraulic conditions for the experiments are shown in Table 8.1. Experiments are divided into three conditions; (A) bottom-shear generated flow (open-channel flow), (B) wind-shear generated flow and (C) combined wind/stream flow. The parameters are defined as follows, H : the flow depth, $U_{a,max}$: the maximum wind velocity, U_{*a} : the friction velocity in the air layer calculated from the log-law, U_{*b} : the friction velocity in the water layer, Fr ($=U_m/\sqrt{gH}$) : Froude number, and η' ($\equiv\sqrt{\eta^2}$) : the intensity of surface-wave fluctuations, respectively. As for (B) wind-induced flow, winds of several speeds were blown over a still water in recirculating flume (valve-closed) and non-recirculating flume (valve-open). As for (C) combined wind/stream flow, the stream condition was changed to three patterns, so called, Fr=0.32 (sub-critical flow), 0.80 (near-critical flow) and 1.50 (super-critical flow). The wind condition was changed to three patterns, that is to say, $U_{a,max}$(m/s)=1.49 (smooth region), 4.39 (incompletely rough region) and 8.41 (rough region).

8.3 Theoretical Considerations

8.3.1 Gas Transfer Coefficient K_L in Wind Water Wave

O'Connor (1983) has applied the film model in the smooth situation and the renewal model in the

rough situation, and expanded semi-theoretically the relation between K_L and the friction velocity U_{*a} in the air flow by using the continuity of momentum across the interface, as follows:

$$K_L \equiv K_{LS} = \frac{D_m}{\delta_l} = \left[\frac{D_m}{\nu_w}\right]^{2/3} \left[\frac{\rho_a}{\rho_w}\right]^{1/2} \frac{\kappa^{1/3}}{\Gamma_0} U_{*a} \propto U_{*a} : Smooth\ Situation \tag{8.7}$$

$$K_L \equiv K_{LR} = \sqrt{D_m r} = \left[\frac{\rho_a \nu_a}{\rho_w \nu_w} \frac{D_m U_{*a}}{\kappa z_e}\right]^{1/2} \propto \sqrt{U_{*a}} : Rough\ Situation \tag{8.8}$$

$$\frac{1}{z_a} = \frac{1}{z_e} + \frac{\lambda_1 U_{*a}}{\nu_a} \exp(-U_{*a}/U_{*t}) \tag{8.9}$$

where Γ_0 : the normalized thickness of viscous sublayer, ν_w : kinematic viscosity of water, κ : Karman constant, z_e : equilibrium roughness, and U_{*t} : the transitional shear velocity, respectively. Therefore, the transfer coefficient in the transitional region is given as follows:

$$\frac{1}{K_L} = \frac{1}{K_{LS}} + \frac{1}{K_{LR}} = \frac{1}{\left[\frac{D_m}{\nu_w}\right]^{2/3} \left[\frac{\rho_a}{\rho_w}\right]^{1/2} \frac{\kappa^{1/3}}{\Gamma(U_{*a})} U_{*a}} + \frac{1}{\left[\frac{\rho_a \nu_a}{\rho_w \nu_w} \frac{D_m U_{*a}}{\kappa z_a (U_{*a})}\right]^{1/2}} \tag{8.10}$$

$$\begin{aligned} \Gamma(U_{*a}) &= \Gamma_0 \frac{U_{*a}}{U_{*c}} \exp(1 - U_{*a}/U_{*c}) \quad for U_{*a} \geq U_{*c} \\ &= \Gamma_0 \qquad for U_{*a} \leq U_{*c} \end{aligned} \tag{8.11}$$

where U_{*c} is the critical velocity of U_*. From equation (8.7)～(8.11), we can see that K_L is proportional to $U_{*a}{}^1$ in the smooth region (K_{LS}), $U_{*a}{}^{1/2}$ in the rough region (K_{LR}) and $U_{*a}{}^2$ (at maximum) in the transitional region, respectively.

8.3.2 Relation between Intensity of Surface-Wave Fluctuations η' and K_L

Dobbins (1964) has proposed the surface renewal frequency r and the length scale L in open-channel flow in the following.

$$r \propto \frac{\rho_w L E_s}{\sigma} \tag{8.12}$$

$$L \propto \left(\frac{\nu_w{}^3}{E_s}\right)^{1/4} \tag{8.13}$$

where σ and E_s are the surface tension and the turbulent energy per unit mass of liquid in the vicinity of the surface. He expressed the enhanced surface area due to surface distortions as the function of Froude number. In the present study, we consider the increased area C_A and E_s, as follows:

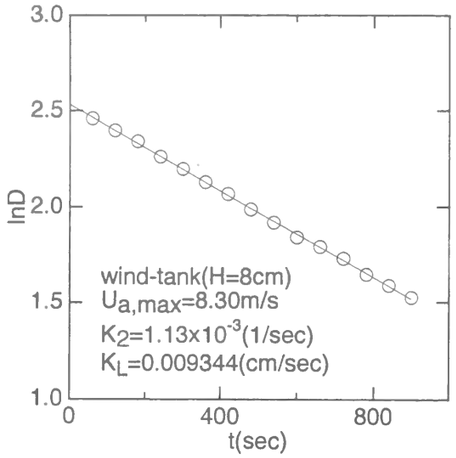

Fig.8.3 Time variation of dissolved oxygen deficit D.

$$C_A = 1 + A\left(\frac{\eta'}{H}\right)^2 \tag{8.14}$$

$$E_s \propto \frac{1}{2}\rho_w g \eta'^2 \tag{8.15}$$

where A is a constant coefficient. From the above mentioned, K_L is expressed by the surface-renewal model in this way.

$$K_L \propto \left(\frac{D_m}{\sigma}\right)^{1/2} \rho_w^{7/8} (g\nu_w)^{3/8} \left(1 + A\left(\frac{\eta'}{H}\right)^2\right) \eta'^{3/4} \propto \left(1 + A\left(\frac{\eta'}{H}\right)^2\right) \eta'^{3/4} \tag{8.16}$$

Therefore, the following relation is obtained:

$$K_L \propto \eta'^{3/4} \quad for A << H^2$$
$$K_L \propto \eta'^{11/4} \quad for A >> H^2 \tag{8.17}$$

8.4 Distribution of K_L

8.4.1 Time variation of D ($\equiv C_s$ - C) and Vertical Distribution of K_2

In wind-water waves (valve-closed), the bulk mean velocity is zero, and the reaeration coefficient K_2 is calculated in the following equation.

$$K_2 = -\frac{\partial}{\partial t} \ln D(t) \tag{8.18}$$

where $D(t)$ ($\equiv C_s$ - $C(t)$, C_s : saturation concentration of dissolved gas, $C(t)$: instantaneous concentration) is the dissolved oxygen deficit (mg/l). Fig.8.3 is an example of the time variation of D, together with the approximation line. K_2 is calculated from this line by using Eq.(8.18).

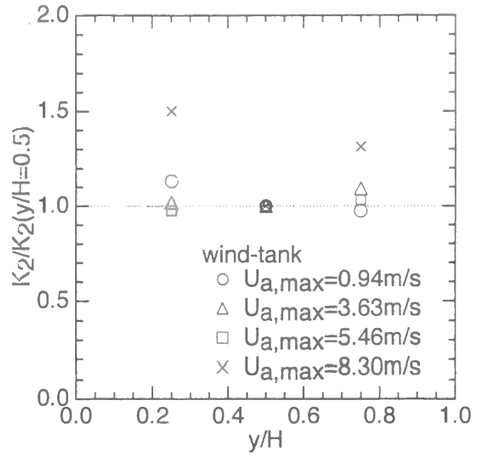

Fig.8.4 Vertical distribution of reaeration coefficient K_2.

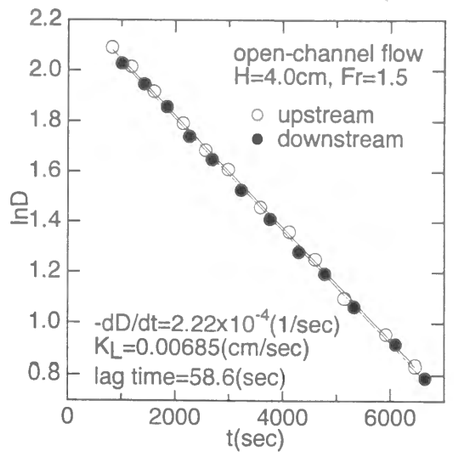

Fig.8.5 Example of the two-point measurement.

Generally, the gas concentration in water changes greatly in the thin concentration boundary layer very near the water interface, and it is almost constant in the bulk, therefore, completely mixed situation. This means that the gas transfer is controlled by the liquid phase, and it is, therefore, preferable to use the gas transfer coefficient K_L for evaluating the gas transfer flux F across the interface.

$$F \equiv K_L D(t) = K_2 \frac{V}{A} D = K_2 H D \tag{8.19}$$

where V : the water volume, A : the water surface area, and H : the flow depth, respectively. To confirm the validity of Eq.(8.19), it is necessary to examine the independence of K_2 on the vertical axis. Fig.8.4 shows the vertical distribution of K_2 normalized by the value of half-depth (y/H=0.5). There is not a great difference to the vertical direction regardless of the wind speed. Therefore, the value of K_2 at the half-depth was used to calculate K_L hereafter.

On the other hand, when the flow has a mean velocity, it is necessary to measure DO concentrations at two points, as pointed out by Moog (1995). In this situation, K_2 is expressed by the following equation including the convection term in the Eq.(8.18).

$$K_2 = -\frac{\partial}{\partial t} \ln D(t,x) - U_{w,mean} \frac{\partial}{\partial x} \ln D(t,x) \tag{8.20}$$

where $U_{w,mean}$ is the bulk mean velocity in water. In the right-hand side of the above equation, the first term is an acceleration one (one-point measurement, K_{acc}) and the second term is a convection one (K_{conv}). Fig.8.5 is an example of the two-point measurement.

8.4.2 K_L in Wind Water Wave

Fig.8.6 shows the distribution of K_L versus U_{*a} in wind-water wave (valve-closed). The semi-theoretical equations (8.7)～(8.11) (solid line) and the approximate functions by Chu and Jirka (1995) are also described together in this figure. It can be seen that K_L increases significantly at $U_{*a} \fallingdotseq$ 10cm/s and again become milder at $U_{*a} \fallingdotseq$ 40cm/s, which agree well with the experimental curves of Chu and Jirka. It seems that these phenomena have a close relationship with the condition of surface-wave fluctuations. The roughness-shear relationship is shown in Fig.8.7, where roughness size z_a is calculated

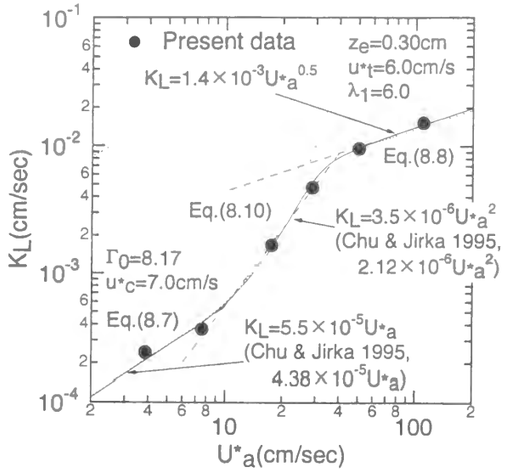

Fig.8.6 Gas transfer coefficient K_L in wind-water wave (valve-closed).

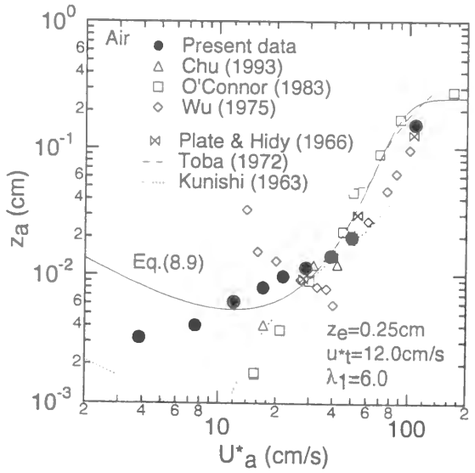

Fig.8.7 Roughness height z_a versus U_{*a} in wind-water wave (valve-closed).

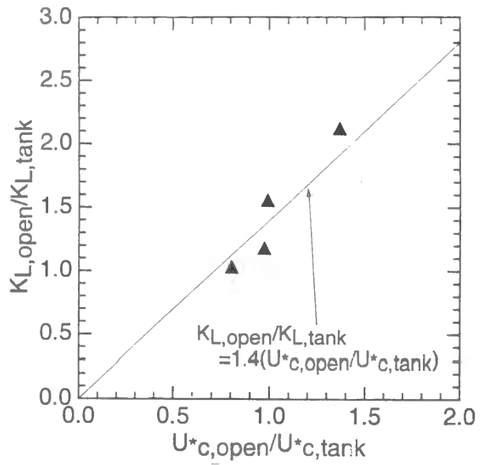

Fig.8.8 Ratio of gas transfer coefficient $K_{L,open}/K_{L,tank}$ versus ratio of friction velocity $U_{*c,open}/U_{*c,tank}$.

by applying the log-law to the wind velocity distribution. Various experimental data are also plotted, together with the Eq.(8.9). From Figs.8.6 and 8.7, one can see that both of z_e are in a good agreement with each other, which means that the physical aspect (wind velocity) and the chemical aspect (concentration) are connected with each other by O'Connor's semi-theoretical formula of Eqs.(8.7)～(8.11).

Eloubaidy and Plate (1972) have proposed the following equation in wind-water wave (valve-open) by using the friction velocity U_{*c} ($=\sqrt{(\tau_b+\tau_w)/\rho_w}=\sqrt{gHS_p}$) on the assumption that Krenkel and Orlob's (1963) idea is effective.

$$K_L = C\frac{U_{*w}H}{\nu_w}U_{*c} \tag{8.21}$$

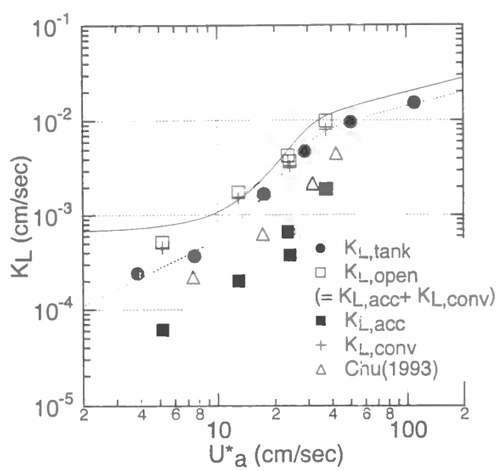

Fig.8.9 Gas transfer coefficient K_L in wind-water wave (valve-open).

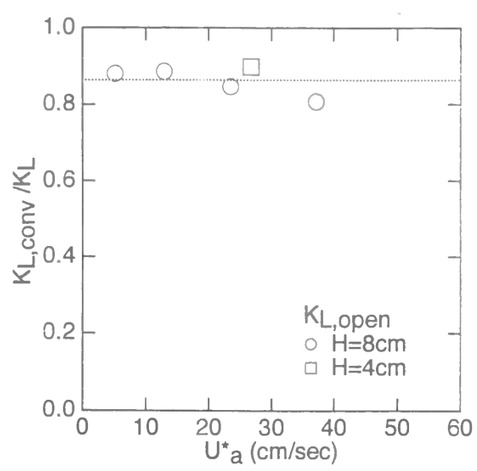

Fig.8.10 Rate of convection term $K_{L,conv}/K_L$ in wind-water wave (valve-open).

where τ_b ($=\rho_w U_{*b}^2$) and τ_w ($=\rho_w U_{*w}^2$) are shear stress at the bottom bed and the free surface, and S_p is the pressure-adjusted channel slope. It can be supposed that U_{*b} has the possibility of affecting K_L in non-recirculating flume. Fig.8.8 shows the distribution of $K_{L,open}/K_{L,tank}$ versus $U_{*c,open}/U_{*c,tank}$. It can be seen that $K_{L,open}/K_{L,tank}$ is almost in proportion to $U_{*c,open}/U_{*c,tank}$.

Fig.8.9 shows the distribution of K_L in wind-water waves (valve-open), together with the data in recirculating flume ($K_{L,tank}$). An approximation curve considering the convection effect in Fig.8.8 is also described in this figure. The distribution of K_L in non-recirculating flume ($K_{L,open}$) seems similar to that in recirculating flume ($K_{L,tank}$). However, the value in non-recirculating flume becomes greater as U_{*a} decreases, which is well reproduced by the approximation curve. Fig.8.10 shows the rate of convection term $K_{L,conv}/K_L$. It can be seen that the ratio has a constant value (about 0.8～0.9) regardless of the wind velocity and the flow depth. As a result, the convection term takes a greater part in K_L.

8.4.3 K_L in Open-Channel Flow

Fig.8.11 shows the distribution of K_L versus U_{*b} in open-channel flow, together with the empirical formula including the effect of Froude number by Thackston and Krenkel (1969) and the large-eddy and small-eddy models. From this figure, it can be shown that the small-eddy model is applicable to the small zone of U_{*b}. However, this model is not applicable in the larger zone of U_{*b}. There occurs an effect of Froude number on K_L, as pointed out by Dobbins (1964) and Thackston and Krenkel (1969). In this figure, the approximation curve considering the effect of Froude number is also described by solid line. The ratio of $K_{L,conv}$ to K_L is shown in Fig.8.12. The value is almost same as that in wind wave (compare Fig.8.10 with Fig.8.12), which implies that the ratio is independent whether the shear is impose on the bottom wall or the free surface.

Fig.8.13 is the distribution of K_L against the turbulent dissipation rate ε near the free surface (the averaged value in the surface-influenced layer). The values of ε were evaluated from the -5/3 power law of energy spectrum. K_L is in a proportion to $\varepsilon^{1/4}$, which implies the validity of small-eddy model. In larger zone of ε, the influence of Froude number occurs, as mentioned before.

8.4.4 K_L in Combined Flow

Fig.8.14 shows the distribution of K_L versus U_{*a} in combined wind/stream flows, together with the

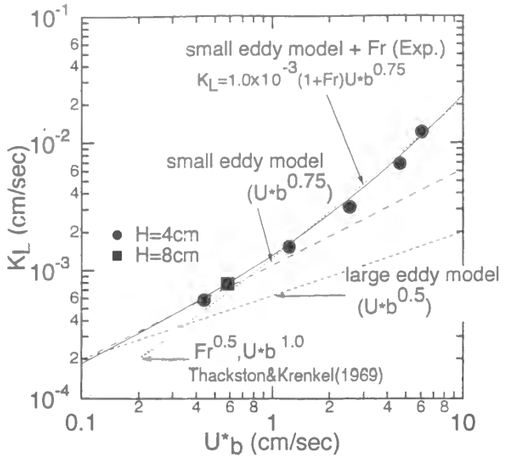

Fig.8.11 Gas transfer coefficient K_L in open-channel flow.

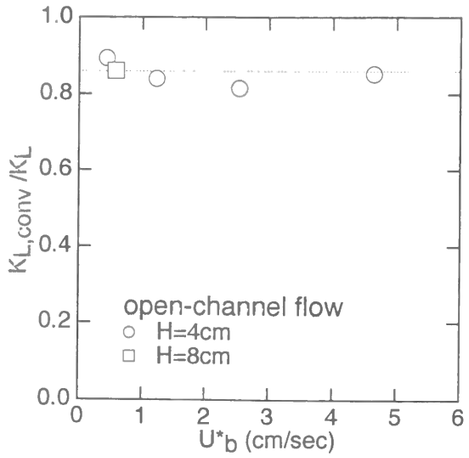

Fig.8.12 Rate of convection term $K_{L,conv}/K_L$ in open-channel flow.

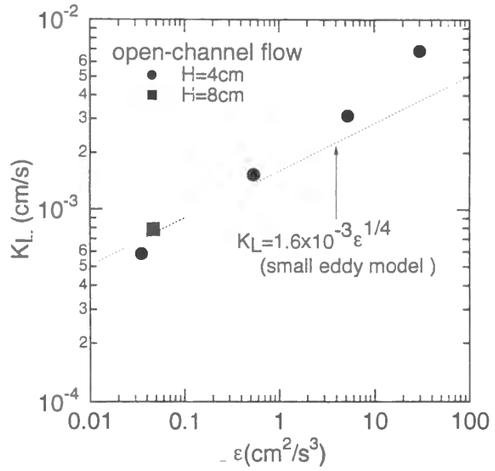

Fig.8.13 Evaluation of small-eddy model in open-channel flow.

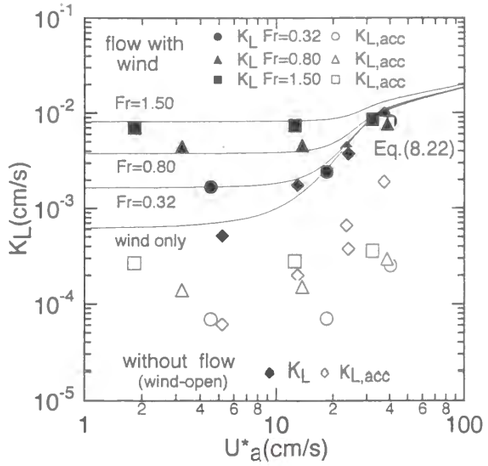

Fig.8.14 Gas transfer coefficient K_L in two-layer flows.

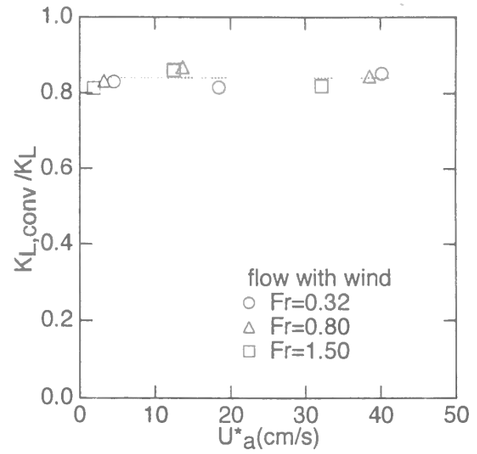

Fig.8.15 Rate of convection term $K_{L,conv}/K_L$ in two-layer flows.

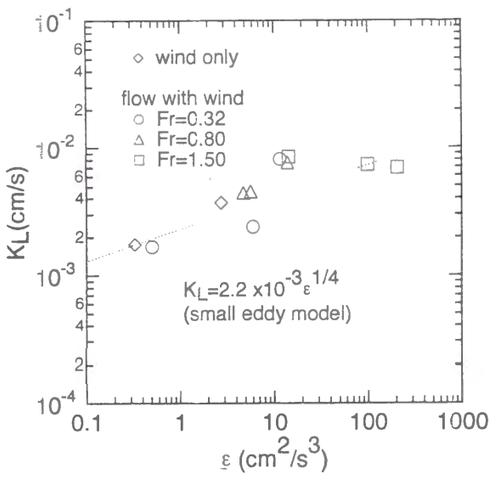

Fig.8.16 Evaluation of small-eddy model in two-layer flows.

data in wind-water wave (valve-open). Chu (1993) has estimated the distribution of K_L in combined flow by using the square-root matching technique.

$$K_L = \sqrt{K_{L,wind}^2 + K_{L,water}^2} \tag{8.22}$$

in which, $K_{L,wind}$ and $K_{L,water}$ are the values in wind-water wave and in open-channel flow, respectively. In this figure, Eq.(8.22) using the semi-theoretical curves in Fig.8.9 and Fig.8.11 is also described by solid curves. This prediction shows a good agreement with the measured values. It can be seen that K_L increases more largely as the Froude number increases in a slower wind speed. The same characteristics are pointed out by Chu (1993). These facts mean that K_L is greatly affected by the relative velocity of both layers, *i.e.* air/water interface layer.

Fig.8.15 shows the value of $K_{L,conv}/K_L$. The value is almost same as that in wind wave and open-channel flow. In this way, the convection term has an important influence on K_L regardless of the flow depth and the shear conditions. Fig.8.16 is the distribution of K_L versus the turbulent dissipation rate ε near the free surface, together with the data in wind-water wave (valve-open). This figure shows that the small-eddy model is valid irrespective of the flow conditions.

8.5 Criterion of Bottom-Shear and Wind-Induced Turbulence

8.5.1 Relationship between η' and K_L

As mentioned before, the gas transfer across the interface is closely related to the turbulence structure of the turbulence-generated point. However, in combined wind/stream flow, both the bottom shear and the wind shear are important for the gas transfer, and it is necessary to find the parameter which

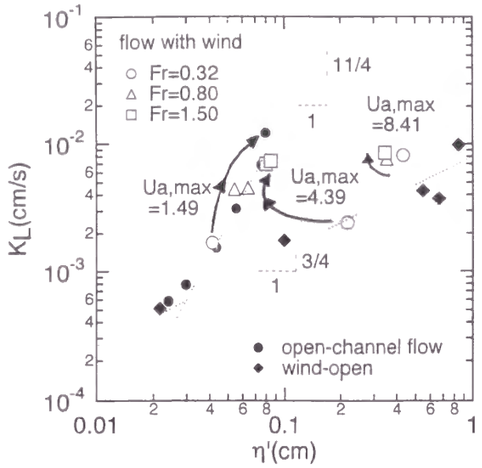

Fig.8.17 Distribution of K_L against intensity of surface-wave fluctuations η'.

can express both characteristics. There occur surface-wave fluctuations when the gas is transferred across the interface, which have a close relationship with the gas transfer.

Fig.8.17 shows the distribution of K_L against the intensity of surface-wave fluctuations η'. It can be seen that K_L is in proportion to the power of η' in both the wind-water wave and the open-channel flow (As a result, wind wave : $K_L \sim \eta'^{3/4}$, open-channel : $K_L \sim \eta'^{11/4}$). The gas transfer rate is greater in open-channel flow than that in wind-water wave when the values of η' are same in both cases. This means that the smaller eddies have a great effect on the gas transfer because the high-frequency component is more predominant in the surface wave of open-channel flow than that of wind wave. These powers of η' correspond to the Eq.(8.15). In combined flow, the value of K_L in Fig.8.17 is located between the two curves and approaches the value that is affected more greatly.

8.5.2 Criterion based on K_L and Dissipation Rates ε

In air-water combined flow, the relative velocity of both layers has a great effect on the gas transfer. In particular, it is confirmed that the small-eddy model is predominant irrespective of the flow conditions. Jirka and Brutsaert (1984) suggested a simple relationship for the relative importance of bottom-shear turbulence and of wind-shear turbulence on the gas transfer, on the basis of estimation of the near-surface turbulent energy dissipation rates ε_s.

$$\begin{aligned} &\varepsilon_s/\varepsilon_b \ll 1 : \textit{Bottom–Shear Controlled Transfer} \\ &\varepsilon_s/\varepsilon_b \gg 1 : \textit{Wind–Shear Controlled Transfer} \end{aligned} \tag{8.23}$$

where ε_b is defined as follows:

$$\varepsilon_b = 0.4\frac{U_{*b}^3}{H} \tag{8.24}$$

Chu (1993) has proposed the criteria for wind and stream dominance in combined flow with an expansion of Jirka and Brutsaert's idea, as follows:

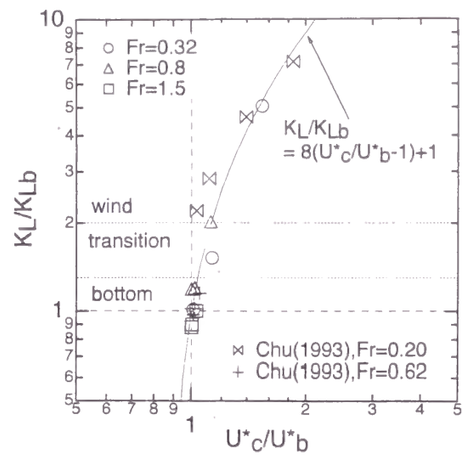

Fig.8.18 Distribution of K_L/K_{Lb} versus U_{*c}/U_{*b}.

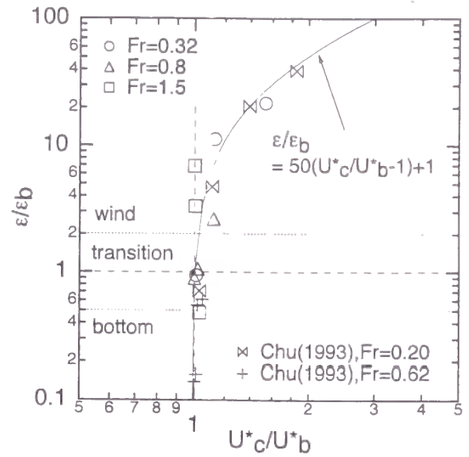

Fig.8.19 Distribution of $\varepsilon/\varepsilon_b$ versus U_{*c}/U_{*b}.

$$\begin{aligned} &\varepsilon_s/\varepsilon_b < 0.5\,(K_L/K_{Lb} < 1.3) : \textit{Bottom–Shear Transfer} \\ &0.5 < \varepsilon_s/\varepsilon_b < 2\,(1.3 < K_L/K_{Lb} < 2) : \textit{Transition} \\ &\varepsilon_s/\varepsilon_b > 2\,(K_L/K_{Lb} > 2) : \textit{Wind–Shear Transfer} \end{aligned} \tag{8.25}$$

where K_{Lb} is the gas transfer coefficient caused by the bottom-shear turbulence. Fig.8.18 shows the distribution of K_L/K_{Lb} versus U_{*c}/U_{*b}. The value of K_{Lb} is calculated from the approximation curve in Fig.8.11 by substituting U_{*b}. In this figure, the experimental data by Chu (1993), Eq.(8.25) and the approximation curve are also described together. The point, *i.e.* $U_{*c}/U_{*b}=K_L/K_{Lb}=1$, means the open-channel flow. Furthermore, Mattingly (1977) has proposed the following equation of K_L in the two-layer flows.

$$\frac{K_L}{K_{Lb}} = 1 + 0.2588(U_a - U_{w.mean})^{1.618}$$

$$K_{Lb} = 0.101\frac{U_{w.mean}^{0.607}}{H^{1.689}} \tag{8.26}$$

However, this equation is inappropriate in view of the dimension. From Fig.8.18, it can be seen that K_L/K_{Lb} is proportional to U_{*c}/U_{*b}. Its value switches also from the stream dominance to the wind dominance condition with an increase of the wind velocity, but the switchover becomes not so conspicuous with the increase of Froude number.

Fig.8.19 shows the distribution of $\varepsilon/\varepsilon_b$ versus U_{*c}/U_{*b}. The value increases monotonically as U_{*c}/U_{*b} increases in the same matter as K_L/K_{Lb}. However, the rate of increase in $\varepsilon/\varepsilon_b$ is much greater than that in K_L/K_{Lb}. This means that the dissipation rate and the gas transfer are closely related with each other even in combined flow.

Fig.8.20 is the distribution of $\varepsilon/\varepsilon_b$ versus K_L/K_{Lb}. In this figure, Eq.(8.25) and the approximation curve calculated from Figs.8.18 and 8.19 are also plotted together. It can be seen that there exists some relation between K_L/K_{Lb} and $\varepsilon/\varepsilon_b$. However, both criteria does not necessarily coincide with each other. In other words, $\varepsilon/\varepsilon_b$ is almost proportional to K_L/K_{Lb} in low Froude-number condition. However,

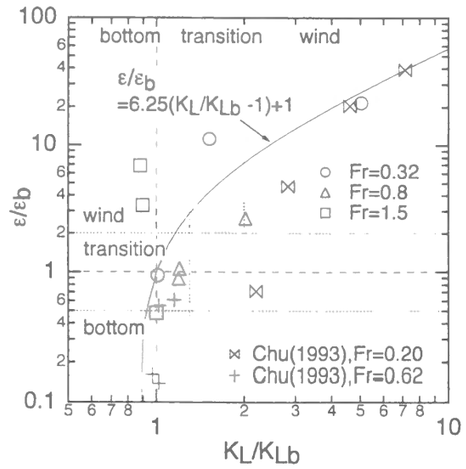

Fig.8.20 Distribution of $\varepsilon/\varepsilon_b$ versus K_L/K_{Lb}.

there are not same characteristics in high Froude-number condition. This means that the dissipation rate is not the only parameter to evaluate the gas transfer characteristics in combined flow.

8.6 Conclusions

In this study, a relation between turbulence structure and gas transfer coefficient near the free surface was evaluated. Fig.8.21 shows the conclusions of chapter 8. The gas transfer coefficient in wind-water wave (valve-open) can be evaluated by the expansion of wind-water wave (valve-closed) considering the convection effect. The gas transfer in open-channel flow can be expressed by the small-eddy model including the effect of Froude number. Furthermore, in combined wind/stream flow, the gas transfer could be explained by the square-root matching technique. Finally, the relation of criteria both in the gas transfer coefficient and the energy dissipation rate was clarified.

Notations

A : constant coefficient, water surface area
C : instantaneous concentration of dissolved gas
C_A : increased area
C_s : saturation (equilibrium) concentration of dissolved gas
D : dissolved oxygen deficit ($=C_s - C$)
D_m : molecular diffusivity of the gas in the liquid
d : half height of air channel
E_s : turbulent energy per unit mass of liquid in the vicinity of the surface
F : gas transfer flux
Fr : Froude number ($=U_m/\sqrt{gH}$)
H : flow depth
K_2 : reaeration coefficient
K_{acc} : acceleration term of K_2

- K_L
  - (1)Wind-Wave (Valve Closed)
    ⇒ $K_L = \text{func.}(U_{*a}) = 1/(1/K_{LS} + 1/K_{LR}) = \text{func.}(\eta'^{3/4})$
  - (2)Wind-Wave (Valve Open)
    ⇒ $K_L = \text{func.}(U_{*b}, U_{*a})$
  - (3)Open-Channel Flow
    ⇒ $K_L = \text{func.}(Fr, U_{*b}^{3/4}) = \text{func.}(\eta'^{11/4})$
  - (4)Combined Flow
    ⇒ $K_L = \sqrt{(K_{L,wind\text{-}wave})^2 + (K_{L,open\text{-}channel})^2}$
- z_e ⇒ Wind Velocity = Concentration
- Convection Effect
  ⇒ $K_{L,conv}/K_L = 0.8 \sim 0.9$ (Constant Value)
- $K_L \sim \varepsilon$ ⇒ "Small-Eddy Model" is effective

Fig.8.21 Conclusions of chapter 8.

K_{conv} : convection term of K_2
K_L : gas transfer coefficient
K_{Lb} : gas transfer coefficient caused by the bottom-shear turbulence
$K_{L,conv}$: convection term of K_L
$K_{L,open}$: K_L in wind wave (valve-open)
$K_{L,tank}$: K_L in wind wave (valve-closed)
$K_{L,water}$: K_L in open-channel flow
$K_{L,wind}$: K_L in wind wave (valve-open)
K_{L0} : K_L at 20℃
L : length scale
R_* : turbulent Reynolds number
r : mean frequency of surface renewal
Sc : Schmidt number ($=\nu/D_m$)
S_p : pressure-adjusted channel slope
U_a : wind velocity
$U_{a,max}$: maximum wind velocity
U_m : bulk mean velocity
$U_{w,mean}$: bulk mean velocity in water
U_* : friction velocity
U_{*a} : friction velocity in air layer
U_{*b} : friction velocity in water layer
U_{*c} : critical velocity of U_*, friction velocity ($=\sqrt{(\tau_b+\tau_w)/\rho_w} = \sqrt{gHS_p}$)

$U_{*c,open}$: U_{*c} in wind wave (valve-open)
$U_{*c,tank}$: U_{*c} in wind wave (valve-closed)
U_{*t} : transitional shear velocity
U_{*w} : friction velocity at the interface
u : instantaneous streamwise velocity component
v : instantaneous vertical velocity component
V : water volume
x : streamwise direction
y : vertical direction from the channel bed
y' : distance from the free surface (=H-y)
z : vertical direction from water surface
z_e : equilibrium roughness

Greek symbols
δ_l : thickness of film
ε : turbulent energy dissipation rate
ε_b : near-surface turbulent energy dissipation rates caused by bottom shear
ε_s : near-surface turbulent energy dissipation rates caused by wind shear
Γ_0 : normalized thickness of viscous sublayer
η' : intensity of surface-wave fluctuations ($\equiv\sqrt{\overline{\eta^2}}$)
κ : von Karman constant
ν : kinetic viscosity
ν_a : kinetic viscosity of air
ν_w : kinetic viscosity of water
ρ_a : density of air
ρ_w : density of water
θ : temperature collection coefficient (=1.0241)
σ : surface tension

References

[1] Broecker, H.Ch. and Siems, W. : The role of bubbles for gas transfer from water to air at higher windspeeds. Experiments in the wind-wave facility in Hamburg, *Gas Transfer at Air-Water Interfaces*, W. Brutsaert and G.H. Jirka (eds.), Reidel Pub., pp.229-236, 1984.
[2] Brumley, B. H. and Jirka, G. H. : Air-water transfer of slightly soluble gases : Turbulence, interfacial processes and conceptual models, *Physico Chemical Hydrodynamics*, Vol.10, No.3, pp.295-319, 1988.
[3] Chan, W.C. and Scriven, L.E. : Absorption into irrotational stagnation flow : A case study in convective diffusion theory, *Ind. Engng Chem. Fundam.*, Vol.9, No.1, pp.114-120, 1970.
[4] Chu, C.R. : Experiments on gas transfer and turbulence structure in free surface flows with combined wind/bottom shear, *Ph.D Thesis presented to Cornell University*, 1993.
[5] Chu, C.R. and Jirka G.H. : Turbulent gas flux measurements below the air-water interface of a grid-stirred tank, *Int. J. Heat Mass Transfer*, Vol.35, No.8, pp.1957-1968, 1992.
[6] Chu, C.R. and Jirka G.H. : Reaeration in combind wind/stream driven flows, *Air-Water Gas Transfer*, B. Jahne and E.C. Monahan (eds.), AEON Verlag, pp.79-88, 1995.
[7] Danckwerts, P.V. : Significance of liquid-film coefficients in gas absorption, *Indust. and Eng. Chem.*, Vol.43, No.16, pp.1460-1467, 1951.

[8] Dobbins, W.E. : BOD and oxygen relationships in streams, *J. Sanitary Eng.*, ASCE, Vol.90, SA3, pp.53-78, 1964.
[9] Dobbins, W.E. : BOD and oxygen relationships in streams ; Closure, *J. Sanitary Eng.*, ASCE, Vol.91, SA5, pp.49-55, 1965.
[10] Elmore, H.L. and West, W.F. : Effect of water temperature on stream reaeration, *J. Sanitary Eng.*, ASCE, Vol.87, SA6, pp.59-71, 1961.
[11] Eloubaidy, A.F. and Plate, E.J. : Wind shear-turbulence and reaeration coefficient, *J. Hydraulic Eng.*, ASCE, Vol.98, HY1, pp.153-170, 1972.
[12] Fortescue, G.E. and Pearson, J.R. : On gas absorption into a turbulent liquid, *Chem. Eng. Sci.*, Vol.22, pp.1163-1176, 1967.
[13] Harriott, P. : A random eddy modification of the penetration theory, *Chem. Engng Sci.*, Vol.17, pp.149-154, 1962.
[14] Higbie, R. : The rate of absorption of a pure gas into a still liquid during short periods of exposure, *AIChE Trans.*, Vol.31, pp.365-390, 1935.
[15] Hirayama, K., Matsuo, T., Imaoka, M. and Katayama-Hirayama, K. : Presentation of an equation for estimating reaeration coefficients based on a turbulence intensity model, *Journal of Hydraulic Engineering*, JSCE, No.521/II-32, pp.181-191, 1995 (in Japanese).
[16] Jirka, G.H. and Brutsaert, W. : Measurements of wind effects on water-side controlled gas exchange in riverine systems, *Gas Transfer at Air-Water Interfaces*, W. Brutsaert and G.H. Jirka (eds.), Reidel Pub., pp.437-446, 1984.
[17] Jirka, G.H. and Ho, A.H.-W. : Measurements of gas concentration fluctuations at water surface, *J. Hydraulic Eng.*, ASCE, Vol.116, No.6, HY3, pp.835-847, 1990.
[18] Krenkel, P.A. and Orlob, G.T. : Turbulent diffusion and the reaeration coefficient, *Transactions*, ASCE, Vol.128, No.3491, pp.293-323, 1963.
[19] Lamont, J.C. and Scott, D.S. : An eddy cell model of mass transfer in the surface of a turbulent liquid, *AIChE J.*, Vol.16, pp.513-519, 1970.
[20] Liss, P.S. and Merlivat, M. : Air-sea gas exchange rates, *The Role of Air-Sea Exchange in Geochemical Cycling*, Reidel Pub., pp.113-127, 1986.
[21] Lewis, W.K. and Whitman, W.G. : Principles of gas absorption, *Indus. and Eng. Chem.*, Vol.16, No.12, pp.1215-1220, 1924.
[22] Mattingly, G.E. : Experimental study of wind effects on reaeration, *J. Hydraulic Eng.*, ASCE, Vol.103, HY3, pp.311-323, 1977.
[23] Moog, D.B. : Stream reaeration and the effects of large-scale roughness and bedforms, *Ph.D Thesis presented to Cornell University*, 1995.
[24] Moog, D.B. and Jirka, G.H. : Macroroughness effects on stream reaeration, *Air-Water Gas Transfer*, B. Jahne and E.C. Monahan (eds.), AEON Verlag, pp.89-99, 1995.
[25] Nezu, I. and Nakayama, T. : Fundamental study at air-water interfaces with wind shear, *28th IAHR Congress*, IAHR, 1999c.
[26] Nakayama, T. and Nezu, I. : Relationship between turbulence structures and gas transfer across air-water interface, *Journal of Hydraulic Engineering*, JSCE, No.635/II-49, pp.85-95, 1999f (in Japanese).
[27] Nezu, I., Nakayama, T. and Inoue, R. : Influence of turbulence structure on gas transfer across air-water interface, *Journal of Applied Mechanics*, JSCE, Vol.2, pp.673-684, 1999h (in Japanese).
[28] Nezu, I., Nakayama, T. and Inoue, R. : Relation between turbulence structure and gas transfer coefficient near the free surface, *Proc. of Water, Environment, Ecology, Socio-Economics, and Health Engineering*, pp.203-216, 1999i.
[29] Nakayama, T. and Nezu, I. : Turbulence structures of wind water waves, *Journal of Hydraulic*

Engineering, JSCE, No.642/II-50, 2000a (in Japanese).
[30] O'Connor, D.J. : Wind effects on gas-liquid transfer coefficients, *J. Environmental Eng.*, ASCE, Vol.109, No.3, pp.731-752, 1983.
[31] O'Connor, D.J. and Dobbins, W.E. : The mechanism of reaeration in natural streams, *J. Sanitary Eng.*, ASCE, Vol.82, SA6, pp.1115-1144, 1956.
[32] Plate, E.J. and Friedrich, R. : Reaeration of open channel flow, *Gas Transfer at Air-Water Interfaces*, W. Brutsaert and G.H. Jirka (eds.), pp.333-346, 1984.
[33] Thackston, E.L. and Krenkel, P.A. : Reaeration prediction in natural streams, *J.Sanitary Eng.*, ASCE, Vol.95, SA1, pp.65-93, 1969.
[34] Theofanous, T.G., Houze, R.N. and Brumfield, L.K. : Turburent mass trrasfer at free, gas-liquid interfaces, with applications to open-channel, bubble and jet flows, *Int. J. Heat Mass Transfer*, Vol.19, pp.613-624, 1976.

CHAPTER 9

RELATIONSHIP BETWEEN COHERENT STRUCTURE AND GAS TRANSFER ACROSS AIR-WATER INTERFACE

Abstract

Instantaneous structures in both air and water layers were measured by using PIV method in wind water waves. Furthermore, turbulence structures at various phase of wind waves were evaluated by applying phase-averaged method. Reynolds stress distributions are much different with each layer. Reynolds stress contributions take a greater value on windward side of wave crest. It became clear that these phenomena are closely related to the generation mechanisms of coherent vortices both in air and water layers, which approach the wave periods in the increase of wind velocity.

Furthermore, the relationship was evaluated between the increase of surface area and the gas transfer coefficient across the interface in two-layer flows by using cross-correlation coefficients evaluated from two sets of ultrasonic depth-measuring instruments in comparison with VTR. It was clarified that the surface area has little effect on gas transfer against former studies. Furthermore, it became clear that the smaller-scale eddies contribute greatly to the greater gas transfer in open-channel flow than those in wind-wave.

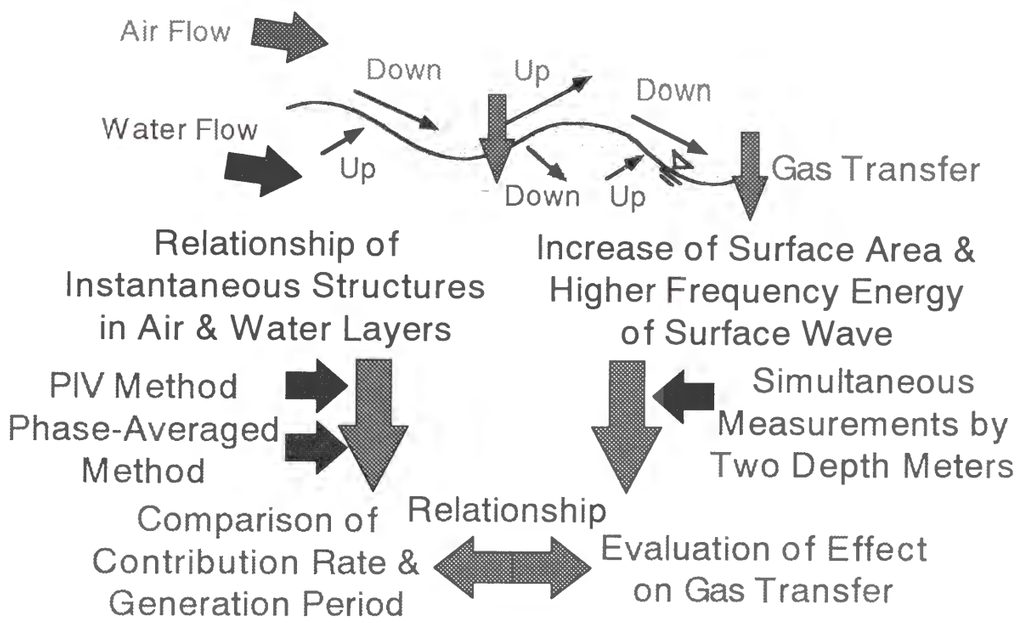

CHAPTER 9 RELATIONSHIP BETWEEN COHERENT STRUCTURE AND GAS TRANSFER ACROSS AIR-WATER INTERFACE

Parts of this chapter were presented and submitted in the following papers.

[1] Nakayama, T. and Nezu, I. : Bursts near the free surface in open-channel flows and their relationship with turbulence structures, *Journal of Hydraulic Engineering*, JSCE, No.635/II-49, pp.31-40, 1999e (in Japanese).
[2] Nakayama, T. and Nezu, I. : Relationship between turbulence structures and gas transfer across air-water interface, *Journal of Hydraulic Engineering*, JSCE, No.635/II-49, pp.85-95, 1999f (in Japanese).
[3] Nakayama, T. and Nezu, I. : Turbulence structures of wind/stream combined flow, *Journal of Hydraulic Engineering*, JSCE, 1999m (in Japanese, to be accepted).
[4] Nakayama, T. and Nezu, I. : Turbulence structures of wind water waves, *Journal of Hydraulic Engineering*, JSCE, No.642/II-50, 2000a (in Japanese).
[5] Nakayama, T. and Nezu, I. : Effect of increase of surface area and other factor on gas transfer in two-layer flows, *Annual Journal of Hydraulic Engineering*, Vol.44, pp.891-896, 2000b (in Japanese).
[6] Nezu, I. and Nakayama, T. : Instantaneous structures of air and water layers in wind water waves, *Annual Journal of Hydraulic Engineering*, Vol.44, pp.897-902, 2000c (in Japanese).

9.1 Introduction

In the former chapter, the relationship between the turbulence structures in air/water layers and the gas transfer mechanism across the interface in two layer flows was examined. On the other hand, it is necessary to make clear the dynamics of instantaneous and coherent structures in both layers in order to evaluate the mutual interaction across the air-water interface. Chang *et al.* (1971) have calculated the phase-averaged wind velocity and turbulence intensity of air layer over each phase of wind water waves. They evaluated the energy spectra of each phase related to the coherent structures. Takeuchi *et al.* (1977) have furthermore examined the instantaneous Reynolds stress in the same flow and pointed out that the higher shear occurs downwind of the wave crests. Kato and Sano (1971) conducted the similar experiment and estimated the relation between turbulence structure and surface-wave fluctuations and the cross-spectra in wind waves. Furthermore, Kawai (1981, 1982) has evaluated qualitatively the instantaneous air-separation behind the wave crest by using the visualization technique of small particles. At that time, he considered the condition when the separation occurs. On the base of these former researches, Kawamura and Toba (1988) have conducted very interesting experiments about the coherent structure of air flow over wind waves. They compared the bursting phenomena over wind waves with those over fixed beds, and supposed two models, that is to say, the "*big burst*" model and the "*small burst*" model, which contribute greatly to the mutual interaction near the interface.

On the other hand, as for the internal structure of water layer in wind waves, Okuda (1982a, 1982b, 1982c) has conducted the experiments about the internal vorticity structure, the streamline pattern and the pressure distribution, respectively. They pointed out that there exist the higher vorticity regions on the leeward of crests and that it is impossible to predict the streamline profiles from a water-wave theory. About the velocity distribution, Esfahany and Kawaji (1996) have shown that the water velocity under the crest is faster than that under the trough, which is the same as the direct numerical simulation (DNS) by Komori *et al.* (1993). Rashidi *et al.* (1991) evaluated the relationship between the coherent structure and the gas transfer characteristics by using the visualization of hydrogen bubble. Furthermore, Komori *et al.* (1993) have suggested the conceptual model about the relationship of coherent vortices in both layers. They pointed out that the coherent vortices go upward where the separated flow reattaches in the air layer, and that the surface-renewal eddies go downward near the same places in the water layer, which are closely related to the gas transfer across the interface.

By the way, Akai *et al.* (1977) examined the difference of auto-correlation functions of surface-wave fluctuations when the surface shapes change in two-layer flows about the suggestion by Hanratty and Engen (1957). On the other hand, when the gas transfer coefficient K_L was evaluated, the surface-renewal model proposed by Danckwerts (1951), *etc.* have been often used on the assumption that the surface area scarcely changes, except for some suggestions that the surface-renewal rate can be directly given by using the generation period of surface-renewal eddies, for example, Rashidi *et al.* (1991) and Komori *et al.* (1993). By the way, Nakayama and Nezu (1999f) have experimentally verified that the gas transfer coefficient K_L in open-channel flows is much larger than that in wind waves even though the surface-wave fluctuations in both flows are same with each other due to the difference of enhanced surface area. Furthermore, Dobbins (1964) and Thackston and Krenkel (1969) have applied the renewal model and proposed a formula including the effect of Froude number to account for enhanced surface area due to surface distortions in open-channel flow. In the same manner, Rashidi *et al.* (1991) have extended the renewal model to evaluate K_L including the effect of the "*patch*" (the area that looks like rising at the free surface) area and frequency by visualization technique on the assumption that there occur no waves.

In this way, though there have been some researches about the turbulence and coherent structures in wind water waves, it is not clear quantitatively where both coherent vortices occur and how is their

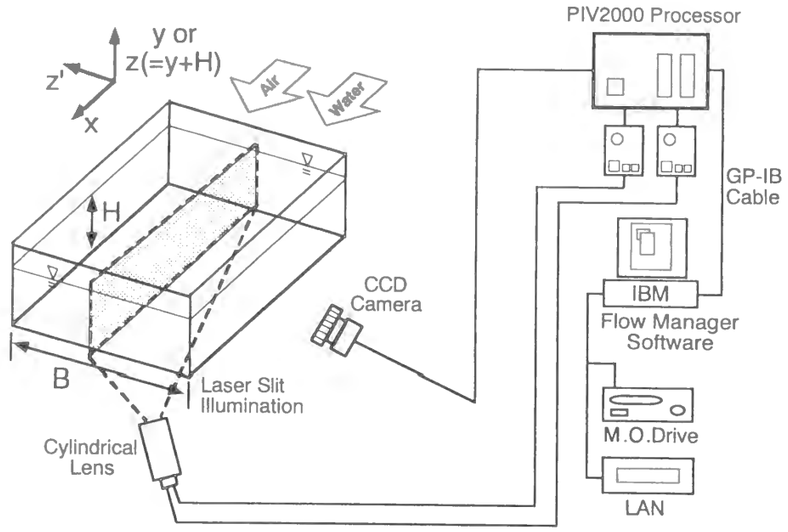

Fig.9.1 Schematic arrangements for PIV system.

relation with each other. Furthermore, these studies were conducted on a specific wind speed or water velocity, and it is not clear about the relationship between the increasing surface area and the gas transfer coefficient in two-layer flows. So, in this study, firstly, PIV method and phase-averaged method were used for evaluating the instantaneous structures in both layers and the relationship with each other. Secondly, the effect of increase of surface area and other factor on gas transfer was evaluated by conducting the simultaneous measurements of two depth meters.

9.2 Experimental Apparatus and Procedures

The experiments were conducted in a tilting wind-water tunnel of 16m long, 40cm wide and 50cm deep in the same way as in the former chapters. Coordinate axis in the streamwise direction is defined as x. As for the vertical direction, the upward direction from the bottom is defined as y. The upward and downward directions from the interface are defined as z and y' (=H-y, H is the flow depth), respectively. Instantaneous velocities for the streamwise and vertical components are $u(t)$ and $v(t)$, respectively.

The instantaneous measurements by using PIV system (DANTEC-made) were conducted in the following. The YAG Lasers of double pulses were illuminated in the center of channel vertically from the bottom-wall or above the top-wall and the images of tracers were taken by using a CCD camera (pixel resolutions : 1008 × 1018) that was set besides the side-wall at the time-interval of 0.6sec. Furthermore, wind velocity was accurately visualized by using the fog generator. In this measuring system, the vector maps can be monitored almost in a real time. The schematic arrangements for this PIV system are shown in Fig.9.1.

The simultaneous measurements by two sets of depth meters were conducted in the following. The LDA system (DANTEC-made) was fixed at the center of channel (y'/H=0.1) 9m downstream of the channel entrance for measuring the instantaneous velocity. At the same time, one ultrasonic depth-measuring instrument (KEYENCE-made) was set above the free surface as a fixed probe, and the other was moved horizontally as a movable probe, both of which were synchronized with the LDA, as

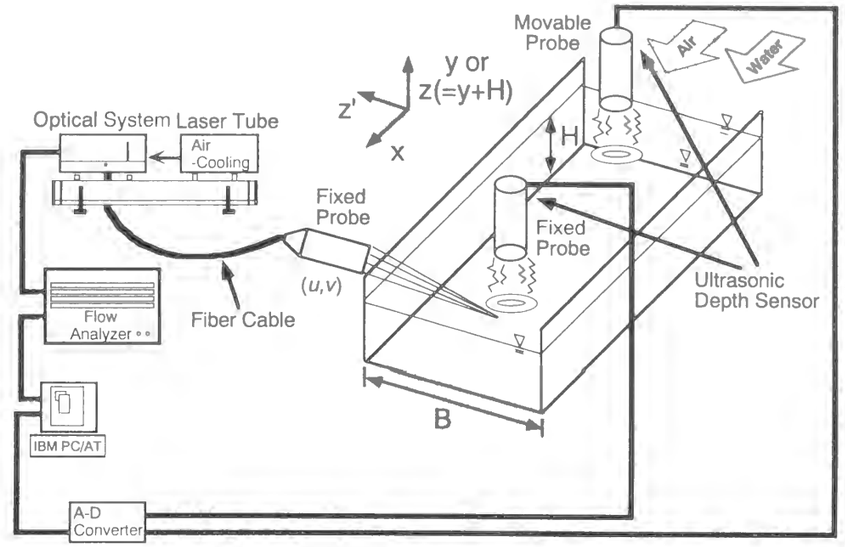

Fig.9.2 Simultaneous measurements by using two sets of depth meters.

Table 9.1 Hydraulic conditions for air-water interactions.

Wind-Water Wave (Valve-Closed)

case	H (cm)	$U_{a,max}$ (m/s)	$U_{w,mean}$ (cm/s)	U^*a (cm/s)
d2wa	8.0	0.94	0.00	3.84
d2wb	8.0	1.79	0.00	7.56
d2wd	8.0	3.63	0.00	17.51
d2wf	8.0	5.46	0.00	28.67
d2wh	8.0	8.30	0.00	50.29
w1f0	4.0	1.49	0.63	5.34
w2f0	4.0	4.39	5.63	21.37
w3f0	4.0	8.41	9.39	37.99

Open-Channel Flow

case	H (cm)	$U_{w,mean}$ (cm/s)	Fr	U^*b (cm/s)
d1f1	4.0	6.8	0.10	0.44
d1f2	4.0	20.2	0.32	1.22
d1f3	4.0	50.2	0.80	2.53
d1f4	4.0	92.9	1.50	4.64
d1f5	4.0	123.5	2.00	6.06
d2f1	8.0	11.2	0.32	0.56

Wind/Stream Combined Flow

case	H (cm)	$U_{a,max}$ (m/s)	$U_{w,mean}$ (cm/s)	Fr	U^*a (cm/s)	U^*b (cm/s)
w1f1	4.0	1.49	20.30	0.32	4.52	1.25
w2f1	4.0	4.39	20.26	0.32	18.45	1.20
w3f1	4.0	8.41	20.59	0.33	40.20	1.22
w1f2	4.0	1.49	50.47	0.81	3.20	2.57
w2f2	4.0	4.39	51.83	0.83	13.66	2.61
w3f2	4.0	8.41	59.24	0.95	38.57	2.61
w1f3	4.0	1.49	98.27	1.57	1.82	4.67
w2f3	4.0	4.39	98.64	1.58	12.49	4.77
w3f3	4.0	8.41	101.84	1.63	32.19	4.93

shown in Fig.9.2. The sampling time was 60sec, and sampling frequency was about 150Hz. As for the measurement of dissolved oxygen (DO) concentrations, please see the chapter 8.

Hydraulic conditions for the experiments are shown in Table 9.1, in the same as in the former chapters. Experiments are divided into three conditions; (A) bottom-shear generated flow (open-channel

flow), (B) wind-shear generated flow and (C) combined wind/stream flow. The parameters are defined as follows, H : the flow depth, $U_{a,max}$: the maximum wind velocity, U_{*a} : the friction velocity in the air layer calculated from the log-law, U_{*b} : the friction velocity in the water layer, Fr ($=U_m/\sqrt{gH}$) : Froude number, and η' ($\equiv\sqrt{\overline{\eta^2}}$) : the intensity of surface-wave fluctuations, respectively. As for (B) wind-induced flow, winds of several speeds were blown over a still water. As for (C) combined wind/ stream flow, the stream condition was changed to three patterns, so called, Fr=0.32 (sub-critical flow), 0.80 (near-critical flow) and 1.50 (super-critical flow). The wind condition was changed to three patterns, that is to say, $U_{a,max}$(m/s)=1.49 (smooth region), 4.39 (incompletely rough region) and 8.41 (rough region).

9.3 Theoretical Considerations

9.3.1 Phase-Averaged Method

The instantaneous velocity fluctuation is written in component form as follow;

$$u_i(x,t)=U_i(x)+\tilde{u}_i(x,t)+u_i'(x,t) \tag{9.1}$$

where U_i is the time-averaged mean velocity, $\tilde{u}_i$ is the wave-induced perturbation and u_i' is the turbulent fluctuation, respectively. The phase average is defined in the following by conducting the simultaneous measurements of the velocity fluctuations and the surface-wave fluctuations.

$$\langle u_i(x,t)\rangle=\lim_{N\to\infty}\frac{1}{N}\sum_{n=0}^{N-1}u_i(x,t+nT)=U_i(x)+\tilde{u}_i(x,t) \tag{9.2}$$

where T is the wave period measured by the depth meter. Therefore, Eq.(9.1) can be converted into the following Eq.(9.3).

$$u_i'(x,t)=u_i(x,t)-\langle u_i(x,t)\rangle \tag{9.3}$$

9.3.2 Distribution of Cross-Correlation Coefficient

On the assumption that the wind wave has a small amplitude and that proceeds to the positive streamwise-direction, the surface-wave fluctuations at the different positions in the streamwise direction can be expressed as follows;

$$\eta_1(0,t)=A\cos(-\omega t) \tag{9.4}$$

$$\eta_2(x,t)=A\cos(kx-\omega t) \tag{9.5}$$

where $k=2\pi/\lambda$, $\omega=2\pi f$, A : amplitude, λ : wave length, k : wave number, f : frequency, and ω : angular frequency, respectively. The intensities of surface-wave fluctuations at two points can be given in the following.

$$\eta_1'^2=\frac{1}{T}\int_0^T\eta_1(0,t)^2dt=\frac{A^2}{2}\quad(T\to\infty) \tag{9.6}$$

$$\eta_2'^2=\frac{1}{T}\int_0^T\eta_2(x,t)^2dt=\frac{A^2}{2}\quad(T\to\infty) \tag{9.7}$$

Therefore, the cross-correlation coefficient between the different points can be given as follow;

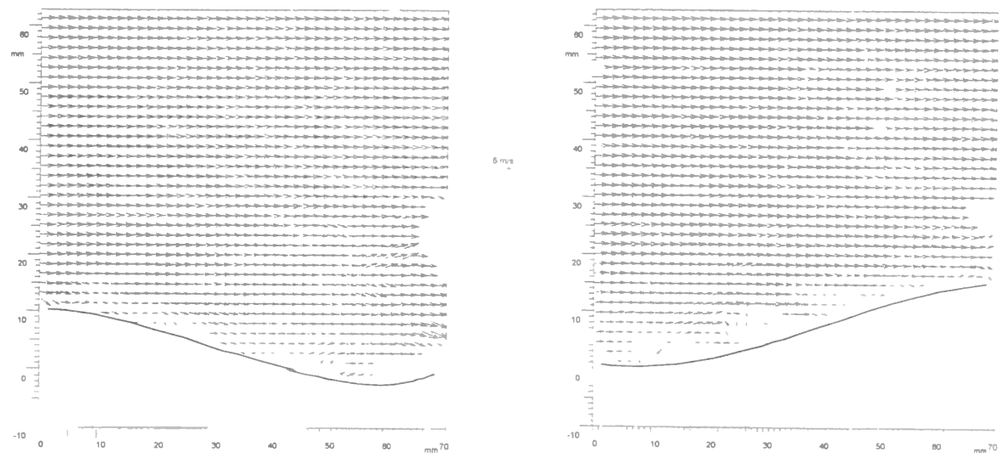

(a) leeward of crest (b) windward of crest

Fig.9.3 Instantaneous wind-velocity vectors of air layer.

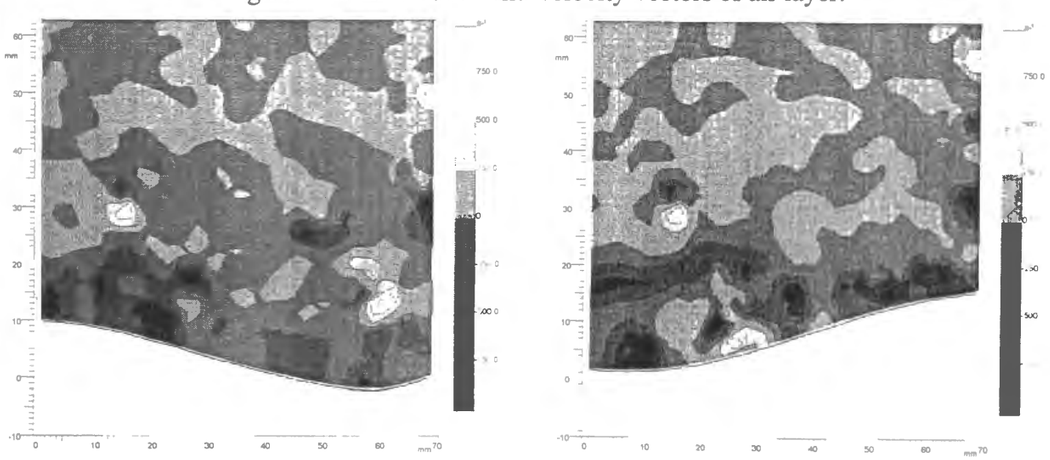

(a) leeward of crest (b) windward of crest

Fig.9.4 Instantaneous spanwise vorticity contours of air layer.

$$C_{\eta_1\eta_2}(x)=\frac{\int_0^T\eta_1(0,t)\cdot\eta_2(x,t)dt}{T\cdot\eta_1'\cdot\eta_2'}=\cos(kx)\quad(T\to\infty) \tag{9.8}$$

The above equation means that the cross-correlation coefficient is sine wave in the amplitude of unit if the surface wave can be assumed to sine wave.

9.4 Relationship of Instantaneous Structures in Both Layers

9.4.1 Instantaneous Structures in Air and Water Layers

9.4.1a Instantaneous Structure in Air layer

Figs.9.3(a) and (b) show the instantaneous wind-velocity vectors of air layer on the leeward and

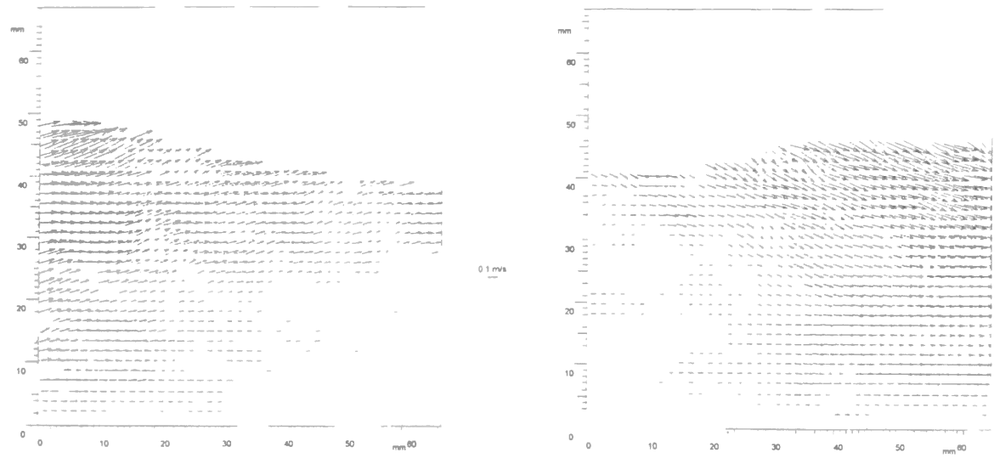

(a) leeward of crest (b) windward of crest

Fig.9.5 Instantaneous velocity vectors of water layer.

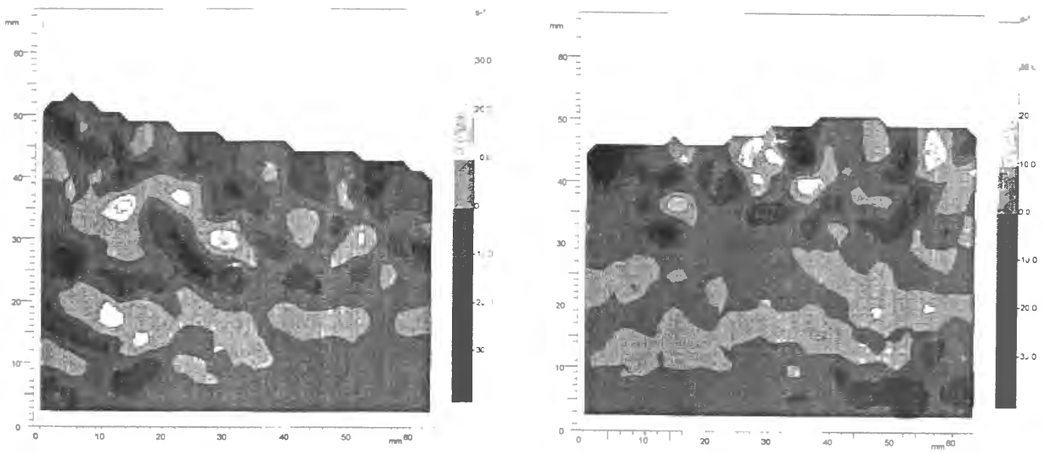

(a) leeward of crest (b) windward of crest

Fig.9.6 Instantaneous spanwise vorticity contours of water layer.

windward of the crest in the center of channel about the case $U_{a,max}$=8.41m/s (rough region at the experimental case of Nakayama and Nezu (2000a)) by using PIV method. In these figures, the wind blows from left to right. On the leeward of the crest in Fig.9.3(a), there exist the separated downward flows from the top of crest in the same way as Kawai (1981, 1982). Figs.9.4(a) and (b) show the instantaneous spanwise vorticity contours Ω_a ($=\partial v/\partial x-\partial u/\partial z$, counterclockwise direction is positive) corresponding to Figs.9.3(a) and (b). At the low wind speed case (free surface is tranquil), there occurred quasi-periodically higher vorticity-regions in the same way as the smooth open-channel flow in chapter 3. On the other hand, the higher vorticity-regions of negative values spread over the leeward and windward sides of the crest in the higher wind-velocity case, which implies that the vorticity distribution greatly depends on the locality of the wind waves.

9.4.1b Instantaneous Structure in Water layer

Figs.9.5(a) and (b) show the velocity vectors of water layer in the same case as Figs.9.3(a) and (b).

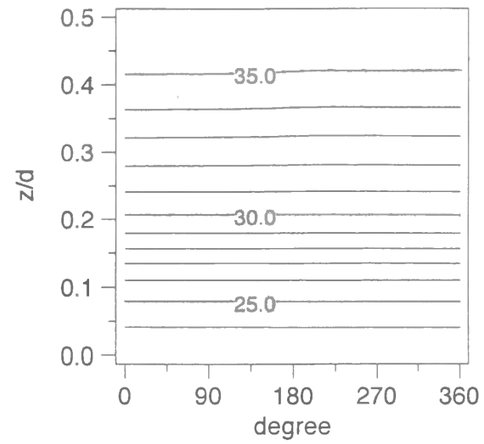

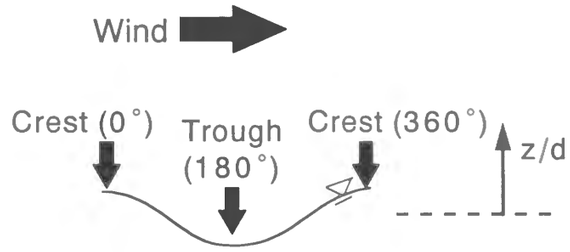

(a) Smooth Region ($U_{a,max}$=1.49m/s)

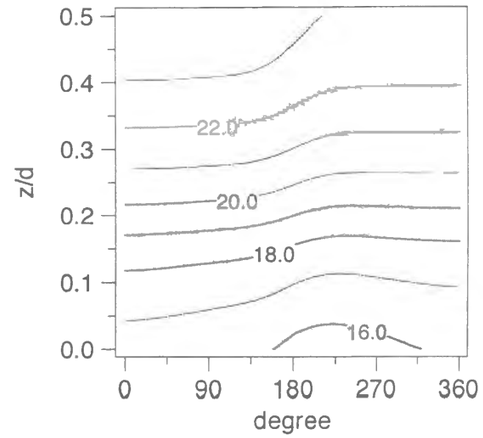

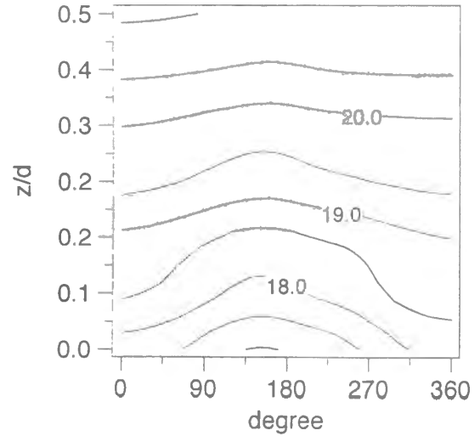

(b) Incompletely Rough Region ($U_{a,max}$=4.39m/s) (c) Rough Region ($U_{a,max}$=8.41m/s)

Fig.9.7 Contours of phase-averaged mean wind velocity $<U>/U_{*a}$ of air layer.

From Fig.9.5(a), it can be seen that the upward flows of higher velocity are generated on the leeward of the crest. On the other hand, the downward flows of higher velocity are generated on the windward of the crest. These velocity vectors are quite coincident with the experiments by Okuda (1982b) and the calculations by Komori *et al.* (1993). However, the experiments by Esfahany and Kawaji (1996) are quite different from these studies and the vertical velocities are opposite, which means that the accuracy of the experiments by Esfahany and Kawaji (1996) is doubtful. In this way, it is found that the flow of the wind waves cannot be predicted by the use of a water-wave theory. The instantaneous spanwise vorticity contours Ω_w ($=\partial v/\partial x-\partial u/\partial y$, counterclockwise direction is positive) are shown in Figs.9.6(a) and (b). Though Okuda (1982a) has pointed out that there exists the higher vorticity region on the leeward of the crest, the space of measuring points of his experiment is rough due to the point measurement and therefore, it is not clear whether his suggestion is correct or not. It can be seen that there are more higher vorticity regions on the leeward of the crest in Fig.9.6(a) than on the windward in Fig.9.6(b).

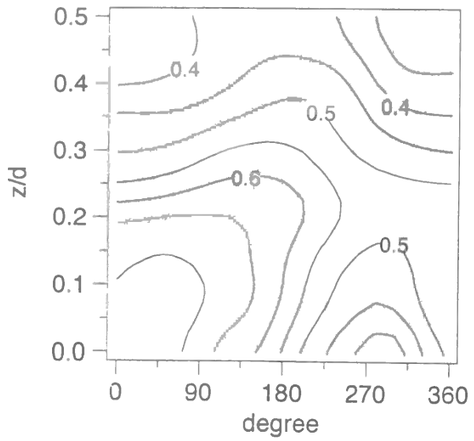

Fig.9.8 Contour of Reynolds stress $-\overline{u'v'}/U_{*a}^2$ of air layer.

9.4.2 Turbulence Structures at Each Phase by Phase-Averaged Method

9.4.2a Turbulence Structure in Air layer

Figs.9.7(a)-(c) show the contours of phase-averaged mean wind velocity $<U>/U_{*a}$ at the cases $U_{a,max}$=1.49m/s (smooth region), 4.39m/s (incompletely rough region), and 8.41m/s (rough region), respectively. In these figures, d is the half height of air layer and U_{*a} is the friction velocity of air layer evaluated from the log law of wind velocity. As for the numerical values in the horizontal axis, 0 and 360 degrees correspond to the crest of the wave and 180 degree corresponds to the trough of the wave. In these figures, the wind blows from left to right. It can be seen that the wind velocity becomes faster near the crest due to the effect of acceleration as the wind speed increases and the wind waves develop. This characteristic is very similar to the experiment by Chang *et al.* (1971) and the velocity distributions over fixed bed. The contour of Reynolds stress $-\overline{u'v'}/U_{*a}^2$ in the case $U_{a,max}$=8.41m/s is shown in Fig.9.8. Takeuchi *et al.* (1977) have pointed out that the shear becomes larger on the leeward of the crest. In this figure, the shear attains a greater value near the crest, and in particular, the shear develops greatly from the top of the crest to the upward of leeward side.

9.4.2b Turbulence Structure in Water layer

Fig.9.9 shows the contours of mean velocity $<U>/U_{*w}$ at the cases $U_{a,max}$=8.41m/s, where U_{*w} is the friction velocity of water layer evaluated from the log law of water velocity near the free surface, in the same way as Nakayama and Nezu (2000a). As is the same with the wind velocity, the water velocity takes a greater value near the crest, which was also in the turbulence intensities u' and v'. Fig.9.10 shows the contour of Reynolds stress $-\overline{u'v'}/U_{*w}^2$. The shear takes a positive value ($-\overline{u'v'}>0$) on the leeward of the trough (180° ～360°) and its value agrees roughly with that in air layer (due to $\rho_a U_{*a}^2=\rho_w U_{*w}^2$). However, on the windward of the trough (0° ～180°), the shear takes a negative value ($-\overline{u'v'}<0$), which is quite different from the value in air layer ($-\overline{u'v'}>0$). This disagreement of Reynolds stress may be closely related to the higher vorticity region on the leeward of the crest, as mentioned before.

9.4.3 Relationship of Coherent Structures in Both Layers

9.4.3a Fractional Contributions to Reynolds Stress

Kawamura and Toba (1988) have evaluated the fractional contributions to Reynolds stress at each

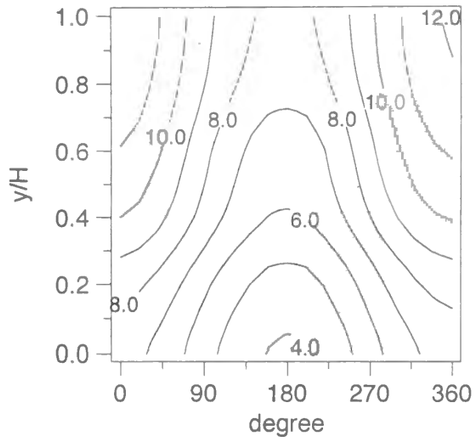

Fig.9.9 Contours of mean velocity $<U>/U_{*w}$ of water layer.

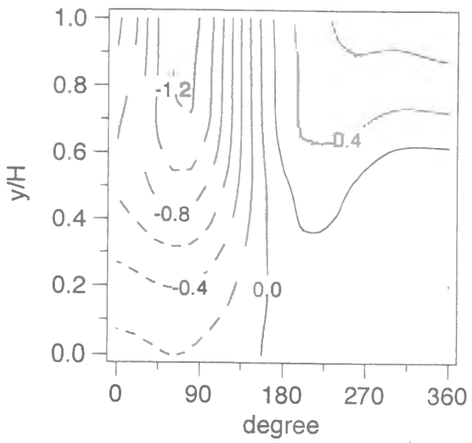

Fig.9.10 Contour of Reynolds stress $-\overline{u'v'}/U_{*w}^2$ of water layer.

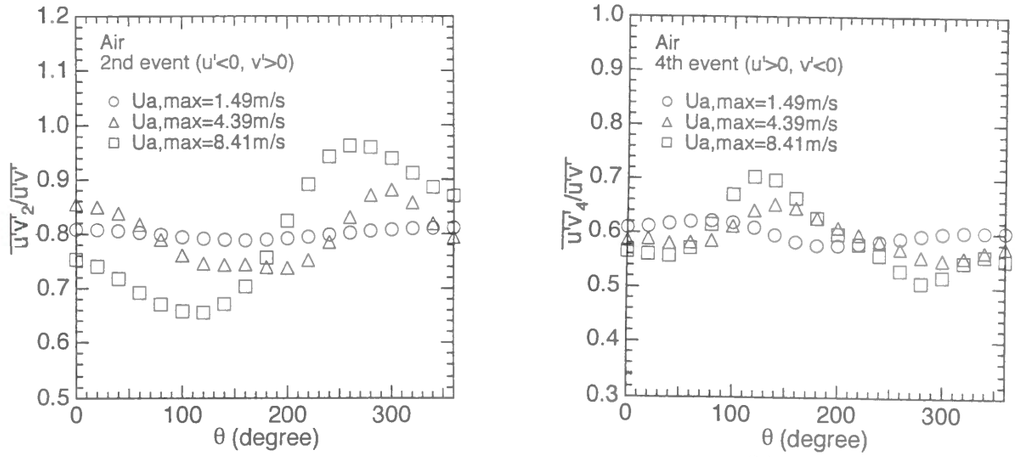

(a) ejection (b) sweep

Fig.9.11 Fractional contributions to Reynolds stress in air layer.

phase of wind waves about ejection ($u'<0$, $v'>0$) and sweep ($u'>0$, $v'<0$) in the log layer of air flow above the 2-D wind waves, and pointed out that the former becomes greater on the windward of the crest and the latter on the leeward. Fig.9.11 is the fractional contributions to Reynolds stress about ejection (RS_2) and sweep (RS_4) when the wind speed changes. At that time, the values were averaged within the inner layer ($z_+<0.2R_*$). It can be seen that ejection takes a greater value on the windward of the crest and sweep on the leeward, respectively, which is similar to the experiment by Kawamura and Toba (1988). Furthermore, the difference between each phase cannot be seen as the wind velocity becomes smaller.

Fig.9.12 shows the fractional contributions of each event in the water layer near the free surface ($y'/H<0.2$), that is to say, RS_1($u'>0$, $v'>0$), RS_2($u'<0$, $v'>0$), RS_3($u'<0$, $v'<0$), and RS_4($u'>0$, $v'<0$), respectively. Because the sign of Reynolds stress in water layer becomes reversed near the trough (Fig.9.10), the value of each event was normalized by U_{*w}^2 instead of $\overline{u'v'}$. In the water layer, the contributions of RS_1

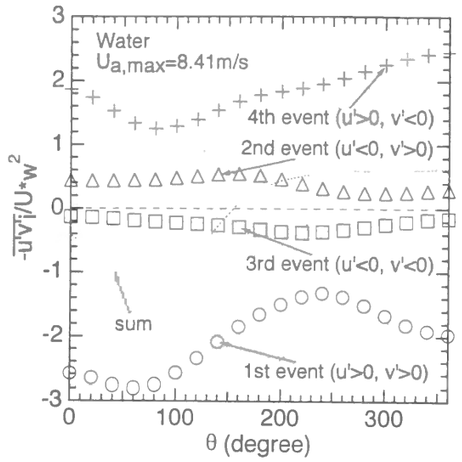

Fig.9.12 Fractional contributions of each event in water layer.

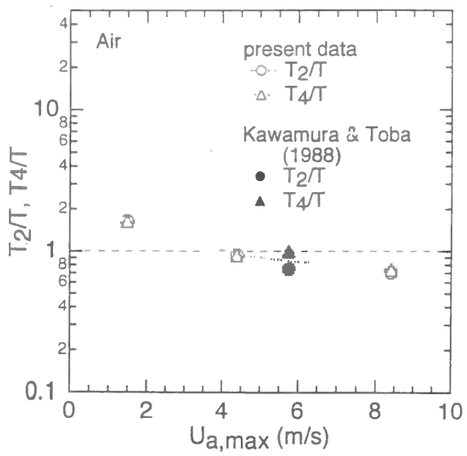

Fig.9.13 Distribution of the generation periods in air layer.

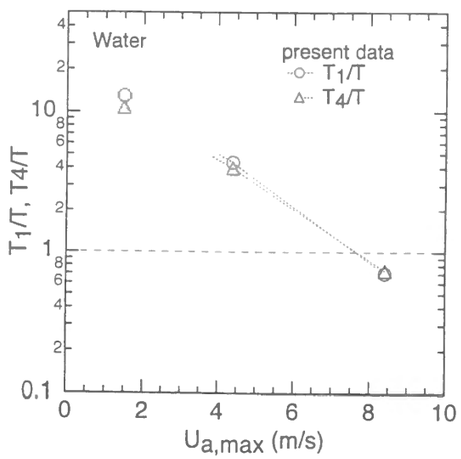

Fig.9.14 Distribution of the generation periods in water layer.

and RS_4 are much larger than those of RS_2 and RS_3, which is very different from those in air layer. In particular, RS_1 takes a greater value on the leeward of the crest and RS_4 on the windward. This means that the downward momentum transfer with high-speed becomes active on the leeward of the crest, which coincides well with the conceptual model suggested by Komori *et al.* (1993).

9.4.3b Comparison of Generation Periods of Coherent Vortices

Kawamura and Toba (1988) have compared the generation number of ejection and sweep with that of wind waves and pointed out that the former is generated more frequently than the latter, which resulted in the suggestion of the "*small burst*" model superior to the "*big burst*" model. Fig.9.13 shows the distribution of the generation periods in air layer normalized by the wave period T_2/T and T_4/T versus $U_{a,max}$. At that time, the "*half-value threshold levels*" were used in the same way as in chapter 3. In this figure, the value evaluated by Kawamura and Toba (1988) when the threshold level equals to $10\overline{u'v'}$ was plotted together. It can be seen that the values T_2/T and T_4/T decrease as the wind becomes

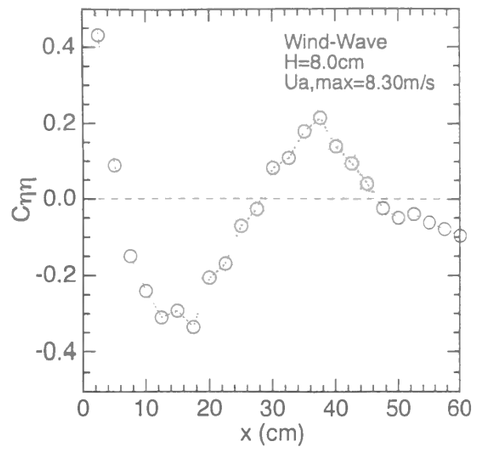

Fig.9.15 Distribution of cross-correlation coefficient $C_{\eta\eta}$ of surface-wave fluctuations.

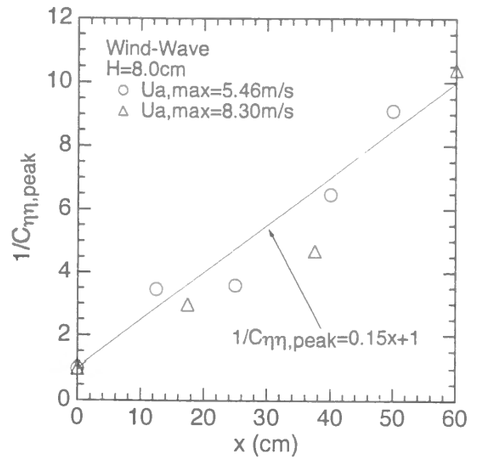

Fig.9.16 Reverse of local peak value of $C_{\eta\eta}$.

faster, which implies that the generation of coherent vortices is restricted by the wave period and that the rate of small burst predominates over that of big burst. On the other hand, Fig.9.14 shows the distribution of T_1/T and T_4/T in water layer. The values of water layer are much larger than those of air layer in the smaller wind speed, and the values of both layers approach the same value with each other as the wind is faster. This phenomenon means that the coherent vortices generated in the water are dependent on the wind waves and that a pair of vortices is generated both in air and water layers in the faster wind speed.

9.5 Effect of Surface Area and Other Factor on Gas Transfer

9.5.1 Comparison between VTR Image and Cross-Correlation Measurement

9.5.1a Distribution of Cross-Correlation Coefficient

Firstly, it is necessary to examine whether the distribution of correlation coefficients is almost equal to the real free-surface shape before evaluating the surface area by using the depth meters. Fig.9.15 shows the distribution of cross-correlation coefficient $C_{\eta\eta}$ of surface-wave fluctuations in 2-D wind waves when one depth meter is fixed at x=0 in the center of the channel and the other is moved to the streamwise direction. It can be seen that the peak value decreases as x increases in spite of the quasi-periodical space. Akai *et al.* (1977) have pointed out that the auto-correlation function versus lag time in 2-D waves takes the same distribution as Fig.9.15, which shows that "*Taylor's frozen-turbulence hypothesis*" is effective in wind waves.

9.5.1b Damping Characteristics of Peak Values

Though the amplitude of $C_{\eta\eta}$ does not decrease in the streamwise direction as expressed in Eq.(9.8) on the assumption that the wind wave can be regarded as a small amplitude wave, the value really does decrease. Therefore, it is necessary to add the damping correction to $C_{\eta\eta}$ in order to evaluate the surface area from the cross-correlation coefficient. Fig.9.16 shows the reverse of $C_{\eta\eta,peak}$ (local peak value of $C_{\eta\eta}$) versus x. Linear relations can be seen in both two cases, and the approximate line evaluated by the least-square method is also described in this figure. Fig.9.17 is the corrected value of

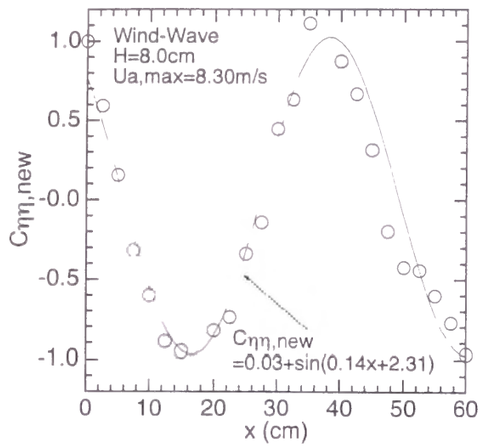

Fig.9.17 Corrected value of $C_{\eta\eta}$ considering damping effect.

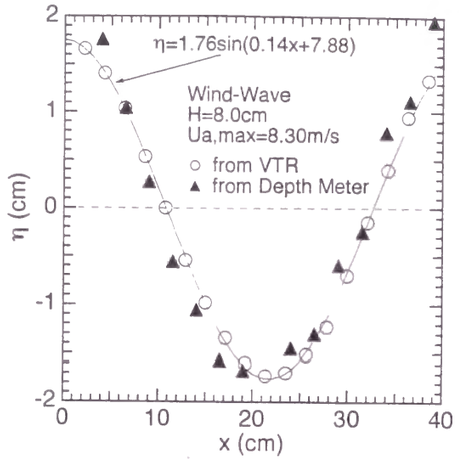

Fig.9.18 Distribution of $\eta=AC_{\eta\eta,new}$.

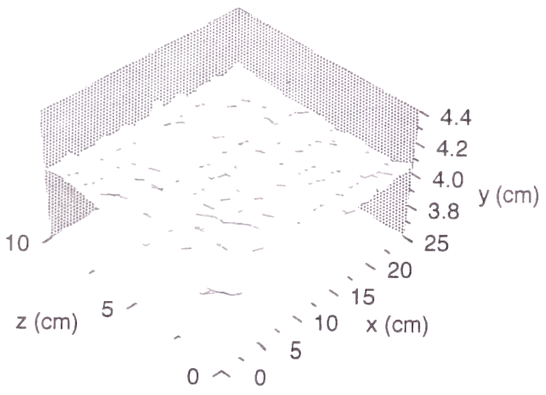

Fig.9.19 Shape of water surface in open-channel flow.

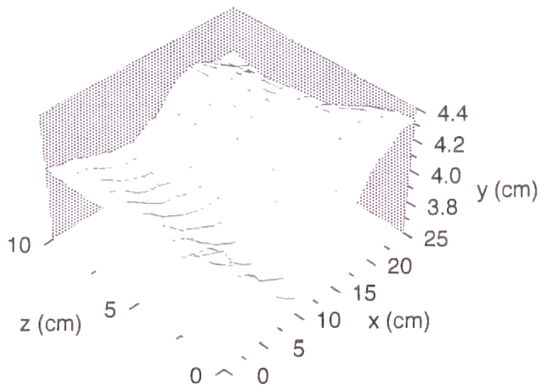

Fig.9.20 Shape of water surface in wind waves.

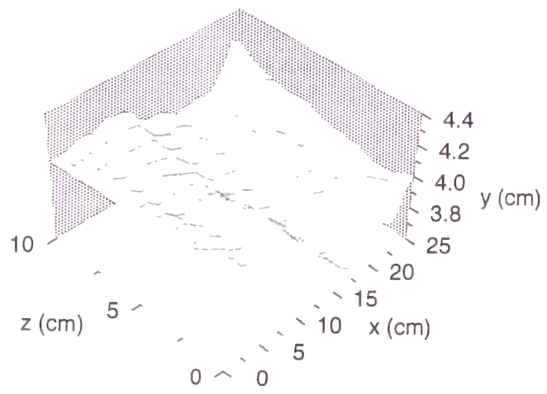

Fig.9.21 Shape of water surface in two-layer flows.

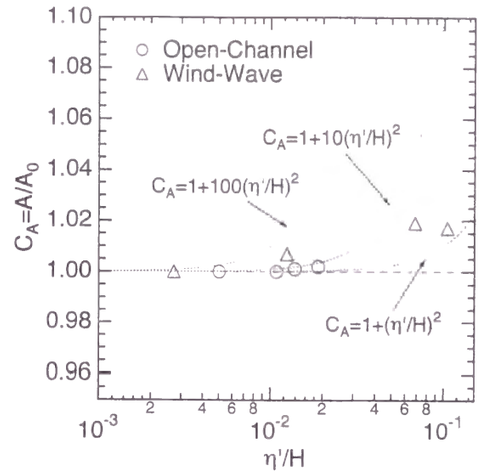

Fig.9.22 Increasing rate of surface area $C_A=A/A_0$.

$C_{\eta\eta}$ by using the line in Fig.9.16, together with the approximate curve. The distribution of $C_{\eta\eta,new}$ is quite similar to Eq.(9.8), which means that the damping correction is fairly correct.

9.5.1c Comparison with VTR Image

Fig.9.18 shows the distribution of $\eta=AC_{\eta\eta,new}$, where A is a significant wave height, together with the surface shape estimated from VTR (phase-averaged value of more than at least 30 samples). The distributions estimated from VTR and calculated by cross-correlation are well coincident with each other for periods and curvatures, which means that this method is very effective.

9.5.2 Variations of Water Surface

9.5.2a Shape of Water Surface

Fig.9.19 shows the shape of water surface in open-channel flow at Fr=1.50. There occur randomly a lot of disturbances in spite of small amplitude. Fig.9.20 shows the shape of water surface in wind waves of $U_{a,max}$=8.41m/s. Though there exist 2-D waves with quite a longer wave-length, there are less disturbances than those in open-channel flow. Fig.9.21 shows the shape of water surface in two-layer flows (Fr=1.50 and $U_{a,max}$=8.41m/s). There occurs small disturbances over wind waves and the wave length is twice as long as in wind waves due to the effect of greater convection.

9.5.2b Variations of Surface Area

Fig.9.22 shows the increasing rate of surface area $C_A=A/A_0$ in open-channel flow and wind wave. The surface area was calculated by the triangular meshes. It can be seen that the increasing rate is almost zero in both flows because the former formula supposed by Dobbins (1964) and Thackston and Krenkel (1969) are for the actual river with rough bed (C_A=1.0+0.3Fr^2 or 1.0+$Fr^{1/2}$). Furthermore, the increasing rate in wind wave is a little greater than that in open-channel flow, which is inconsistent with the experimental data by Nakayama and Nezu (1999g) and Eq.(8.17). Therefore, the effect of surface area on the gas transfer can be almost ignored in smooth open-channel flow.

9.5.3 Evaluation of Effects on Gas Transfer

9.5.3a Energy Spectra of Surface-Wave Fluctuations

It has been pointed out that the -5 power law in wind waves proposed by Phillips (1958) is mostly

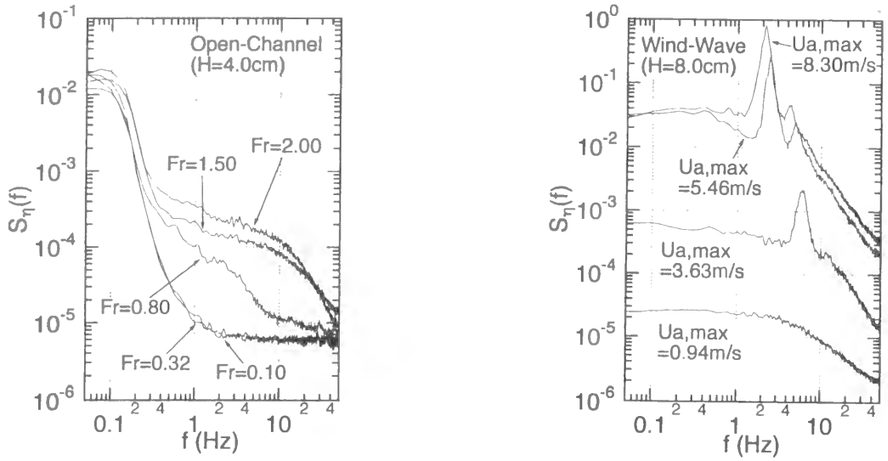

(a) open-channel flow (b) wind wave

Fig.9.23 Energy spectra of surface-wave fluctuations $S_\eta(f)$.

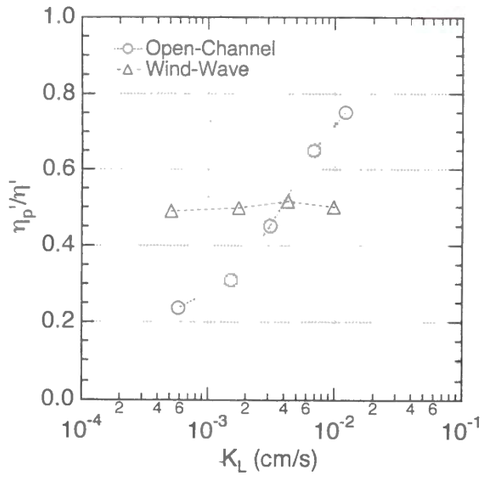

Fig.9.24 Ratio of the intensity of surface-wave fluctuations by the higher frequency component η_p' to the total intensity η'.

effective instead of a little modification. By the way, Nezu (1977) pointed out the slope of power law in open-channel flow changes from -5 in sub-critical flow to -3 in super-critical flow as the Froude number increases. Figs.9.23(a)-(b) show the energy spectra of surface-wave fluctuations $S_\eta(f)$ in open-channel flow and wind waves. For calculating the spectra, the ensemble average was conducted over about 40 samples. In wind waves, the gradient is milder at the higher frequency region by the scatter of supersonic waves due to the larger amplitude of waves. In open-channel flow, the -5 power law is effective in the smaller Froude number, and the energy shifts to the higher frequency region as the Froude number increases.

Fig.9.24 shows the ratio of the intensity of surface-wave fluctuations by the higher frequency component η_p' to the total intensity η' versus K_L, where η_p' is defined as follow;

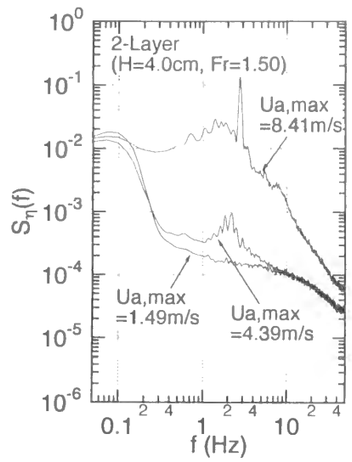

Fig.9.25 Energy spectra of surface-wave fluctuations $S_\eta(f)$ in two-layer flows.

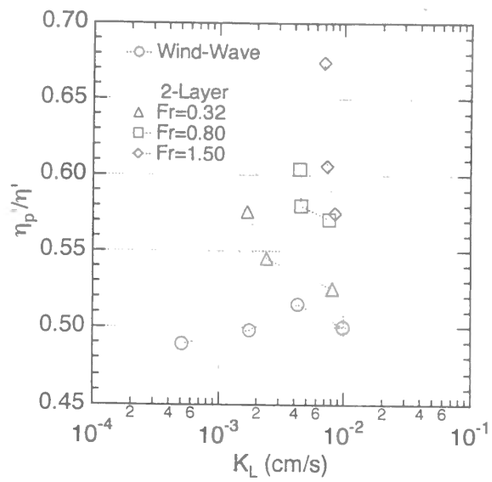

Fig.9.26 Distribution of η_p'/η' in two-layer flows.

$$\eta_p'^2 = \int_{f_p}^{\infty} S_\eta(f)\,df \tag{9.9}$$

where f_p is the transitional frequency from the -5 power law to the -3 power law in open-channel flow, and the upper limit of dominant frequency in wind waves, respectively. It can be seen that η_p'/η' is almost constant in wind waves and that the value gradually approaches one as K_L increases in open-channel flow. This implies that the relation $K_L \sim \eta^{3/4}$ is effective when S_η takes the -5 power law regardless of open-channel flow or wind waves, and that the gas transfer is more promoted ($K_L \sim \eta^{1/4}$) in open-channel flow than that in wind wave due to the predominance of the energy of the smaller-scale surface-wave in open-channel flow at the higher Froude number.

9.5.3b Extension to Two-Layer Flows

Fig.9.25 shows S_η in two-layer flows (Fr=1.50). It can be seen that the effect of wind velocity becomes greater over the hole frequency region as the wind becomes faster. Fig.9.26 shows the distribution of η_p'/η' in two-layer flows, where f_p is the upper limit of the predominant wave motion. The value η_p'/η' increases as the velocity of water layer becomes faster, which means that the energy rate of higher-frequency component increases. The increasing rate is larger as the wind is smaller. In this way, the value η_p'/η' becomes a good measure of the contributions of higher-frequency component in two-layer flows. Fig.9.27 shows the conceptual model about the relationship between K_L and η'. As for two-layer flows, the values are located between the two lines depending on the rate of higher-frequency energy. This relationship is very effective because it is not necessary to use the relation between friction velocities and K_L in this situation, which does not depend on the shear conditions.

9.6 Conclusions

In this study, firstly, PIV method and phase-averaged method were used for evaluating the instantaneous structures in both layers and the relationship with each other. Fig.9.28 shows the

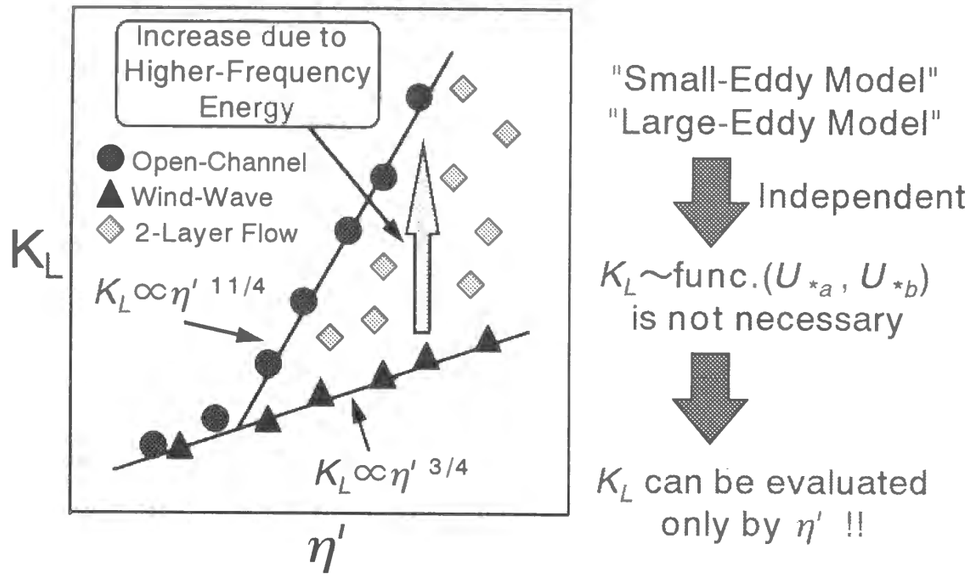

Fig.9.27 Conceptual model about the relationship between K_L and η'.

Fig.9.28 Conclusions of chapter 9.

conclusions of chapter 9. It was clarified that the separation of air flow on the leeward of the crest is closely related to the higher vorticity region of water on the leeward. Furthermore, the coherent vortices generated in the water depend on the wind waves and in the faster wind speed a pair of vortices is generated both in air and water layers.

Next, the effect of increase of surface area and other factor on gas transfer was evaluated by conducting the simultaneous measurements of two depth meters. As a result, it was found that the

effect of enhanced surface area on the gas transfer can be almost ignored in smooth open-channel flow. The energy of the smaller-scale surface-wave fluctuations contributes greatly to the rapid increase of gas transfer.

Notations

A : significant wave height, water surface area
C : instantaneous concentration of dissolved gas
C_A : increased area ($=A/A_0$)
$C_{\eta\eta}$: cross-correlation coefficient
$C_{\eta\eta,new}$: corrected value of $C_{\eta\eta}$ considering the damping effect
$C_{\eta\eta,peak}$: local peak value of $C_{\eta\eta}$)
D_m : molecular diffusivity of the gas in the liquid
d : half height of air channel
E_s : turbulent energy per unit mass of liquid in the vicinity of the surface
Fr : Froude number ($=U_m/\sqrt{gH}$)
f : frequency
f_p : the transitional frequency of power law or the upper limit of dominant frequency
H : flow depth
K_L : gas transfer coefficient
k : wave number ($=2\pi/\lambda$)
L : length scale
RS_i : contribution rate of i-th event
R_* : turbulent Reynolds number
r : mean frequency of surface renewal
S_η : energy spectra of surface-wave fluctuations
T : wave period
T_i : generation period of i-th event coherent vortex
U_a : wind velocity
$U_{a,max}$: maximum wind velocity
U_m : bulk mean velocity
$U_{w,mean}$: bulk mean velocity in water
U_* : friction velocity
U_{*a} : friction velocity in air layer
U_{*b} : friction velocity in water layer
U_{*w} : friction velocity at the interface
u : instantaneous streamwise velocity component
$-\overline{uv}$: Reynolds stress
v : instantaneous vertical velocity component
x : streamwise direction
y : vertical direction from the channel bed
y' : distance from the free surface ($=H-y$)
z : vertical direction from water surface

Greek symbols
ε : turbulent energy dissipation rate

η : surface-wave fluctuations
η' : intensity of surface-wave fluctuations ($=\sqrt{\overline{\eta^2}}$)
η_p' : the intensity of surface-wave fluctuations by the higher frequency component
λ : wave length
κ : von Karman constant
ν : kinetic viscosity
ν_a : kinetic viscosity of air
ν_w : kinetic viscosity of water
θ : degree of wave phase
ρ_a : density of air
ρ_w : density of water
Ω_a : instantaneous spanwise vorticity in air layer ($=\partial v/\partial x - \partial u/\partial z$, counterclockwise direction is positive)
Ω_w : instantaneous spanwise vorticity in water layer ($=\partial v/\partial x - \partial u/\partial y$, counterclockwise direction is positive)
ω : angular frequency ($=2\pi f$)

References

[1] Akai, M., Inoue, A. and Aoki, S. : Structure of a co-current stratified two-phase flow with wavy surface, *Theor. Appl. Mech.*, Vol.25, pp.445-456, 1977.
[2] Banner, M.L. and Melville, W.K. : On the separation of air flow over water waves, *J. Fluid Mech.*, Vol.77, pp.825-842, 1976.
[3] Belcher, S.E., Harris, J.A. and Street, R.L. : Linear dynamics of wind waves in coupled turbulent air-water flow. Part 1. Theory, *J. Fluid Mech.*, Vol.271, pp.119-151, 1994.
[4] Chang, P.C., Plate, E.J. and Hidy, G.M. : Turbulent air flow over the dominant component of wind-generated water waves, *J. Fluid Mech.*, Vol.47, pp.183-208, 1971.
[5] Danckwerts, P.V. : Significance of liquid-film coefficients in gas absorption, *Indust. and Eng. Chem.*, Vol.43, No.16, pp.1460-1467, 1951.
[6] Dobbins, W.E. : BOD and oxygen relationships in streams, *J. Sanitary Eng.*, ASCE, Vol.90, SA3, pp.53-78, 1964.
[7] Esfahany, M.N. and Kawaji, M. : Turbulence structure under a typical shear induced wave at a liquid/gas interface, *AIChE Symposium Series*, pp.203-210, 1996.
[8] Hanratty, T.J. and Engen, J.M. : Interaction between a turbulent air stream and a moving surface, *AIChE J.*, Vol.3, No.3, pp.299-304, 1957.
[9] Hsu, C.-T., Hsu, E.Y. and Street, R.L. : On the structure of turbulent flow over a progressive water wave : theory and experiment in a transformed, wave-following co-ordinate system, *J. Fluid Mech.*, Vol.105, pp.87-117, 1981.
[10] Kawai, S. : Visualization of airflow separation over wind-wave crests under moderate wind, *Boundary-Layer Met.*, Vol.21, pp.93-104, 1981.
[11] Kawai, S. : Structure of air flow separation over wind-wave crests, *Boundary-Layer Met.*, Vol.23, pp.503-521, 1982.
[12] Kawamura, H. and Toba, Y. : Ordered motion in the turbulent boundary layer over wind waves, *J. Fluid Mech.*, Vol.197, pp.105-138, 1988.
[13] Kato, H. and Sano, K. : An experimental study of the turbulent structure of wind over water waves, *Report of the Port and Harbour Research Institute*, Vol.10, No.1, pp.1-42, 1971.
[14] Komori, S., Nagaosa, R. and Murakami, Y. : Turbulence structure and mass transfer across a

sheared air-water interface in wind-driven turbulence, *J. Fluid Mech.*, Vol.249, pp.161-183 1993.
[15] Lemmin, U., Scott, J.T. and Czapski, U.H. : The development from two-dimensional to three-dimensional turbulence generated by breaking waves, *J. Geophys. Res.*, Vol.79, No.24, pp.3442-3448, 1974.
[16] Lombardi, P., Angelis, V.D. and Banerjee, S. : Direct numerical simulation of near-interface turbulence in coupled gas-liquid flow, *Phys. Fluids*, Vol.8, No.6, pp.1643-1665, 1996.
[17] Longuet-Higgins, M.S. : Capillary rollers and bores, *J. Fluid Mech.*, Vol.240, pp.659-679, 1992.
[18] Luchik, T.S. and Tiederman, W.G. : Timescale and structure of ejections and bursts in turbulent channel flows, *J. Fluid Mech.*, Vol.174, pp.529-552, 1987.
[19] Nezu, I. : Turbulent structure in open-channel flows, *Ph.D Thesis presented to Kyoto University*, 1977 (in Japanese).
[20] Nakayama, T. and Nezu, I. : Bursts near the free surface in open-channel flows and their relationship with turbulence structures, *Journal of Hydraulic Engineering*, JSCE, No.635/II-49, pp.31-40, 1999e (in Japanese).
[21] Nakayama, T. and Nezu, I. : Relationship between turbulence structures and gas transfer across air-water interface, *Journal of Hydraulic Engineering*, JSCE, No.635/II-49, pp.85-95, 1999f (in Japanese).
[22] Nakayama, T. and Nezu, I. : Turbulence structures of wind/stream combined flow, *Journal of Hydraulic Engineering*, JSCE, 1999m (in Japanese, to be accepted).
[23] Nakayama, T. and Nezu, I. : Turbulence structures of wind water waves, *Journal of Hydraulic Engineering*, JSCE, No.642/II-50, 2000a (in Japanese).
[24] Nakayama, T. and Nezu, I. : Effect of increase of surface area and other factor on gas transfer in two-layer flows, *Annual Journal of Hydraulic Engineering*, Vol.44, pp.891-896, 2000b (in Japanese).
[25] Nezu, I. and Nakayama, T. : Instantaneous structures of air and water layers in wind water waves, *Annual Journal of Hydraulic Engineering*, Vol.44, pp.897-902, 2000c (in Japanese).
[26] Okuda, K. : Internal flow structure of short wind waves ; Part I. On the internal vorticity structure, *J. Oceanogr. Soc. Japan*, Vol.38, pp.28-42, 1982a.
[27] Okuda, K. : Internal flow structure of short wind waves ; Part II. The streamline pattern, *J. Oceanogr. Soc. Japan*, Vol.38, pp.313-322, 1982b.
[28] Okuda, K. : Internal flow structure of short wind waves ; Part II. Pressure distribution, *J. Oceanogr. Soc. Japan*, Vol.38, pp.331-338, 1982c.
[29] Okuda, K. : Internal flow structure of short wind waves ; Part II. The generation of flow in excess of the phase speed, *J. Oceanogr. Soc. Japan*, Vol.40, pp.46-56, 1984.
[30] Phillips, O.M. : The equilibrium range in the spectrum of wind-generated ocean waves, *J. Fluid Mech.*, Vol.4, pp.426-434, 1958.
[31] Rashidi, M., Hetsroni, G. and Banerjee, S. : Mechanisms of heat and gas transport at gas-liquid interfaces, *Int. J. Heat Mass Transfer.*, Vol.34, No.7, pp.1799-1810, 1991.
[32] Takeuchi, K., Leavitt, E. and Chao, S.P. : Effects of water waves on the structure of turbulent shear flow, *J. Fluid Mech.*, Vol.80, pp.535-559, 1977.
[33] Thackston, E.L. and Krenkel, P.A. : Reaeration prediction in natural streams, *J.Sanitary Eng.*, ASCE, Vol.95, SA1, pp.65-93, 1969.

CHAPTER 10

CONCLUSIONS

10.1 Overall Results

In this study, the relationship between the turbulence and coherent structures in both layers and the gas transfer across the interface was evaluated in view of the physical and chemical aspects. At that time, three types of turbulent conditions were examined; that is to say, (A) bottom-shear generated turbulence, (B) wind-shear generated turbulence and (C) combined wind/stream turbulent conditions. In open-channel flow, the turbulence and coherent structures near the free surface greatly depend on the Froude number, and are closely related to the bursting phenomena near the wall. In wind-water wave, there exists the interfacial shear, which greatly affects the momentum and energy transfer from the air to the water layer. In two-layer flows, the turbulence and coherent structures are greatly dependent on the relative velocity. These turbulence and coherent structures are closely related to the gas transfer. The enhanced surface area can be ignored and the higher frequency energy of surface-wave fluctuations contribute much to the gas transfer.

10.2 Specific Findings

"Chapter 1" introduced the motivation, scope and objectives of this thesis. Furthermore, the overviews of each chapter are briefly mentioned.

"Chapter 2" examined the turbulence and the coherent structure near the free surface in smooth open-channel flow. It was found that the free surface affects greatly the damping characteristics of turbulence intensity near the free surface in quiet open-channel flow in comparison with the DNS data in duct flow. However, when the Froude number increases and the surface-wave fluctuations occur, this damping characteristic disappears. So, the relationship between the turbulence structure near the free surface and the surface-wave fluctuations was considered by the simultaneous measurements of LDA (Laser-Doppler anemometer) and the ultrasonic depth meter. These turbulence characteristics are closely related to the coherent structure, and therefore, the space-time correlation structures were considered in order to relate to the Chapter 3.

"Chapter 3" estimated the variation of turbulent energy redistributions near the free surface including the effect of Froude number. Next, PIV (Particle-Image Velocimetry) method is used to measure evolutionary patterns of coherent vortices. In this chapter, a relationship between the "*bursting phenomenon*" generated near the wall and the "*surface renewal eddies*" near the free surface was evaluated in the flows whether or not the surface-wave fluctuations are generated at the free surface. It was clarified that the agglemeration occurs in the higher Froude number flow and that this results in the longer bursting-period and the increase of turbulence intensity.

"Chapter 4" described the numerical simulation by using RSM (Reynolds stress model). The turbulent redistribution near the free surface could be reproduced by considering the effect of Froude number and the surface-wave fluctuations. At that time, two methods, that is to say, (1) giving the boundary conditions of the turbulent redistributions at the free surface, and (2) the extension of Shir model, were used.

"Chapter 5" applied the rough-bed flow with large roughness elements. The tendency toward isotropy becomes stronger near the roughness elements in comparison with smooth open-channel flow. As for the coherent structure, the inhomogeneity of the coherent structure predominates near the rough bed, which results in the generation of boil near the free surface. Furthermore, the wave-induced flow is evaluated for comparing "*wave-effect*" with "*turbulence-effect*".

"Chapter 6" examined the turbulence structure at the air-water interface with wind shear above the still water. Firstly, the fundamental characteristics of wind waves were considered in view of the

momentum transfer and the relation between roughness height and surface wave, *etc*. Furthermore, the turbulence structures across air-water interface were evaluated. At that time, LFT (Linear Filtration Technique) method was used for decomposing the velocity component into the mean, wave and turbulence components. The energy budgets in both air and water layers are closely related with each other, and the energy transfer through the air-water interface increases when the wind velocity increases.

"Chapter 7" extended the knowledge of former chapters to the two-layer flows when both the bed shear and the interfacial shear coexist. In this chapter, the mixing-length model in wind wave is extended in the air flow of two-phase flows. As for the roughness height, it was clarified that the value has a close relationship with the relative velocity of both layers.

"Chapter 8" relates the characteristics of gas transfer across the interface to the previous empirical models including the effects of shear velocity and dissipation rate by measuring the DO (dissolved oxygen) concentrations. About two-layer flows, these models were expanded by considering the effect of the bed and interfacial shears, and the gas transfer coefficient in two-layer flows could be estimated by using the square-root matching technique.

"Chapter 9" completed the mechanism of relationship between the coherent structures in both layers and the gas transfer across the interface. By using PIV and the phase-averaged method, it was found that the separation of air flow on the leeward of the crest is closely related to the higher vorticity region of water on the leeward. In the faster wind speed, there occurs a pair of vortices both in air and water layers. Furthermore, the effect of enhanced surface area on the gas transfer could be ignored in open-channel flow, and the higher frequency-energy of surface-wave fluctuations contributes greatly on the rapid increase of gas transfer.

10.3 Directions for Further Works

Fig.10.1 shows an applicability of this study. As for the physical aspect, mixing-length model, shear stress and energy budget across air-water interface in two-layer flows can be used for conducting a numerical simulation of atmosphere-water global-circulation. At that time, by using the predominant condition of shear stress, it is possible to treat river and ocean together, that is to say, as a circulation system. Furthermore, the relationship between the intensity of surface-wave fluctuations η' and the gas transfer coefficient K_L is very effective because it is not necessary to use the relation between friction velocities and K_L in this situation, which does not depend on the shear conditions. In particular, if these findings are combined with GIS, GPS and artificial satellite data, it will result in the construction of better air-water combined-model, which is very effective for the forecast of climate change, movement of pollutant and chemical substance in view of the global environment problems on earth.

A continuation of this research should include the following areas of studies in the future, as shown in Fig.10.2 :

(1) Extension to the breaking waves, hydraulic jump, and jet flows, *etc*. These flows are accompanied by the air bubble, and therefore, would have a greater contribution to the environmental problems in the near future.

(2) The measurements of the flow with air bubbles may be very difficult and have a limitation of accuracy in the present measuring systems. In this sense, the numerical simulations including the unsteady effects (LES and DNS) may be much important for predicting the interfacial flow situations. Furthermore, the refinements of boundary conditions at the interface are urgently necessary.

(3) Water sound accompanied by the air bubble is important as the environmental function of hearing in the waterfronts. This sound may be closely related to the turbulence structure and it is necessary to make clear the relation.

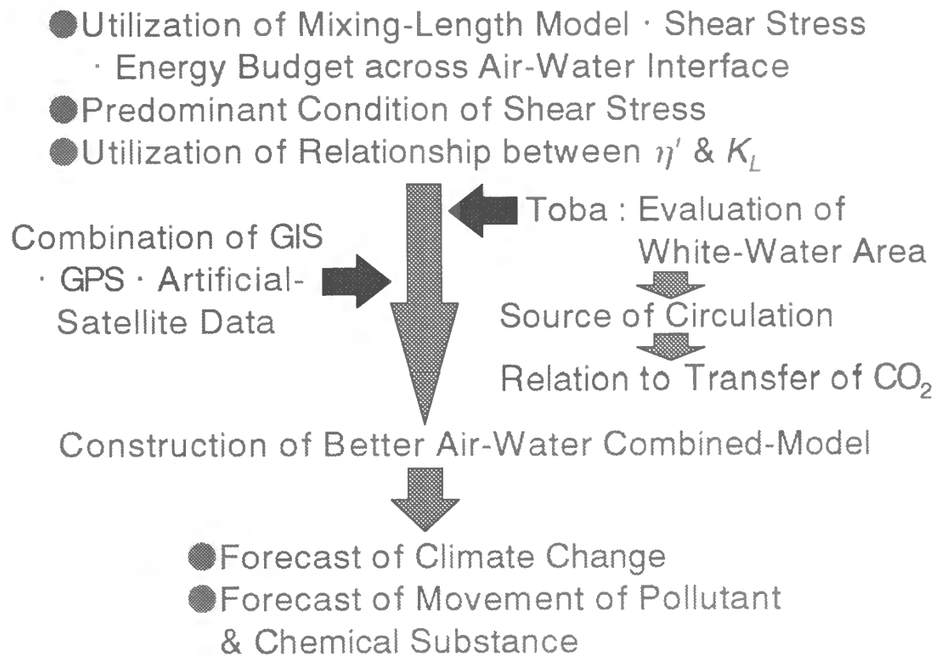

Fig.10.1 Applicability of this study.

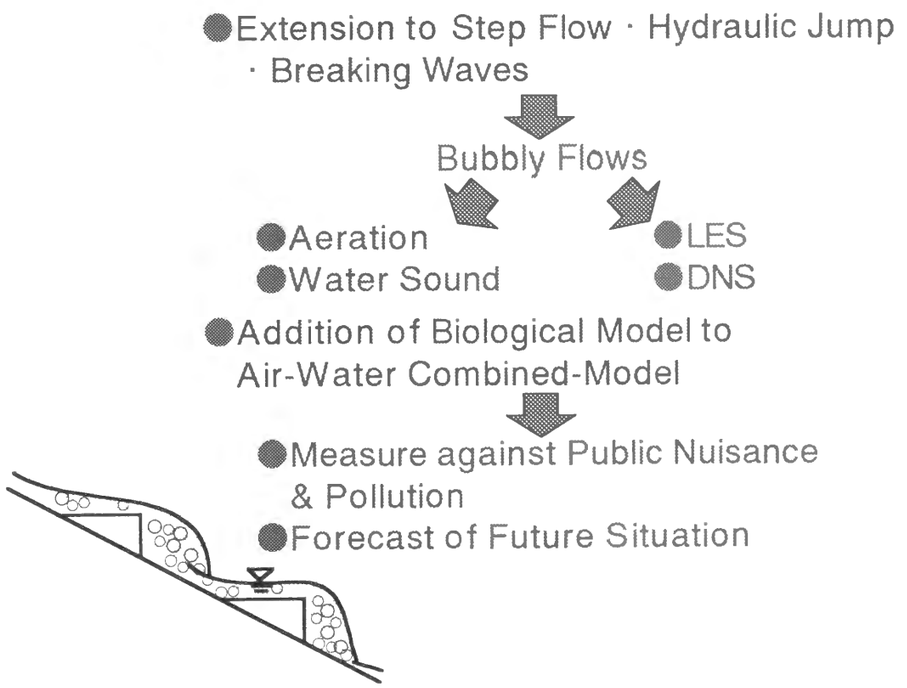

Fig.10.2 Directions for further works.

(4) In view of global environment problems, it is urgent to add biological model to air-water combined model. This will become the measure against public nuisance and pollution and the forecast of future situation of these substances.